Mark D. Allendorf, Renhao Dong, Xinliang Feng, Stefan Kaskel, Dariusz Matoga, Vitalie Stavila

# Electronic Devices Using Open Framework Materials

**Erstveröffentlichung in / First published in:**

*Chemical Reviews* 2020, 120(1), S. 8581-8640 {Zugriff am: 04.08.2022}. ACS Publications. ISSN 1520-6890.

DOI: https://doi.org/10.1021/acs.chemrev.0c00033

Final edited form was published in "Chemical Reviews 2020, 120(1), S. 8581-8640. ISSN 1520-6890.
https://doi.org/10.1021/acs.chemrev.0c00033

# Electronic Devices Using Open Framework Materials

Mark D. Allendorf,[†*] Renhao Dong,[‡] Xinliang Feng,[‡] Stefan Kaskel,[§] Dariusz Matoga,[‖] Vitalie Stavila[†]

[†]Chemistry, Combustion, and Materials Science Center, Sandia National Laboratories, Livermore, CA 94551 USA

[‡]Center for Advancing Electronics Dresden (cfaed) and Faculty of Chemistry and Food Chemistry, Technische Universität Dresden, 01062 Dresden, Germany Zimmerman, Jonathan A <jzimmer@sandia.gov>[§]Department of Inorganic Chemistry, Technische Universität Dresden, Bergstrasse 66, 01062 Dresden, Germany

[‖]Faculty of Chemistry, Jagiellonian University, Gronostajowa 2, 30-387 Kraków, Poland

## ABSTRACT

Open framework materials (OFM) constitute a large and growing class of nanoporous crystalline structures that is attracting considerable attention for electronic device applications. This review summarizes the most recent reports concerning electronic devices enabled by either of the two primary categories of OFM, Metal-Organic Frameworks (MOFs) and Covalent-Organic Frameworks (COFs). Devices in which the OFM plays an active role (as opposed to acting only as a selective sorbent or filter) are the principal focus, with examples cited that include field-effect transistors, capacitors, memristors, and a wide variety of sensing architectures. As a brief tutorial, we also provide a concise summary of various methods of depositing or growing OFM on surfaces, as these are of crucial importance to the deployment of electronic OFM. Finally, we offer our perspective concerning future research directions, particularly regarding what in our view are the biggest challenges remaining to be addressed. Based on the literature discussed here, we conclude that OFM constitute a unique class of electronic materials with characteristics and advantages that are distinct from either conventional inorganic semiconductors or organic conductors. This suggests a bright future for these materials in applications such as edge computing, resistive switching, and mechanically flexible sensing and electronics.

Final edited form was published in "Chemical Reviews 2020, 120(1), S. 8581-8640. ISSN 1520-6890.
https://doi.org/10.1021/acs.chemrev.0c00033

## CONTENTS

Final edited form was published in "Chemical Reviews 2020, 120(1), S. 8581-8640. ISSN 1520-6890.
https://doi.org/10.1021/acs.chemrev.0c00033

Final edited form was published in "Chemical Reviews 2020, 120(1), S. 8581-8640. ISSN 1520-6890.
https://doi.org/10.1021/acs.chemrev.0c00033

## 1. Introduction

The categories of nanoporous materials known as Metal-Organic Frameworks (MOFs)[1,2] and Covalent Organic Frameworks (COFs)[3] continue to grow in both their number and the galaxy of applications for which they are being considered. For the purposes of this article we designate them simply as Open Framework Materials (OFM). They share the common feature of having supramolecular structures assembled from metal nodes and organic linkers to form a crystalline lattice with rigid nanoporosity. The nodes consist of either transition metal cations or clusters (MOFs) or the main-group elements C, N, Si, B, and P (COFs), whereas the linkers are rigid, multitopic organic molecules with chemical functionalities of various types. These materials span an enormous compositional and structural landscape, driven by their versatile combination of long-range order and rational structure-function relationships. Encouragingly, aspects of their chemistry that initially limited their appeal relative to more traditional porous materials such as zeolites are being addressed. For example, materials with exceptional thermal stability,[1] lack of water reactivity,[4,5] and acceptable cost[6] have been reported during the past decade. OFM are now recognized as a unique category of materials filling a large gap between fully inorganic and organic materials. As a result, commercial interest is increasing, with several small companies founded that offer MOF-based technologies, bulk quantities, and custom synthesis.

In addition to traditional uses of nanoporous materials, such as gas storage, separation and catalysis, the potential of OFM to play a role in the world of electronics is generating great interest. In 2011 some of us discussed the status of the MOF field *vis a vis* electronics. Philosophically, this took the form of a "roadmap," somewhat like the International Technology Roadmap for Semiconductors that was first published in 1998.[7] Its primary purpose, however, was to highlight areas where major research efforts were needed to develop OFM for use in electronic devices. As of its writing in 2010, fewer than 800 articles on topics related to MOFs for optoelectronics were published between 1999 and 2010. Today, a search of MOF or COF with various device-related terms identified over 2100 articles for the period 2017-October 2019, covering virtually all of the major application spaces, including chemical and biological sensing, logic, and energy conversion (e.g. photovoltaics and fuel cells) and storage (e.g. supercapacitors and batteries). No doubt some articles merely reference the potential of OFM for these applications and no fewer than 130 review articles were found. Nevertheless, this enormous volume of work demonstrates a remarkable expansion within less than a decade and is testament to the realization that many opportunities exist to exploit the advantages of OFM for electronic devices.

The primary aim of this article, of course, is to inform the reader regarding the most recent developments and progress toward OFM-based devices, as well as to highlight areas where major knowledge gaps identified in the original[8] and updated[9] MOF roadmaps have been addressed. These include the need for improved film growth methods, an expanded catalogue of dielectric and conducting OFM, and assembly of fully functional devices with electronic readout. With so many recent review articles focused on this subject, however, it is reasonable to ask why another one is needed. Our answer is that most of the previous reviews are limited to particular subtopics or refer to electronic devices in only a peripheral way. At least thirty focus directly on sensing (the word "sensor" or "sensing" appears in the title),[10-32] consider specific sensing-related properties (e.g. electrical conductivity or luminescence),[14,24,33-35] or review particular fabrication methods such as thin-film growth required for device fabrication.[20,23,36-40] Here, our approach is both more specific than some but also more general than others: more specific in that we focus primarily on actual devices, as opposed to materials with properties that make them attractive for electronic

Final edited form was published in "Chemical Reviews 2020, 120(1), S. 8581-8640. ISSN 1520-6890.
https://doi.org/10.1021/acs.chemrev.0c00033

applications. Narrowing the focus further, for the most part we include only literature appearing since the revised MOF electronic materials roadmap published in 2017. Alternatively, this review is more general than some previous ones, in that we consider not only sensors (unavoidable, as this is such an important device-related topic), but also logic, memory, and resistance switches (memristors). We also review the latest developments concerning fabrication methods.

An additional motivation for this review is to place these developments in the context of the much wider world of microelectronics. Although there is no consensus that Moore's Law[41,42] is at an end (see for example the final International Technology Roadmap for Semiconductors[7]), there are strong indications that certain fundamental and economic limits are being reached. For example, it was very recently announced that the smallest usable gate length, 5 nm (~90 silicon atoms), has been achieved.[43] Another metric, switching energy, appears to be plateauing as well (Figure 1) and some analysis suggests that the dominant factor in the departure from Moore's Law is heat generation.[44] For these and other reasons, the semiconductor industry is at an historical turning point following decades of progress. A symptom of this change is the advent of specialized computers optimized for particular uses. Starting in 2011, the computational hardware capacity of application-specific computers (defined as those that perform "automated computations that are incidental to their primary task") exceeded that of so-called general-purpose computers (defined as those "whose functionality is directly guided by their human users").[45]

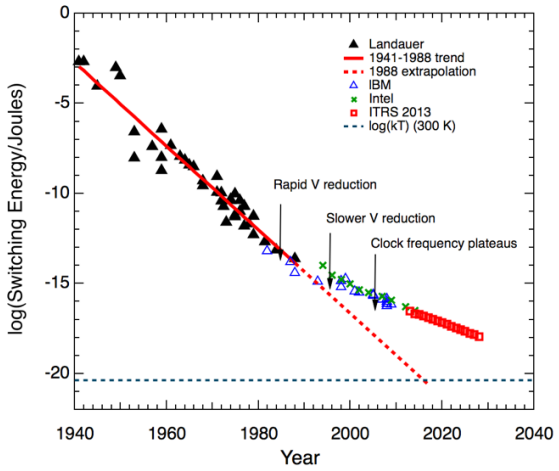


**Figure 1.** Historical data for switching energy from various published sources; see Ref. 44 for details. Red line is a linear fit to the Landauer data and the dashed red line is Landauer's 1988 extrapolation toward the thermal fluctation energy *kT*. Adapted with permission from Ref. 44. Copyright 2017 IEEE.

The trend from general-purpose to application-specific computing may provide an important motivation for developing OFM as a new class of electronic materials. For example, OFM possess a combination of properties that place them somewhere between conventional inorganic and organic semiconductors. Because OFM are crystalline, their properties may be less affected by disorder than amorphous organic polymers, leading to improved properties. Alternatively, compared with crystalline inorganic semiconductors, OFM possess vastly greater chemical tailorability due to the individual chemistries of the nodes and linkers. Moreover, their nanoporosity provides a totally new design element that allows emergent properties to be achieved by careful infiltration of the pores with guest species.[46] A range of semiconducting and optical

properties have also been demonstrated. Of course, other nanoporous materials as well as nano- or mesoporous templating materials have some of these same characteristics. However, few if any of these can provide the full "materials genome" exhibited by OFM.

Has progress been made? Definitely. Although there are no commercial devices to our knowledge that incorporate OFM materials, numerous proof-of-concept demonstrations have been reported in just the past three years. Importantly, fabrication techniques are also steadily advancing and the factors controlling them are better understood. Finally, an increasing number of measurements of fundamental properties such as charge mobility are being reported, which contributes to better understanding of the mechanisms controlling OFM charge transport.[34] These developments reflect a greater awareness of the very real challenges that must be addressed to develop OFM for electronic devices.

It is important to emphasize, however, that conventional semiconductors should not be the metric by which OFM are judged as electronic materials. It is sometimes asked whether OFM will ever outperform these materials. Although this question cannot be fully answered without specifying a particular property, function, and device type, if the comparison is with silicon the answer is likely to be no. For example, intrinsic electron and hole mobilities for crystalline silicon at 300 K are 1450 – 1610 $cm^2(V•s)^{-1}$ and 300 – 400 $cm^2(V•s)^{-1}$, respectively (Hall effect),[47] whereas the highest values reported for an OFM are 116 $cm^2(V•s)^{-1}$ (electrons, FET)[48] and ~220 $cm^2(V•s)^{-1}$ (holes, Hall).[49] It is almost certainly the case that, regardless of whether OFM properties become better than conventional materials, they will likely never displace silicon or even less entrenched inorganic semiconductors because the commercial investment in these is so great. However, the reported mobilities for OFM considerably exceed those of typical crystalline organic semiconductors, which now are in the 1 – 10 $cm^2(V•s)^{-1}$ range.[50] It will be apparent below that OFM deserve to be judged on the merits of their unique combination of properties, i.e. nanoporosity, crystallinity, and highly tailorable structure. For example, the ability to tailor the electrical conductivity of OFM without resorting to doping is far greater than for silicon. Similarly, OFM bandgaps exhibit a range of values comparable to semiconducting organic polymers. Moreover,because of their crystalline structure rational bandgap tuning is possible to a greater extent than in disordered materials.

The sections of this review can be briefly summarized as follows. Section 2 provides an overview of fabrication techniques developed for OFM. Our purpose is to acquaint the reader with the primary methods now available, which are essential for integration of OFM with device hardware. We include both important initial reports for specific approaches as well as noteworthy recent developments, as this is a rapidly advancing field. Section 3 addresses the most recent advances in the use of OFM as active materials for both chemical and physical sensors. Sensors are by far the best developed category of OFM-enabled electronic devices. In contrast, memory and logic applications have received much less attention, but activities on this topic are gaining speed. Section 4 thus proceeds with a review of recent efforts to develop OFM-based FETs. Particular emphasis is placed on 2D materials, which are promising because of their ordered structure of stacked layers, which enables efficient interlayer charge transfer. Particularly interesting from a device perspective are their potential topological phenomena, magnetic properties, diverse exciton physics, and ability to integrate 2D OFM with other 2D materials. Research to develop OFM as dielectric materials is also reviewed. Finally, although devices assembled from FETs constitute a multi-billion-dollar industry, trends in the semiconductor industry discussed above point to the need for alternative device types. Consequently, we devote

Final edited form was published in "Chemical Reviews 2020, 120(1), S. 8581-8640. ISSN 1520-6890.
https://doi.org/10.1021/acs.chemrev.0c00033

a separate section to resistive switches (also known as memristors). This is an application for which OFM appear to be particularly well suited, in part due to ordered porosity that can enhance ion transport rates. Moreover, their hybrid organic-inorganic structure and relatively mild processing conditions make them suitable for flexible electronics and edge computing, as well as for biocompatible devices. Omitted from this review are optoelectronic devices, in particular LEDs. Although this is a large and growing activity within the field of OFM, particularly involving luminescent MOFs as emitters, we are unaware of any electroluminescent OFM. Consequently, the primary challenge facing their use is optimization of OFM luminescent properties and not their integration with other materials to create functional devices. Nevertheless, even with this rather severe limitation the more than 500 references cited here clearly demonstrate that OFM electronics is an extremely vigorous area of research that justifies a review only three years after the second roadmap appeared.[9]

## 2. Fabrication and Integration of OFM with (Opto)electronic Devices

To design materials with desired properties and functionality, it is essential to establish the relationships between the composition, the periodic arrangement of molecules and atoms, and fabrication/processing conditions. OFM were originally developed as bulk materials for gas storage and catalysis, but recently more advanced applications are using well-defined OFM thin films in electronic, photonic, and optical devices. This poses unique challenges in terms of their fabrication and integration with other materials, as devices based on OFM represent a radical shift in terms of synthesis and processing compared with traditional inorganic and purely organic materials. Inorganic materials can be deposited on various surfaces using chemical and physical approaches, including sputtering,[51] electrochemical plating,[52] thermal evaporation,[53] molecular beam epitaxy (MBE),[54] chemical vapor deposition (CVD),[55] atomic layer deposition (ALD),[56] and pulsed laser deposition (PLD).[57] Organic materials, on the other hand, can be processed using solid-state and solution techniques and deposited on surfaces by techniques such as melting,[58] laser ablation,[59] spin coating,[60] and casting.[61] Unlike these traditional electronic materials, OFM often require conditions for nucleation and growth that these conventional processing methods difficult and sometimes impossible. OFM are not as thermally stable as many inorganic materials, which makes high-temperature solid-state approaches unusable. Organic compounds, on the other hand, are often processed from solution at or near room temperature. OFM by definition are solid materials that are not reversibly solvated and may display reactivity to solvents (e.g. hydrolytic instability in the presence of water) that can limit or prevent suspending them as nanoparticles in solution. Consequently, there is a need for facile processing methods that permit high-quality, large-area growth on substrates such as silicon wafers and on individual devices.

It is important to note that the properties of OFM films are not necessarily identical to those of the bulk material, even though the crystalline porous structure is often maintained in the film.[62-65] For example, H. Kitagawa and coworkers recently discovered that a 2D layered MOF undergoes a structural transformation upon uptake of water or pyridine.[66] Although there are examples of physisorption-induced structural changes (gate-opening effects) in MOF films, the Kitagawa report is the first example of a chemisorption-induced structural response by a MOF thin film. Such effects are not well understood but surface reconstructions and substrate-film interactions are surely involved. No doubt the particular method used to grow the film will have an effect as well. This is a nascent research area that was recently reviewed.[67]

The first step in the fabrication of OFM-based devices involves deposition of a film or coating on a surface, ideally with some spatial control. Depending on the specific application, device fabrication may impose a number of requirements in terms of composition, morphology, homogeneity, and mechanical robustness. For optoelectronic applications there are additional requirements for thickness, crystallinity, transparency, and film orientation, which governs the pore direction relative to the substrate. The deposition of OFM thin films can be achieved by *in situ* and *ex situ* techniques. *In situ* methods rely on substrate functionalization to allow preferential nucleation of OFM and subsequent film growth[68-72] whereas *ex situ*[73-77] methods are based on direct deposition of previously synthesized OFM crystals or nanoparticles on surfaces. Many materials can be used as substrates, including oxides, silicon, silicon nitride, graphite, gold, copper, and many other metals. There is a significant body of literature concerning this subject matter and a number of reviews have been published over the past decade discussing various aspects of this topic.[8,9,22,30,36-38,46,78-96] In addition to OFM deposition, control over the film orientation may be required, which can be achieved using surface treatments such as self-assembled monolayers (SAMs)[68,96] and polymer coatings.[97] Finally, patterning and confining the OFM to specific locations is critical for certain device applications; this area also has been recently reviewed.[9,37,98,99] Our objective in this section, therefore, is to provide the reader with a basic familiarity with the various OFM integration methods, citing a few influential early references. We then review the most recent developments (primarily work published after 2015) concerning both *in-situ* and *ex-situ* techniques that are particularly suitable for integrating OFM with (opto)electronic devices.

Although a number of methods have been developed to integrate OFM with (opto)electronic devices, none are sufficiently general to be applied to a wide range of these materials. It is unfortunately still necessary in most cases to consider each OFM as having unique requirements for growing it as a film. Special consideration must be given to charge and mass transport in nanoporous OFM, as these are critical for device applications. The most appealing methods for device applications are those that allow film thickness to be controlled, with uniformly sized crystals, suitable pore orientation, and strong adhesion to the substrate. In general, the protocols for integration with functional devices have certain limitations. For example, only layer-by-layer liquid epitaxy, gas-phase synthesis, and Langmuir-Blodgett methods lead to well oriented films. Nevertheless, the proof-of-concept examples highlighted here point to great progress in just the past few years.

### 2.1 Solvothermal synthesis

Solvothermal synthesis was one of the first methods to be successfully employed for synthesizing OFM thin films. This method involves immersing substrates in precursor solutions and heating to enable reactivity and film nucleation.[100,101] Since thermal treatment can lead to both heterogeneous crystallization on substrates as well as homogeneous crystallization in bulk solutions, the challenge with solvothermal synthesis is to favor the former by creating multiple crystallization centers on the substrate to control the growth and yield crystalline materials and continuous films. This is especially challenging for COFs, which are often isolated as amorphous products. Yaghi and co-workers recently developed a new route to overcome this difficulty by using *tert*-butyloxycarbonyl and 4-(tert-butoxycarbonylamino)-aniline groups to protect the amine functionality of the linker and avoid the formation of amorphous polyimines. This method enables controlled synthesis of well-oriented thin films of COF-112 with and uniform thickness of 190 nm.[102] Using the solvothermal approach, complex heterostructures could be obtained as well, such

Final edited form was published in "Chemical Reviews 2020, 120(1), S. 8581-8640. ISSN 1520-6890.
https://doi.org/10.1021/acs.chemrev.0c00033

as periodically eclipsed pi-stacking columns of 2D COFs for direct charge carrier transport. Sun *et al*. perfected this method and reported the solvothermal synthesis of a COFTFPy-PPDA film on single layer graphene.[101] The synthesis involves covalent imine-type condensation of 1,3,6,8-tetrakis(p-formylphcnyl)pyrene (TFPy) and p-phenylenediamine (PPDA). Notably, the vertical field-effect transistor constructed from the COFTFPy-PPDA/graphene heterostructure showed ambipolar charge carrier behavior with the current density on/off ratio (>$10^5$) and high on-current density (>4.1 A $cm^{-2}$).[101]

The solvothermal method allows incorporation of multiple different metal centers in MOFs, such as in the formation of a Fe/Ni/Co-MIL-53 trimetallic MOF that is an active oxygen evolution reaction (OER) catalyst.[103] Modulators are widely used in the solvothermal synthesis of Zr and Hf-based MOFs, with Zr/Hf clusters first coordinating to modulators, then exchanging modulators with the organic linkers.[104] In a variation of this method, Lin *et al.* reported the synthesis of Zr/Hf-based metal-organic layers (MOLs) using formic acid and water as modulators (Figure 2).[105,106] The materials can exist as both 2D-MOLs and 3D-MOFs as they are connected by similar metal-oxo clusters, with key differences in the topology and dimensionality of the metal-ligand connection. Finally, although most of the OFM film growth methods were developed for relatively simple organic ligands such as BTC or BDC, methods of growing films incorporating larger, more complex linkers have also been developed. For example, Morris and co-workers used solvothermal synthesis to isolate a metalloporphyrin MOF consisting of [5,10,15,20-(4-carboxyphenyl)porphyrin]Co(III) (CoTCPP) units bound by linear trinuclear Co(II)-carboxylate clusters.[107]

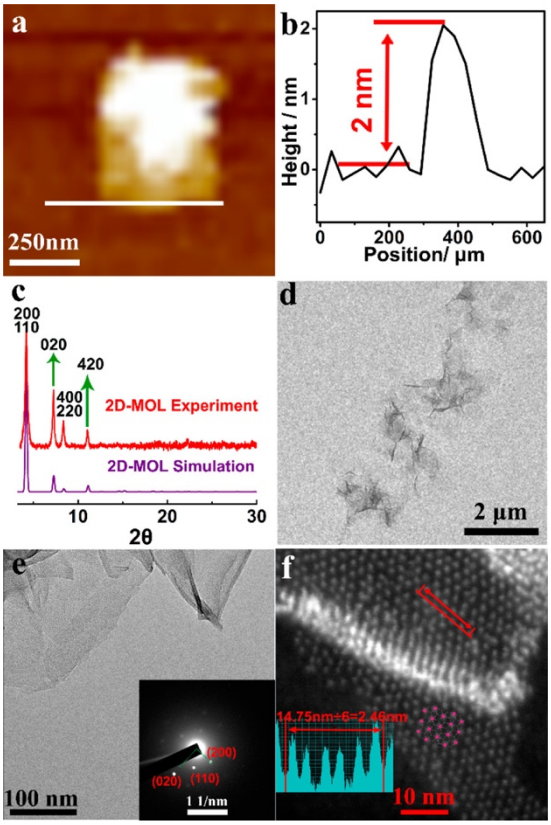

Final edited form was published in "Chemical Reviews 2020, 120(1), S. 8581-8640. ISSN 1520-6890.
https://doi.org/10.1021/acs.chemrev.0c00033

**Figure 2.** (a) AFM topography of a Hf-based 2D-MOL. (b) Height profile along the white line in (a). (c) PXRD pattern of 2D-MOL compared with the simulated one from the double-decker model. (d) TEM imagine of 2D-MOL. (e) HRTEM and SAED images of 2D-MOL. (f) HAADF images of 2D-MOL overlaid with a structural model showing $Hf_{12}$ SBUs. Reproduced with permission from Ref. 106. Copyright 2017 American Chemical Society.

### 2.2 Microwave-assisted synthesis

Although this is a relatively recent development, microwave-assisted heating is now widely employed for OFM synthesis and provides a means to increase the rate of film growth.[108-116] The rate acceleration occurs by efficient heating of the reaction mixture by "microwave dielectric heating," by which microwave energy is absorbed by a solution or a suspension and then converted into heat. Microwave heating was originally used for rapid production of MOF powders. The precursors are typically dissolved or dispersed in a solvent and then the mixture is heated in a microwave oven from a few seconds to a few hours to form the desired reaction product.[117-120] For example, Ni and Masel used microwave-assisted solvothermal synthesis to produce MOF-5 particle sizes ranging from 200 nm to 4 μm in less than a minute under varying reactant concentrations.[118] Serre and co-workers optimized the synthesis of sub-100 nm uniform MIL-88A(Fe), and obtained better yields compared to conventional solvothermal synthesis.[121] Extending the method beyond powders, Chen *et al.* used this technique to synthesize a Zn-Ni honeycomblike MOF structure as a supercapacitor electrode material with remarkable electrochemical performance, a specific capacity of 237.4 mAh $g^{-1}$ at 1 A $g^{-1}$, one of the highest performances reported so far for MOFs.[122] For film growth, substrates comprised of inorganic carbon or carbon-coated materials are particularly attractive, as these are efficient microwave absorbers. Yoo *et al*. presented a microwave-induced method to synthesize MOF-5 on carbon coated porous alumina surfaces, with nearly full surface coverage achieved in 30 seconds at 500 W irradiation power.[123] Microwave heating can also be used for the rapid synthesis of various COF materials. For example, COF-5 can be synthesized in as little as 20 minutes by microwave heating to give a highly porous material (BET S.A. = 2099 $m^2$ $g^{-1}$) in good yields (68−95%).[119] Zhao *et al*. synthesized a 2D imine COF, LZU-1, with a surface area of 729 $m^2$ $g^{-1}$, and created continuous thin films on silicon substrates.[102] Microwave approaches are not without disadvantages, however; they may also lead to the formation of by-products and thin film contamination.[124]

### 2.3 Low-temperature self-assembly

In selected cases, it is possible to grow OFM films directly by self-assembly from solutions, or by immersing substrates in the mother solution of the OFM so that the growth can take place at low temperatures.[96] This synthesis is widely used for systems with a strong thermodynamic driving force to form the product and low activation energies for the process. Dincă and co-workers synthesized an electronically conductive metal-organic graphene (MOG) analogue $Ni_3(HITP)_2$ (HITP = 2,3,6,7,10,11-hexaiminotriphenylene) by reacting $NiCl_2{\cdot}6H2O$ with HATP (2,3,6,7,10,11-hexaaminotriphenylene) in aqueous ammonia to obtain electrically conducting pellets and films.[125] Marinescu and coworkers successfully isolated conducting and semiconducting thin films of thiolate based MOFs using low-temperature solution synthesis approaches.[126,127] Chen *et al.* synthesized thiolate 2D MOFs based on the benzenehexathiol ligand (BHT) using a liquid-liquid interfacial reaction, with $Ag_3BHT_2$ thin films reaching an electrical conductivity of as high as 363 S $cm^{-1}$.[128]

Final edited form was published in "Chemical Reviews 2020, 120(1), S. 8581-8640. ISSN 1520-6890.
https://doi.org/10.1021/acs.chemrev.0c00033

Controlled growth can be also achieved from solutions containing the OFM. Such methods were successfully applied in the cases of $[Cu_3(BTC)_2]$,[129] MIL-88B,[68] MOF-5,[130] as well as various ZIFs.[131,132] Repeated immersion steps in freshly prepared mother solutions enable the attachment of seeds and their further growth.[70,133] In the case of $[Cu_2(pzdc)_2(pyz)]_n$ (CPL-1; pzdc = pyrazine-2,3-dicarboxylate; pyz = pyrazine)[70], the MOF tends to form plate-like crystals in which the *b* plane is much larger than others. After five cycles, a dense layer of crystals forms a continuous film with preferred orientation in the (010) direction. Lu and Hupp deposited ZIF-8 on Si substrates and controlled the thickness of the film by the number of deposition cycles. No preferred orientation is found, but a very precise control of film thickness is achieved as the film thickens of 100 nm every cycle.[133] The use of appropriately prepared mother solution for film growth is a very powerful method. If sufficient time is allowed, continuous films can be achieved that in some cases are oriented. However, the fabrication of films by this route is relatively slow and requires greater understanding of the reactivity in the system than other approaches.[89,95]

## 2.4 Sonochemical synthesis

Sonochemical or ultrasound-assisted synthesis has been extensively used for the preparation of COFs[134,135] and MOFs[136-141] in bulk and thin film form. The field of ultrasound-assisted (sonochemical) synthesis of MOFs was recently reviewed, and the effects of various factors, such as power, reagent concentration, solvents, reaction time are discussed in details.[142] For example, Jhung *et al.* compared the synthesis of MIL-53(Fe) by ultrasound, microwave, and conventional electric heating methods, finding that the reaction rate is comparable for all three methods.[143] As expected, the size of the deposited MOF particles is inversely correlated with nucleation rate (conventional heating << microwave < ultrasound).

Recent examples of sonochemical OFM synthesis include the report by Tang and coworkers, who used this method to produce ultrathin Ni-Co MOF nanosheets (UMOFNs) as precursors for supercapacitor electrodes.[144] They reacted $Ni^{2+}$, $Co^{2+}$ and BDC ligands in DMF/$H_2O$/EtOH in the presence of trimethylamine, which produced a colloidal suspension that was then sonicated for 8 hours at 40 kHz, yielding nanosheets as thin as 3.1 nm.[144] These could be deposited as a continuous film on glassy carbon electrodes. The resulting nanocomposite electrode exhibited a specific capacitance as high as 360 F g-1 at a current density of 1.5 A $cm^{-2}$ for electrocatalytic $O_2$ evolution, thirty-four times higher than the bulk composite electrode. Sonochemistry is also suitable for OFM integration with carbon nanotubes and graphene to form carbon material/COF composites[134] and can be used to isolate nanosheets of CoTDA (TDA = 2,5-thiophene-dicarboxylate),[145] $[Zn(BDC)(H_2O)]_n$,[146] Mn–UMOFNs,[147] and hybrid MOF nanosheets based on various metals.[148] The structure and morphology of manganese-based UMOFNs is shown in Figure 3, which are promising materials for high-energy-density lithium anodes.[147] High-purity COFs can also be isolated by this approach, shown by Yang et al. for COF-1 and COF-5.[135]

Final edited form was published in "Chemical Reviews 2020, 120(1), S. 8581-8640. ISSN 1520-6890.
https://doi.org/10.1021/acs.chemrev.0c00033

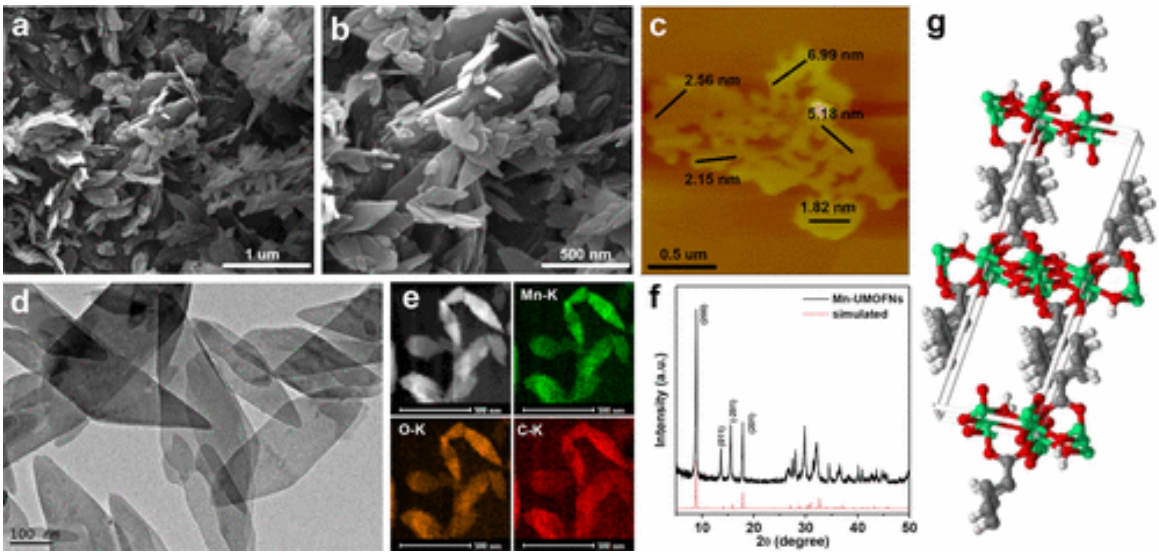


**Figure 3.** (a, b) SEM micrographs of the Mn-UMOFNs. (c) AFM of the obtained Mn-UMOFNs, showing the ultrathin nature of the nanosheets. (d) TEM image of the as-fabricated Mn-UMOFNs. (e) STEM and the corresponding EDS mapping images of the as-fabricated Mn-UMOFNs. (f) measured and simulated PXRD patterns. (g) Layered crystal structure of Mn/Ni-UMOFNs. Color scheme: Mn/Ni, green; O, red; C, gray (H atoms are omitted for clarity). Reproduced with permission from Ref. 147. Copyright 2017 American Chemical Society.

## 2.5 Electrochemical approaches

Researchers at BASF first developed the electrochemical synthesis of HKUST-1 and since then the procedure has been used extensively and expanded to produce other MOFs.[97,149-157] In this method, the metal source, which serves as the electrode, is placed in the linker solution containing the electrolyte. When an appropriate voltage or current is applied, the metal source dissolves and releases the metal ions near the surface of the electrode. Then the metal ions react with the organic linkers in the solution and the MOF is generated near the electrode surface.[158] The electrochemical synthesis method exhibits several advantages, including short synthesis time, milder synthesis conditions, and tunable thickness, and often allows the formation of OFM films without any surface pretreatment.[158] Fischer and co-workers published a comprehensive review of electrochemical fabrication techniques for MOFs and their applications.[86] Notable developments since 2016 include convergent and divergent paired electrodeposition of Cu/Zn-based MOFs,[159] anodic electrodeposition of carboxylate-based MOFs on ITO,[150] and synthesis of MOFs with high intrinsic proton conductivity.[152]

Ameloot *et al.* showed that, by modifying the reaction conditions it is possible to coat the metal electrodes by continuous HKUST-1 films. By applying an anodic voltage to Cu electrodes immersed in a $H_3BTC$ inker solution, MOF layers were formed in 30 min or less. Various thicknesses (2 to 50 μm) could be obtained by varying the voltage and frequency of the applied tension. Zhang and co-workers prepared ultrathin MOF nanosheets by electrochemical exfoliation,[160] and reported excellent performance for Fe-Co nanosheets in OER with an overpotential of 211 mV at a current density of 10 mA $cm^{-2}$.[160] Hauser *et al*. reported recently the

synthesis of a series of Cu(II) and Zn(II) MOF thin films on ITO substrates that were coated with metallic copper and zinc, then served as the metal cation source during the anodic dissolution and electrochemical MOF film growth.[150]

An alternative to using the electrode as the metal source is based on *in situ* generation of the metal ions, provided by anodic dissolution of a metal electrode or by galvanic displacement with a more noble metal. For example, HKUST-1 can be synthesized by either the anodic oxidation of the metallic substrate (Cu) or by galvanic displacement of copper with a more noble metal (e.g. Ag).[71,72] It was proposed that the metal ions are released in the vicinity of the anode, where they react with the linker, and that the voltage controls the concentration of metal ions. A higher voltage induces a higher concentration of ions near the surface, leading to more nucleation events and smaller crystals compared to lower voltages. Another noticeable advantage is the very short time required for growth. However, this method does not provide any control over the orientation of the crystals and may be difficult to scale-up.

Hod *et al.* presented an electrophoretic deposition[161] approach that consists in moving the negatively charged OFM particles in solution towards the positively charged electrode within an electric field. MOF particles are simply suspended in a nonpolar organic solvent, placed into a flask containing two electrodes and a potential difference of 90 V is applied for *ca.* 3 hours to get full surface coverage. The method was tested for four different MOFs: NU-1000, UiO-66, HKUST-1, and Al-MIL-53. Patterned structures could be produced using this approach by applying photolithography prior to the electrophoretic deposition. After removing the photoresist a layer of a MOF different from the first can be electrophoretically deposited.

These and other studies reported to date reveal that the applied voltage, current density, solvent, electrolyte, and temperature affect the quality of the resulting OFM films and coatings.[71,162,163] Mechanistic insight into the factors controlling electrochemical MOF film growth is beginning to emerge. An interesting example of MOF-5 thin film synthesis based on cathodic electrodeposition rather than anodic dissolution was reported by Li and Dincă.[157] The authors showed that the slow introduction of base equivalents to deprotonate the carboxylic acid linker is the key step in the formation of MOFs. In the original publication by Yaghi and coworkers on the synthesis of MOF-5, triethylamine was used as a base by vapor diffusion and a mixture of DMF and chlorobenzene was used as a solvent instead of pure DMF.[164] Later on, all the literature applied DMF in their solvothermal synthesis procedures. As described earlier, DMF is slowly decomposing to form dimethylamine which acts as a base to deprotonate the carboxylic acid linkers. It was pointed out that the decomposition of DMF depends on many factors including the metal ion concentration, pH, and temperature, leading to a large range of reaction times required for different MOFs. Li and Dincă addressed this problem by producing $OH^-$ as a base to deprotonate the linker directly at the electrode (Figure 4). This elegant solution yielded a phase-pure MOF-5 film of 20 − 40 μm thickness in only 15 minutes at room temperature, which is much faster growth than achieved by conventional solvothermal reaction.

Final edited form was published in "Chemical Reviews 2020, 120(1), S. 8581-8640. ISSN 1520-6890.
https://doi.org/10.1021/acs.chemrev.0c00033

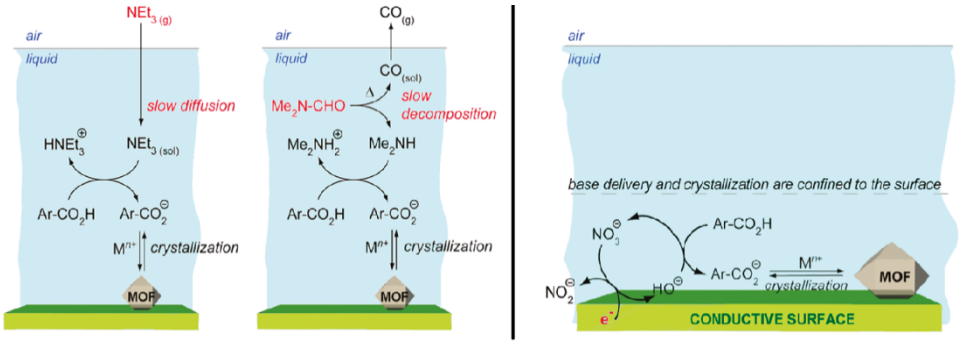


**Figure 4.** Approach to electrochemically create a hydroxyl acting as a base to facilitate MOF-5 nucleation on a substrate developed by Dincă and coworkers. Reprinted with permission Ref. 157 Copyright 2015 American Chemical Society.

## 2.6 Gas-phase synthesis

Gas-phase deposition processes have only recently been used to synthesize OFM films. This method typically involves three steps: (*i*) precursor vaporization, (*ii*) precursor transport through the gas phase and (*iii*) OFM deposition on the substrate. There are two types of gas-phase processes for OFM: physical vapor deposition (PVD) and chemical vapor deposition (CVD). Only a few OFM have been synthesized by PVD processes, mainly because of the lack of volatile yet stable precursors above 300 °C.[165] Müller-Buschbaum and co-workers explored the PVD approach for a Europium-imidazolate framework,[166] as well alkaline and rare earth metal imidazolates under thermal vacuum conditions (215 °C and 0.1 Pa).[167] Lotsch and co-workers used femtosecond pulsed-laser deposition (femto-PLD) to fabricate ZIF-8 films impregnated with polyethylene glycol. By washing the films with ethanol, the polyethylene glycol additive can be removed, leading to ZIF-8 films on sapphire substrates.[168] Ameloot and co-workers demonstrated a novel CVD process for synthesizing high-quality films of ZIF-8.[169] In addition to acceptable control over thickness, ALD permits highly conformal coatings, even on high-aspect-ratio features (Figure 5). ZIF-8 was synthesized on silicon pillars with a 25:1 aspect ratio by vapor-solid transformation of 25 nm ALD zinc oxide films. Krypton physisorption shows a type I shape of the isotherms, showing adsorption and saturation in the low-pressure range, which corresponds to filling of the ZIF-8 micropores. The CVD process enables lift-off patterning and deposition of continuous films on flexible substrates.

Final edited form was published in "Chemical Reviews 2020, 120(1), S. 8581-8640. ISSN 1520-6890.
https://doi.org/10.1021/acs.chemrev.0c00033

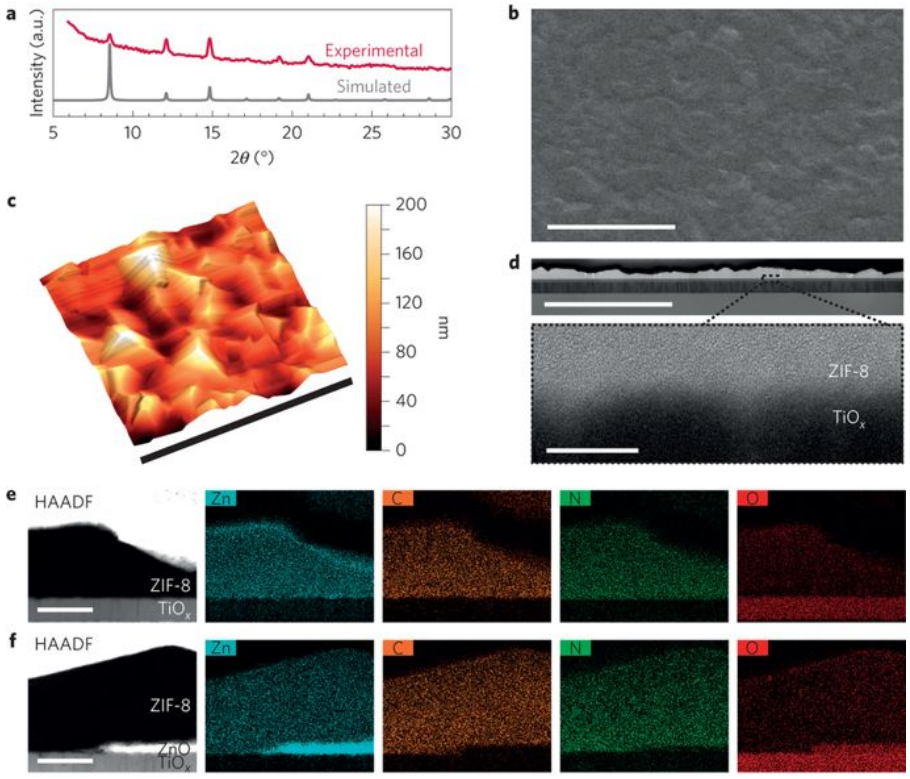


**Figure 5.** (a) X-ray diffraction pattern of a ZIF-8 CVD film and simulated pattern for ZIF-8. (b) Scanning electron microscopy top view. (c) 3D rendered AFM topograph. (d) Focused-ion beam TEM cross section. Inset: high-resolution magnification of the interface between ZIF-8 and the titanium oxide substrate. (e) HAADF and EDS cross-section maps of a completely transformed film. (f) HAADF and EDS cross-section maps of a partially transformed film. Scale bars, 2 μm for **b**–**d**, 20 nm for inset in **d**, 100 nm for **e**–**f**. Reproduced with permission from Ref. 169. Copyright 2015 Nature Publishing Group.

## 2.7 Atomic Layer Deposition

Atomic layer deposition (ALD) is a thin film deposition technique which involves sequential reaction of chemical precursors on the surface of a substrate to form monolayers or sub-monolayers of thin films. An advantage of ALD for synthesizing OFM films is the possibility to run the process in enitrely in the gas phase, thereby avoiding solvents that are incompatible with many processes used today in microelectronics.[165,170-179] However, the deposited films are not always crystalline and may require additional treatment. For example, sequential reactions of $ZrCl_4$ and 1,4-benzenedicarboxylic acid produce amorphous films. Lausund *et al.* showed that that an amorphous film can be crystalized into UiO-66 by treatment in acetic acid vapor.[176] Deposition of MOF-5 amorphous thin films by ALD was achieved at 225-350 °C using zinc acetate and 1,4-benzenedicarboxylic acid as precursors. The MOF-5 films can be crystalized by treatment in humid air and solvothermal reaction in DMF.[179] Copper(II) 2,2,6,6-tetramethyl-3,5-heptanedionate and $H_2BDC$ were used as precursors for ALD synthesis of Cu(BDC). A narrow deposition window (180–190 °C and 0.2 kPa) is critical for obtaining crystalline films. It was

Final edited form was published in "Chemical Reviews 2020, 120(1), S. 8581-8640. ISSN 1520-6890.
https://doi.org/10.1021/acs.chemrev.0c00033

proposed that the presence of the protonated β-diketone ligand of the copper precursor is required for the process by enhancing the mobility of the reacting species during OFM crystallization.[180]

## 2.8 Langmuir–Blodgett deposition

The Langmuir-Blodgett deposition method was introduced by H. Kitagawa's group for porphyrin-based structures, and since then extended to a number of OFM.[181-184] The layers of desired material are made in a Langmuir–Blodgett apparatus, then are transferred one after another onto a substrate, sometimes with intervening washing steps. The layers stack by weak interactions, such as π-stacking, hydrogen bonding, or van-der-Waals interactions. The first thin films synthesized using this approach were NAFS- 1 and NAFS-2 frameworks. NAFS-1 consists of cobalt-containing porphyrine units (CoTCPP) linked together by binuclear copper paddlewheels into a two-dimensional array (Figure 6). Pyridine molecules bind the axial position of the copper ions perpendicularly to the layers and ensure correct π- stacking, with an average tilt angle of only 0.3° relative to the substrate. NAFS-2 has no pyridine moiety to control the packing and as a result the average tilt angle between the layers is larger and reaches 3°. Interestingly, no bulk versions of these structures exist; they can only be isolated in thin film form on surfaces. The Langmuir–Blodgett technique has been used to prepare 2D monolayer films of HKUST-1, $[Cu_2(BDC)_2(bpy)]$, $Al_{12}O(OH)_{18}(H_2O)_3(Al_2(OH)_4)(BTC)_6$, $[M_3O(C_{16}N_2O_8H_6)_{1.5}(H_2O)_3](NO_3)$ (M-soc-MOF, M = In and Ga).[185] This approach allows growth on various substrates over several square centimeters, uniformly and with controllable density of the crystals. OFM assemblies can also be fabricated as freestanding sheets. In addition, this Langmuir-Blodgett method can translate the orientation of the channel network from the individual crystal to the macroscopic scale to create hierarchical systems.

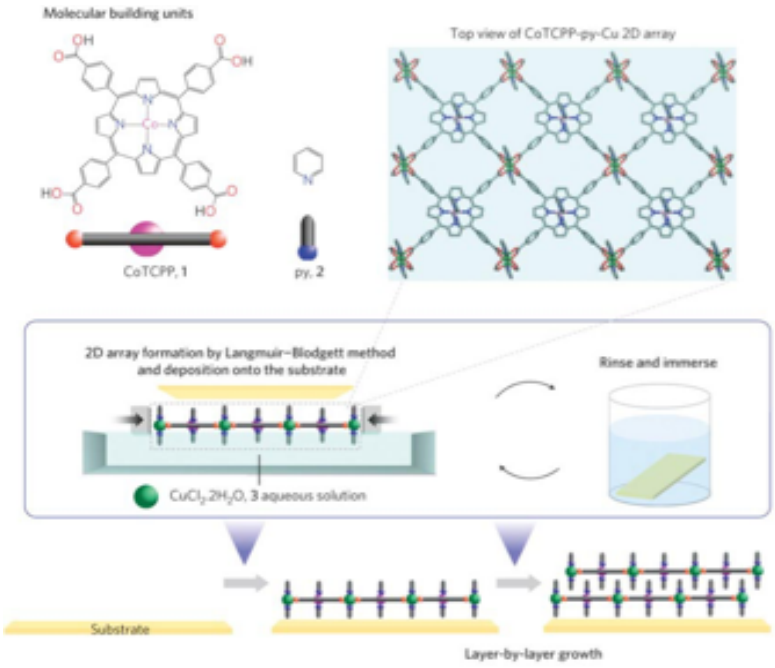


**Figure 6.** Schematic representation of the Langmuir-Blodgett fabrication method for NAFS-1. The solution mixture of CoTCPP and pyridine molecular building units is spread onto an aqueous solution of copper(II) chloride in a Langmuir trough. The 2D arrays are deposited onto the

substrate by the horizontal dipping method. Reproduced with permission from Ref. 185. Copyright 2010 Nature Publishing Group.

### 2.9 Layer-by-layer growth

A powerful technique for thin film MOF synthesis is the so-called layer-by-layer (LbL) growth, which is also known as liquid-phase epitaxy.[186-188] The principle is composed of sequentially immersed into a solution containing the metal salt, a washing solution to remove excess metal precursor and a solution containing the organic linker. Layer-by-layer growth of thin films represents an appealing approach to deposit films with controlled thickness by combining the metal precursor and the organic linker in a sequential manner.[186,188-193] During immersion, ligand exchange reactions take place and the metal ion bind to the upper layers of ligands and *vice versa*, allowing the building of the OFM structure. The growth is thus controllable down to the level of single molecular layers and is solely dependent on self-assembly. Liu *et al*. were able to incorporate multiple functionalities into porphyrin-based MOFs for photovoltaic applications.[194] The LbL method was recently extended to a number of COFs. The first step includes exfoliation of bulk materials in solution, followed by stacking the layers on a periodic fashion on a substrate by vacuum-assisted filtration or dip coating to form continuous films. The methods to exfoliate COFs have been recently reviewed by Tang and co-authors.[38]

Recent applications of the LbL method of MOF growth include conformal shells of HKUST-1 on plasmonic gold nanorods,[195] integration of HKUST-1, ZIF-67 and ZIF-8 with graphene oxide for supercapacitor applications,[196] $Cu_2(F_2AzoBDC)_2(dabco)$ films with photoswitchable proton conduction,[197] and Zn-SURMOF-2 films as crystalline chromophore assemblies.[198] A recent review article by Heinke and Wöll covers the many other applications of the SURMOFs (surface-mounted MOFs),[199] enabled by their unique structure and morphology.

### 2.10 Patterning of OFM films and coatings

Strategies for patterning OFM films have been extensively reviewed in recent years.[9,37,98,99] Here, we summarize a few recent developments with particular emphasis on device integration and nanotechnology applications. Armon *et al*. developed a clever way to micro-pattern MOFs by reacting appropriate precursors by local laser heating. The laser-induced heating leads to rapid crystallization of MOF nanoparticles in solution, and allows simultaneous synthesis and patterning of MOF coatings (Figure 7).[200] Selective laser sintering was also employed recently as a 3D printing technique to fabricate MOF–polymer mixed matrix films by using thermoplastic polyamide 12 (PA12) with powders of ZIF-67, $NH_2$-MIL-101(Al), MOF-801, HKUST-1, and ZIF-8.[201] A number of COFs with imine or β-ketoenamine linkages were co-assembled with a 3D-printing template, Pluronic F127, to form hydrogels with suitable shear thinning and rapid self-healing properties. When the Pluronic F127 is removed, an amorphous-to-crystalline transformation occurs to form crystalline and mechanically robust 3D monoliths.[202] Using lithographically controlled wetting and conventional ink-jet printing, Ruigomez *et al*. synthesized an imine-based COF called RT-COF-1 with a layered hexagonal structure . The synthesis occurs at room temperature and enables fabrication of low-cost micro- and sub-micropatterns of RT-COF-1 on $SiO_2$ and flexible acetate paper.[203]

Final edited form was published in "Chemical Reviews 2020, 120(1), S. 8581-8640. ISSN 1520-6890.
https://doi.org/10.1021/acs.chemrev.0c00033

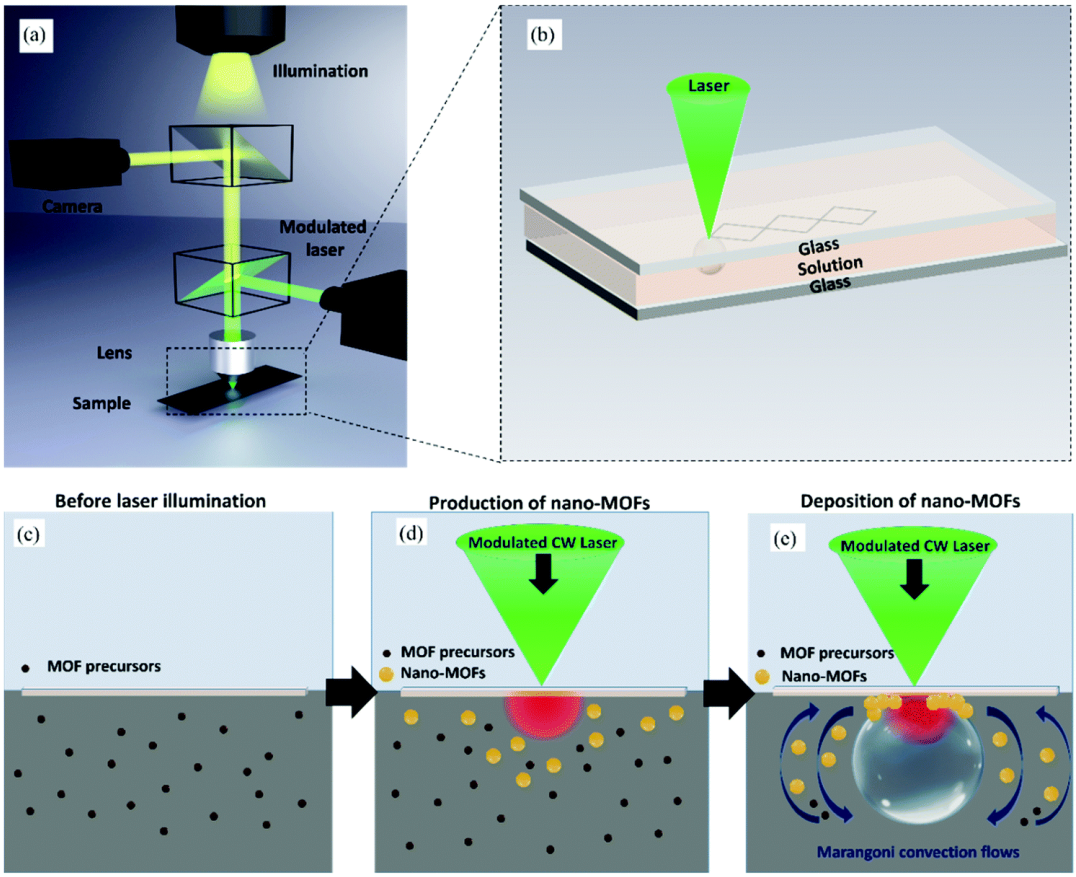


**Figure 7.** (a) Concomitant MOF synthesis and patterning by a modulated laser beam using a dichroic mirror, with the lens focusing the laser on the (b) upper substrate/liquid interface of a solution containing MOF precursors. The solution (c) is heated by the laser, producing nano-MOFs (d) and increasing the vapor pressure until a microbubble is formed and convection flows carry the nano-MOFs, some of which are pinned (e) at the solution/microbubble/substrate interface. Reproduced with permission from Ref. 200. Copyright 2019 The Royal Society of Chemistry.

## 2.11 Post-synthetic film modification

As mentioned above, none of the OFM film growth methods developed thus far can be considered truly general, in the same way that techniques such as CVD and ALD of inorganic materials are. One strategy to address this is post-synthetic modification of an existing film. Advantages of this approach include the possibility to incorporate metal ions with multiple coordination geometries that might not assemble into a desired MOF structure, inclusion of reactive linkers, and the use of guest molecules as a design element. Illustrative and recent examples of these are discussed below.

**2.11.1 Electroactive linkers.** Kung *et al.* reported the post-synthetic metalation of free-base porphyrin linkers used for the growth of MOF-525 thin films.[204] The films show clear electrochemical response due to the electroactivity of the porphyrin linkers. Usov *et al.* demonstrate in-situ spectroelectrochemical measurements of the electroactive MOF $Zn_2(NDC)_2(DPNI)$ (NDC = 2,7-naphthalene dicarboxylate, DPNI = N,N′-di(4-pyridyl)- 1,4,5,8-naphthalenetetracarboxydiimide) and report that the twice-reduced dianion species is stable over the timeframe of the experiment.[205] Farha and Hupp[204] reported that NU-901, a MOF based on Zr-

Final edited form was published in "Chemical Reviews 2020, 120(1), S. 8581-8640. ISSN 1520-6890.
https://doi.org/10.1021/acs.chemrev.0c00033

nodes and TBAPy linker ($H_4$TBAPy = 1,3,6,8-tetrakis(p-benzoic acid)pyrene), can be electrochemically synthesized and showed electrochromism due to an one-electron oxidation of the linker. Ahrenholtz *et al*. solvothermally prepared a thin film of a Co-porphyrin based MOF (5,10,15,20-(4-carboxyphenyl)porphyrin]Co(III)) on FTO glass and showed that the redox-hopping of the porphyrin linker can be explained by a non-Nernstian behavior.[107]

**2.11.2 Covalently incorporated electroactive moieties.** Halls *et al*. presented a post-synthetic modification of different Al- and Zn-MOFs in which an uncoordinated amine site on the linker reacts with ferrocenecarboxylic anhydride.[206] The resulting ferrocene-functionalized MOF film exhibted a reversible electrochemical response when prepared on a basal plane pyrolytic graphite working electrode. Meilikhov *et al.* presented a covalent modification of MIL-53 ([Al(OH)-(BDC)]$_n$) with 1,1′-ferrocenediyl-dimethylsilane.[207] The reaction takes place at an unsaturated Al−H bond between two $AlO_6$ octahedra and thereby represents a functionalization at the inorganic part rather than the organic linker of the MOF. Very recently, Hod *et al*. installed ferrocene carboxylate at the $Zr_6(\mu_3\text{-}O)_4(\mu_3\text{-}OH)_4(OH)_4(H_2O)_4$ nodes of the NU-1000 framework that itself already contains 1,3,6,8- tetrakis(p-benzoate)pyrene as an electroactive linker.[208] A ferrocene loading of one molecule per node was reached and the ferrocene units were electrochemically active. An interesting feature of these films is their blocking behavior to cation penetration through the film when the ferrocene was oxidized to ferrocenium. The electroactive pyrene linker became redox-silent in that case as well, implying a shift in redox potential of the MOF linker due to the large number of positively charged ferrocenium.

**2.11.3 Non-covalently incorporated electroactive moieties.** Dragasser *et al*. introduced ferrocene from the vapor phase into a layer-by-layer deposited HKUST-1 film on a gold electrode. The conductivity of these films was 2 x $10^{-9}$ S·cm$^{-1}$ and no clear ferrocene signal was observed in the cyclic voltammogram.[209] Chang *et al*. introduced ferrocene in a one-step solvothermal treatment of $In(NO_3)_3 \cdot 5H_2O$ and 4,5- imidazoledicarboxylic acid in the presence of the guest molecule.[210] How the ferrocene is bound within the MOF was not described, but it appears to be trapped within the pores in a ship-in-a-bottle fashion, since no adsorption takes place when putting the bare MOF into a ferrocene solution. The modified glassy carbon electrode is conditioned by cyclic voltammography in 0.5 mol L$^{-1}$ sulfuric acid for 20 cycles to enable robust electrochemical cycling. After this treatment the cyclic voltammogram showed a clear and stable peak for ferrocene. Lu *et al*. reported that covering a substrate with polyaniline before the solvothermal treatment leads to good film growth of HKUST-1, MIL-68 and $Zn_2(BDC)_2DABCO$.[97] This method is effective irrespective of the substrate and its general applicability to stainless steel, copper, and platinum substrates was demonstrated.

**2.11.4 Guest molecule incorporation to modulate electrical conductivity.** The use of guest molecules as a design element was discussed by some of us in a recent perspective article.[46] Its potential for increasing the electronic conductivity of a nominally insulating MOF was first demonstrated by Talin et al., who introduced 7,7,8,8-tetracyanoquinododimethane (TCNQ) into the pores of HKUST-1. [211] The TCNQ infiltration increased the electronic conductivity by 8 orders of magnitude. This high-electrical conductivity and relatively low thermal conductivity suggested potential for thermoelectric applications.[212] Alternatively, the MOF can be used as a template for forming a network of conducting polymer strands. Lu *et al.* described the electrochemical synthesis of polyaniline within the pores of HKUST-1, which yielded a conductivity of 0.125 S·cm$^{-1}$ after doping with iodine.[97] Incorporation of semiconducting polythiophene in MOFs (NU-1000,[213] MIL-177,[214] and HKUST-1[215]) also renders the framework electronically conductive. The

conductivity can be tuned over a wide range depending on the amount of polythiophene present. In selected cases, the introduction of polythiophene into the pores gives rise to an enhanced charge separation lifetime upon irradiation.[214]

## 3. Sensors based on electrical conductivity and related properties

Sensors are analytical devices that can deliver immediate information concerning the presence of specific substances or ions in a complex sample (chemical sensors) or of physical stimuli acting on a sample (physical sensors). However, this is insufficient to subdivide this enormous topic. Other common categories used to describe sensors are the material responsible for detection (e.g. biosensors, MOF-based sensors), the specific analyte targeted (e.g. volatile organic compounds, biomolecules), the transduction mechanism (e.g. electrical, optoelectronic, optical), the device architectures (e.g. chemoresistor, chemicapacitor), and the detection method used (e.g. potentiometry, refractometry). With regard to OFM for sensing applications, the first comprehensive review appeared in 2011[216] and was focused on MOFs and the topic was included in the two MOF roadmaps published in 2014[8] and 2017.[9] In this section, we highlight the most recent progress on electrically transduced sensors based on OFM (primarily MOFs) sensing materials covering literature from 2016 onwards. A few selected earlier case studies that made a considerable impact in the field are also included. We first summarize recent developments on chemosensors, grouped according to the sensing architectures in Figure 8 and corresponding measurement techniques. All OFM used for sensing gas-phase analytes (listed in Table 1) are discussed in subsections 3.1-3.3 whereas detection of analytes from liquid phases, realized in electrochemical cells, is described in subsection 3.4. In the last part we additionally describe recent developments regarding OFM-based physical sensors (subsection 3.5). An extensive class of OFM-based biosensors, understood as those containing biorecognition units (e.g. cells, enzymes, nucleic acids, antibodies, aptamers) is not covered.[217] These devices, which utilize non-conductive MOFs as adsorbents, are used for detecting bio-relevant analytes in solution and were recently reviewed.[21] We also exclude sensors employing chemical-to-optical-to-electrical transduction mechanisms, as distinguished from chemical-to-electrical/electrochemical-to-electrical mechanisms (electrically-transduced), as this topic is very large and has been recently covered in reviews on luminescent MOFs[24] and COFs[38] as well as on intensively developed optical fiber based chemical sensors.[218] Very recent examples of the use of optical fibers integrated with MOFs for detection of chemicals include ZIF-8 for sensing VOCs,[219] small gaseous molecules[220] and $CO_2$ from humid gas;[221] HKUST-1 for detection of $CO_2$[222] and nitrobenzene from solution;[223] as well as UiO-66 for chemical vapor sensing.[224]

The range of applications requiring sensors is vast and includes environmental monitoring of pollutants and toxins, chemical threat detection (e.g. sensing of explosives and other warfare agents), medical diagnostics (e.g. sensing relevant biomolecules), food safety and quality control (e.g. sensing of biological and chemical contaminants, allergens and humidity), and industrial process management and safety (e.g. sensing of chemical hazards and contaminants). Due to their exceptionally tunable structures and intrinsic porosity, OFM have been tested for many these applications. In principle, any OFM property that changes as a result of interacting with an analyte could be used as transduction method. Exploring the potential of MOFs as chemosensing materials began more than a decade ago with simple, yet powerful means of transducing a signal, such as a change in color, luminosity, or mechanical properties.[1,3] Since these early works the field has evolved and is currently rapidly expanding to include both optical[3] and electronic sensor devices

Final edited form was published in "Chemical Reviews 2020, 120(1), S. 8581-8640. ISSN 1520-6890.
https://doi.org/10.1021/acs.chemrev.0c00033

that feature MOFs as active components.[11,13] Considering MOF-based sensors that utilize optical property change, luminescence-based detection, recently comprehensively reviewed,[24] is among the most desirable transduction mechanisms for its relative ease of use and broad adaptability.

On the other hand, given the simplicity and compatibility with common electronic technologies, electrically transduced sensors are a highly sought-after alternative. However, this option often necessitates electrically conducting frameworks, which are still rare.[225,226] Nevertheless, recent discoveries of such materials led to construction of first MOF-based chemiresistors and chemitransistors. To move beyond the dielectric limitations of most OFM, alternative approaches have been developed, such as conductive MOF composites[227,228,229] and using the electrical response from a dielectric (such as a change of capacitance or electrostatic potential) for transduction. [9,11,13] Naturally, both general approaches towards electrical sensors are closely related to the development of methods to integrate OFM with electronic circuits and devices, as discussed above.

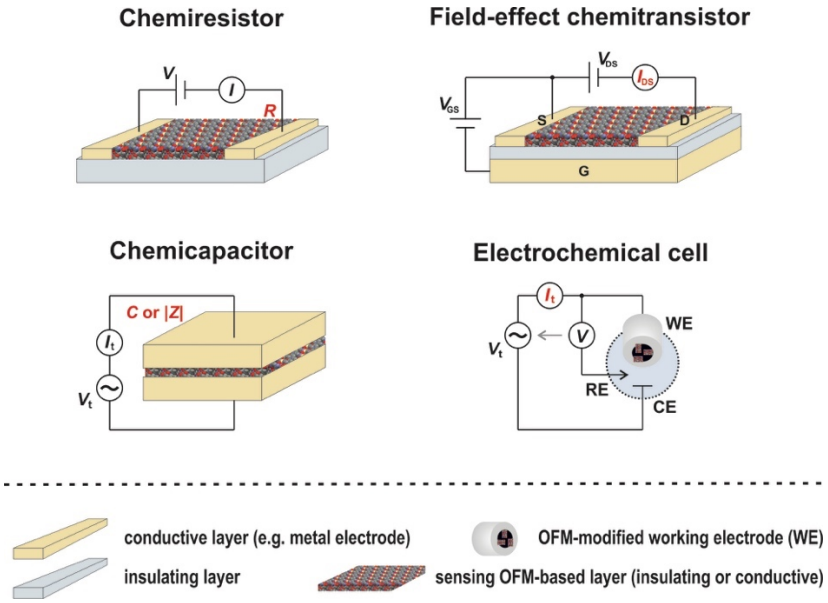


**Figure 8.** Schematic diagrams of OFM-based sensor devices: (i) chemiresistor, (ii) chemicapacitor, (iii) bottom-gated field-effect chemitransistor and (iv) three-electrode electrochemical cell. Response readouts are marked in red: (i) *R* - resistance based on output current *I* and applied DC voltage *V*; (ii) *C or* |*Z*| - capacitance or impedance of a dielectric OFM layer under applied AC voltage $V_t$; (iii) $I_{DS}$ - current under applied gate-source $V_{GS}$ and drain-source $V_{DS}$ DC voltages (G -gate, S-source, D-drain); and (iv) $I_t$ – faradaic current associated with reduction or oxidation of the analyte in solution (WE OFM-modified working electrode, CE - counter electrode, RE - reference electrode.

### 3.1 Chemiresistor gas sensors and conductometry

This approach uses electrical circuits with a sensing material whose resistance *R* (inverse of a conductance *G*) depends on the concentration of a given analyte (Figure 8). Interactions between the analyte and the sensing material modify either the concentration of charge carriers or their

Final edited form was published in "Chemical Reviews 2020, 120(1), S. 8581-8640. ISSN 1520-6890.
https://doi.org/10.1021/acs.chemrev.0c00033

mobility, both of which contribute to the overall conductance. Conductometric measurement relies on monitoring the direct current (DC) *I* through the resistor under a constant bias voltage *V* (*R* = *V*/*I*). Consequently, the resistive material must have at least moderate electrical conductivity to enable changes in current and voltage to be observed. As will be seen below, this is a particularly fruitful strategy, with several reports demonstrating both high sensitivity and high selectivity. Chemiresistors are also appealing because they are simple to fabricate. In general, two strategies to achieve this have been explored, based on either an OFM alone or as a composite with a conducting material.

**3.1.1 Pristine MOFs.** Several intrinsically semiconducting MOFs have been shown to be effective active sensing elements in chemiresistors, without the need for doping or other additives to improve the conductivity. Until very recently this field remained dormant due to the lack of materials with suitable conductivity.[225]The strategy was initially realized in 2014 by Zhang and coworkers who reported the use of cobalt-based ZIFs, $[Co(mim)_2]$[230] (ZIF-67), and $[Co(im)_2]$[231] (mim = 2-methylimidazolate; im = imidazolate) for sensing formaldehyde and trimethylamine vapors, respectively. In spite of the favorable detection limits achieved (5 ppm for formaldehyde and 2 ppm for trimethylamine), elevated temperatures were necessary to overcome the low conductivity of the MOFs. Moreover, the devices exhibited relatively long response-recovery times, on the order of several minutes to one hour. Consequently, extending this strategy to the detection of other analytes awaits an understanding of the origin of the slow 'turn-off' responses and observed selectivities.

With the advent of MOFs with higher conductivity, construction of room-temperature chemiresistive sensors based on pristine MOFs became possible. Layered MOFs with a topology analogous to graphene, 'metal-organic graphene analogues (MOGs)' are particularly effective, as they combine high electronic conductivity with the ability to modify the framework metal ion (Ni, Cu) and coordinating functional group (amine or hydroxyl). In 2015 Dincă and coworkers demonstrated the use of $Cu_3(HITP)_2$ (HITP = 2,3,6,7,10,11-hexaiminotriphenylene) for chemiresistive sensing of sub-ppm levels of ammonia. This MOF exhibits bulk conductivity of 0.2 S $cm^{-1}$ at room temperature. The chemiresistor, fabricated by drop-casting a dispersion of the MOF onto interdigitated gold electrodes, showed reversible linear 'turn-on' responses to $NH_3$ over the 0.5-10 ppm range.[232] In a follow-up work, using this MOF along with two other conductive isostructural analogues, $Cu_3(HHTP)_2$ (HHTP = 2,3,6,7,10,11-hexahydroxytriphenylene) and $Ni_3(HITP)_2$, they constructed a sensor array capable of discriminating five different categories of volatile organic compounds: alcohols, ketones/ethers, aliphatic hydrocarbons, aromatic hydrocarbons and amines.[233] In this prototype MOF-based chemiresistive sensor array, the nature of the metal had the largest impact on the direction of the response, suggesting that an electron transfer mechanism between analyte molecules and the metal centers is responsible for sensing. However, the observed dependence on analyte concentration (which may be either an increase or decrease in resistivity for the same analyte) indicates that a competing mechanism, hypothesized to involve hydrogen bonding with the organic linkers, is simultaneously operative.

An important advance in the sensing device integration of 2D MOFs from the metal-catecholate family was demonstrated by Mirica and coworkers. They fabricated a series of chemiresistors utilizing direct self-assembly of $Cu_3HHTP_2$ and Ni-CAT-1 MOGs on shrinkable PE or PS films with pre-patterned graphitic IDEs.[234] M-CAT-1 (M = Ni, Co) materials are composed of two distinct types of alternating stacked layers: 2D $[M_3(HHTP)_2(H_2O)_6]_n$ MOF separated by supramolecular layers including discrete complexes of $[M_3(HHTP)(H_2O)_{12}]$.[235] These

Final edited form was published in "Chemical Reviews 2020, 120(1), S. 8581-8640. ISSN 1520-6890.
https://doi.org/10.1021/acs.chemrev.0c00033

sensors could selectively detect $H_2S$, $NH_3$ and NO gases at 20-80 ppm levels. Reduction of the NO and $H_2S$ detection limits to sub-pm levels was discussed in a follow-up paper in which Ni-CAT-1 and $Ni_3HITP_2$ were integrated with cotton or polyester fabrics via direct growth from solution.[236] The resulting SOFT sensors were the first examples of wearable, flexible textile-supported chemiresistive MOF-based sensors. Remarkably, they retained their performance at 18% RH and proved fully recoverable after washing in water.

Another approach to MOGs in high-performance sensing devices was developed by Xu et al., who used a spray LbL liquid-phase epitaxy method to fabricate thin films of $Cu_3HHTP_2$ with controllable thickness on various substrates (sapphire, quartz, Si, $Si/SiO_2$) patterned with gold IDEs.[237] The resulting $NH_3$ gas sensors surpassed several performance parameters for their bulk powder analogs.[233,234] In particular, they exhibited selective detection of ammonia from 10 other reducing gases, including $H_2$, CO, acetone, methanol, ethanol, methane, n-hexane, benzene, toluene and ethylbenzene. Moreover, they displayed the highest response of 129% and shorter response and recovery times by 54% and 10%, respectively, compared to the reported gas sensors based on $Cu_3HHTP_2$ powders, nanorods or thick films.[237] In addition, they showed low detection limit of 0.5 ppm $NH_3$, comparable with its powder counterpart,[233] and excellent long-term stability and reproducibility. Another spray-coating approach was adopted by Behrens *et al.* who used water-based dispersions of $Cu_3HHTP_2$ nanoplatelets to prepare MOF coatings on glass slides or flexible polycarbonate foils.[238] Apart from easily accessible pore systems, such coatings showed good interparticle contacts yielding conductivity of 0.045 S $cm^{-1}$ that surpasses all formerly reported measurements. The fabricated devices were capable of chemiresistive methanol sensing with high, fast and reversible responses. The origin of the chemiresistive thin-film response of $Cu_3HHTP_2$ was recently investigated by Marti-Gastaldo and coworkers.[239] Through a combination of experimental data and computational modeling, they linked the response of this MOG to the direct interaction of gas molecules with the metal centers, which was postulated to slightly distort the internal structure of the layer or change the coordination geometry of the metal node. As a result, the bandgap of the material was modified. This mechanism is consistent with previous experimental findings that suggested a relationship between the nature of metal, involving charge transfer between the analyte and the metal ions, and the intensity and selectivity of the turn-on response.[232,233,237] Very recently, however, Dincă and co-workers reported new important critical insights into structure and electrical transport of layered $Cu_3HHTP_2$ and $Ni_3HITP_2$ MOGs.[240] Variable-temperature conductivity measurements carried out on fabricated single-crystal based devices indicated intrinsic metallic nature of $Ni_3HITP_2$ in contrast to activated electrical transport observed for its polycrystalline films. The apparent semiconducting behavior of such films was hypothesized to be the effect of anisotropy and grain boundaries. For both MOFs the authors demonstrated that rod devices with significant out-of-plane contributions exhibit higher conductivities than polycrystalline pellets, with values up to 150 S $cm^{-1}$ for $Ni_3HITP_2$ and 1.5 S $cm^{-1}$ for $Cu_3HHTP_2$. Additionally, HRTEM microscopy studies revealed that both layered MOFs are not isostructural due to differences in stacking modes and this observation may be relevant to analysis of electrical transport properties for 2D MOFs in general.

Very recently Mirica *et al.* reported another family of layered MOFs with potential for gas sensing: nickel phthalocyanine- and nickel naphthalocyanine-based bimetallic systems (with either bridging Cu or another Ni center). Using these for chemical recognition they could detect and differentiate $NH_3$, $H_2S$ and NO by chemiresistance.[241] The devices they fabricated exhibited excellent detection limits (sub-ppm $NH_3$ and ppb $H_2S$ and NO) at low applied voltages within 1.5 min of exposure, even under 18% RH (Table 1). Moreover, the sensors showed exceptional

Final edited form was published in "Chemical Reviews 2020, 120(1), S. 8581-8640. ISSN 1520-6890.
https://doi.org/10.1021/acs.chemrev.0c00033

sensitivities, with highest responses ($-\Delta G/G_0$) reaching 45% for $NH_3$, 98% for $H_2S$, and -657% for NO). Positive or negative responses were observed depending on the analyte used and regardless of the presence of the second metal center that linked nickel phthalocyanines into polymeric framework structures. EPR and XPS studies with two types of probes, electron-donating $H_2S$ and electron-accepting NO molecules, revealed that the sensing mechanism involves charge transfer interactions induced by the gaseous analytes adsorbed on the surface of MOF pores.

Although the examples above demonstrate that $NH_3$, $H_2S$ and NO are easily detected using MOFs of various types, chemiresistive detection of gaseous hydrocarbons by semiconductive $Cu[Ni(pdt)_2]$ is also feasible. This was recently demonstrated by Long and coworkers (Figure 9).[242] Surprisingly, the magnitude of the chemiresistive response in this case was independent of either analyte binding strength or total adsorption capacity. Instead, the conductivity increased linearly only (if not disturbed by nanoconfinement effects) with the quantity of gas adsorbed in the framework and the sensitivity correlated strongly with specific heat capacity of the adsorbate. Additionally, combined time-resolved conductance and adsorption measurements revealed faster equilibration of the chemiresistive response than gas adsorption, which indicates that interparticle contacts limit conduction and extrinsic charge transport at crystalline surfaces is most responsive to analyte adsorption. This work presents a new approach for the development of chemiresistive OFM sensor materials that focuses on gas adsorption properties.

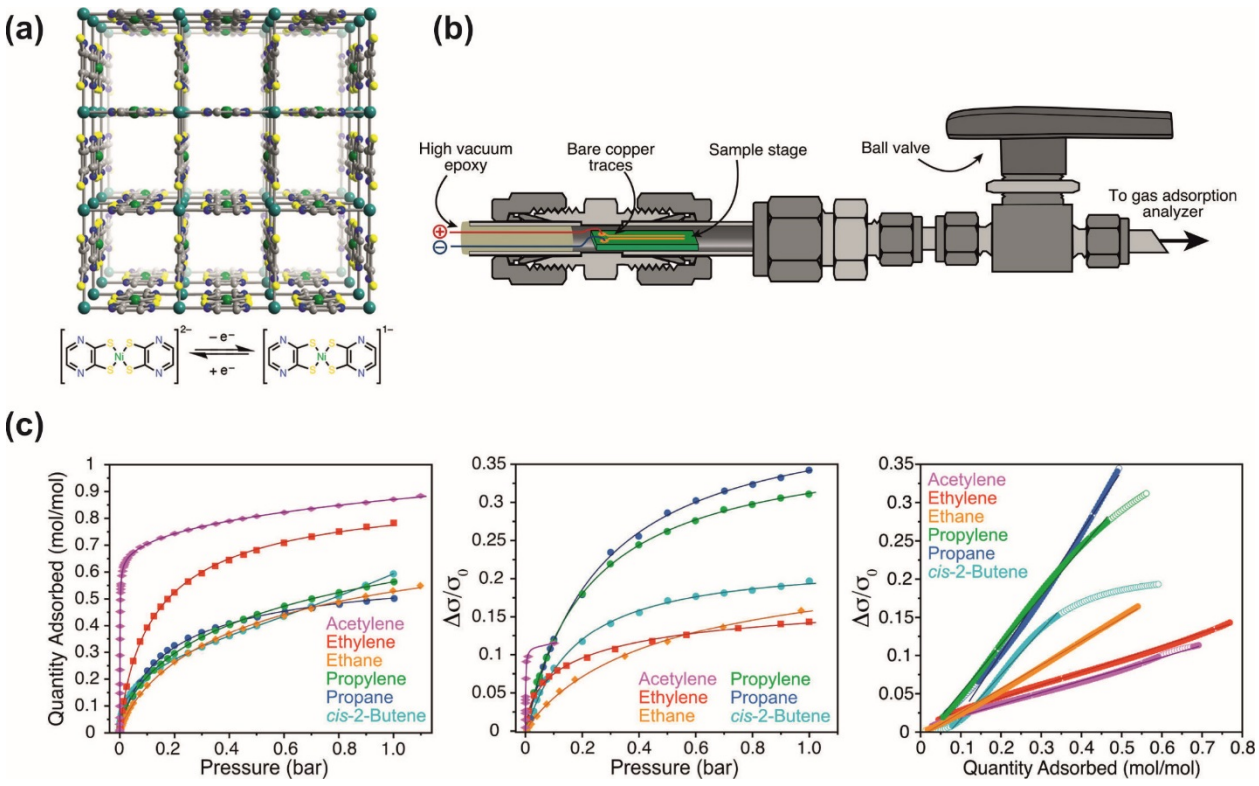


**Figure 9.** Chemiresistive sensing of gaseous hydrocarbons by $Cu[Ni(pdt)_2]$ MOF: (a) crystal structure of the MOF with one-dimensional channels and redox-active $Ni(pdt)_2$ entity; (b) schematic diagram of the conductivity cell used for in situ conductance measurements on a gas adsorption analyzer; (c) Room temperature gas adsorption (left) and conductivity (middle)

isotherms as well as conductivity-amount adsorbed profiles. Adapted with permission from Ref. 242. Copyright 2019 American Chemical Society.

Zirconium MOFs are appealing for sensing because of their high thermal and chemical stability, even at low pH. This makes them attractive to detecting acidic gases such as $CO_2$, $SO_2$ and $NO_2$, as demonstrated by Dmello *et al*. These authors employed amine-functionalized zirconium-based UiO-66-$NH_2$ for resistive detection of these gases.[243] Since electrical conductivities of UiO-66 family are relatively low (e.g. ~$3.8 \times 10^{-8}$ S cm$^{-1}$ at 300 K for UiO-66, based on DFT calculations[244] and are borderline between semiconductive and insulating solids, the sensing penalty was a high operating temperature (150$^o$C) that is undesirable for practical applications. At this temperature, the UiO-66-$NH_2$-based device showed responses of 21.6, 7.6 and 11.4% for 10 ppm $SO_2$, 10 ppm $NO_2$ and 5000 ppm $CO_2$, respectively, as well as short response/recovery times and low (1 ppm) $SO_2$ detection limit. In contrast, no detectable resistance changes were observed for non-functionalized UiO-66 and the sensitivity was significantly lower for UiO-66-OH and UiO-66-(OH,$NH_2$). The authors explained the unique sensing properties of the amine-functionalized MOF by the formation of effective charge-transfer complexes via acid-base interactions with the $NH_2$ groups.

**3.1.2 Pristine COFs.** Despite progress in the development of chemiresistive gas sensors based on MOFs, challenging synthesis of intrinsically conducting π-conjugated COFs, as well as the difficulty in controlling both the COF crystallinity and formation of a stable electrode interface, are responsible for the fact that these materials have still received relatively little attention for electrically-transduced sensing of gases.[245,246] The use of COFs as sensing materials so far has been mostly reported for luminescence-based sensing in liquid phases.[38] However, first reports of COFs as the active materials for chemiresistive sensing of gases were recently published. An amorphous heptazine-based organic framework (denoted as HMP-TAPB-1) was used for the chemiresistive detection of 1–200 ppm $NH_3$ at RT and under ambient conditions in the 23–85% RH range (Table 1).[247] The sensor device showed increased responses ($R_{air}/R_{gas}$) with humidity (e.g. 16.6 at 47% RH and 70.1 at 84% RH towards 50 ppm $NH_3$) as well as response and recovery times of 65 and 9 s, respectively. Its high selectivity towards ammonia over other VOC analytes was explained by the presence of electron withdrawing heptazine units. Another new layered COF (denoted as COF-DC-8), containing a macrocyclic metallic site, was obtained by the reaction of 2,3,9,10,16,17,23,24-octa-amino-phthalocyanine nickel(II) and pyrene-4,5,9,10-tetraone.[241] It showed the highest bulk electrical conductivity ($2.51 \times 10^{-5}$ S cm$^{-1}$ at RT) among intrinsically conductive COFs. By $I_2$ doping this could be further increased by three orders of magnitude. Upon integration into chemiresistors, it showed excellent responses to $NH_3$, $H_2S$, NO and $NO_2$ gases with ppb limits of detection (Table 1). The highest negative responses were obtained for oxidizing gases, whereas the largest positive increases in resistance occurred for reducing gases. Collectively, EPR and XPS studies indicated that the sensing mechanism involved surface adsorption and charge transfer interactions between nickelphthalocyanine component of the COF and the analytes.

**3.1.3 OFM composites.** The second general strategy for constructing an OFM-based chemiresistor relies on the formation of composites as sensing materials. In this approach an electrically nonconducting OFM plays the role of an analyte receptor, often to improve an overall sensor selectivity and/or sensitivity, and the function of electrical transduction is given to another conductive component of the composite. Various conductive materials have been used to prepare chemiresistive MOF composites. In particular, several devices were constructed with MOF@SMO

Final edited form was published in "Chemical Reviews 2020, 120(1), S. 8581-8640. ISSN 1520-6890.
https://doi.org/10.1021/acs.chemrev.0c00033

sensing heterostructures (SMO = semiconductor metal oxide). Following the series of formaldehyde, acetone, and $H_2$ sensors based on MOFs coated on ZnO nanowires (ZIF-8/67@ZnO),[248,249,250] several new studies were published using this approach. In the first study, Wu et al. fabricated a ZnO/ZIF-8 core-shell nanorod film on a glass substrate, with a fine-grained, thin and porous ZIF-8 coating. Devices assembled from this material exhibited an excellent selective sensing response for $H_2$ over CO.[251] A facile chemical solution deposition method was used to control the composite microstructure. The formation of the ~110-nm thick ZIF-8 shell made it possible to introduce additional oxygen vacancies in the complex film. As a result, the sensitivity for $H_2$ was enhanced for the ZIF-8@ZnO nanorod film compared with a pure ZnO film. Moreover, owing to the small grain size (<140 nm) of the ZIF-8 coating, its molecular sieving effect was significantly strengthened. Consequently, the ZIF-8@ZnO nanorod film showed no response for CO molecules at 200 ˚C. In a related work, Zhou *et al.* studied the correlation between the pore size of MOFs used for coating ZnO nanorods and the size of gaseous analyte molecules.[252] By their systematic investigation using ammonia, hydrogen, ethanol, acetone and benzene as probe molecules with various kinetic diameters (2.89-5.85 Å) and two types of coatings (ZIF-8 with ~3.4-Å pores and ZIF-71 with ~4.8-Å pores), they demonstrated selective sensing by MOF@ZnO nanorods via molecular sieving. In another work, Liu *et al*. employed $In_2O_3$ nanofibers coated with ZIF-8 for chemiresistive detection of $NO_2$ at ppb levels.[253] They found that the resistive response depended on the composition of the ZIF-8@$In_2O_3$ heterostructure. Devices with 1:4 ZIF-8/$In_2O_3$ (Zn/In molar ratio) showed the highest resistive response of 16.4 to 1 ppm $NO_2$ over air with a LOD of 10 ppb. This ZIF-8@$In_2O_3$ composite also exhibited enhanced humidity resistance compared to prisitine $In_2O_3$.

Variations on the MOF@SMO strategy were also described for heterostructures involving nanoparticles or microparticles of SMOs instead of SMO nanorods. Kalidindi and coworkers assembled cobalt-based ZIF-67 over $SnO_2$ nanoparticles and considered this material for $CO_2$ resistive sensing.[254] The coating improved the sensing response of pristine tin oxide up to twelve-fold for 50% $CO_2$ level and up to two-fold for 5000 ppm $CO_2$ (with a response $R_{gas}/R_{air} - 1 = 16.5\%$ at 205ºC). This improved performance was explained by changes of electronic structure at the interface of $SnO_2$ and ZIF-67, as revealed by XPS measurements. In another work, Ren *et al.* grew ZIF-8 shell on the surface of ZnO microspheres to explore its sensing behavior towards ethanol.[255] When exposed to ethanol vapor at 160°C the synthesized ZIF-8@ZnO core-shell material exhibited much higher sensor response ($R_{air}/R_{gas}$ = 35.90), selectivity and stability as compared to pristine ZnO microspheres ($R_{air}/R_{gas}$ = 14.54).

Even more complex heterostructures have been implemented to enhance sensor sensitivity and selectivity and impart new transduction mechanisms such as a photoresponse. In particular, the use of three-component composites, in which a heterostructure such as MOF/nanoparticle/metal oxide (outer layer/middle layer/core) is the sensing material, have been demonstrated for gas sensing. Weber *et al.* used this strategy to enhance both sensitivity and selectivity of devices for hydrogen detection.[256] In the first step ZnO nanowires were vapor-grown on a device support with IDEs and subsequently decorated with Pd nanoparticles by atomic layer deposition to reach maximal signal responses. Finally, a ZIF-8 nanomembrane was formed as an outer molecular sieve layer via partial solvothermal conversion of the ZnO surface. The ZIF-8@Pd@ZnO device showed high responses ($R_{air}/R_{gas}$ = 3.2, 4.7, 6.7) at 10, 30 and 50 ppm concentrations of $H_2$ in the presence of VOCs such as benzene, toluene, ethanol, and acetone in air at 200ºC. In a related report, a bifunctional device for simultaneous detection and removal (by oxidation) of formaldehyde was proposed based on a Au@ZnO@ZIF-8 composite.[257] The

Final edited form was published in "Chemical Reviews 2020, 120(1), S. 8581-8640. ISSN 1520-6890.
https://doi.org/10.1021/acs.chemrev.0c00033

fabricated devices required intense photoirradiation (Xe lamp) to obtain a photoresponse. Nevertheless, measurable responses were achieved for concentrations of 0.25 to 100 ppm formaldehyde at room temperature, even in the presence of humidity and toluene interferences. The introduction of plasmonic gold nanorods enhanced visible-light-driven charge carrier generation on the ZnO surface and ZIF-8 improved analyte selectivity. One disadvantage of this approach are the relatively high temperatures required for MOF@SMO growth. Wang *et al.*[258] addressed this problem by incorporating a POM into ZIF-8@ZnO to enhance its sensitivity and selectivity towards formaldehyde. The fabricated POM@ZIF-8@ZnO device showed an improved formaldehyde sensing ability in RT air under Xe lamp irradiation with ~ 0.4 ppm LOD and excellent selectivity over ethanol. The POM component was responsible for enhancing the sensing ability due to its property to inhibit electron-hole recombination in semiconducting materials.

MOFs combined with (semi)conductors other than SMOs have also been explored, including GO, graphite, and carbon nanoparticles. Three examples are of particular interest. First, in 2015 Travlou *et al.* described the formation of Cu-BTC/GO composites capable of ammonia sensing with 4% normalized resistance ($\Delta R/R_0$) increase at 100 ppm but relatively slow response times (>10 min). [259] After an initially irreversible increase in resistance upon first exposure to $NH_3$, the sensing became reversible. This unusual behavior was explained by the collapse of the MOF structure and the ability of the resulting amorphous phase to weakly adsorb ammonia. Second, searching for new methods to incorporate MOFs to create chemiresistive sensors, Mirica and coworkers prepared ball-milled $Cu_3HHTP_2$, M-CAT-1 (M = Co, Ni) or Fe-HHTP MOFs/graphite blends that were pressed into pellets and mechanically abraded onto the surface of paper substrates with IDEs.[260] An array of four chemiresitor devices was able to detect and differentiate $NH_3$, NO, and $H_2S$ at 80 ppm from each other and from water at 7000 ppm. The formation of composites with graphite not only facilitated integration with other materials but also improved the electrical contact between the MOF and the IDEs. The relatively high LOD were linked to blocked pores and reduced surface areas for analyte interaction in the ball-milled composites. Finally, a new concept of utilizing MOF/carbon blends was presented by Kaskel and coworkers, who constructed the first MOF-based threshold sensors with electrical transduction.[261] They fabricated a series of chemiresistive sensing composite membranes based on dynamic MOFs (*i.e.* structurally flexible). They combined DUT-8(Ni), ELM-11 (Cu) and MIL-53(Al) with carbon nanoparticles (CNP) and PTFE binder. The working principle of these sensors relies on the volume change of the MOF particles upon analyte adsorption which disrupts the percolating carbon-particle network, resulting in a significant resistance change (Figure 10). The observed responses ($\Delta R/R_0$) were repeatable and reached a colossal 7500% for switchable DUT-8 MOF and n-butane detection and covered a wide range of gas concentrations 20-80%. Recently this general concept was successfully used for selective threshold sensing of $CO_2$ in mixtures with methane at high pressure by use of MIL-53(Al) composite[262] as well as for moisture threshold sensing by use of JUK-8 composite (Figure 10).[263]

Final edited form was published in "Chemical Reviews 2020, 120(1), S. 8581-8640. ISSN 1520-6890.
https://doi.org/10.1021/acs.chemrev.0c00033

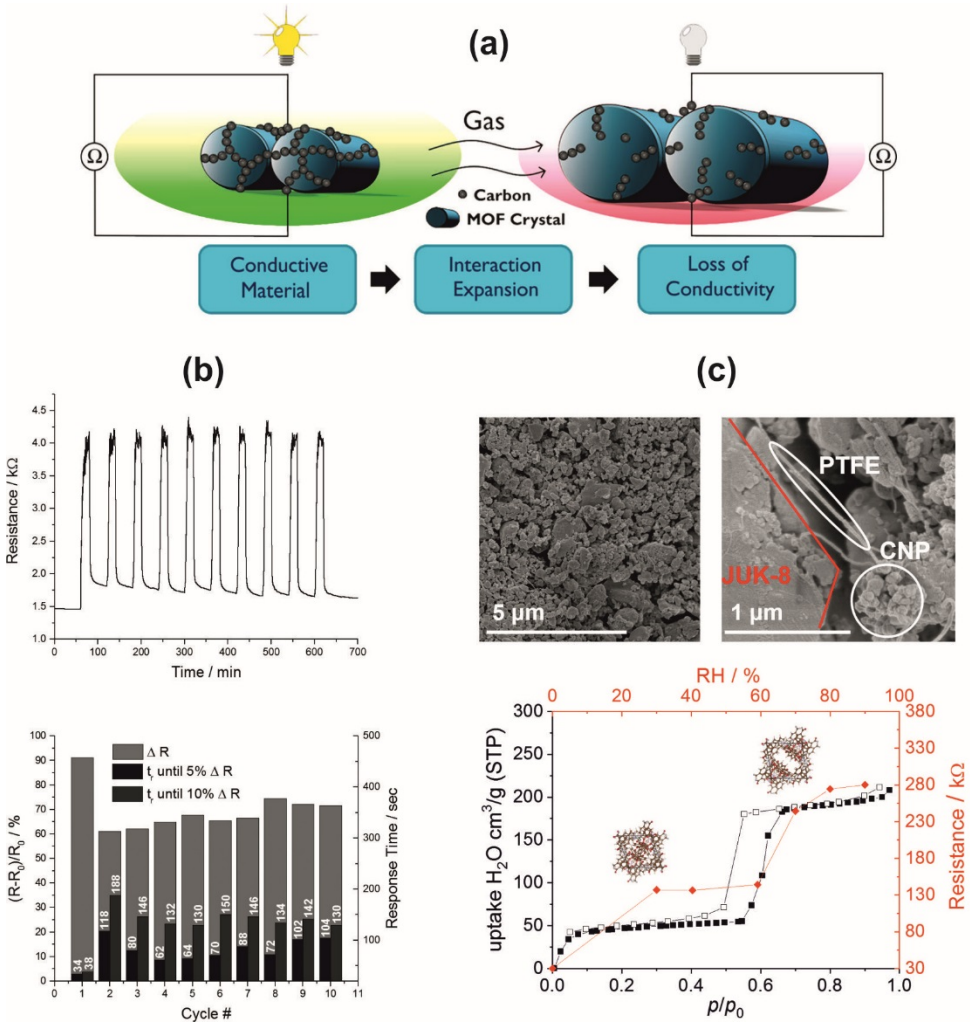


**Figure 10.** Threshold sensors based on switchable OFM composites: (a) schematic illustration of working principle; (b) resistance responses of the MIL-53/CNP/PTFE to *n*-butane upon cycling in dry atmosphere. Adopted with permission from Ref. 256. Copyright 2017 American Chemical Society. (c) SEM images and resistance responses of the JUK-8/CNP/PTFE towards humidity compared with water vapor uptake at 298K.

Instead of coating semiconducting materials with OFM to reach chemiresistive sensing composites, another approach is to incorporate semiconducting polymers within the nanopores, as was demonstrated by Uemura, Kitagawa and coworkers.[264] They polymerized 3,4-ethylenedioxythiophene (EDOT) molecules in the cavities of MIL−101(Cr) and obtained a series of MOF/PEDOT conducting composites that retained high porosity. By using this "best-of-both-worlds" approach they fabricated a chemiresistor with a MOF active layer having $S_{BET}$ = 1038 $m^2/g$ and $\sigma > 10^{-7}$ S $cm^{-1}$. The device efficiently detected $NO_2$ up to a 10 ppm level with a LOD (extrapolated) of 60 ppb at room temperature. An alternative approach using an inorganic semiconductor was adopted by Hupp and coworkers, who introduced one-dimensional strands of oxy-tin(IV) into mesoporous zirconium-based NU-1000 MOF via repetitive solvothermal installation.[265] The resulting composite with 'conductive-glass' (tin oxide) was deposited on IDEs by suspension drop-casting; the fabricated final device had a reversible conductance response to 5% $H_2$ in air or nitrogen.

Final edited form was published in "Chemical Reviews 2020, 120(1), S. 8581-8640. ISSN 1520-6890.
https://doi.org/10.1021/acs.chemrev.0c00033

### 3.2 Chemicapacitor gas sensors and impedimetry

These transduction mechanisms are based on alternating current (AC) electrical circuits with a capacitor, a device that consists of two conducting electrodes separated by an insulating (dielectric) sensing material. The current-voltage $V(t)$-$I(t)$ characteristic of the capacitor in the frequency ($f$) domain defines its impedance $Z$, which is the AC analogue to DC resistance. The complex representation of impedance includes resistance $R$ as the real part and capacitive reactance $X_C$ as the imaginary part (eq. 1). The capacitive reactance is inversely proportional to capacitance $C$ (eq. 2), which is a function of the dielectric constant ($\varepsilon_r$) of the sensing material, the area of each electrode $A$, the vacuum permittivity ($\varepsilon_0$), and the separation distance $d$ between the electrodes, *i.e.* thickness of the dielectric layer (eq. 3):

$$Z = \frac{V(t)}{I(t)} = \mathrm{Re}Z + \mathrm{Im}Z = R + \mathrm{j}X_C \quad (1)$$

$$X_C = -\frac{1}{2\pi f C} \quad (2)$$

$$C = \varepsilon_r \frac{\varepsilon_0 A}{d} \quad (3)$$

The interaction of the analyte with the dielectric sensing material modifies its dielectric constant $\varepsilon_r$ and/or its thickness $d$, both of which contribute to the overall capacitance and impedance. Two electrical readouts ($C$ or $|Z|$, *i.e.* scalar $Z$) are the most commonly used in impedimetric (impedance spectroscopy) measurements as the primary sensing response to analyte concentration.

**3.2.1 Impedance as the primary sensing response.** MOF-based impedance sensors are among the earliest developments in the integration of OFM with sensing hardware, likely because this transduction mechanism does not require the OFM to be intrinsically conducting. Moreover, a variety of material morphologies can be used, including single crystals, pellets, and composites. Such devices seems to be particularly well suited to detect water vapor[266,267] and other polar molecules such as alcohols.[266] More recently, Ruan and coworkers improved the performance of their earlier devices[267] by forming a composite of $NH_2$-MIL-125 (Ti) with $FeCl_3$.[268] This device showed improved sensitivity and shorter response time (11 s) compared with pristine MOF-based capacitor. The sensitivity to water was further improved (with comparable response time, 17 s) when $NH_2$-MIL-125 (Ti) or its composite were replaced by MIL-101(Cr) nanoparticles (Table 1).[269] Zheng and coworkers prepared a layered mixed-metal MOF, $[CoCa(notpH_2)(H_2O)_2]ClO_4$ (CoCa). Using single crystals of the material their device showed reversible impedance responses of ca. three orders of magnitude within 55-95% RH at 25°C with short response and recovery times (35 and 49 s, respectively).[270] Obtaining MOF crystals of sufficient size to form devices is not always feasible, so these authors also prepared devices using pellets formed from the MOF powders. Sensor response was clearly inferior; much longer times were required for equilibration of adsorption and desorption of water molecules (ca. 600 and 200 s for round and square pellets, respectively). Without pressure to form a pellet, a powdered sample showed response and recovery times (62 and 76 s) comparable to those of single crystals. Tanase and coworkers reported a unique example of dual impedance and luminescent response to humidity for a pelletized mixed-metal MOF, $[Eu(H_2O)_2(mpca)_2Eu(H_2O)_6W(CN)_8]$ (EuW), placed between copper electrodes.[271] This device exhibited good sensitivity and repeatability as well as response-recovery times of 380-390 s, when cycled within 53-100% RH at 500 Hz and 21 °C. Zhang and coworkers reported another

Final edited form was published in "Chemical Reviews 2020, 120(1), S. 8581-8640. ISSN 1520-6890.
https://doi.org/10.1021/acs.chemrev.0c00033

humidity sensor based on a layered MOF, [Cd(TMA)(DPP)$_{0.5}$($H_2O$)], which showed similar sensitivity to the $FeCl_3$/$NH_2$-MIL-125 (Ti) composite in the 11-97% RH range when compared to performance of humidity sensors based on various materials.[272] The first COF-based impedimetric humidity sensing was recently reported.[273] A new porous crystalline layered COF with boron ester linkages (denoted as COF-TXDBA) was obtained by the reaction of truxene (10,15-dihydro-5*H*-diindeno[1,2-*a*:1′,2′-*c*]fluorene, TX) and 1,4-phenylenediboronic acid (DBA). The COF-TXDBA based sensor exhibited impedance decrease by three orders of magnitude in the 11–98% RH range, with excellent reversibility as well as response and recovery times of 37 s and 42 s, respectively.

The first impedance sensors to detect ammonia were recently reported by Li et al. and were based on two different proton-conducting MOFs comprised of 2-substituted 1*H*-imidazole-4,5-dicarboxylate linkers. [274,275] The capacitor with the highest response used pelletized [Ba(o-CbPh$H_2$IDC)($H_2O$)$_4$] placed between Pt mesh electrodes. The response of this device was 243% to 25 ppm $NH_3$ under 98% RH at 30 °C and showed the lowest LOD of 1 ppm at 75% RH.[274] Importantly, it was also selective against interfering gases, such as $N_2$, $O_2$, $H_2$, benzene, acetone, CO, $CO_2$, $H_2S$, ethanol, and methanol. Apart from high sensitivity at high relative humidity and low temperature, it was reversible over 10 cycles. The sensor showed no proton conduction and no ammonia recognition in the absence of water or under dry ammonia at 30 °C. Clearly, the formation of a proton conduction pathway involving water is required, pointing to either a vehicle or a Grotthuss mechanism for the ion transport, dependent on RH. Another example of an impedance ammonia sensor was reported by the same group using a proton-conductive copper-based layered [Cu(*p*-IPhHIDC)] MOF.[275] The fabricated chemicapacitor showed a remarkable impedance response of 8620% to 130 ppm $NH_3$ gas with an LOD of (2 ppm) at room temperature and 68% RH. Similar to the Ba-MOF based device, this sensor was selective to several interferants ($N_2$, $O_2$, $H_2$, benzene, CO, $CO_2$, methanol) and showed excellent reversibility. However, a disadvantage of the sensing mode represented by these two devices is that water molecules are essential for impedance-based ammonia detection.

**3.2.2 Capacitance as the primary sensing response.** Capacitance as a transduction mechanism was one of the earliest uses of a MOF as an active sensing layer, using a composite with an organic binder.[266] Integration with CMOS was demonstrated later in a 2011 report by Qiu *et al.*,[276] whereby water vapor sensing was shown using HKUST-1 film. Analogous capacitors with HKUST-1 films were also used for alcohol and VOC sensing by Zeinali and coworkers.[277,278] Recently, this group carried out humidity sensing using a capacitor fabricated from an electrochemical film of HKUST-1 grown on a copper plate electrode.[149] This device was much more sensitive (ca. four orders of magnitude) than the earlier composite device of Qiu and coworkers.[276] Using the same MOF, De Smet et al. demonstrated an elegant fabrication of a chemicapacitor by in-situ electrochemical growth of HKUST-1 layers directly on custom-fabricated planar copper IDEs consisting of 100 electrodes (to increase the device capacitance), each 6-8 μm high and 50 μm wide, and separated from each other by 50 μm gaps.[279] The device could sense methanol and water vapor and exhibited fast (~120-150 s) and reversible response to these analytes (with higher sensitivity for water) in the 100-8000 ppm range at 20 kHz and 30 °C. The time-dependent capacitance response followed diffusion-controlled kinetics and the equilibrium response followed Langmuir adsorption model. The differences between devices based on the same MOF (HKUST-1) reported by various groups clearly demonstrate that the performance of each sensor design is unique. In particular, it depends on the area of the electrodes, thickness of the dielectric layer, and detailed fabrication method. Capacitance response to water using a series of MOFs, Al-isophthalate CAU-10 MOFs with various linker substituents, was reported.[280,281] However, the sensitivity of these devices to 40-

Final edited form was published in "Chemical Reviews 2020, 120(1), S. 8581-8640. ISSN 1520-6890.
https://doi.org/10.1021/acs.chemrev.0c00033

60% RH range was relatively low (0.13 pF/%RH) and the devices showed long (12 min) response times due to slow characteristics of the gas mixing system. Omran and coworkers also reported a capacitance based sensing of water and several VOCs by a layered copper-benzenedicarboxylate MOF that was epitaxially grown on SAM-functionalized Au IDEs.[282] The capacitance changes were found to be linear within various ranges up to 1.7% for acetone, and up to 65% RH.

De Smet and coworkers have continued their development of CMOS-integrated MOF-polymer composites, reporting fabrication of capacitive sensor devices with planar Al electrodes covered with thin films formed by drop-casting MIL-53-$NH_2$ (Al) nanoparticles dispersed (20 wt%) in a polyimide matrix (Matrimid®).[283] The device with the polymer-MOF composite as an affinity layer was used to detect methanol vapor at 28 °C. Upon exposure to 5000 ppm methanol, the reversible chemicapacitive response of the sensor was nearly double that of a device coated with MOF-free polymer, with a lower LOD and faster response time. In a subsequent paper, they expanded their study to cover mixed-matrix membranes with various MOF loadings (0-100 wt%) as well as additional analytes, including a series of alcohols and water in the gas phase.[284] The impedance response was reproducible and reversible for all devices and the maximum capacitance responses to methanol and water were found for the composite containing 40 wt% MIL-53-$NH_2$ in the polymer (e.g. five-fold increase in response to 1000 ppm methanol was observed compared to devices coated with Matrimid® only). Discrimination of other alcohols, ethanol and 2-propanol, from methanol and water was possible based on different response times. In general, these composite-based chemicapacitors show promise in chemical sensors for tuning of affinity of sensing layers by changing their compositions.

MOF-based chemicapacitive sensing has been advanced by other groups as well. Eddaoudi, Salama and coworkers targeted toxic gases as analytes and reported the fabrication of an $H_2S$ sensor by solvothermal growth of a yttrium fumarate MOF (Y-fum) film on SAM-functionalized gold IDEs.[285] This device exhibited sensitivity in the 0.1 to 100 ppm range with a remarkable LOD (extrapolated) of 5.4 ppb at 22 °C. High selectivity to $H_2S$ in the presence of $CH_4$, $NO_2$, $H_2$ and $C_7H_8$ interferents was also shown. More recently, they reported the first MOF-based $SO_2$ sensor (Figure 11).[286] An indium-based MOF (MFM-300) was coated solvothermally on pre-functionalized IDEs, using an OH-terminated SAM as an attachment layer, similar to the yttrium-based sensor. This device showed a linear response to $SO_2$ within 75 to 1000 ppb range, low LOD of 5 ppb, and selectivity over several gases including $CH_4$, $CO_2$, $NO_2$, $H_2$, propane, and toluene. Its excellent stability and reproducibility, even in the presence of water vapor, suggests its potential for practical application.

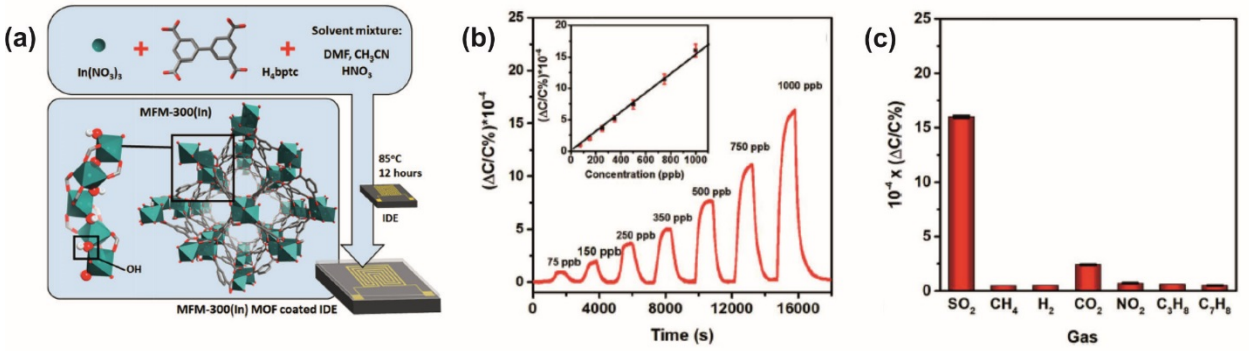

**Figure 11.** MFM-300 (In) MOF-based chemicapacitive $SO_2$ sensor: (a) Schematic representation of the solvothermal preparation of thin film on IDEs; (b) Detection in the 75 to 1000 ppb concentration range, inset: linear response for the corresponding range; (c) selectivity to other gases at 1000 ppb. Adapted from Ref. 286 under a Creative Commons Attribution-NonCommercial 3.0 Unported Licence. Published by The Royal Society of Chemistry in 2018.

An interesting comparison of IDE-capacitive and quartz crystal microbalance (QCM)-based transduction mechanisms for MOF-based sensors was published recently by Chappanda *et al.,* using a ZIF-8 thin film as the example sensing material and acetone as an analyte.[287] The IDE capacitors showed the advantages of higher sensitivity, lower detection limit, better short-term stability as well as smaller device size and lower cost. On the other hand, the QCM devices proved superior in selectivity with respect to humidity, reduced effect of temperature on the sensitivity, and lower actuation energy cost. They also compared the capacitance and impedance responses for the IDE devices, finding that the capacitive transduction was more sensitive to acetone, due to the properties of ZIF-8 films whose impedance decreased when exposed to acetone.

### 3.3 FETs, Kelvin probe gas sensors and potentiometry

Although field-effect transistors (FETs) have been successfully used as sensors based on many organic and inorganic channel materials, FET devices based on pristine MOFs as channel materials have not been used for sensing applications yet.[288,289] These devices consist of a semiconductive sensing material (channel) placed between source (S) and drain (D) electrodes, and a third gate (G) electrode, separated by a dielectric layer (Figure 8). As compared to chemiresistor sensors, an extra gate electrode in a FET is used to control the drain current ($I_{DS}$) flowing through the sensing channel, by a perpendicular electric field originating from the applied gate-source voltage, $V_{GS}$. This electric field modulates the density of mobile charge carriers in the channel material. In general, the magnitude of the drain current $I_{DS}$, which is an electrical readout in a FET device, depends on the applied gate-source $V_{GS}$ and drain-source $V_{DS}$ electrode DC voltages, the width-to-length ratio of the channel ($W/L$), the capacitance of the gate insulator per unit area ($C$), the charge carrier mobility in the channel ($\mu$), and the so-called the threshold voltage ($V_T$), which is proportional to the difference between the work functions of the gate and the sensing channel (eq. 4):

$$I_{DS} = \frac{\mu CW}{L}\left[(V_{GS} - V_T)V_{DS} - \frac{V_{DS}^2}{2}\right] \quad (4)$$

As compared to capacitance devices, tunable charge carrier mobility in the semiconductor material (by gate voltage) allows higher sensitivity of FET sensors. Simultaneously, FET devices can provide insight into the sensing mechanism with in-depth characterization of the active semiconductors. A few recent papers present construction and detailed characterizations of MOF-based. [48,242,290-293] or COF-based[101] FET devices (MOFFETs or COFFETs). The rare MOFFET examples involved one of two material types: (1) layered frameworks as channel materials, such as conjugated $Cu_3BHT$ (which has record-high conductivity and charge mobility[48]); porous Ni-CAT-1 with excellent hole mobility;[293] $Ni_3(HIB)_2$ with slight back-gate dependent conductance;[291] or (2) guest@MOF structures, such as $[(CH_3)_2NH_2]^+$ ions in a series of proton-conducting In-isophtalate compounds;[292] $K^+$ ions in a mixed-valence $K_xFe_2(BDP)_2$ framework;[294] or imidazole molecules in a proton-conducting Im@HKUST-1.[290] Contrary to FET devices using the layered materials (e.g. Ni-CAT-1), the guest-loaded MOFs are rather poor candidates for potential FET

Final edited form was published in "Chemical Reviews 2020, 120(1), S. 8581-8640. ISSN 1520-6890.
https://doi.org/10.1021/acs.chemrev.0c00033

sensing applications because their surface areas are much lower than those of the pristine materials. In addition to the aforementioned MOFFETs, a COFFET device with a vertical field-effect transistor (VFET) architecture, was recently fabricated based on the heterostructure of $COF_{TFPy-PPDA}$ film and single-layer graphene (SLG).[101] This pioneering device with ambipolar charge carrier behavior under lower modulating voltages, demonstrated its application prospect in flexible organic electronic devices. However, to our knowledge, CHEMFET sensing involving OFM has so far been reported only for the case of an organic-based FET (OFET sensor) in which a Cd-MOF was used as a component of a sensing composite for detecting explosives.[295] Other OFET related examples without sensing studies include surface modifications of the gate dielectric layer by an HKUST-1 film to tune and optimize the device parameters[296] and bulk modification of the active layer by HKUST-1 to improve its environmental stability.[297]

All of the above-mentioned examples represent important steps towards implementation of OFM as active porous conducting materials in CHEMFET sensors. In general, the principle underlying signal transduction in CHEMFETs is modulation of the gate electrode chemical work function or of the channel semiconductor by a change in surface functionalization or adsorbed surface species. Changes of work function can be probed using the Kelvin Probe (KP) method and this approach to sensing gas-phase analytes was adopted by a few groups. The response of the KP sensor is the work function difference, i.e. the contact potential difference (CPD). Although the KP technique allows one to consider MOFs that are not sufficiently conducting for use in FETs, its main disadvantage lies in the difficulty in miniaturizing oscillating electrodes, which makes KP devices unsuitable for real-life applications. This approach to sensing was described in earlier reviews[9,11,13] and no new publications have appeared since then. Therefore, the MOFs and corresponding analytes considered thus far are listed in Table 1 without detailed description.[298-304] These studies demonstrate that MOF-based CHEMFET devices are feasible and could potentially be used for sensing gas-phase analytes in near future.

### 3.4 Electrochemical sensors for solution-phase analytes

Electrically transduced detection of analytes from liquid phases requires the presence of a liquid-solid interface that is realized in electrochemical cells, typically in a three-electrode configuration comprising working (WE), counter (CE) and reference electrodes (RE) connected to a potentiostat (Figure 8). In general, electrochemical sensing can be realized by either (i) potentiometric measurements that generate a response in the form of potential under zero current conditions (with a two-electrode configuration); (ii) voltamperometric measurements that give a response in the form of current, with the applied potential as a driving force (waveform potential in voltammetry or single-potential in amperometry); or (iii) impedimetric measurements with a current response to AC potentials applied at various frequencies. Electrochemical sensing is of particular interest for contacting aqueous solutions with electronics in applications such as medical diagnostics and environmental monitoring.

OFM can be used in electrochemical sensors to modify the liquid-solid interface, i.e. to modify working electrodes in electrochemical cells. There are numerous examples of electrochemical sensors in which a MOF plays a passive role. For example, the MOF may serve as a selective molecular sieve or an adsorbent, in either pristine form or as a component of a composite. These uses have been recently reviewed.[18,21,305] Compared to MOFs, COFs are still rarely applied in electrochemical sensing but examples in which they serve as carriers or immobilizing matrices in composites are on a rise.[306-313] Most commonly, voltamperometric techniques that can detect only redox-active species have been used in OFM-based electrochemical

Final edited form was published in "Chemical Reviews 2020, 120(1), S. 8581-8640. ISSN 1520-6890.
https://doi.org/10.1021/acs.chemrev.0c00033

sensors. Analytes such as various heavy metal ions (e.g. $Pb^{2+}$, $Cd^{2+}$, $Cu^{2+}$), anions (e.g. nitrites), biomolecules (e.g. glucose, glutathione, dopamine), and water contaminants (e.g. hydroquinone, hydrazine, nitrobenzene) have been targets. As a representative illustration of highly sensitive ion detection, an electrochemical sensor for trace quantities of cadmium ions based on conducting UiO-66-$NH_2$@PANI composite (PANI = polyaniline) was recently published.[314] A glassy carbon electrode (GCE) was modified with the composite and this was used for reductive accumulation of cadmium from solution. After this step, differential pulse-stripping voltammetry was employed for quantitative determinations. The modified electrode showed the lowest LOD value (0.3 µg/L) compared to other $Cd^{2+}$ sensors, a linear response in the 0.5-600 µg/L range, and high repeatability. Another elegant example of voltammetric and amperometric detections was reported by Wei et al.,[315] who prepared a composite electrocatalyst comprising a flexible carbon cloth anode covered with Co-ZIF67 in the form of well-aligned leaf-like nanosheets. The electrode exhibited low LOD, wide detection range, and excellent selectivity for glucose biomolecules under physiological conditions. Another approach towards electrochemical biomolecule sensing was recently described by Wang et al. who fabricated a flexible carbon fiber microelectrode coated with $Cu(INA)_2$ MOF in the context of nonenzymatic sweat sensors.[316] [XXXX] This rime-inspired MOF film showed highly selective and sensitive sensing performances for simultaneous determination of lactate and glucose in a wide range of pH values.

First *in vivo* chemical detection using MOFs integrated with implantable flexible electrochemical sensors was recently reported by Ling *et al*.[317] The MOF-modified screen-printed electrodes were first employed for *ex vivo* monitoring important nutrients such as ascorbic acid, glycine, L-tryptophan and glucose. The sensors showed LOD values of 14.97, 0.71, 4.14, and 54.60 µmol/L, respectively, and were capable of retaining their performance under extreme deformation. Follow-up experiments using live cells and mice demonstrated that the MOF-modified sensors are biologically safe to cells (with 84 and 95% cell viabilities after 24 hours) and can detect L-tryptophan in blood and interstitial fluids of animals. This work shows great promise for future use of OFM in implantable flexible electronics and sensing.

Unlike the above examples, in which a non-conductive OFM was used to increase sensitivity by acting as a preconcentrator, a MOF used as active electrical element for electrochemical sensing of ions was recently described.[318] A series of conductive layered MOFs, $Cu_3HHTP_2$ and M-CAT-1 (M = Co, Ni) were drop-casted onto a GCE and subsequently covered with a layer of an ion-selective membrane (ISM) to form an ion-selective electrode (ISE) for potentiometric sensing. The MOF component played the role of an efficient ion-to-electron transducer. The resulting sensors showed near-Nernstian linear responses within wide range of $NO_3^-$ or $K^+$ ion concentrations (ca. $10^{-6}$-$10^{-2}$ M), as well as good potential stability (Figure 12). This first demonstration of ion-to-electron transduction using a conductive MOF may stimulate further developments of OFM-based ion-selective electrodes and potentiometric sensors.

Final edited form was published in "Chemical Reviews 2020, 120(1), S. 8581-8640. ISSN 1520-6890.
https://doi.org/10.1021/acs.chemrev.0c00033

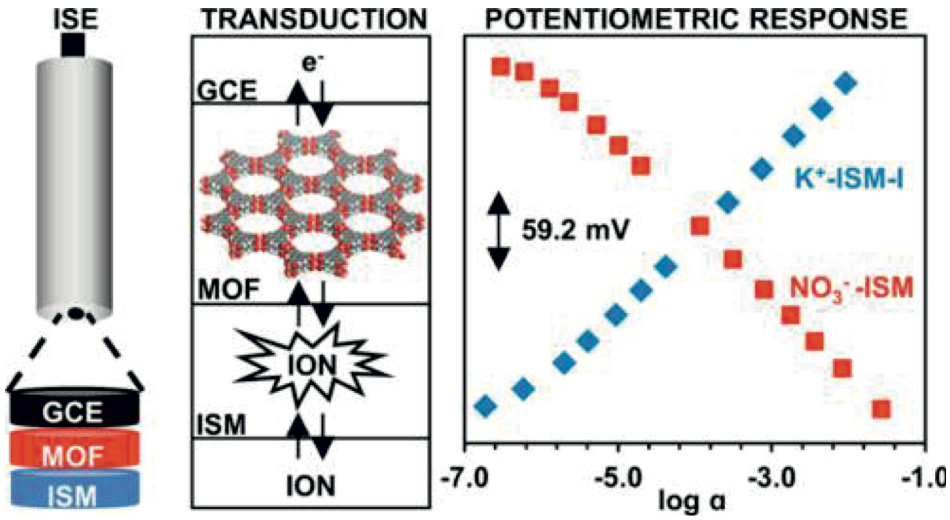


**Figure 12.** Potentiometric ion sensing involving conductive $Cu_3HHTP_2$ and M-CAT-1 (M = Co, Ni) MOFs: (left) schematic representation of an ion-selective electrode with modifying layers; (middle) illustration of the ion-to-electron transduction mechanism; (right) representative potentiometric responses Ni-CAT-1 based sensors to $NO_3^-$ and $K^+$ ions. Reproduced with permission from Ref. 318 Copyright 2018 American Chemical Society.

### 3.5 Electrically transduced physical sensors

The first OFM-based physical sensor, i.e. a device that responds to changes in a physical property of a material and tranduces this information as an electrical signal, was recently reported as a strain sensor for detecting human body motion (Figure 13).[319] Previously, the concept of strain-based detection by utilizing OFM was used for chemical sensing.[320] The HKUST-1 thin film was integrated with a microcantilever surface and a strain created at the interface was measured as a piezoresistive response to water vapor, alcohols and $CO_2$. In the case of the physical sensor device its essential element is a thin film of iodine doped copper-tricarboxytriphenylamine ($I_2$@CuTCA) fabricated on gold/polyethylene (PE) flexible substrate via a liquid-phase epitaxy approach. The working principle of the sensor is based on structure deformation-induced change of conductivity of the material. This modulation of the charge-carrier hopping process leads to a threshold current response with major conductance variation between 2.5 and 3.3% strain level (Figure 13). The $I_2$@CuTCA crack-type piezoresistor exhibits ultrahigh sensitivity with a gauge factor exceeding 10000 in the above-mentioned deformation range for several thousand operating cycles. In an intriguing new application space, the sensor was employed in a smart kneecap to differentiate among various human body motions and to estimate the energy consumption during exercises (Figure 13d). In general, this proof-of-concept demonstrates the potential of both OFM and this transduction mechanism for detecting motion in a variety of applications.

Final edited form was published in "Chemical Reviews 2020, 120(1), S. 8581-8640. ISSN 1520-6890.
https://doi.org/10.1021/acs.chemrev.0c00033

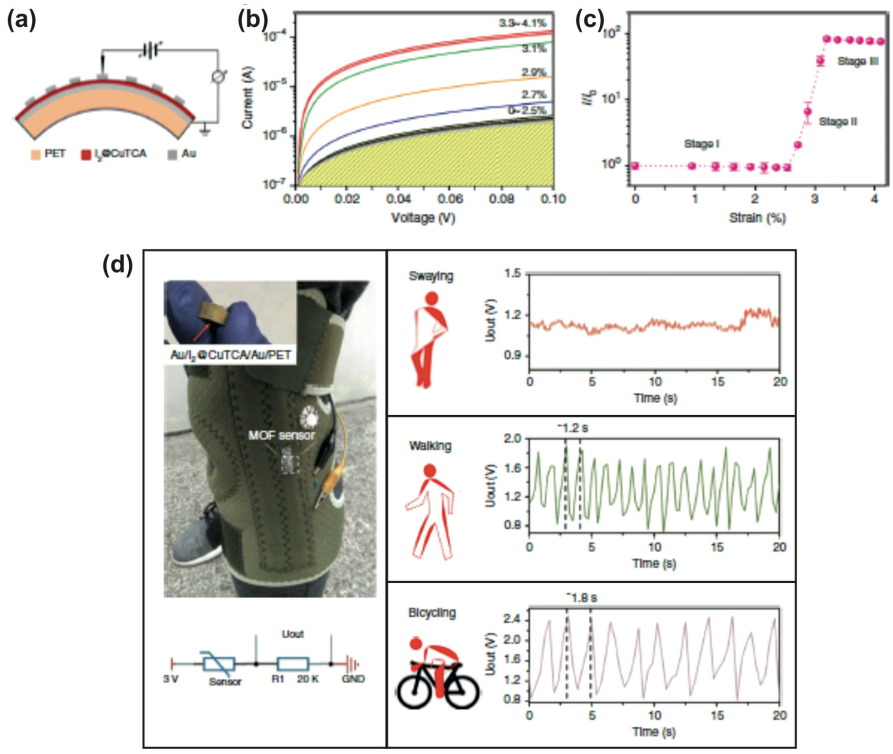


**Figure 13.** Electromechanical properties of the $I_2$@CuTCA nanofilm strain sensor: (a) schematic illustration of the bended device structure fabricated on PET substrate; (b) current-voltage curves of the Au/$I_2$@CuTCA/Au device under various bending strains; (c) evolution of the device current as a function of the bending strains; (d) human body motion recognition: smart kneecap with integrated MOF sensor and a 20kΩ resistor R1 (left), and its strain-responding voltage output signals ($U_{out}$), falling on the resistor R1, under leg swaying, walking, and bicycling. Adapted from Ref. 319 under a Creative Commons Attribution 4.0 Licence (CC BY 4.0). Published by Nature Publishing Group in 2018.

Very recently, a new type of OFM-based physical sensor was reported as a photosensor capable of detecting a broad wavelength range from UV to near IR (400-1575 nm).[321] This proof-of-concept photodetector device was based on a semiconducting 2D conjugated MOF film (see also Sect. 4.1.1), $(NH_4)_3Fe_3(THT)_2$, containing deprotonated THT and $NH_4^+$ counterions, and featuring high charge carrier mobility of 230 $cm^2\ V^{-1}\ s^{-1}$ and narrow IR bandgap of 0.45 eV at room temperature. Photocurrent responses of the device were systematically investigated dependent on temperature as well as incident laser wavelength and power. The device showed a significantly improved performance upon cooling to 77K due to the suppression of thermally generated charge carriers. Low-temperature parameters such as specific detectivity, voltage responsivity and noise equivalent power were maintained over the entire excitation range and are comparable to those of first graphene- and phosphorus-based photodetectors. Furthermore, the devices show stable and reproducible photoswitching behavior as a function of time. This work for the first time brings 2D conjugated MOFs toward reliable and robust broadband photodetector application. These findings demonstrate the feasibility of integrating 2D conjugated MOFs as active elements into broadband photodetectors as well as the high potential of these materials for optoelectronic applications in general.

Final edited form was published in "Chemical Reviews 2020, 120(1), S. 8581-8640. ISSN 1520-6890.
https://doi.org/10.1021/acs.chemrev.0c00033

**Table 1. Electrical sensors for gas-phase analytes based on pristine OFM.[a]**

| Sensing material /MOF dimensionality | Setup (architecture) Integration method | Method (Electrical readout) Max avg response observed | Analyte | LOD | Experimental range | Environment /remarks | Ref./ year |
|---|---|---|---|---|---|---|---|
| **Chemiresistors and conductometry** | | | | | | | |
| $Co(mim)_2$ (ZIF-67) 3D | **- chemiresistor: Ag-Pd/$Co(mim)_2$/Ag-Pd** - paste coating on IDEs | conductometry (resistance $R$) $R_{gas}/R_{air}$ = 13.9 (100 ppm) | HCHO | 5 ppm | 5-500 ppm 5-50 ppm (linear response) | air, <70% RH, 150 °C lower responses for methanol, acetone | 230/2014 |
| $Co(im)_2$ 3D | **- chemiresistor: Ag-Pd/$Co(im)_2$/Ag-Pd** - paste coating on IDEs | conductometry (resistance $R$) $R_{gas}/R_{air}$ = 14.1 (100 ppm) | $N(CH_3)_3$ | 2 ppm | 2-500 ppm 2-50 ppm (linear response) | air, <70% RH, 75 °C lower responses for formaldehyde, TEA | 231/2014 |
| $Cu_3HITP_2$ 2D | **- chemiresistor: Au/$Cu_3HITP_2$/Au** - suspension dropcasting on IDEs | conductometry/ (conductance $G$) $\Delta G/G_0$ = 2.5% (10 ppm) | $NH_3$ | 0.5 ppm | 0.5-10 ppm (linear response) | air and $N_2$, <60%RH, RT isostructural $Ni_3HITP_2$ not operative; | 232/2015 |
| Array of 2D MOFs: $Cu_3HHTP_2$/$Cu_3HITP_2$/ $Ni_3HITP_2$ | **- array of chemiresistors: Au/$Cu_3HHTP_2$/$M_3HITP_2$/Au** (M = Cu, Ni) - 'drawing' with pellets on IDEs on paper or suspension dropcasting on IDEs on $Al_2O_3$ | conductometry (conductance $G$) $\Delta G/G_0$ ~ from -9 to 4% (at 200 ppm) | alcohols ketones/ethers aliphatic $C_xH_y$ aromatic $C_xH_y$ amines | N/A | 200 ppm | $N_2$, RT multiple analyte sensing; Ni-based sensor mostly displays an opposite direction of response to Cu-based MOFs; | 233/2015 |
| Array of 2D MOFs: $Cu_3HHTP_2$/ Ni-CAT-1 | **- array of chemiresistors: GR/$Cu_3HHTP_2$/Ni-CAT-1/GR -** direct growth on IDEs drawn on shrinkable films (PS- or PE-based blends) | conductometry (resistance $R$) $\Delta R/R_0$ = 0.7% (80ppm $NH_3$) Cu-MOF $\Delta R/R_0$ = -1.8%, -1.7% (80ppm NO) Cu-MOF, Ni-MOF $\Delta R/R_0$ = 0.5%, 4.2% (80ppm $H_2S$) | $H_2S$, $NH_3$, NO | N/A | 2.5-80 ppm (linear response) | $N_2$, RT multiple analyte sensing, including water presence | 234/2016 |

Final edited form was published in "Chemical Reviews 2020, 120(1), S. 8581-8640. ISSN 1520-6890.
https://doi.org/10.1021/acs.chemrev.0c00033

| | | | | | | | |
|---|---|---|---|---|---|---|---|
| | | Cu-MOF, Ni-MOF | | | | | |
| Ni-CAT-1 (2D) or $Ni_3HITP_2$ (2D) | **- chemiresistor: Au/$Ni_3HXTP_2$ on textile/Au** (X = H, I) - direct growth on textiles (cotton, polyester) | Conductometry (conductance *G*) -$\Delta G/G_0$ = -49%, 81% (80ppm NO) Ni-CAT-1, $Ni_3HITP_2$ -$\Delta G/G_0$ = 98%, 97% (80 ppm $H_2S$) Ni-CAT-1, $Ni_3HITP$ | NO<br>$H_2S$ | 1.4; 0.16 ppm (Ni-CAT-1; $Ni_3HITP_2$)<br>0.23; 0.52 ppm (Ni-CAT-1; $Ni_3HITP_2$) | 5-80 ppm (linear response)<br>0.1-80 ppm (NO)<br>1-80 ppm ($H_2S$) | $N_2$, <18% RH (5000 ppm $H_2O$), RT; first wearable flexible chemical sensor based on (semi)conductive MOFs; other gas-phase analytes also tested: $H_2O$, CO, $NH_3$, acetone, 2-butanone, ethanol, ethanol, benzene | 236/2017 |
| $Cu_3HHTP_2$ (2D) | **- chemiresistor: Au/$Cu_3HHTP_2$/Au** - spray LbL liquid-phase epitaxial fabrication of a thin film on IDEs | conductometry (resistance *R*) $\Delta R/R_0$ = 129% (100 ppm) | $NH_3$ | 0.5 ppm | 1-100 ppm (linear response) | dry air, RT | 237/2017 |
| $Cu_3HHTP_2$ (2D) | **- chemiresistor: Cu-$Ag_{paste}$/$Cu_3HHTP_2$/Cu-$Ag_{paste}$** - spray-coating of water-based MOF nanoplatelet dispersions on glass slides or PC foils | conductometry (resistance *R*) $\Delta R/R_0$ ~125% (glass slide) $\Delta R/R_0$ ~35% (PC foil) | methanol | N/A | N/A | dry and water-saturated Ar, RT | 238/2018 |
| NiPC-M or NiNPC-M (2D) (M = Cu, Ni) | **- chemiresistor: Au/Ni(N)PC-M/Au** (M = Cu, Ni) - dropcasting of water-based MOF suspension onto IDEs | conductometry (conductance *G*) -$\Delta G/G_0$ = 43-45% (80 ppm $NH_3$ 30 min) -$\Delta G/G_0$ = 64%, 98% (80 ppm $H_2S$, 10 min) NiPC-Ni, -Cu -$\Delta G/G_0$ = -657%, -397% (1 ppm NO, 30 min) NiPC-Ni, -Cu | $NH_3$<br>$H_2S$<br>NO | 0.31; 0.33 ppm<br>32; 19 ppb<br>1.1;1.0 ppb<br>above for NiPC-Ni; -Cu (within 1.5 min) | 2-80 ppm<br>0.2-20 ppm<br>0.02-1.0 ppm<br>(linear responses within 1.5 min) | < 18% RH (5000ppm $H_2O$), RT | 322/2019 |

Final edited form was published in "Chemical Reviews 2020, 120(1), S. 8581-8640. ISSN 1520-6890.
https://doi.org/10.1021/acs.chemrev.0c00033

| | | | | | | | |
|---|---|---|---|---|---|---|---|
| $Cu[Ni(pdt)_2]$ (3D) | **- chemiresistor: Cu/$Cu[Ni(pdt)_2]$/Cu** - powder pellet formed between Cu rail electrodes | conductometry/ (conductivity $\sigma$) $\Delta\sigma/\sigma_0$ = 11.5% (0.1 bar, $C_2H_2$) 14.4% (1 bar, $C_2H_4$) 15.8% (1 bar, $C_2H_6$) 19.7% (1 bar, $C_4H_8$) 31.1% (1 bar, $C_3H_6$) 34.2% (1 bar, $C_3H_8$) | $C_xH_y$: acetylene, ethylene, ethane, *cis*-2-butene propylene, propane | N/A | linear responses, dependent on adsorbate, up to 0.34-0.76 (moles of adsorbate per mole of $Cu[Ni(pdt)_2]$ ) | RT, pure adsorbates | 242/2019 |
| $UiO\text{-}66\text{-}NH_2$ (3D) | **- chemiresistor: steel-$Ag_{paste}$/UiO-66-$NH_2$/ steel-$Ag_{paste}$** - powder pellet formed between steel rod electrodes | conductometry (resistance $R$) $-\Delta R/R_0$ = 21.6% (10 ppm $SO_2$) $-\Delta R/R_0$ = 7.6% (10 ppm $NO_2$) $-\Delta R/R_0$ = 11.4% (5000 ppm $CO_2$) | $SO_2$, $NO_2$, $CO_2$ | 1 ppm 10 ppm 5000 ppm | 1-10 ppm (linear response for $SO_2$) | $N_2$, 150 °C | 243/2019 |
| HMP-TAPB-1 (2D) | **- chemiresistor: Ag–Pd / HMP-TAPB-1/ Ag–Pd** - dropcasting of ethanol-based paste onto IDEs | conductometry (resistance $R$) $R_{air}/R_{gas}$ = 16.6 (50 ppm, 47%RH) = 70.1 (50 ppm, 84% RH) | $NH_3$ | 1 ppm | 5-200 ppm (linear response) | air, RT, 23–85% RH, selective over other VOC analytes | 247/2018 |
| COF-DC-8 (2D) | **- chemiresistor: Au/COF-DC-8/Au** - dropcasting of water-based COF suspension onto IDEs | conductometry (conductance $G$), 40 ppm, 30min $-\Delta G/G_0$ = 39 % ($NH_3$) $-\Delta G/G_0$ = 62% ($H_2S$) $-\Delta G/G_0$ = -3939% (NO) $-\Delta G/G_0$ = -6338% ($NO_2$) | $NH_3$ $H_2S$ NO $NO_2$ | 70 ppb 204 ppb 5 ppb 16 ppb | 2-10 ppm 5-80 ppm 0.02-40 ppm 2-40 ppm | $N_2$, RT | 241/2019 |
| **Chemicapacitors and impedimetry** | | | | | | | |
| Fe-BTC (3D) | **- chemicapacitor: Au/Fe-BTC/Au** film paste screen-printed on IDEs | impedimetry (impedance $\|Z\|$): $\Delta\|Z\|/\|Z_0\|$ = 5.4% (2.5%RH) | $H_2O$ | N/A | 0-2.5% (linear response) | 1 Hz, 120 °C, responsive also to methanol and ethanol (lower sensitivity) | 266/2009 |
| $NH_2$-MIL-125 (Ti) (3D) | **- chemicapacitor: Ag–Pd/ $NH_2$-MIL-125/Ag-Pd** coating nanoparticles on IDEs | impedimetry (impedance $\|Z\|$): $\Delta\|Z\|$ = 123.58 to 4.50 MΩ (from 11 to 95%RH) | $H_2O$ | N/A | 11-95% (linear response) | 100 Hz, RT | 267/2013 |
| MIL-101 (Cr) (3D) | **- chemicapacitor: Ag–Pd/MIL-101/Ag-Pd** | impedimetry (impedance $\|Z\|$): | $H_2O$ | N/A | 33-95% (linear response) | 100 Hz, RT | 271/2017 |

Final edited form was published in "Chemical Reviews 2020, 120(1), S. 8581-8640. ISSN 1520-6890.
https://doi.org/10.1021/acs.chemrev.0c00033

| | | | | | | | |
|---|---|---|---|---|---|---|---|
| | coating on IDEs | $\Delta\|Z\|$ = 108 to 0.0558 MΩ (from 33 to 95%RH) | | | | | |
| $[CoCa(notpH_2)(H_2O)_2]ClO_4$ (CoCa) (2D) | **- chemicapacitor: Au/CoCa/Au** - single crystal (or pressed pellet) between plate electrodes | impedimetry (impedance $\|Z\|$): $\Delta\|Z\|$ = 250 to 0.28 MΩ (from 55 to 95%RH) | $H_2O$ | N/A | 55-95% (linear response) | 1 kHz, 25°C | 270/2015 |
| $[Eu(H_2O)_2(mpca)_2Eu(H_2O)_6W(CN)_8]$ (EuW) (3D) | **- chemicapacitor: Cu/EuW/Cu** - pressed pellet between plate electrodes | impedimetry (impedance $\|Z\|$): $\Delta\|Z\|$ = 1.48 to 1.30 MΩ (from 53 to 100%RH) | $H_2O$ | N/A | 53-100% (threshold sensor) | 500 Hz, 21°C | 271/2017 |
| $[Cd(TMA)(DPP)_{0.5}(H_2O)]$ (CdL) (3D) | **- chemicapacitor: Ag–Pd/CdL/Ag-Pd** paste coating on IDEs | impedimetry (impedance $\|Z\|$): $Z_{11\%RH}/Z_{97\%RH}$ = 352 | $H_2O$ | N/A | 11-97% (threshold sensor) | 100 Hz, 20°C | 272/2018 |
| COF-TXDBA | **- chemicapacitor: Ag–Pd/** COF-TXDBA **/Ag-Pd** paste coating on IDEs | impedimetry (impedance $\|Z\|$): $\Delta\|Z\|$ = ~$10^5$ to $10^2$ kΩ (from 11 to 98%RH) | $H_2O$ | N/A | 11-98% | 100 Hz, 25°C | 273/2017 |
| [Ba(*o*-$CbPhH_2IDC)(H_2O)_4$] (3D) | **- chemicapacitor: Pt/Ba-MOF/Pt** - pressed pellet between plate electrodes | impedimetry (impedance $\|Z\|$): $-\Delta\|Z\|/\|Z_0\|$ = 243% (25ppm, 98%RH) | $NH_3$ | 1ppm (75%RH) | 1-25ppm (75%RH) 3-25ppm (85%RH) 5-25ppm (98%RH) (linear responses) | air, 30 °C, 75−98% RH | 274/2018 |
| [Cu(*p*-IPhHIDC)] (2D) | **- chemicapacitor: Pt/Cu-MOF/Pt** - pressed pellet between plate electrodes | impedimetry (impedance $\|Z\|$): $-\Delta\|Z\|/\|Z_0\|$ = 8620% (130 ppm, 68%RH) | $NH_3$ | 2ppm (68%RH) | 0-130 ppm at 68–98% RH (linear responses) | air, RT, 68–98% RH | 275/2018 |
| $Cu_3BTC_2$ (3D) | **- chemicapacitor: Cu/$Cu_3BTC_2$/Cu-$Al_{dots}$** - solvothermal film growth on a plate electrode | impedimetry (capacitance $C$) : $\Delta C$= 1.5 pF per %RH (10-90%RH) | $H_2O$ | N/A | 10-90% (linear response) | 1MHz, 25°C | 276/2011 |
| $Cu_3BTC_2$ (3D) | **- chemicapacitor: Cu/$Cu_3BTC_2$/Cu-$Ag_{paste}$** - electrochemical film growth on a plate electrode | impedimetry (capacitance $C$): $\Delta C/C_0$ = ~7% (500ppm EtOH) $\Delta C/C_0$ = ~24% (500ppm MeOH) | ethanol, methanol | 150.5 ppm 47.3 ppm | 250-1000ppm (linear response) | 1MHz, 25°C | 277/2016 |
| $Cu_3BTC_2$ (3D) | **- chemicapacitor: Cu/$Cu_3BTC_2$/Cu-$Ag_{paste}$** - dropcasting of nanoparticle suspension on a plate electrode | impedimetry (capacitance $C$): $\Delta C/C_0$ = 101.5% (500ppm EtOH) $\Delta C/C_0$ = 125.3% (500ppm MeOH) | ethanol, methanol, isopropanol, acetone | 71.05 ppm 61.99 ppm 77.80 ppm 100.18 ppm | 250-1500ppm (linear response) | 1MHz, 10%RH, 25°C | 278/2016 |

Final edited form was published in "Chemical Reviews 2020, 120(1), S. 8581-8640. ISSN 1520-6890.
https://doi.org/10.1021/acs.chemrev.0c00033

| | | | | | | | |
|---|---|---|---|---|---|---|---|
| | | $\Delta C/C_0$ = 65% (500ppm isopropanol)<br>$\Delta C/C_0$ = 12.5% (500ppm acetone) | | | | | |
| $Cu_3BTC_2$ (3D) | **- chemicapacitor: Cu/$Cu_3BTC_2$/Cu-$Ag_{paste}$**<br>- electrochemical film growth on a plate electrode | impedimetry (capacitance *C*) :<br>$\Delta C$= 1.13 pF per ppm (20-100ppm)<br>$\Delta C/C_0$ = 30% (50ppm) | $H_2O$ | 5.45 ppm | 20-100 ppm (linear response) | 1MHz, 25°C | 149/2019 |
| $Cu_3BTC_2$ (3D) | **- chemicapacitor: Cu/$Cu_3BTC_2$/Cu**<br>- electrochemical film growth on IDEs (no =100) | impedimetry (capacitance *C*):<br>$\Delta C$= 5.57 pF (1000ppm MeOH) | methanol<br>$H_2O$ | N/A | 100–8000 ppm (response follows Langmuir adsorption model) | 20 kHz, 30°C | 279/2017 |
| CAU-10 (Al):<br>CAU-10-H/$SO_3H$,<br>CAU-10-$NO_2$/$SO_3H$<br>& CAU-10-OH/$SO_3H$<br>(3D) | **- chemicapacitor: Au/CAU-10/Au**<br>- pressed pellet between plate electrodes | impedimetry (capacitance *C*) :<br>$\Delta C$= 0.13 pF per %RH (40-60%RH) | $H_2O$ | N/A | 0-100% | 1039 Hz, 27°C | 281/2015<br>280/2016 |
| $Cu_2BDC_2$ (2D) | **- chemicapacitor: Au/$Cu_2bdc_2$/Au**<br>LbL liquid-phase epitaxial fabrication of a thin film on IDEs | impedimetry (capacitance *C*) :<br>$\Delta C$= ~0.5 fF per %RH ($H_2O$)<br>$\Delta C$= ~0.4-4.4 fF (VOCs) | $H_2O$<br>VOCs: acetone, ethanol, methanol, toluene | N/A | 5-65 %RH (linear response)<br>0.5-1.7% (acetone)<br>0.28-1.1% (EtOH)<br>0.32-1.4% (MeOH)<br>125-500ppm ($C_7H_8$) (linear responses) | 1MHz, 20-22°C | 282/2015 |
| Y-fum (3D) | **- chemicapacitor: Au/Y-fum/Au**<br>thin film solvothermally grown on IDEs | impedimetry (capacitance *C*):<br>$\Delta C/C_0$ = 0.0016% (1000ppb) | $H_2S$ | 5.4 ppb | 0.1 to 100 ppm (linear response) | $N_2$, 22°C, selective vs. $CH_4$, $NO_2$, $H_2$ and $C_7H_8$; | 285/2016 |
| MFM-300 (In) (3D) | **- chemicapacitor: Au/MFM-300/Au**<br>thin film solvothermally grown on IDEs | impedimetry (capacitance *C*):<br>$\Delta C/C_0$ = 0.0016% (1000ppb) | $SO_2$ | 5 ppb | 75 to 1000 ppb (linear response) | $N_2$, 22°C, selective vs. $CH_4$, $CO_2$, $NO_2$ and $H_2$; responsive at 5-85%RH | 286/2018 |
| **Chemitransistors and potentiometry** | | | | | | | |

| | | | | | | | |
|---|---|---|---|---|---|---|---|
| $Cu_3BTC_2$ (3D) | **- Kelvin Probe: Au or Pt/$Cu_3BTC_2$/Au** screen printing or drop coating | potentiometry (CPD), e.g.: ~ 0.01V at 100°C (pentanal) ~ 0.02V at 80°C ($NH_3$) ~ 0.04V at 80°C ($H_2S$) ~ 0.12V at 200°C (ethanol) ~ 0.08V at 200°C (acetone) | pentanal, $NH_3$ $H_2S$ ethanol acetone | N/A | 1 ppm 5 ppm 2 ppm 15 ppm 5 ppm | 25-200°C, 40%RH, responses strongly dependent on temperature and on back electrode | 303/2011 |
| $Cu_3BTC_2$ (3D) | **- Kelvin Probe: TiN/$Cu_3BTC_2$/Au** drop coating | potentiometry (CPD), e.g. 40%RH, pentanal: ~ 15mV (10 ppm), synt. air ~ 27mV (10 ppm), $O_2$-free | pentanal, ethanal, propanal, hexanal | N/A | 2-10 ppm | synthetic air (20% $O_2$, 80% $N_2$) and $O_2$-free, 25°C, 0-50 %RH; negligible responses to other aldehydes | 298/2013 |
| Mg-MOF74 Co-MOF74 (3D) | **- Kelvin Probe: TiN/MOF-74/Au** drop coating | potentiometry (CPD): ~ 5-8 mV (400-4000 ppm), both MOFs | $CO_2$ | N/A | 400-4000 ppm | synthetic air (20% $O_2$, 80% $N_2$), 25 and 40°C, 40 and 50 %RH cross-sensitive to ethanol | 302/2014 |
| $Cu_3BTC_2$ (3D) | **- Kelvin Probe: TiN/$Cu_3BTC_2$/Au** drop coating | potentiometry (CPD), e.g. in dry air: ~ 0-5 mV (propanal) ~ 0-10 mV (acetone) ~ 11-32 mV (1-propanol) ~ 6-27 mV (2-propanol) | 1-propanol 2-propanol, propanal, acetone, propane | N/A | 10-50 ppm | synthetic air (20% $O_2$, 80% $N_2$), 25 °C, 0 and 40 %RH, negligible response to propane | 302/2014 |
| $M_3BTC_2$ (M = Co, Ni, Cd, Al) (3D) | **- Kelvin Probe: TiN/$M_3BTC_2$/Au** drop coating | potentiometry (CPD), e.g. in $N_2$: ~ 80 mV (50 ppm, n-butanol, M = Cd) | ethane, pentane, hexane, heptane, methanol, ethanol, 2-propanol, n-butanol | N/A | 10, 25,50 ppm | synthetic air (20% $O_2$, 80% $N_2$) and $N_2$, 25 °C, varying RH cross-sensitive to RH, similar responses regardless of M, stronger | 323/2014 |

Final edited form was published in "Chemical Reviews 2020, 120(1), S. 8581-8640. ISSN 1520-6890.
https://doi.org/10.1021/acs.chemrev.0c00033

| | | | | | | | |
|---|---|---|---|---|---|---|---|
| | | | | | | responses for alcohols | |
| $Cu_3BTC_2$ (3D) | **- Kelvin Probe: TiN/$Cu_3BTC_2$/Au** drop coating | potentiometry (CPD), for 10 ppm alcohols: 1-2.9 mV (40% RH) 9.3-21.8 mV (0% RH) | methanol, ethanol, 1-propanol 2-propanol | N/A | 2-50 ppm (linear response at 40%RH) (log response at 0%RH) | synthetic air (20% $O_2$, 80% $N_2$) and $N_2$, 25 °C, varying RH decreasing responses with increasing RH, highest sensitivity to 1-propanol | 324/2014 |
| $Zn_3BTC_2$ (3D) | **- Kelvin Probe: Au/$Zn_3BTC_2$/Au** drop coating | potentiometry (CPD), e.g. for 10 ppm propanol: ~0.02 mV (40% RH) ~0.07 mV (0% RH) | methanol, ethanol, propanol | N/A | 5-30 ppm | synthetic air (20% $O_2$, 80% $N_2$) and $N_2$, 25°C, varying RH, stronger responses for alcohols with longer alkyl chains | 300/2016 |
| M-MOF74 (M = Mg, Ni, Co, Zn) and en-Mg-MOF74 (en functionalized) (3D) | **- Kelvin Probe: Au/MOF-74/Au** drop coating | potentiometry (CPD), e.g. for en-Mg-MOF74: ~12 mV (4000 ppm, 40% RH) | $CO_2$ | N/A | 400-4000 ppm | synthetic air (20% $O_2$, 80% $N_2$) and $N_2$, 25°C, varying RH, decreasing responses with increasing RH, stronger response for Mg-MOF74, en -Mg-MOF shows higher responses and stability vs RH | 301/2016 |
| UiO-66-$NH_2$ (3D) | **- Kelvin Probe:** drop coating | potentiometry (CPD): ~75 mV (150 ppb, 0% RH) | DMMP | 0.3 ppb (0%RH) 2.0 ppb (50% RH) | 3-150 ppb | 0 and 50% RH | 304/2016 |

[a] The following are used throughout the table and are defined as follows: $G = 1/R$; $\Delta R = R_{gas}-R_0$; $\Delta G = G_{gas}-G_0$; $\Delta\sigma = \sigma_{gas} - \sigma_0$, $\Delta|Z = |Z|_{gas} - |Z|_0$, $\Delta C = C_{gas} - C_0$. Index '0' refers to values recorded in the absence of an analyte.

Final edited form was published in "Chemical Reviews 2020, 120(1), S. 8581-8640. ISSN 1520-6890.
https://doi.org/10.1021/acs.chemrev.0c00033

## 4. Logic and Memory

In this section we discuss recent progress toward integrating OFM into logic and memory devices. These devices enable data storage or logic processing via application of current or voltage to an OFM layer. Since the publication of the updated roadmap in 2017 by some of us,[9] several milestones in OFM-based devices have been realized. We emphasize that both the OFM chemistries and the processing/integration of OFM in electronic devices are important.[325] Here, we review state-of-the-art OFM-based logic and memory devices, including field-effect transistors and spintronics (resistance memories and switching are discussed in Section 5). The literature discussed highlights both the diversity of roles that OFM can play in these devices and recently developed understanding concerning the relevant structure-performance relationships.

### 4.1 (Semi-)Conducting MOFs for Field-Effect Transistors

Field-effect transistors (FETs) are arguably the most important class of microelectronic devices in modern physics from both scientific and application standpoints. FETs are fabricated on an insulating substrate by deposition of thin layers of the four main components: 1) source and drain electrodes between which the current is controlled; 2) a semiconductor as a variably conducting element; 3) an insulating gate dielectric; and 4) a gate electrode (Figure 14).[326,327] The thickness of each of these layers varies from few-nanometer electrode adhesion layers to few hundred-nanometer thick dielectric layers. Applying a voltage to the gate electrode causes charge carrier depletion or enhancement in the semiconductor, thereby tuning the current flowing between the source and drain terminals. In practical digital circuits, the device is optimized for ON/OFF switching based on the logic input on the gate terminal. In addition, FETs are also highly useful experimental tools for in-depth characterization of semiconductors. The threshold voltage and charge carrier mobility are two key parameters that determine the device performance.

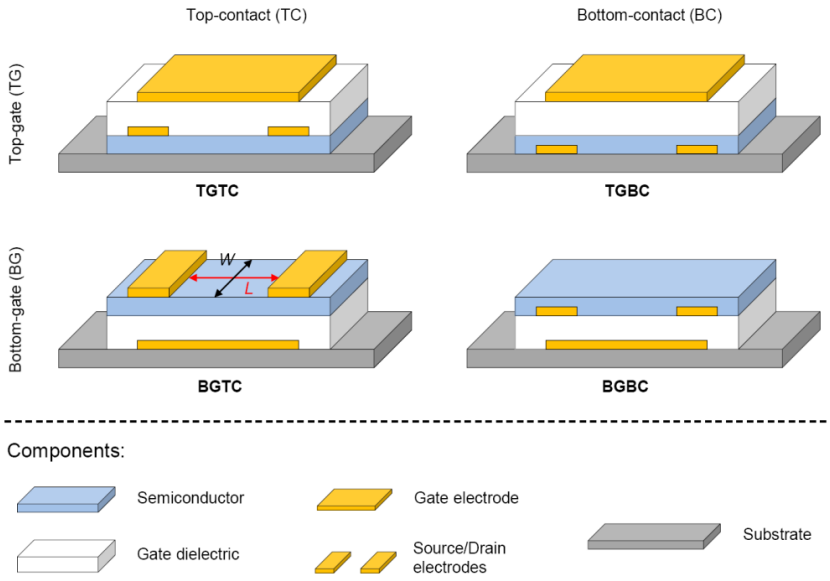


**Figure 14.** Scheme of the four fundamental FET structures: top gate, top contacts (TGTC); top gate, bottom contacts (TGBC); bottom gate, top contacts (BGTC); bottom gate, bottom contacts (BGBC). Reproduced with permission from Ref. 327. Copyright 2009 John Wiley & Sons, Inc.

Final edited form was published in "Chemical Reviews 2020, 120(1), S. 8581-8640. ISSN 1520-6890.
https://doi.org/10.1021/acs.chemrev.0c00033

Depending on the arrangement of the components, four typical FET structures result with top-gate (TG) or bottom-gate (BG) architecture in combination with top-contacts (TC) or bottom-contacts (BC). However, in all four types the insulating dielectric layer separates the gate electrode from the semiconductor and source/drain electrodes. The channel length (*L*) and channel width (*W*) are shown in the BGTC structure (Figure 14). Each of the four FET structures has advantages and disadvantages with regard to the electrical performance and device fabrication. An important process is the transfer of charge carriers between the source and drain electrodes and the semiconductor, which is accompanied by an energy barrier. Both experiments and simulations show that TGBC- and BGTC-FETs are less influenced by the barrier height than the other two. The TGBC architecture additionally provides self-encapsulation of the semiconducting layer and the channel area by the dielectric (Figure 14). This leads to improved device resistance to environmental influences. Moreover, TGBC FETs can be fabricated by large-scale printing technologies that in combination with organic materials/polymers affords low-cost, fully flexible electronic devices. In BGBC structures, the semiconductor is deposited on top of the source/drain electrodes and the electrode surface can be modified by organic monolayers or by thin metal oxide layers to decrease the impact of the energy barrier on the transfer efficiency of charge carriers. In contrast, the TGTC architecture does not allow modification of the electrode surface as the electrodes are deposited directly onto the semiconductor. Nevertheless, the BGBC structure tends to provide lower charge carrier mobility values compared to BGTC FETs. It should be noted that the thermal evaporation of metal source/drain electrodes through a shadow mask on top of the semiconductor can damage the organic material in the BGTC and TGTC architectures.

As will be evident below, significant progress has been made in synthesizing and characterizing new 2D MOFs, in both polycrystalline and single-crystal formats, and exploiting them for device integration. These developments are summarized in Table 2, which shows the reported FET performance based on conductive MOFs. These findings demonstrate the potential for developing MOFs as new types of active semiconductors for logic circuits, which already exhibit the advantages in chemical and structural diversity, inherent porosity, high performance, high stability and multi-functions. The challenges of rational band gap tuning, electrical conductivity enhancement, and facile processing for device fabrication are of burgeoning interest.

**Table 2. Performance of FET devices using conductive MOFs.**

| MOF | Conductivity type | FET structure | Electrical conductivity ($S\ cm^{-1}$) | Charge mobility ($cm^2(V•s)^{-1}$) | Threshold voltage (V) | On/off ratio | Ref. |
|---|---|---|---|---|---|---|---|
| Cu-BHT Polycryst. film | Metallic | BGTC | ~1580 | 99 (*h*) 116 (*e*) | - | 10 | 48 |
| Ni-HIB Polycryst. film | - | BGTC & BGBC | GΩ | - | - | - | 291 |
| $Ni_3HITP_2$ Polycryst. film | *p*-type | BGTC | 40 | 48.6 | ~1.1 | $2\times10^3$ | 293 |

| | | | | | | | |
|---|---|---|---|---|---|---|---|
| $K_xFe_2BDP_3$ ($0 \leqslant x \leqslant 2$) single crystal | *n*-type | BGBC | $10^{-2}$-$10^{-7}$ | $10^{-4}$-0.84 | - | - | 294 |

**4.1.1 2D Conjugated MOFs for FET devices.** Typical three-dimensional (3D) MOFs comprised of first-row transition metal ions and hard electron donors such as carboxylates lack supramolecular conjunction, leading to very low electrical conductivity (<$10^{-8}$ S/cm).[225] Several strategies to increase these to values useful for a variety of device applications have been demonstrated, including through-bond and through-space framework designs,[34,225] incorporating redox-active ligands into the frameworks,[328] and doping with guest molecules such as $I_2$[329]and TCNQ.[211] An early exception was Cu[Cu(pdt)$_2$] (pdt = 2,3-pyrazinedithiolate), reported by Kitagawa and coworkers in 2009, with a conductivity of $6\times10^{-4}$ S cm$^{-1}$ at 300 K.[330] The first FET to employ an OFM was reported by Gu and coworkers, who used $Cu_3BTC_2$ as the dielectric layer of a film-based organic FETs (OFETs).[296] The MOF thin film was first prepared by a liquid-phase epitaxial[331] approach to modify the $SiO_2$/Si substrate. A thiophene-based semiconducting polymer of PTB7-Th was then deposited on the MOF film surface followed by two top Au electrodes on the semiconducting film. This SURMOF/polymer-based OFET exhibited a hole mobility of ~1.0 $\times10^{-2}$ cm$^2$(V•s)$^{-1}$, an on/off ratio of $10^3$, and a threshold voltage less than 10 V. This performance was superior to that of an OFET without the SURMOF (average hole mobility of ~$5.0\times10^{-3}$ cm$^2$(V•s)$^{-1}$ and threshold voltage > 13 V). The performance enhancement was mainly attributed to the highly crystalline, homogeneous, and low-k $Cu_3BTC_2$ SURMOF grown on the $SiO_2$/Si substrate and the smaller interface trap density in the OFET. However, it was challenging to realize high-mobility semiconductive MOFs for logic electronics.

Recent advances in the synthesis and characterization of 2D conjugated MOFs is opening new possibilities for OFM-based electronic devices, in particular those requiring high charge mobility and either semiconducting or metallic behavior. These materials are layer-stacked structures comprised of planar ligands and linkages with high in-plane conjugation and weak out-plane van der Waals interaction, demonstrate that these have much higher electrical conductivities (>0.1 S cm$^{-1}$) than typical 3D frameworks.[39,40,226,325,332]. In 2012, Yaghi and coworkers[235] reported the first fully *π-d* conjugated, graphene-like 2D MOF, Cu-catecholates (HHTP-Cu), which exhibited room temperature (RT) conductivity as high as ~0.2 S cm$^{-1}$ (Figure 15). Since then, it has been commonly accepted that the development of highly conductive 2D MOFs strongly relies on the design of planar linking units and organic ligands for the construction of a *π-d* conjugated system. To date at least a dozen varieties of 2D conjugated MOFs have been reported, based on triphenylene (hexahydroxytriphenylene, HHTP;[235] hexaaminotriphenylene, HATP;[125] hexathiolatedtriphenylene, HTTP[333]; triphenylenehexaselenol, $H_6$TPHS;[334] phenylene(benzenehexathiol), BHT;[335] hexaaminobenzene, HAB;[336] triaminotrithiolatedbenzene, TATTB;[337] hexahydroxybenzene, HHB;[338] benzenehexaselenol, BHS;[339] phthalocyanine (Pc$M_1$NH;[340] Pc$M_1$OH[341-343]); coronene (perthiolatedcoronene, PTC[294,344]); and dibenzo[g,p]chrysene (dibenzo[g,p]chrysene-2,3,6,7,10,11,14,15-octaol, 8OH-DBC)[345] derivatives with functional groups (-OH, -$NH_2$, -SeH or -SH). Figure 15 presents selected 2D conjugated MOFs reported since 2012 and the corresponding performance in electrical conductivity and band gaps. The highest MOF electrical conductivities achieved are 40 S cm$^{-1}$, 160 S cm$^{-1}$, and 2500 S cm$^{-1}$ for 2D conjugated MOF films of HITP-Ni,[336] BHT-Ni[346] and BHT-Cu,[48] respectively. These materials have been integrated as electrode materials for applications in

electrocatalysis,[333,342,347-353] chemiresistive sensors (discussed in Section 3),[232,233,237-239,289] energy storage[345,354-360 361 362] and superconductivity.[363]

Final edited form was published in "Chemical Reviews 2020, 120(1), S. 8581-8640. ISSN 1520-6890.
https://doi.org/10.1021/acs.chemrev.0c00033

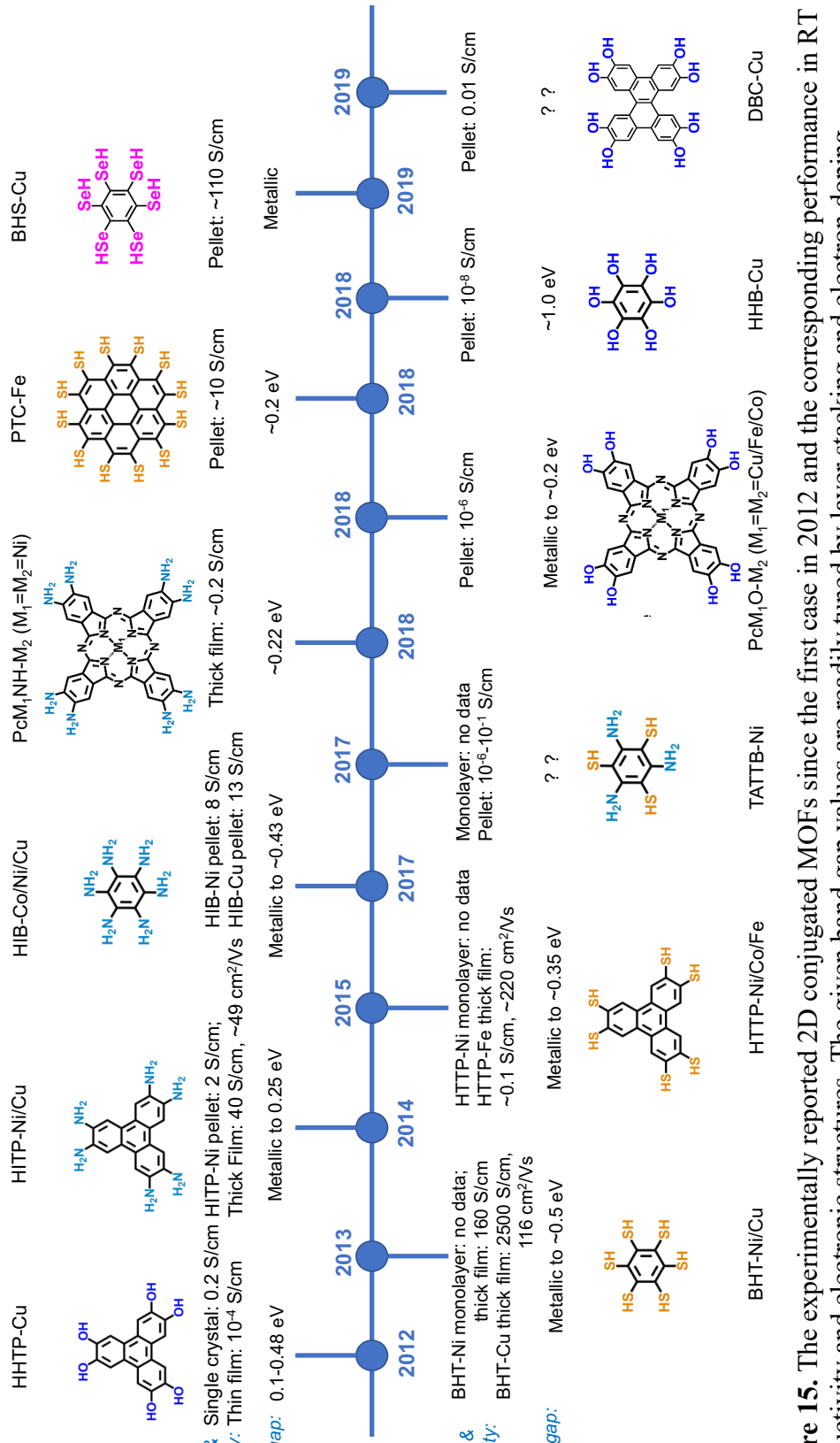


**Figure 15.** The experimentally reported 2D conjugated MOFs since the first case in 2012 and the corresponding performance in RT conductivity and electronic structures. The given band gap values are readily tuned by layer stacking and electron doping.

Final edited form was published in "Chemical Reviews 2020, 120(1), S. 8581-8640. ISSN 1520-6890.
https://doi.org/10.1021/acs.chemrev.0c00033

Early work by Nishihara and coworkers revealed that 2D MOF with high electrical conductivity are feasible. They synthesized multi-layer, crystalline BHT-Ni nanosheets with a lateral size of ~100 μm and a thickness of 1-2 μm at a $H_2O/CH_2Cl_2$ interface.[335] The authors further treated as-prepared film with tris(4-bromophenyl)ammoniumyl hexachloroantimonate, which led to a oxidized nanosheet. The as-prepared film displayed a conductivity of 2.8 S $cm^{-1}$ by four-probe measurement based on van der Pauw pattern, whereas the oxidized sheet exhibited conductivity as high as $1.6 \times 10^2$ S $cm^{-1}$. Both BHT-Ni sheets showed increased conductivity upon heating, with activation energies of 26 and 10 meV, respectively, suggesting the material is a semiconductor. However, the photoelectron spectroscopy and first-principles calculations indicate that both samples are metallic.

Further exploration of 2D structures formed from BHT and related ligands demonstrates that these materials can exhibit both unusual electronic behaviors (e.g. metal-semiconductor transformations) and exceptional charge transport properties. Zhu and co-workers replaced the Ni centers with Cu centers in BHT-Ni and synthesized free-standing, polycrystalline BHT-Cu 2D MOF films with thickness that could be tailored from 20 nm to 200 nm at the $CH_2Cl_2/H_2O$ interface (Figures 16a).[48] Synchrotron GIXRD and XPS analysis suggested that the BHT-Cu possessed a 2D lattice in the formula of $[Cu_3C_6S_6]_n$ with a hexagonal unit cell ($a = b = 8.76$ Å and $c = 3.38$ Å) in a AA stacking mode (Figure 16b). An in-line four-probe conductivity measurement revealed a high conductivity of $1.58 \times 10^3$ S/cm in a 150 nm-thick film at 300 K and the conductivity decreased upon cooling (Figure 16c). Later Nishihara and coworkers[346] combined the reported ultraviolet photoemission valance band spectrum[342] with band structure calculations to reveal that this material is also metallic in nature. To further characterize the charge transport properties, a FET device was built with a BGBC device geometry on a $SiO_2/Si$ substrate and 30 nm-thick gold patterns as the source and drain electrodes (Figure 16d). The FET measurements showed an ambipolar charge transport behavior with high carrier mobilities (99 $cm^2(V•s)^{-1}$ for holes and 116 $cm^2(V•s)^{-1}$ for electrons) but a small on/off ratio (~10). This behavior is typical for a FET fabricated from a gapless conductor. However, the observed mobility surpasses all previously reported organic ambipolar devices. Recently, Melot and Marinescu et al. demonstrated an unprecedented transition from a metal to a semiconductor in a polycrystalline $Co_3(HTTP)_2$ 2D MOF films upon heating from 50 K to 350 K.[127] The transition temperature largely depends on the film thickness, the solvents trapped in the pores and the oxidation of the metal centers.[126] These intriguing but also apparently conflicting results clearly indicate that additional research concerning the manipulation of the electronic band structure of these materials is needed. For example, strategies such as doping or modulation of the effective carrier mass value by temperature could lead to very promising FET devices based on similar coordination polymers.

Final edited form was published in "Chemical Reviews 2020, 120(1), S. 8581-8640. ISSN 1520-6890.
https://doi.org/10.1021/acs.chemrev.0c00033

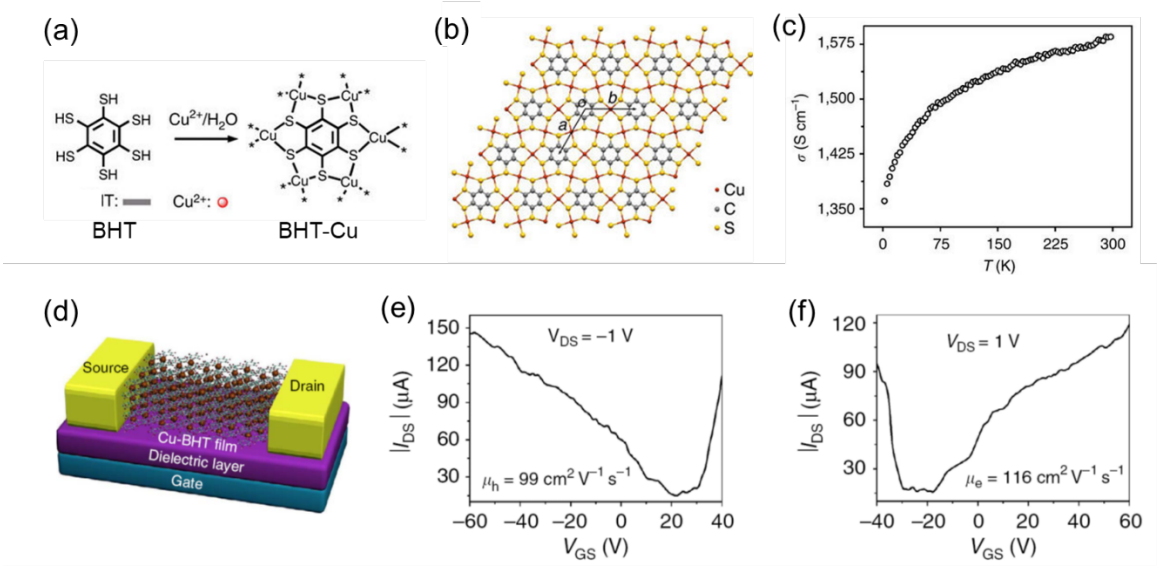


**Figure 16**. (a) Schematic synthesis of BHT-Cu MOF. (b) Schematic structure of the 2D lattice of BHT-Cu with cell parameters of $a = b = 8.76$ Å. (c) Temperature-variable conductivity measurement on a 150-nm film by in-line four-probe method. (d) Illustrative scheme of BHT-Cu-based FET. (e and f) Output characteristics of BHT-Cu-based FET. Reproduced with permission from Ref. 48. Copyright 2015 Nature Publishing Group.

In 2017, a new family of 2D conjugated MOF films was reported by coupling hexaiminobenzene (HAB) ligands with a series of metal centres ($Ni^{2+}$, $Cu^{2+}$, $Co^{2+}$) employing interfacial synthesis strategy.[291]The polycrystalline layer-stacked films were prepared with thickness raging from <10 nm to 2 μm. HAB-Ni MOF film was integrated into a BGTC-type FET device and showed a gate-dependent conductance down to 4 K. However, due to the low crystallinity of these MOF films, the resistance dropped in the GΩ range. Subsequently, Dincă and co-workers synthesized highly crystalline $M_3(HIB)_2$ MOF (M = Cu and Ni) by the solvothermal method.[336] The electrical conductivity of the pressed pellets, measured by the van der Pauw method under vacuum and in the dark, was 8.0 S cm$^{-1}$ for $Ni_3(HIB)_2$ and 13 S cm$^{-1}$ in $Cu_3(HIB)_2$ at 300 K. The variable-temperature conductivity measurement showed an increase of conductivity from 200 to 400 K, revealing a semiconducting behavior in $M_3(HIB)_2$. DFT calculations revealed anisotropic electrical properties in both MOFs with metallic character in the ab direction and semiconducting character in the c direction of the Brillouin zone. The authors concluded that the thermally activated hopping over grain boundaries (i.e., interparticle transport) dominated the temperature dependence of conductivity in the bulk polycrystalline pellets, giving rise to apparent semiconducting behavior in otherwise intrinsically metallic solids.

The materials discussed above reveal the potential of 2D conjugated MOFs as a new generation of electroactive layers, although their performance is still limited for a logic electronic device. In 2014, Dincă et al. utilized the HATP monomers and achieved the hydrothermal synthesis of polycrystalline $Ni_3(HITP)_2$ 2D MOF film with a thickness of ~500 nm by placing a quartz substrate in the bulk solution. [125] Although the obtained film was not homogeneous or smooth, as discussed above it behaves as a semiconductor with a high conductivity of 40 S cm$^{-1}$. However, the corresponding semiconducting parameters, including charge carrier type, carrier mobility, and

Final edited form was published in "Chemical Reviews 2020, 120(1), S. 8581-8640. ISSN 1520-6890.
https://doi.org/10.1021/acs.chemrev.0c00033

carrier concentration, remain to be determined. As mentioned in Section 3.1.1, single-crystalline rods of $Ni_3(HITP)_2$ were integrated into a four-probe device by the same group recently, which revealed higher conductivity up to 150 S $cm^{-1}$.[240] In 2017, Xu et al. employed an air-liquid interfacial growth method to prepare a high-quality, free-standing, polycrystalline $Ni_3(HITP)_2$ film with smooth (RMS roughness of ~1 nm) and dense surface.[293] MOF films were initially transferred onto the solid substrates via a Langmuir–Schaefer transfer method. Next, a FET device was fabricated by a BGTC device geometry based on a 105 nm-thick membrane as the active channel material, 50 nm thick Au thin films as the source and drain electrodes, and heavily doped *p*-type Si as the gate electrode. From the transfer characteristics of five devices, *p*-type depletion behavior and a typical threshold voltage of ~1.1 V and a high carrier mobility of 48.6 $cm^2(V•s)^{-1}$ were found. The device moreover displayed on/off current ratios as high as 2000. The observed mobility is competitive with state-of-the-art solution-processed organic and inorganic semiconductors, a remarkable feature for a material that consists for a significant part of empty pore space. The authors pointed out that no saturation current was observed and that the device showed gapless conductor behavior, similar to the BHT-Cu case.

**4.1.2 Conductivity mechanisms.** The above-reported 2D conjugated MOFs display exciting electrical conductivity and potential for logic electronic circuits, but the nature of the charge transport remains ambiguous. Very recently, Dong et al.[49] reported a study of MOF conductivity using time-resolved terahertz spectroscopy (TRTS), an all-optical, contact-free method capable of addressing the nature of charge transport.[364] These authors synthesized a large-area free-standing multilayer $(NH_4)_3Fe_3(THT)_2$ 2D MOF film by an interfacial method in which aqueous and $CHCl_3$ phases host THT and iron precursors, respectively (Figure 17a). The film thickness is tunable by the reaction time (from 20 nm to ~2 μm after 72 reaction hours). DFT calculation of the electronic structures revealed a semiconducting behaviour with a bandgap of ~350 meV. The achieved porous thin films of $(NH_4)_3Fe_3(THT)_2$ supported band-like charge carrier transport, directly demonstrated from the observed Drude-type complex photoconductivity. A room temperature mobility of ~220 $cm^2(V•s)^{-1}$ was estimated from TRTS (Figure 17b), which represented a record mobility in the reported MOFs. Notably, this mobility value was independently verified using Hall effect measurements based on a Hall bar structure of the $(NH_4)_3Fe_3(THT)_2$ film (Inset image in Figure 17c). The Hall geometry of the MOF layer on a $Si/SiO_2$ (300 nm) wafer was fabricated using cold ablation via ultrafast laser pulses. After that, a 5 nm-thick Cr layer and a 150 nm-thick Au layer were deposited as the metallic contacts by electron beam lithography. The Hall effects were investigated with temperature from 100 K to RT and a vertical magnetic field that reached ±2.5 T. The quantitative agreement between the inferred THz and Hall mobilities demonstrated that band-like charge carrier transport was operative in the samples in both, the AC and DC limit. The analysis of the temperature dependence for the conductivity from both methods revealed that scattering rates and hence mobilities are primarily limited by impurity scattering so that the inferred mobilities constitute lower limits (Figure 17b). Thermally excited carriers were responsible for the temperature dependence of the four-probe conductivity, as opposed to a reduction in the DC mobility of the carriers (Figure 17c). These results illustrated the potential for high-mobility semiconducting MOFs as active materials in thin film optoelectronic devices.

Final edited form was published in "Chemical Reviews 2020, 120(1), S. 8581-8640. ISSN 1520-6890.
https://doi.org/10.1021/acs.chemrev.0c00033

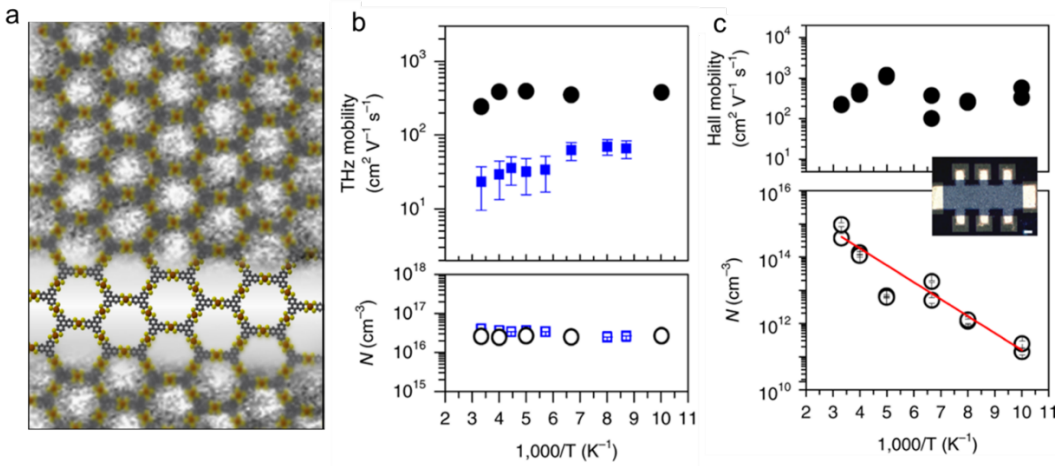


**Figure 17.** (a) A high-resolution transmission electron microscopy image of the $(NH_4)_3Fe_3(THT)_2$ 2D conjugated MOF together with the structural schematic (grey, yellow and orange: carbon, sulfur and iron atoms, respectively). (b and c) Charge transport studies by THz spectroscopy and Hall effect measurements, respectively. Scale bar: 100 μm. Reproduced with permission from Ref. 49. Copyright 2018 Nature Publishing Group.

Despite the initial success in obtaining efficient charge transport in 2D conjugated MOFs, many key issues remain to be addressed. In particular, the electrical properties throughout powders or films of these materials can be highly inhomogeneous. This results from a combination of small crystalline domains (tens of nanometers in size are typical), grain boundaries, defects, and the random orientation of nanocrystals. These morphological and microstructural features severely limit effective electron delocalization and long-range charge transport. Defects generated by uncoordinated sites, edges, and impurities are equivalent to heavily doping the 2D conjugated MOFs, causing variations in the electronic structures that are difficult to eliminate. Film quality is still far from sufficient for reliable device performance; control over lateral dimensions, thickness, and uniformity at a large-scale is still very limited. Moreover, tailoring of 2D MOF structures at the molecular scale is still quite difficult due to the limited variety of organic ligands and synthetic methodologies for assembling them into MOFs. Beyond the state-of-the-art, highly crystalline 2D conjugated MOF monolayershave not yet been achieved. These critical synthetic issues have hampered efforts to achieve a full understanding of intrinsic charge transport features in 2D conjugated MOFs.

DFT and other theoretical approaches are shedding insight into the detailed nature of intrinsic charge transport in 2D OFM, however. A wide variety of electronic states are predicted, some of which are highly unusual and indicative of topological insulator (TI) behavior. For example, band structure calculations with spin orbit coupling (SOC) near the Fermi level reveal that an undoped BHT-Ni monolayer is a narrow-gap semiconductor with an indirect gap of ~0.11 eV,[365] whereas a TI state is predicted in both a Dirac band and a flat band opened up by SOC ~0.5 eV above the undoped Fermi level. The band gap of the Dirac band is $\Delta 1$ = 13.6 meV, while the band gap between the flat band and the top branch of the Dirac band is $\Delta 2$ = 5.8 meV. From the edge state calculation the nontrivial topological gapless edge states can be recognized, which connect the band edge states between $K$ and $K'$ to form a 1D Dirac cone at the boundary of the Brillouin zone, signifying a 2D TI. It has also been confirmed that the high structural tunability available in 2D conjugated MOFs allows their electronic structure to be engineered by varying the metal ion and

Final edited form was published in "Chemical Reviews 2020, 120(1), S. 8581-8640. ISSN 1520-6890.
https://doi.org/10.1021/acs.chemrev.0c00033

molecular ligands as well as by various layer stacking arrangements (Figure 15). For example, DFT calculations predict that bulk HTB-Ni is metallic.[366] In contrast, monolayer HITP-Ni is predicted to be a semiconductor with a small indirect band gap (~0.12-0.25 eV), but converting to structures with two or more layers shrinks the band gap to zero, making it metallic.[367,368] When Ni is replaced by Cu, the monolayer is metallic.[369] It is thus evident that the highly delocalized electronic states expected for the 2D conjugated MOFs not only improves the intrinsic electrical conductivity but also creates the potential to use these materials as electroactive layers in logic circuit applications.

Although very intriguing, these predictions are not in full agreement with experiment. The temperature-dependent electrical conductivity and Seebeck coeeficient measurements of HITP-Ni demonstrate that it is an n-type semiconductor.[125,370] In contrast, the transfer curve measured for a HITP-Ni FET device indicates that the material is p-type and displayed gapless conductivity behavior.[293]An explanation for the semiconducting-metallic discrepancy was provided by theoretical consideration of the effects of grain boundary, strike-slip, and layer-layer displacement defects. DFT calculations showed that, for example, interlayer discplacements can produce bandgaps ranging from nearly zero to 0.16 eV.[368] This hypothesis is supported by recent four-point probe conductivity measurements by Day et al.,[240] who found non-zero conductivity near 0 K for a single-crystal device, consistent with metallic behavior. In contrast, a polycrystalline device showed conductivity approaching zero at 0 K, in agreement with semiconducting behavior. These results highlight the need for better understanding of OFM defects as well to develop film growth methods with reproducible defect concentrations or alternatively, processes that can nucleate single-crystal OFM on device substrates.

In addition, it is still an open question whether high-performance electrically conductive MOFs necessarily require the incorporation of in-plane conjugated structures. A series of recently reported layered HHTP-lanthanide MOFs have metal centers located in-between the linker layers were synthesized.[371] The HHTP-lanthanide MOFs do not possess in-plane $\pi$-$d$ conjugation but nevertheless display high electrical conductivity (up to 0.05 S $cm^{-1}$). These findings demonstrate that charge transport by $\pi$-$\pi$ stacking between organic ligands also contributes to the high bulk conductivities.[240]

### 4.1.3 Single-crystal MOF-based FETs

A challenge in fabricating OFM-based FETs stems from the fact that charge transport occurs only in the first few molecular layers of the semiconductor. Electronic percolation within these layers is required for device operation. Importantly for polycrystalline OFM films, several effects of the particle-particle and semiconductor-dielectric interfaces, such as grain boundaries, interfacial adhesion, and roughness, affect contact quality and charge carrier transport and are therefore expected to interfere with the interpretation of the device performance. Single crystal OFM-based FETs should minimize such effects and allow the intrinsic charge transport properties to be determined. Unfortunately, methods of growing single-crystal OFM layers have yet to be developed that can be used for wafer-scale patterning and fabrication of devices for both measurement of charge transport properties as well as logic and memory functions.

Until the recent work by Day et al., measurements of charge transport in MOFs have been limited to studies of pressed pellets[372] and analysis of data obtained from polycrystalline thin films. However, such measurements often probe only interparticle or grain boundary contacts, precluding a fundamental understanding of long-range charge transport. Contactless measurements can

Final edited form was published in "Chemical Reviews 2020, 120(1), S. 8581-8640. ISSN 1520-6890.
https://doi.org/10.1021/acs.chemrev.0c00033

provide a good probe of intrinsic charge transport, such as flash photolysis time-resolved microwave conductivity (FP-TRMC)[294,373] and time-resolved terahertz spectroscopy,[49,343] although they cannot directly yield the sign of the charge carriers. This knowledge can be obtained from measurements of the Seebeck coefficient. [212,370,374]Development of growth methods for single crystals and techniques to delaminate them into single layers will enable not only fundamental studies of structure–properties relations, but also the development of MOF-based functional devices when long-range free carrier motion is required. For example, single-crystal FET measurements enable determination of both the mobility and charge carrier sign, while the devices can be fabricated to resemble functional architectures. However, reports of single-crystal MOF FETs are still rather limited. Two recent reports from Long and coworkers (Aubrey et al.[294]) and Dincă and coworkers (Xie et al.[375]) made a major contribution to the understanding electrical conductivity measurements on MOFs, highlighting the importance of single crystal devices to achieve a reliable fundamental understanding of the structure-electronic property relationship.

Aubrey et al. fabricated single-crystal FET devices through drop-casting $K_xFe_2(BDP)_3$ ($0 \leq x \leq 2$; BDP = 1,4-benzenedipyrazolate, Fe(II)/Fe(III) mixed-valence) onto FET-ready silicon substrates prefabricated with interdigitated microelectrode arrays.[294] $Fe_2(BDP)_3$ MOF comprises one-dimensional chains of $\mu^2$-pyrazolate-bridged iron(III) octahedra oriented parallel to the (001) direction. Here, the controlled reductive insertion of potassium into $Fe_2(BDP)_3$ to access $K_xFe_2(BDP)_3$, which exhibits a mixed-valence state for a range of $x$, together with broad-band charge delocalization. The achieved $K_xFe_2(BDP)_3$ consists of a polydisperse mixture of acicular microcrystals ranging in size from less than 100 nm to greater than 20 μm in length. Significantly, the long axis of each crystal is parallel to the pyrazolate-bridged iron chains, the expected direction for conduction. Then, platinum/carbon composite contacts were deposited at the interface between the single microcrystals and the patterned microelectrodes to improve mechanical stability and increase contact area. The transfer current outputs were measured based on the single-crystal FET devices and the related carrier mobilities were obtained with varying the K composition. The transcurrent in $Fe_2(BDP)_3$ device increases with both positive and negative gating voltages, corresponding to an ambipolar charge transport. The calculated average electron and hole mobilities of $Fe_2(BDP)_3$ are $\mu_e = 2 \times 10^{-3}$ $cm^2(V•s)^{-1}$ and $\mu_h = 6 \times 10^{-4}$ $cm^2(V•s)^{-1}$, respectively. Upon reduction of potassium naphthalenide up to $K_{0.98}Fe_2(BDP)_3$, the trans currents increased and a peak electron mobility of 0.84 $cm^2(V•s)^{-1}$ was achieved, and then slightly decreased on further reduction. The conductivity also increased from $3.53\times10^{-7}$ S $cm^{-1}$ to 0.025 S $cm^{-1}$ of the reduced $K_{0.98}Fe_2(BDP)_3$. The above single-crystal FET measurements reveal that the added electrons are delocalized over the framework as conduction electrons. In contrast, two-contact, pressed pellet measurements of $K_{0.98}Fe_2(BDP)_3$ gave conductivities at least a million times lower than comparable single-crystal measurements, exemplifying the extreme anisotropy of transport and suggesting that $K_xFe_2(BDP)_3$ is a one-dimensional conductor. Based on this work, the single-crystal FET measurements provide a path towards maximizing conductivity and understanding the underlying electronic structures of this mixed-valence MOF.

Dincă and coworkers investigated the systematic variation of the doping level,[375] i. e., the ratio between $Fe^{2+}/Fe^{3+}$ defects in $Fe_2(BDT)_3$ single crystals and their impact on the electrical conductivity of the MOF. Orange-red single crystals of $Fe_2(BDT)_3$ were isolated under oxygen-free conditions. Upon exposure to air from 1 h to 30 days, $Fe_2(BDT)_3$ crystals undergo a color change from orange to deep black attributed to the oxidation of $Fe^{2+}$ to $Fe^{3+}$. A conductivity measurement on a two-probe single-crystal device of $Fe_2(BDT)_3$ revealed that the electrical conductivity at room temperature increased from $6\times10^{-5}$ S $cm^{-1}$ to 1.8 S $cm^{-1}$. An intervalence

charge transfer (IVCT) between $Fe^{2+}$ and $Fe^{3+}$ led to the population of mid-gap states and thereby to an enhancement in electrical conductivity.[376] These findings based on the single-crystal conductivity measurement demonstrate that inducing metal-based mixed valency is a powerful strategy toward realizing high and systematically tunable electrical conductivity in MOFs.

Finally, in a 2019 work by Pathak et al.,[377] a single crystalline MOF $\{[Cu_2(6\text{-Hmna})(6\text{-mn})]\cdot NH_4\}_n$(6-Hmna = 6-mercaptonicotinic acid, 6-mn = 6-mercaptonicotinate), consisting of a two dimensional $(–Cu–S–)_n$plane, was synthesized from the reaction of $Cu(NO_3)_2$, and 6,6′-dithiodinicotinic acid via the *in situ* cleavage of S-S bonds under hydrothermal conditions. This MOF exhibited a low band gap of 1.34 eV and a high electrical conductivity of ~11 S $cm^{-1}$ based on a four-probe single-crystal device. The integration of $(–Cu–S–)_n$ planes provided a suitable path for facilitating the transfer of electrons along the frameworks, leading to a significant enhancement in electrical conductivity.

### 4.2 Conducting 2D conjugated COFs

COFs are a remarkable class of porous polymers that allow atomically precise linking of building blocks by covalent bonds to form extended structures with periodic skeletons and ordered nanopores.[3,83,378] In 2005, Yaghi and co-workers reported the first example of layer-stacked crystalline 2D COF composed of repeating benzene rings linked by boroxine.[379] Generally, 2D COFs are synthesized from planar building blocks to provide layer-stacked structures that feature the extended planar network and periodic columnar $\pi$-arrays aligned with an atomic precision in vertical direction, i.e., strong in-plane covalent bonding and weak out-plane van der Waals force. Since then, more than one hundred 2D COFs with various porous structures have been synthesized, employing abundant organic building blocks and a rich array of linkage chemistries, including boronate, imine, hydrozone, azine, squaraine, pyrazine, imide, benzimidazole and triazine.[245 244] Due to their chemical and structural diversity, high chemical and thermal stability, porosity and crystallinity, 2D COFs have attracted considerable attention over the past decade with potential applications in gas storage,[380,381] separation,[382-385] catalysis,[386-388] sensing,[241,389] proton conductor,[390-392] optics,[393] magnetics,[394-397] and energy conversion[398] and storage.[399-404]

During the last decade, 2D COFs also have been considered for optoelectronic applications. However, most 2D COFs exhibit extremely low electrical conductivity (< $10^{-10}$ S/cm), which has limited their transport performance in electronic devices. In 2008, Jiang and co-workers reported a *p*-type semiconducting boronic ester TP-COF with pyrene moieties in the backbone through the co-condensation of pyrene-2,7-diboronic acid and 2,3,6,7,10,11-hexahydroxytriphenylene (HHTP).[405] Its electrical conductivity was measured using a two-probe method. The *I-V* profile of TP-COF showed a current of 4.3 nA at 2 V bias voltage compared to only 79 pA for a sample composed of COF precursors. Subseqquently, improved electronic properties were achieved in 2D $\pi$-conjugated COFs by systematic engineering of the framework to favor extended conjugation. For example, integrating photoconductive $\pi$-conjugated building blocks into 2D COF backbones, such as pyrene, thiophene, tetrathiafulvalene, porphyrin, hexabenzocoronene, and phthalocyanine,[406-411] or by employing conjugated linkers such as carbon-carbon bonds[397,412,413] and pyrazine linkages,[241,414,415] yielded 2D COFs constituting a new generation of organic semiconductors. [245,416-419]

Until now, various *p*-, *n*- and ambipolar-type 2D-conjugated COFs have been reported in which their bandgap, ranging from 0.5 eV to 2.5 eV, and HOMO/LUMO levels could be tuned.[83,101,246,378,386,397,405,408,410,411,416,420-433] This high degree of bandgap tunability results from the

Final edited form was published in "Chemical Reviews 2020, 120(1), S. 8581-8640. ISSN 1520-6890.
https://doi.org/10.1021/acs.chemrev.0c00033

wide variety of the building blocks, including those with modified functional groups and various numbers of aromatic building blocks, as well as the pore geometry, layer stacking arrangement, and the degree of π conjugation. Generally, layered 2D COFs exhibit anisotropic charge transport in which the charges prefer to move along the stacked columns. This typically yields intrinsic electrical conductivities of $10^{-10}$-$10^{-6}$ S cm$^{-1}$ for pellet samples.[434] Upon doping with TCNQ or $I_2$, the conductivity can increase to as high as ~$3\times10^{-3}$ S cm$^{-1}$.[397,420] For example, Gu, Ma and coworkers[435] recently demonstrated a record intrinsic electrical conductivity of ~$4\times10^{-3}$ S cm$^{-1}$ along the columnar stacking direction in an imine-based charged 2D COF thin film. Along the in-plane direction, however, the material displays insulating behavior, exemplifying the anisotropic transport behavior in this class of 2D COFs.

Carrier mobilities have also been measured for some 2D conjugated COFs. Values in the 1 – 10 cm$^2$(V•s)$^{-1}$ range are found, comparable to crystalline organic semiconductors but a factor of ten or more lower than the best MOFs.[34,49] A pyrazine-linked triphenylene/pyrene-based 2D conjugated COF was found to have a charge carrier mobility (AC limit) as high as 4.2 cm$^2$(V•s)$^{-1}$ measured by FP-TRMC,[414] whereas a porphyrin-based 2D conjugated COF linked by imine bonds exhibited a an even higher mobility of 8.1 cm$^2$(V•s)$^{-1}$ (AC limit) estimated by FP-TRMC at room temperature.[408] In a recent report, Dong, Feng and coworkers introduced two novel pyrazine(pz)-linked metal-phthalocyanine (MPc)-based conjugated 2D COFs (MPc-pz, M = Zn or Cu), that assembled as van der Waals (vdWs) layer-stacked structures.[434] The MPc-pz materials were synthesized by condensation of 2,3,9,10,16,17,23,24-octaamino-phthalocyaninato metal [II] (OAPcZn or OAPcCu) and tert-butylpyrene-tetraone (tBu-PT) under solvothermal conditions. The resulting materials are polycrystalline p-type semiconductors with calculated band gaps of ~0.6 eV. Hall effect, Van der Pauw, and time-resolved terahertz spectroscopy measurements were coupled with DFT calculations to identify the intrinsic and extrinsic factors controlling the electronic structure and charge transport properties of these COFs. The room-temperature electrical properties were not remarkable: conductivity (~$5\times10^{-7}$ S cm$^{-1}$), charge density (~$10^{12}$ cm$^{-3}$), charge carrier scattering rate (~$3\times10^{13}$ s$^{-1}$), and effective mass (~$2.3m^0$) of the majority carriers (holes). Not surprisingly, changing the metal center in the phthalocyanine moiety from Cu to Zn has a negligible effect on these. However, when compared with state-of-the-art semiconducting COFs, a record mobility up to ~5 cm$^2$(V•s)$^{-1}$ was resolved in the dc limit, which was limited by long-range charge carrier transport across crystalline grain boundaries in the pelletized samples. Both materials revealed a drop in the conductivity upon sample cooling, typical semiconducting behavior, with almost identical activation energies (0.34±0.1 eV). Notably, charge transport was found to be highly anisotropic, with hole mobilities being practically null in-plane and finite out-of-plane for the developed 2D COFs. This work further highlights the potential of high mobility π-conjugated 2D COFs as semiconductors for (opto-)electronics and provides a rational approach to ascertain structure-property relationships. It also suggests that detailed analysis of charge transport properties may offer a reliable path for designing and developing semiconducting COF materials with improved charge transport properties.

### 4.3 Fabrication of COF-enabled devices

Despite their promising charge transport properties, electronic devices integrating insoluble bulk 2D COF powders often exhibit lower efficiency than expected due to challenges in device processing and heterogeneous features arising from interparticle interactions, disordered stacking, crystalline grain boundaries, and defects.[436] Consequently, the development of homogeneous 2D

Final edited form was published in "Chemical Reviews 2020, 120(1), S. 8581-8640. ISSN 1520-6890.
https://doi.org/10.1021/acs.chemrev.0c00033

COF thin films with controlled thickness, morphology, and crystallinity is essential for realizing the full potential of these materials in devices such as FET.[38]

Interface-assisted synthesis, including gas-solid, liquid-solid, air-water and liquid-liquid interfaces, has provided a pathway to prepare large-area thin films of 2D COFs with long-range ordered structures and tailored thickness.[325,332,384,385,437-440] On-surface synthesis under ultrahigh vacuum based on dynamic covalent chemistry (e.g. boronic acid dehydration and Schiff-base reactions) can result in single-layer, structurally-defined 2D COFs.[441-444] However, the crystalline domain size is usually limited to a few dozens of nanometers. Moreover, lift off of COF networks grown on HOPG or Au surfaces and transfer onto various substrates is difficult. As an alternative, an *in-situ* synthesis process can be performed in which the desired substrate is immersed in the reaction mixture, leading to COF film deposition on the substrate via the in-situ condensation reaction. Dichtel and coworkers demonstrated this approach,[445] reporting the growth of oriented thin COF-5 films via condensation of 1,4-phenylenebis(boronic acid) (PBBA) and HHTP on copper (or $SiO_2$)-supported single-layer graphene surface. They successfully obtained oriented thin films with a thickness of ~195 nm, corresponding to ~580 layers. The COF layers are deposited parallel to the substrate and therefore the columnar stacks are positioned in a perpendicular manner. This fabrication technique facilitated the study of the effect of the substrates on the growth of COF films and provided a promising route for the integration of COFs into a variety of devices such as organic photovoltaics.

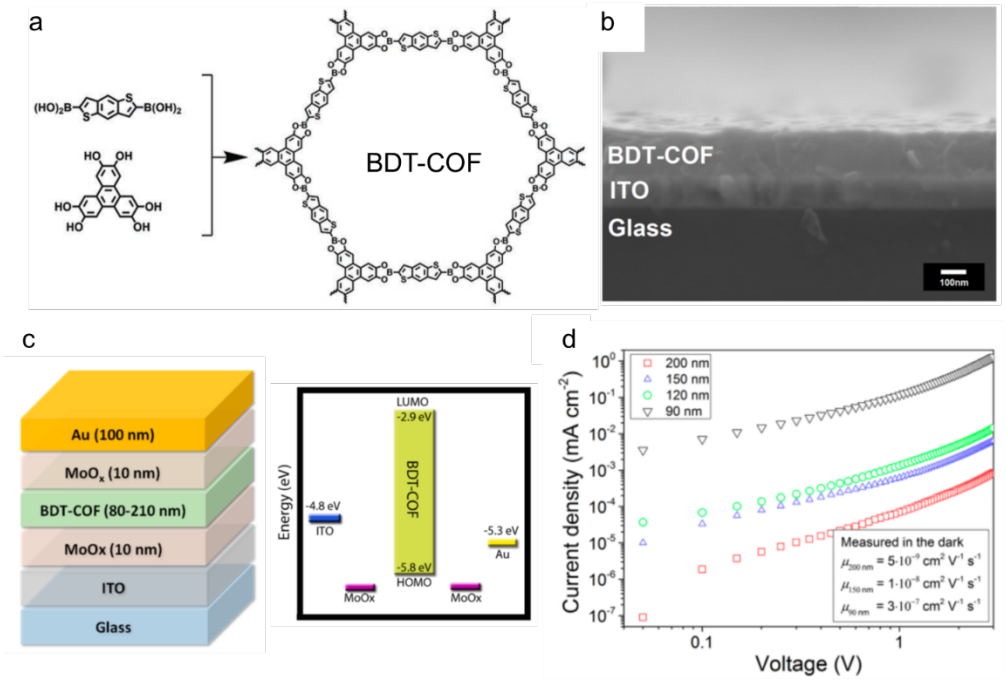


**Figure 18.** (a) Schematic structure of semiconducting BDF-COF. (b) SEM image of BDT-COF thin-film cross section with estimated film thickness of 200 nm on ITO/glass. (c) COF hole-only device layout and the corresponding energy diagram. (d) Current density as a function of voltage (J−V) of hole-only devices containing BDT-COF layers of different film thicknesses. Reproduced with permission from Ref. 428. Copyright 2017 American Chemical Society.

Final edited form was published in "Chemical Reviews 2020, 120(1), S. 8581-8640. ISSN 1520-6890.
https://doi.org/10.1021/acs.chemrev.0c00033

By extending this *in-situ* deposition method, Bein et al. developed a room-temperature vapor-assisted conversion strategy to synthesize benzodithiophene-based BDT-COF film (Figure 18a) via the condensation of 2,3,6,7,10,11-hexahydroxytriphenylene (HHTP) and benzo[1,2-b:4,5-b′]dithiophene-2,6-diyldiboronic acid (BDTBA) on a variety of solid surfaces (such as $SiO_2$ and ITO glass). [63,428,446] The achieved 2D COF films exhibited high crystallinity with hexagonal patterns and tailored film thickness ranging from 90 to 300 nm (Figure 18b). The achievement of continuous 2D COF films on glass surfaces enabled them to be incorporated into devices, enabling their directional charge-carrier transport behavior to be probed.[428] In this case, the in-plane electrical conductivity of up to $5 \times 10^{-7}$ S $cm^{-1}$ was obtained for oriented 90 nm-thick BDT-COF films. The columnar hole mobility was measured in a diode configuration by constructing hole-only devices with the following architecture: Glass/ITO/$MoO_x$/BDT-COF(80-210nm)/$MoO_x$/Au (Figure 18c). Measurements preformed in the dark revealed a thickness dependency of the columnar charge transport, where thinner films exhibited higher hole-mobilities of $3 \times 10^{-7}$ $cm^2(V•s)^{-1}$ compared than thicker films (Figure 18d). This was attributed to intrinsic electronic defects within the stacks of the BDT-COF layers. In addition, under illumination an enhanced hole mobility was observed, thus demonstrating that BDT-COF is a photoactive semiconductor.

By employing a wet-interfacial strategy, Bao and coworkers accomplished large-area, imine-based 2D COF film synthesis (polyTB, consisting of a BDT core bearing extended alkoxy chains and triphenylamine) with controlled thickness from ~2 to 150 nm at a dimethylformamide(DMF)/air interface.[411] Following transfer of the thin film onto a glass substrate, the HOMO and LUMO energies were estimated by UV-Vis and photoelectron spectroscopy to be 5.5 eV and 3.5 eV, respectively. Although the resultant film lacked high crystallinity compared with its powder state, it was self-supporting, allowing facile lift off and transfer onto desired substrates for FET studies (Figure 19a). In this case, the polyTB thin film was transferred to a degenerately doped ($n^{++}$), 2 × 2 cm Si wafer with a 300 nm oxide layer. Then, a 40-nm thick Au source and drain top contacts were deposited through a shadow mask, defining a top-contact transistor with channel length and width of 50 and 4000 μm, respectively. Applying a potential between the source and drain ($V_{SD}$) up to −100 V yielded very low current (<10 pA). However, applying an additional gate voltage ($V_G$), caused the source-drain current [447] to rise by two orders of magnitude (Figure 19b). A charge carrier mobility of $3.0 \times 10^{-6}$ $cm^2(V•s)^{-1}$ and an average on/off ratio of 850 were achieved.

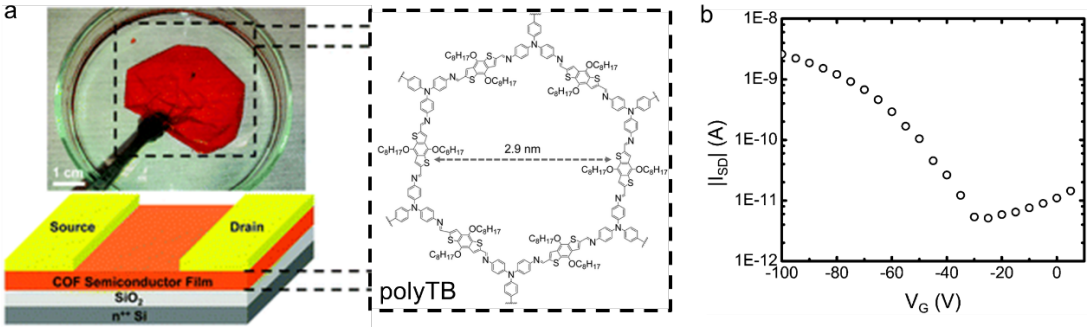


**Figure 19.** (a) The synthesis of polyTB COF thin film at the DMF/air interface and the corresponding BGTC-type thin-film FET device. (b) Transfer curve for polyTB-based FET. Reproduced with permission from Ref. 411. Copyright 2015 The Royal Society of Chemistry.

Final edited form was published in "Chemical Reviews 2020, 120(1), S. 8581-8640. ISSN 1520-6890.
https://doi.org/10.1021/acs.chemrev.0c00033

The repertoire of COF film integration methods was expanded further when Feng and coworkers developed a Langmuir-Blodgett (LB) assisted interfacial synthesis method to synthesize a wide-area crystalline 2D COF monolayer (~0.7 nm in thickness). They accomplished this using a Schiff-base reaction of 5,10,15,20-tetrakis(4-aminophenyl)21H,23H-porphyrin-Co(II) with 2,5-dihydroxyterephthalaldehyde at an air-water interface (Figure 20a).[419] In a typical procedure, a submonolayer of porphyrin monomer was first spread at the air-water interface of a LB trough from chloroform solution and compressed to a surface pressure of 10 mN $m^{-1}$ to promote the formation of a densely packed monomer film. The aldehyde monomer was then added to the subphase and diffused to the interface where 2D polymerization was triggered by the formation of imine bonds between amine and aldehyde groups. The interfacial reaction was allowed to occur for more than four hours (vide infra) to promote the efficient reaction conversion. The resulting wafer-scale 2D imine COF had a monolayer thickness of ~0.7 nm (Figures 20b and c). A remarkable feature of the film was that its outstanding Young's modulus (267±30 GPa), which is comparable to that of graphene. The monolayer 2D COF was used to fabricate a thin-film transistor for a proof-of-concept demonstration of this COF as an active semiconducting layer. The film was horizontally transferred onto an *n*-doped Si wafer with 300 nm $SiO_2$ layer (dielectric), onto which 30 nm thick gold was deposited and used as bottom electrodes. From the transfer curve of the 2DP (Figure 20d), a mobility of $1.3 \times 10^{-6}$ $cm^2(V•s)^{-1}$ and on/off ratio of $10^2$ were obtained. Doping with $I_2$ increased the charge carrier mobility by a factor of more than two orders of magnitude, reaching $1.6 \times 10^{-4}$ $cm^2(V•s)^{-1}$.

Finally, in a very recent report, Park et al. employed a surfactant-monolyaer-assisted interfacial synthesis (SMAIS) approach to achieve large-area growth of crystalline thin (few-layer) films of 2D boronate ester COFs (BECOFs).[448] Using a sulfate surfactant monolayer on a water surface, they first injected the boronic acid-functionalized porphyrin monomer, which diffused to the underside of the monolayer. Following this a second tetrahyroxy-functionalized monomer (e.g. tetrahydroxybenzene) was injected into the aqueous phase. Heating the mixture to 50 °C for seven days to initiate the polymerization reaction produced a free-standing film that had sufficient mechanical strength to be transferred to other substrates for characterization. As a final proof of the utility of this method for device fabrication, they assembled a silicon nanowire FET in which an 11-nm BECOF film was transferred to the surface of the $SiO_2$ gate dielectric to serve as a charge accumulation layer. Upon application of a positive gate voltage, surface charge accumulated at the BECOF-$SiO_2$ interface. This charge was maintained when the gate voltage returned to zero, showing memristor-like behavior. Moreover, short-term potentiation was demonstrated by application of 500-ms pulses.

Final edited form was published in "Chemical Reviews 2020, 120(1), S. 8581-8640. ISSN 1520-6890.
https://doi.org/10.1021/acs.chemrev.0c00033

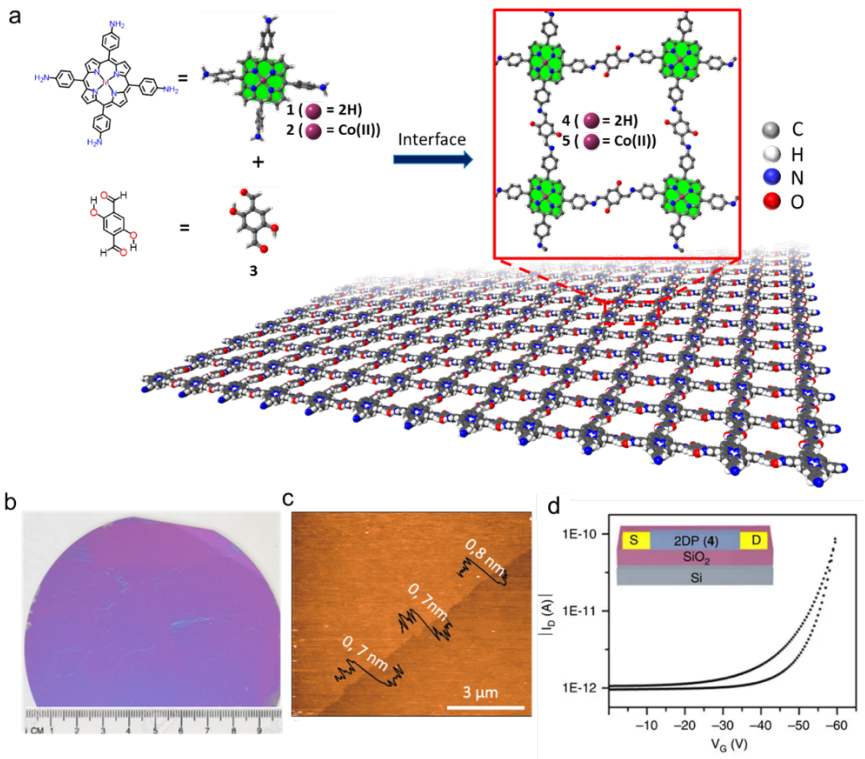


**Figure 20.** (a) Chemical structures of monomers (1, 2 and 3) and imine-based 2D COFs (4 and 5). (b) Photographic image of monolayer 2D COF on 4-inch 300 nm $SiO_2$/Si wafer. (c) AFM image of a monolayer. (d) Transfer curve of a thin film transistor using a 2D COF (4) as an active semiconducting layer at a source to drain voltage of −40 V. Reprinted by permission from Macmillan Publishers Ltd.: Nat. Commun. Ref. 419, copyright 2016.

The three reports from the Bao group[411] and Feng group[419] just discussed clearly show that the development of single- and few-layer 2D COF films enabled by interface-assisted synthesis creates the potential for their use as semiconducting components in thin-film transistors (TFTs). The relatively low mobilities of the polyimine transistors may be attributable to low $\pi$-conjugation through imine bonds, low crystallinity in the thin film, and possible defects, suggesting that improvements in both chemical/structural design and film preparation are required to yield high-mobility devices. In addition, the interfacial methods usually suffer from relatively low yield and an efficient bottom-up route to scalable synthesis of 2D COF films is yet to be achieved. An important recent development that could at least partially address this problem is the formation of 2D COF nanosheets by top-down exfoliation from pre-synthesized 2D COF bulk crystals.[403,413,449-456] Although this strategy potential to produce single-layer or few-layer 2D COFs at large-scale under ambient conditions, it is currently limited by the broad distribution of sheet thicknesses and lateral size, as well as low yield, low structural integrity, and high tendency of the nanosheets to restack. Nevertheless, the controlled synthesis of some single- or multi-layer 2D COFs with fine-tuned lateral size and thickness at the atomic or molecular level is still a critical issue that must be addressed to boost their performance in semiconductor devices.

A very recent development is the report by Xu and coworkers of the synthesis of few-layer crystalline polyimide 2D COF nanosheets via hydrogen-bond-induced preorganization of

Final edited form was published in "Chemical Reviews 2020, 120(1), S. 8581-8640. ISSN 1520-6890.
https://doi.org/10.1021/acs.chemrev.0c00033

pyromellitic acid and melamine, followed by the imidization reaction of the resulting planar hydrogen-bonded networks under solvothermal conditions.[402] The nanosheets thus obtained had an average lateral size of ~4 μm and a thickness of 1.5-2.6 nm. High-resolution TEM certified that the nanosheets are highly crystalline with hexagonal 2D crystal structures and long-range order within the COF nanosheets. Moreover, they could be easily dispersed in ethanol and maintained in this state for >2 months), providing desired processability for subsequent applications. Supported by UV-Vis spectra and DFT calculation of the band structure, this polyimide 2D COF showed a bandgap of 2.2 eV and can function as a semiconducting layer in FET devices. To this end, the COF nanosheets were deposited on *p*-type Si substrates with 300 nm $SiO_2$ by drop coating, followed by thermal deposition of source and drain electrodes comprised of Au films with Ti adhesion layers (30 nm/5 nm). A typical transfer curve ($I_{DS}$*vs*$V_G$ with $V_{DS}$ = 1 V) of the 2D polyimide-based FET device showed *p*-type behavior with a very high on/off ratio of $1.4\times10^4$ and relatively good mobility ($4.3\times10^{-3}$ $cm^2(V\bullet s)^{-1}$) in contrast to the well-known insulator property for linear polyimides. This much-improved mobility value of this 2D polyimide compared with those seen in the 2D polyimines described above ($10^{-6}$ $cm^2(V\bullet s)^{-1}$) is likely not due exclusively to the difference in the chemical components. Rather, the high sample crystallinity and homogeneous features that produce a high-quality interface between semiconductor, $SiO_2$ dielectric and source/drain electrodes must play a major role.

### 4.4 COF-based vertical FETs

Inspired by the progress achieved so far, high crystallinity and closely layer stacking alignment of aromatic moieties as well as in-plane extended π-electron delocalization render 2D conjugated COF films as ideal platforms for charge carrier transport. However, the layer orientation in the 2D conjugated COF films - which generally determines the charge mobility due to the anisotropic transport in the layer stacked structures - is challenging to control when integrated into a device. Similar challenges exist in the field of organic semiconductors, including conducting polymers and organic small molecules, where control of crystal and layer orientation was recognized as a reliable approach to tailor electronic structures and improve charge transport in specific electronic devices.[457-459] For example, conducting conjugated polymers can display different charge mobilities when aligned in edge-on or face-on conformation.[458] This is attributed to the fact that, in edge-on orientation, strong π-orbital overlap between adjacent polymer backbones facilitates intermolecular charge transport to the electrodes. Correspondingly, lateral and/or vertical electronic devices have been developed to clarify the transport mechanism.

An illustrative example is the work of Wang and co-workers, who prepared imine-linked $COF_{TFPy–PPDA}$ thin films by condensation of 1,3,6,8-tetrakis(p- formylphenyl)pyrene (TFPy) and p-phenylenediamine (PPDA) via solvothermal synthesis, using single-layered graphene (SLG)/$SiO_2$-Si to orient the film (Figure 21a).[101] Based on the COF film/SLG heterostructure, a vertical field-effect transistor (VFET) device was constructed. In this architecture, SLG serves as the source electrode and the drain electrode is provided by a 60 nm-thick Au layer deposited on the COF film, thereby vertically stacking the source electrode and channel layer (Figure 21b). This device structure is advantagous because it enables low-power, low-voltage manipulation and high current output. The vertical orientation also facilitates tuning the channel length, which corresponds to the thickness of the COF semiconducting layer. In the device discussed here, the $COF_{TFPy–PPDA}$ thin film serving as transport channel had an average thickness of 50 nm, resulting in excellent ambipolar charge transport (determined by monitoring gate voltages; Figure 21c). These device characteristics can be ascribed to the tunable work function and density of states of

Final edited form was published in "Chemical Reviews 2020, 120(1), S. 8581-8640. ISSN 1520-6890.
https://doi.org/10.1021/acs.chemrev.0c00033

SLG, as well as lower barriers for electron and hole injection. The narrow band gap (1.61 eV) of $COF_{TFPy\text{-}PPDA}$ can also contribute to a lower injection barrier. A high current density and on/off ratio > $10^5$ were achieved at lower manipulating voltages. The maximum on-current density could reach 6.8 A $cm^{-2}$ for holes and 4.1 A $cm^{-2}$ for electrons (Figure 21d). Thus, the VFET provides a universal method for probing the nature of charge transport in layer-stacked 2D COF films, as well as demonstrates their potential for applications in organic electronics.

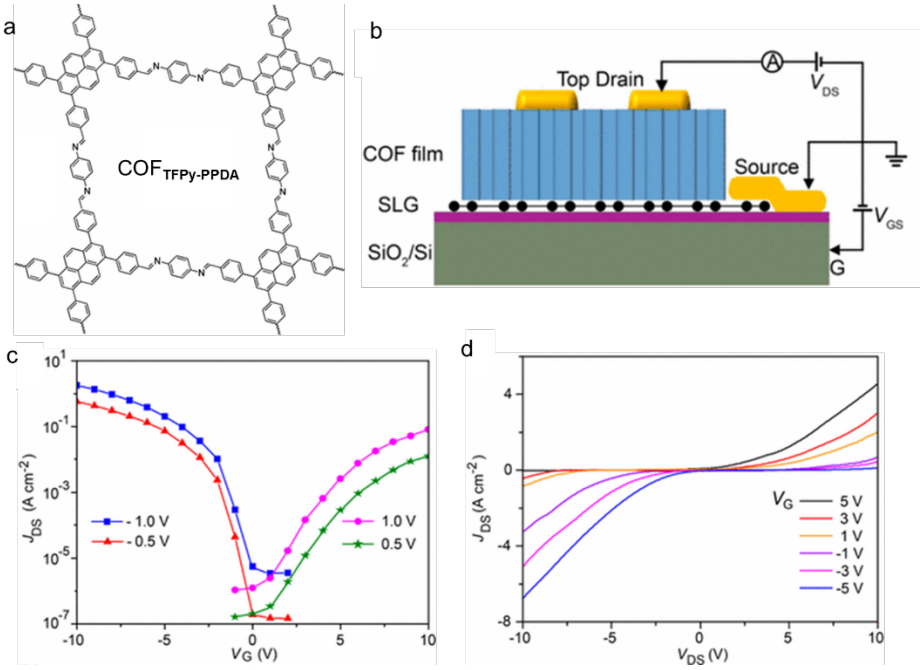


**Figure 21.** (a) Schematic structure of imine-based $COF_{TFPy\text{-}PPDA}$. (b) Module side view of the constructed COF/SLG-VFET device. (c) Transfer characteristics of the ambipolar SLG/$COF_{TFPy\text{-}PPDA}$-VFET at $V_{DS}$ values of -0.5, -1.0, 0.5, and 1.0 V with 50-nm channel length and 300-nm $SiO_2$ gate dielectric. (d) Output characteristics of the ambipolar SLG/$COF_{TFPy\text{-}PPDA}$-VFET depending on various gate voltages. Reproduced with permission from Ref. 101. Copyright 2017 American Chemical Society.

### 4.5 Dielectric OFM for transistors

In recent years, MOFs have garnered significant interest as dielectric materials[460] and the topic is the subject of a recent review.[461] Their crystalline porous structure provides an avenue for the rational design of both high-$\kappa$[462-467] and low-$\kappa$[468-471] dielectrics, with properties readily tailored via the choice of metal nodes, organic linkers, and use of guest molecules. Another advantage is that MOF films exhibit high compatibility with the surface of the substrate, which is imperative for high performance in electronic devices. A remarkably wide range of dielectric constants have been reported for MOFs, from ultralow to collosal high. Reports from 2016 until 2020 concern primarily low-$\kappa$ materials, although new high-$\kappa$ materials have appeared as well. COFs have attracted little interest so far, likely due to the difficulty of forming COF thin films and integrating them with other materials. We are aware of only two papers that consider COFs as dielectric materials, however.[428,472]

Final edited form was published in "Chemical Reviews 2020, 120(1), S. 8581-8640. ISSN 1520-6890.
https://doi.org/10.1021/acs.chemrev.0c00033

Among the best-developed MOFs for low-$\kappa$ applications are ZIFs and there are several recent reports concerning these. Ameloot and coworkers described a variation of their ALD-CVD method of film growth that can deposit ZIF-8 and ZIF-67 in high aspect-ratio vias. [471]In a new twist, Wang et al. used DFT calculations to predict the structural, electronic, and dielectric properties of amorphous ZIFs (a-ZIFs). Their results suggest that all such materials possess ultralow dielectric constants. A potential advantage of amorphous materials is that the absence of grain boundaries and associated defects can make them less susceptible to reproducibility problems resulting from insufficient control over the film growth process. Strategies recently evaluated to achieve a low-$\kappa$ dielectric constant in a MOF include linker functionalization, [473] metal ion substitution,[474] and guest infiltration.[475] New fabrication methods are also appearing. In particular, Ameloot and coworkers described a variation of their ALD-CVD method of film growth that can deposit ZIF-8 and ZIF-67 in high aspect-ratio vias.[471] Synthesis of IRMOFs with nanocrystalline microstructure is another novel approach; $\kappa$ values for MOF-3, MOF-5 and MOF-10 films supported on ITO glass of 1.2, 2.1, and 4.8, respectively, were achieved.[476]

High-$\kappa$ materials refer to materials with dielectric constants generally $\kappa > 4$.[477] The dielectric constant $\kappa$, also referred to as the relative permittivity, describes the degree of electrical polarization a material experiences under an external electric field. As $\kappa$ increases, the resistance to formation of an electric field in the medium will decrease.[9] In general, $\kappa$ increases with increasing material density and the introduction of polarizable atoms and bonds. Currently, a significant effort has been devoted to the development of high-$\kappa$ materials with low electrical leakage and high breakdown voltage for microelectronic devices such as transistors.[478] Silicon-based materials are the dominant gate dielectric layers. However, their relatively low $\kappa$ and large static power dissipation limit the further improvements in performance. In particular, high-$\kappa$ gate dielectrics are required when downsizing microprocessor FETs for fast switching and low leakage. Inorganic metal oxides such as hafnium dioxide ($HfO_2$) and zirconium dioxide ($ZrO_2$) are widely utilized as high-$\kappa$ dielectric materials. However, the integration of these materials into FETs typically requires deposition under high temperatures and expensive vacuum equipment[462] and their relative brittleness inhibits compatability with substrates. Organic polymers, which are solution-processable and afford excellent film topologies for flexible and stretchable electronics, are an alternative, but have low dielectric constants and capacitance than oxides as well as low thermal stability.[478]

To achieve high-$\kappa$ MOF materials, a promising strategy is to trap or coordinate in the pores guest molecules with high polarizability. Of recent significance is the 2016 report of Li et al., who described a 2-fold interpenetrated Zn(dimethylammonium)(TBTC) framework film (TBTC=1,3,5-tris[4-(carboxyphenyl)-oxamethyl]-2,4,6-trimethylbenzene) by electrochemical assembly.[462] This anionic network was balanced by $H_2N(CH_3)^{2+}$ counterions located inside the pores. Thus, the close-packed interpenetration and electronic interaction of the frameworks and trapped solvent guests (dimethylformamide and ethanol) resulted in high $\kappa$ of 19.5. For comparison, $SiO_2$ is 3.9; $ZrO_2$ and $HfO_2$ are both 25.[479] The film exhibited a leakage current of $10^{-7}$ A $cm^{-1}$ at 1 kV $cm^{-1}$ and a breakdown voltage above 10 kV $cm^{-1}$. This MOF film also showed a high mechanical flexibility, which points to potential promising applications in microelectronics. In addition, varying the composition of the MOF backbone enables the high-*k* characteristics to be tuned. For example, the transition metal ions (Fe, Ga, Mn, V, Cr, Zr, Mo) increase the ionic and electronic polarizability due to the presence of *d*-electrons with anisotropic electronic-spatial distributions.[477] In 2017, a niccolite structural MOF reported by Bu, Wang and coworkers, $[(CH_3CH_2)_2NH_2][Fe^{III}Fe^{II}(HCOO)_6]$, exhibited a thermally switchable dielectric constant

Final edited form was published in "Chemical Reviews 2020, 120(1), S. 8581-8640. ISSN 1520-6890.
https://doi.org/10.1021/acs.chemrev.0c00033

transition accompanied by phase transition, with a high-dielectric state in the paraelastic phase and a low-one state in the ferroelastic phase, which is associated with statistical fluctuations of polar cations of diethylamine. Upon cooling from 240 to 227 K, the $\kappa$ values changed from 13 to 16. The same authors also reported similar thermally switchable dielectric constant transition triggered by freezing cations in other niccolite structural MOFs like $[L][Ga^{III}Mn^{II}(HCOO)_6]$ (L= $CH_3NH_3$, $(CH_3)_2NH_2$ and $CH_3CH_2NH_3$).[466,467] Alkaline-earth metals have been employed as well; a series of six strontium-containing MOFs comprised of aromatic nitrogen (e.g. pyrazine) and/or V-shaped ligands exhibit *k* values from 8 – 20. These results, though limited, are encouraging in that the favorable mechanical properties of MOFs and $\kappa$ values to high-$\kappa$ oxides should make them useful replacements for $ZrO_2$ and $HfO_2$ in device applications requiring flexible substrates.

Finally, the increasing number of fundamental studies employing sophisticated diagnostic tools are leading to detailed understanding of the interrelationships between MOF structure and guest molecules affecting the dielectric constant in this diverse class of materials.[480,481] Tan and coworkers employed synchrotron-based infrared reflectivity to measure the dynamic dielectric response of ZIFs, from which they established structure-property relationships involving the nature of the porosity and frequency-dependent structural change. This group also examinded the effects of temperature and pressure on the broadband dielectric response of $Cu_3(BTC)_2$ (HKUST-1).[480] Their results suggest that MOFs have potential to be used in terahertz applications, including high-speed wireless communications. Scatena et al. combined DFT and other theory with impedance spectroscopy, which allowed them to separate the effects of chemi- and physisorbed guest molecules from framework structural features in the iconic MOF $Cu_3(BTC)_2$ (HKUST-1).[481] Theoretical studies are appearing as well.[480,482-484] of particular interest is a molecular dynamics investigaton of self-diffusion in the MOF Co-MOF-74 ($Co_2$(dobdc); dobdc = ,5-dioxo-1,4-benzenedicarboxylate) that shows how motion of polar molecules in the pores can produce a "colossal" dielectric constant on the order of 42,000 at ambient temperature.[483] Together, these works are beginning to identify structure-property relationships that are essential for rational design of dielectric MOFs.

## 5. Resistive switching

Artificial devices that mimic a synapse, the biological equivalent of an analog switch, are currently of intense interest for artificial neural network (ANN) computing.[485] ANN attempt to emulate the computing power of the brain, which is a massively parallel super computer with an estimated $10^{15}$ interconnections. The most extensively investigated analog concept is the memristor (**Figure 22**), a two-terminal device that exhibits memory.[486] Such devices switch from a high-conductivity (low resistance) state to a low-conductivity (high-resistance) state as a result of field-induced chemical or physical changes that alter the resistivity by an amount determined by the quantity of current that has flowed through the device.[486] Ideally, this change is not reversed until a voltage of equal and opposite sign is applied. Although relatively new circuit elements, memristors based on inorganic oxides and other materials are promising for integration in data storage in the form of resistive random-access memory (RRAM).

Final edited form was published in "Chemical Reviews 2020, 120(1), S. 8581-8640. ISSN 1520-6890.
https://doi.org/10.1021/acs.chemrev.0c00033

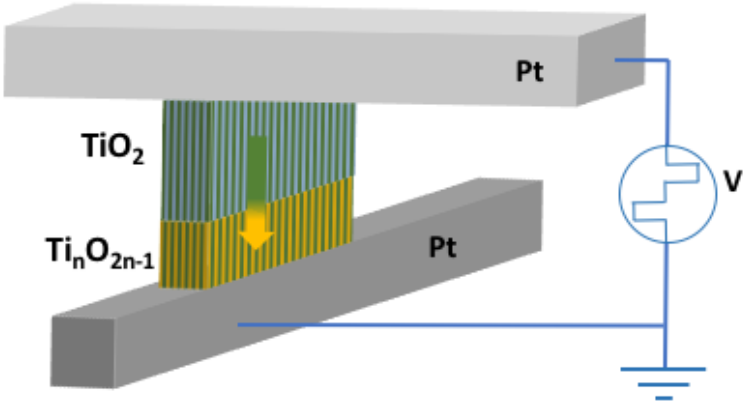


**Figure 22.** Schematic of a bipolar nonlinear memristor, a type of valence-change switch in which application of voltage pulses leads to motion of oxygen vacancies and formation of suboxides (see for example Ref. 487).

A variety of chemical switching mechanisms have been identified that involve motion of ions, including both anion- and cation-based mechanisms as well as defects and vacancies.[488,489] These mechanisms and associated devices have been referred to by various names. Valence-change memory is the most general term, but is often used in the context of anion-based devices. Cation-based devices are known as electrochemical metallization or electroforming memory, programmable metallization cells, or atomic switches. Anion-based devices typically involve motion of oxygen ions, thus a change in the redox state of the material occurs; oxides are commonly used materials. For example, in two-terminal memristors using $TiO_2$ as a conducting channel, applying a voltage above a threshold value $V_{th}$ causes positively charged vacancies to drift toward the oxide-electrode interface (Figure 22). This creates conducting pathways that reduce the barrier to charge transport.[490] The extent of this ionic motion is determined by the flux of electronic charge (holes or electrons) that has flowed through the device, which makes the resistance continuously adjustable and enables WRITE operations that program the device. Once conducting channels are formed, a device READ operation is performed by applying a voltage $<< V_{thr}$ to measure the electrical conductivity. In contrast, cation-based switching typically involves transport of metal ions and can involve filament formation by electrochemical metallization. Electrochemically active metals such as copper or silver are used that are oxidized upon application of a high positive voltage. The resulting metal cations drift through an electrolyte to a cathode where they are reduced, nucleating a metal filament that grows backward toward the anode. Physical contact with the anode turns on the switch. A third type of resistive switches are those operating by purely physical mechanisms. In these, modulation of the conductivity occurs by changing the electronic, magnetic, or ferroelectric properties of a material. A variety of device architectures have been developed on this basis; in addition to resistance switches, they include magnetic tunnel junctions, ferroresistive switches, and phase-change switches.[488]

In general, the switching characteristics of memristive devices are highly dependent on the properties of the barrier material, including the concentration and mobility of both the ionic species and electronic charges and the interactions between these. The processes responsible for switching are stochastic and highly dependent on the nature of the fabrication process, leading to unpredictable switching behaviors and lack of reproducibility.[488,491] It is clear that material

Final edited form was published in "Chemical Reviews 2020, 120(1), S. 8581-8640. ISSN 1520-6890.
https://doi.org/10.1021/acs.chemrev.0c00033

properties are central to achieving the device performance and high degree of reproducibility needed for ANN. Since coupled motion of both ions and electronic charge is required,[486] material and device optimization would benefit from new materials with a high degree of synthetic tailorability, reproducible synthesis/properties, clearly identified transport mechanisms, and ideally, independent control over charge and ion transport.

### 5.1 Material requirements for resistive switching

Key requirements for memristive switches serving as artificial synapses have been identified to enable their use in large-scale ANN.[492] Among these are: low fluctuation and drift to maximize computational accuracy and minimize noise; high resistance in the conducting channel to achieve low currents (< 10 nA) and thus low power consumption; high endurance for repeated training; and reproducible fabrication. Moreover, a linear current-voltage relationship is needed so that Ohm's law can be used for computations and the channel conductance should be linearly proportional to the number and/or amplitude of voltage pulses used for training (i.e., the WRITE step that establishes the channel conductance). Achieving all of these has been difficult using inorganic materials, many of which exhibit nonlinear conductance tuning and poor stability. Mixed-conducting organic materials are promising, but rational design of ion and current transport is difficult due to complex and disordered structures at the molecular and mesoscale.[493,494]

OFM, including MOFs and COFs, offer potential solutions to these problems for several reasons. First, tailorable nanopore size, geometry, and chemical functionalities provide opportunities for designing materials with fast, selective ion transport. This has been demonstrated for protons [495-498] and other ions.[499] OFM crystallinity enhances electronic charge transport by minimizing disorder,[225] in contrast with the disordered nature of materials such as porous carbons, aerogels, and block copolymers. The long-range order of OFM could also be useful for understanding ion injection and transport in organic semiconductors, the mechanisms of which are still not fully understood.[494] Second, the nanopores in OFM provide a new design element for introducing guest molecules to tailor both ion and electronic charge transport.[46] Finally, OFM with 1D, 2D, and 3D porous networks are available, allowing directional ion and charge transport. Anisotropic ion and charge transport are conceivable, which would be advantageous for some switching architectures.[428]

It is important to inject a note of realism regarding OFM as resistive switching materials. Device requirements for practical implementation of memristors are extremely demanding. Repeatable switching behavior over literally billions of READ/WRITE operations is essential, at WRITE/ERASE times of tens of ns or less.[500] The switching speeds, endurance, reproducibility, and retention of the OFM-enabled devices discussed below are very far from the state-of-the-art of either inorganic or organic materials used in memristors.[491] Moreover, device size must be scalable to enable fabrication of large device arrays required for ANN computing. To date, crossbar arrays with memristors as small as 200 x 200 $nm^2$ have been reported using conventional materials such as $TiO_{2-x}$.[492] Fabrication methods for integrating OFM with other materials lag far behind the discovery of new switching phenomena and OFM. Consequently, OFM are very much in the nascent stage of development for these applications. A particularly encouraging development, however, is the report of a resistive memory device in which the switching material is a ruthenium-coordination complex with 2(phenylazo)pyridine) ligands.[501] Although this is molecular system, not a porous supramolecular framework, the proposed switching mechanism (ligand redox with charge balancing by counterion transport) suggests possibilities for using OFM in an analogous

Final edited form was published in "Chemical Reviews 2020, 120(1), S. 8581-8640. ISSN 1520-6890.
https://doi.org/10.1021/acs.chemrev.0c00033

manner. Devices prepared by spin-coating the complex onto a conducting substrate exhibited remarkable endurance, undergoing $10^{12}$ switching cycles and switching times ≤30 ns.

In the following section, we review recent literature describing OFM-based devices and OFM with properties that make them potential candidates for resistive switching (RS) applications, including phase-change MOFs, ferroelectrics, and ion-conducting OFM. Only a few examples of actual devices employing these concepts have been reported, but they are intriguing and suggest future avenues for research to take advantage of the rich variety of structures within this class of materials.

### 5.2 MOF-based devices and switching mechanisms

In most cases switching mechanisms proposed for OFM are speculative, reflecting that correlated ion and charge transport in general is not well understood, even for well-established materials such as semiconducting organic polymers.[494] Charge and ion transport across interfaces are difficult to probe in operating devices. There also is no consensus regarding the most effective approach to modeling these processes in organics[502] much less in mixed ionic-electronic conductors.[503] Consequently, structure-property relationships and clear-cut design rules have not been developed. Nevertheless, it is useful to consider OFM in light of RS mechanisms in conventional organic and inorganic materials. This can reveal both the similarities and unusual properties specific to OFM.

**5.2.1 Cation-conducting OFM.** As discussed above, transport of small cations can provide a mechanism for RS. Memristors based on metal ion modulation of conductivity are well established, but protons are also attractive. Numerous studies focused on OFM for proton-exchange membranes show that transport rates through OFM can be very high. This subject was recently reviewed;[504] research prior to 2013 also has been reviewed.[499,505] Development of proton-conducting COFs is more recent.[392,504] RS involving transport of $Li^+$ is also a possibility, but the high mobility of this ion could lead to increased leakage currents in CMOS devices integrated with the RS.[506]

Proof-of-concept that a proton-transporting OFM can enable RS was recently demonstrated by Yao et al., who described a device in which the nanopores of a chiral MOF serve as a pathway for proton transport.[507] The device, comprised of an OFM single crystal bonded to two silver electrodes, exhibits a low set voltage (~0.2 V) and an ON/OFF ratio > 10. The framework used is comprised of Zn(II) cations coordinated to triazole isophthalate linkers, with an incomplete chain of hydrogen bonds, in which the O1w···O11 bond distance and the O1w—H1w1···O11 bond angle are outside the normal range of hydrogen bonds (Figure 23). This chain runs parallel to the *c* axis of the crystal and exhibits a sharp increase in proton conductivity (vehicular mechanism [504,508]) upon application of a voltage > 0.2 V. This voltage-gated conductivity modulation can serve as a mechanism for RS and a high ON/OFF ratio (>$10^5$) is observed. The structure is chiral, an intriguing consequence of which is that proton transport is unidirectional due to a reordering of water molecules and their associated hydrogen bonds within the pores. Consequently, the device is not only a resistive switch but also a rectifier. This highlights a feature that may be unique to OFM: the ability to control the directionality of ion transport through the use of chirality.

Final edited form was published in "Chemical Reviews 2020, 120(1), S. 8581-8640. ISSN 1520-6890.
https://doi.org/10.1021/acs.chemrev.0c00033

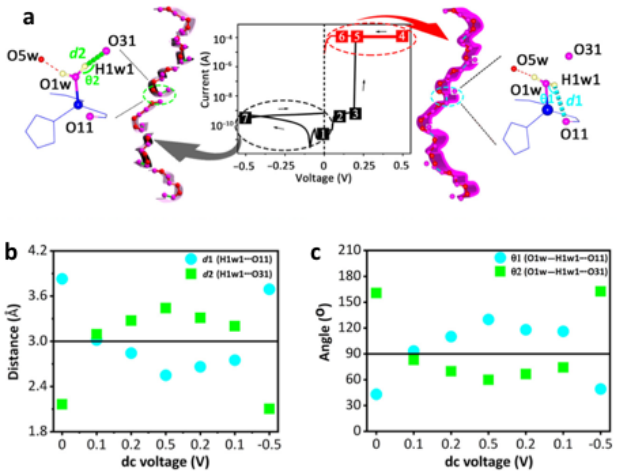


**Figure 23.** (a) Effect of DC bias on the structure of FJU-23-$H_2O$ (viewed along the c axis). Two O-H distances are shown as a function of voltage in the sequence of points labeled 1–7. (b) Comparison of hydrogen bonding distances and angles as a function of applied voltage. Reprinted with permission from Ref. 507 under a Creative Commons Attribution Non-Commercial License 4.0.

The unusual features of the previous device indicate that ion-based based resistive switching by OFM merits further consideration. Proton transport in many organic materials is facilitated by water molecules in the pores, which enable the Grotthuss mechanism.[504,508] However, for electronic devices it is usually desirable to avoid water, since its concentration may vary with temperature and can affect other parts of the device. OFM are appealing from this perspective because proton transport rates comparable to Nafion®, the standard membrane material used in PEM fuel cells, have been achieved at temperatures up to 150 °C without water in the pores.[496] Two primary strategies have been employed to achieve high conductivities, water-free transport, and operation at high temperature. The first strategy, in which linkers having mobile protons are constituents of the framework, yields intrinsically conducting materials and has been implemented in both MOFs and COFs. For example, a 3D MOF with an interpenetrated framework (composition $\{[(Me_2NH_2)_3(SO_4)]_2[Zn_2(ox)_3]\}_n$) is reported to have a conductivity of 1 x $10^{-4}$ S $cm^{-1}$ at 150 °C, likely by a Grotthuss mechanism.[509] XRD reveals extensive hydrogen bonding between sulfate and $Me_2NH_2$ cations, which facilitates proton transport.

The second strategy, one that is more amenable to electronics applications because adsorbed water is not required, is to infiltrate OFM with proton-rich guest molecules. High proton conductivity (0.01 S $cm^{-1}$ at 150 °C, a record at the time) was achieved by infiltrating the mesoporous MOF MIL-101 with nonvolatile acids ($H_2SO_4$ and $H_3PO_4$).[510] Very high proton conductivities were also obtained by infiltrating MOFs with organic molecules such as histamine,[498] imidazole,[495] and 1,2,4-triazole.[496] A unifying conclusion of these reports is that the MOF pores enforce a molecular orientation conducive to fast hopping by the Grotthuss mechanism.[508] This mechanism requires molecular reorientation for proton transfer to occur. For bulk histamine, a 3D network of trans hydrogen bonds exists, leading to a high activation energy for the reorientation. In contrast, histamine captured in the 1D pores of the aluminum MOF $[Al(OH)ndc)]_n$ (ndc = napthalenedicarboxylate) cannot adopt such conformations. Narrower NMR peaks suggest the molecules are more freely rotating, consistent with the low activation barriers of

Final edited form was published in "Chemical Reviews 2020, 120(1), S. 8581-8640. ISSN 1520-6890.
https://doi.org/10.1021/acs.chemrev.0c00033

0.25 eV. Water-free proton conductivity > $10^{-3}$ S $cm^{-1}$ is observed at 150 °C , which is very different from bulk histidine (9.4 x $10^{-6}$ S $cm^{-1}$ at 75 °C).[498]

**5.2.2 Electroforming.** Switching in so-called conductive bridge RAM or electrochemical metallization memory is cation-based and occurs by oxidation of metal atoms at an electrochemically active anode. The resulting cations are transported to an insulating counterelectrode under the influence of an electric field, where they are again reduced. A metal filament begins to grow backward toward the anode, creating a conducting path when it contacts the anode.[491] No MOF-based memristors operating by this mechanism have been reported, although this would seem to be a logical approach given that electrochemical formation of MOFs has been demonstrated in a number of cases.[150,213,511-515] For example, stepwise reduction of HKUST-1 results in formation of what appear to be metallic copper nanowires intercalated with the MOF. This could presumably be reversed, as electrochemical synthesis of this MOF is feasible.[150,512]

Using a related concept, a memory device involving $Cu^{2+}/^{1+}$ reversible reduction was recently described.[516] The active metal cations are thought to be located near the interface of the MOF with the electrode. The device was cycled 6000 times without apparent degradation of properties. Clouding the picture, however, is that the electrochemically grown MOF layer on the electrode was rinsed with methanol but not activated prior to device testing. It is now known that methanol oxidation is involved in the formation of Cu(I) species from HKUST-1 in the presence of an electron acceptor such as 7,7,8,8-tetracyano-quinodimethane (TCNQ).[517]

The first report of a RS device incorporating a MOF, by Yoon et al., also involves transport of metal ions. In this case, switching occurs by selective ion transport through the nanopores of a rubidium-cyclodextrin MOF.[518] The MOF was sandwiched between silver electrodes and facilitated transport of $Ag^{+}$ under applied bias. The mechanism of resistance modulation was hypothesized to be formation of a nanoscale passivating layer (presumably AgO) at the MOF-electrode interface. This conclusion was supported by XPS data and control experiments involving redox-inert gold electrodes.

**5.2.3 Guest-molecule mobility.** In this switching mechanism, ion transport occurs by the motion of charged molecules and one to which OFM are uniquely well suited. Unlike typical nonporous barrier materials used in memresistors, OFM nanopores can be filled with guest species with tailored redox or ion transporting ability. Guest molecules can in fact be used as a new design element to create composite or hybrid electronic materials with emergent properties distinct from either the OFM or guest.[46] Transport of small anions or cations through an electrolyte within the pores is a straightforward example, as in the case of lithium ion transport for batteries. More sophisticated approaches can involve molecular guests, such as molecules with labile protons that can enable proton transport in the absence of water, as discussed above. In the case of RS, Redel and coworkers considered devices incorporating a ferrocene-loaded HKUST-1 SURMOF film grown on gold and patterned with electrodes. This device exhibited reversible and repeatable low- and high-conductivity states.[519] Its electrochemical behavior suggested that filament-forming copper reduction is not the mechanism. Rather, the authors speculate that loosely bound ferrocene $Fe^{2+}$ ions are responsible for conductivity modulation. As in some of the other devices discussed here, although the SURMOF film was activated at 80 C for four hours, this may not have been sufficient to fully remove residual reactant and solvent. Clearly, systematic investigations in which this aspect of the material is controlled are needed to understand the device behavior. Nevertheless,

Final edited form was published in "Chemical Reviews 2020, 120(1), S. 8581-8640. ISSN 1520-6890.
https://doi.org/10.1021/acs.chemrev.0c00033

the wide range of potential guest molecules suggests that a rich chemistry exists for modulating the properties of MOFs for RS.

Another example of guest-enabled resistance switching is the work of Liu et al., in which high- and low-conductance states are achieved by infiltrating with methanol or ethanol the pores of ZIF-8.[520] Unlike HKUST-1, ZIF-8 is comprised of redox-inactive Zn(II) ions coordinated to methylimidazolate linkers. The proposed switching mechanism in this case, which is based on molecular dynamics simulations, is that the dipole moments of alcohol molecules in the ZIF-8 pores become aligned in the direction of an applied electric field. A high ON/OFF ratio of $10^7$ was achieved. However, device performance was not highly reproducible; the device-to-device resistance in the high-conductivity state, for example, varied by more than a factor of thirty. Although this is far from acceptable for nonvolatile memory, it may be sufficient for sensing applications.

**5.2.4 Ferroelectric OFM.** Ferroelectric RAM (F-RAM) was commercialized in the 1990s and has several advantages over flash memory, including lower power consumption, longer retention, and higher READ/WRITE durability ($10^{14}$ cycles or more).[521] The most common material in commercial production is the perovskite lead zirconate titanate [$Pb(Zr,Ti)O_3$], but other inorganic oxides with this structure have been used as well. However, the composition space for creating new ferroelectric oxides is limited, as not all $ABO_3$ combinations are chemically feasible. Organic ferroelectrics are also well known, but high fabrication costs have limited market penetration. Metal-free organic ferroelectrics were not known until recently, including one with spontaneous polarization similar to $BaTiO_3$.[522] Although these new materials could potentially open a new venue to tailorable ferroelectrics, their rigid crystalline structure is a barrier to creating devices on substrates that are bendable or rollable. Polymer ferroelectrics are under development for non-volatile memory applications but suffer from issues such as polarization fatigue.[523] These factors provide another opportunity for OFM, which possess some of the same synthetic versatility as fully organic materials (via the linker). Moreover, OFM are crystalline but are nevertheless soft materials that could be used for biosensor and wearable electronics applications. From an application perspective, they are similar to organics in that their low-temperature processability is compatible with other electronic materials.

So far, in spite of the large number of ferroelectric MOFs that are known,[524] there is only one report of a resistance switchable device employing a ferroelectric MOF as the active material. Pan et al. synthesized a framework constructed of indium ions and 2-amino 1,4-benzenedicarboxylate linkers, which form a three-dimensional interpenetrated network in the β-quartz topology.[525] The ON/OFF current ratio is only 30, but state endurance of 6000 s. Curiously, the $P6_222$ crystal space group makes this MOF structure nonpolar and thus incapable of ferroelectricity. The authors speculate that the mechanism of ferroelectric switching is related to water molecules in the pores, which are bound to the framework via hydrogen bonds with the amino groups on the linkers. Molecular dynamics simulations support this hypothesis, predicting the formation of N···H−O···H−N structures that produce a stable dipole moment (Figure 24). Applying an electric field would presumably align these otherwised randomly oriented dipoles along the field direction. The switching effect was found to decrease with temperature, consistent with thermal weakening of these bonds. This not optimal for device applications and may contribute to the relatively low ON/OFF ratio, as well as to poor fabrication reproducibility. Nevertheless, this example highlights the possibility unique to MOFs and OFM in general that guest molecules in the pores (water in

Final edited form was published in "Chemical Reviews 2020, 120(1), S. 8581-8640. ISSN 1520-6890.
https://doi.org/10.1021/acs.chemrev.0c00033

this case) can be used to design new materials. Guest-induced ferroelectric effects in MOFs were highlighted in a recent mini-review.[526]

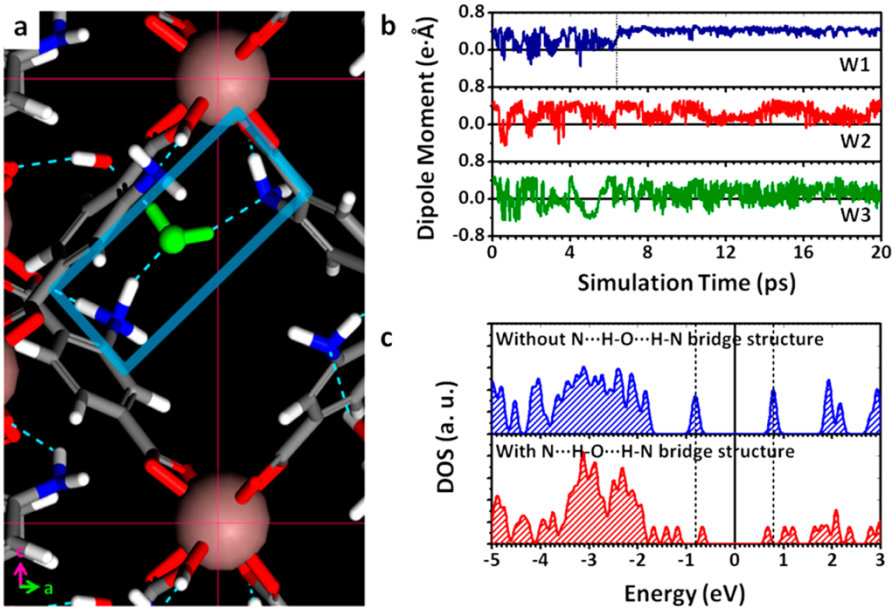


**Figure 24.** (a) Molecular dynamics simulation of the spontaneous formation of bridging N···H–O···H–N by the interaction of guest water molecules with amino groups attached to the linkers the indium-containing MOF. (In, pink; N, blue; O, red; H, white). A water molecule with stable hydrogen bonds is highlighted in green. (b) Time evolution of hydrogen bond formation. Blue: bridging N···H–O···H–N. Red and green: weak and intermittent hydrogen bonds. (c) Local density of states calculations showing a 0.18 eV decrease in the bandgap caused by the formation of rigid N···H–O···H–N hydrogen bonds. (Reproduced from Ref. 525 Copyright 2014 American Chemical Society.)

**5.2.5 Physical switching OFM.** As mentioned above, switching mechanisms based on a purely physical change in the properties of a material are an alternative to chemical mechanisms involving ion transport. In fact, phase-change memory and magnetoresistive switching are very active areas of research for the purpose of developing low-power, high-density, durable, and fast data storage devices.[500] Inorganic phase-change materials undergo a reversible crystalline-to-amorphous transition, a process that has not been reported to date, although crystalline-to-crystalline phase transitions in MOFs are well known.[527] Alternatively, switching between different magnetic states in MOFs has been observed and in one case a nonvolatile magnetic switch was fabricated. Miyasaka and coworkers demonstrated switching between ferrimagnetic and paramagnetic states of a donor-acceptor framework.[528] This material switches by a hybrid mechanism, in which motion of $Li^+$ correlated with a redox reaction implements band-filling control. The $Li^+$ ions serve as dopants: insertion (removal) reduces (oxidizes) bis(1,2,5-thiadiazolo)TCNQ acceptor linkers. This enables the material to be reversibly switched between ferrimagnetic and neutral paramagnetic states. Phenomenologically, this MOF represents a novel giant magneto-electric response material.[529] The properties are already among the best known of this type and should facilitate ion

transport. Moreover, the ability to design donor-acceptor materials with appropriate band alignments suggests potential for greatly increased tailorability relative to inorganics.

**5.2.6 Other RS mechanisms.** Although the previous examples demonstrate a variety of strategies to create resistance-switchable devices using OFM, the mechanisms are far from clearcut. In this regard, several reports describe MOF-based resistance switches for which none of the previously discussed switching mechanism appears to be operative. On the one hand, this suggests that the possibilities for OFM are even greater than imagined based on known phenomena. On the other, however, they highlight the critical need for fundamental studies to identify design rules to guide synthesis.

An example is a device Pan et al. reported in which RS is induced by mechanical strain.[530] A gold-coated polyethylene terephthalate film was used as a substrate for growth of a thin (130 nm) HKUST-1 film. The proposed mechanism involves transport of $Cu^{2+}$ ions to the top electrode under the influence of an applied field, where they are reduced. This variant of an electroforming mechanism is thought to require metal ions in defect sites that are more easily detached from the coordinated BTC linkers. The authors assert that the binding energy of a single BTC carboxylate to the copper dimers is "relatively weak" compared to bonds in metal oxides and can be "disturbed by external means." However, the binding energy of an individual BTC carboxylate bridging the copper dimer in the SBU is 372 kJ $mol^{-1}$, which is too high to be affected by the low voltages or thermal energies present in their experiments. Alternative explanations are that either the $Cu^{+2}$ ions are reduced by application of the set voltage (note that the $Cu^{2+}$ reduction potential is only 0.34 eV vs. SHE) or that residual reactant copper ions in the MOF pores are reduced during switching. Both explanations seem reasonable, as it is likely that the pores contained some water as well as ethanol due to incomplete activation of the film (blow-dried at room temperature).

In an alternative approach, a two-dimensional coordination polymer was formed by surfactant-assisted assembly of tetrakis(4-carboyphenyl)porphyrin (TCPP) ligands with various metal ions (Co, Cu, Zn, Cd).[531] Although referred to as a MOF, it is difficult to ascertain if this very thin layer (~ 7.7 nm thick) is porous. Nevertheless, a RS device was assembled by spin coating a suspension of M-TCPP nanosheets in polyvinylpyrrolidone onto an ITO substrate, followed by evaporation of an aluminum top electrode. The device characteristics are reasonably promising for a prototype: switching from a low resistance to a high resistance state occurred at -0.5 V, with reset voltage of 2.5 V and an on/off ratio of $10^3$. A READ voltage of only 0.1 V was required, retention time of $10^4$ s, and endurance over 1000 switching cycles were observed. Ding et al. performed a thorough investigation of the switching mechanism, obtaining in-situ conducting atomic force microscopy (AFM) and Kelvin Probe Force Microscopy (KPFM) maps of the current read and surface potential of the high- and low-resistance states.[531] RS was determined to occur via a charge trapping-assisted hopping model. The authors hypothesize that the 2D M-TCPP active layer has many trap sites, leading to a relatively high activation energy (442 eV) for charge transport. On the plus side, it should be possible to modulate the trap site charge transport properties by using the coordinating metal and linker functionalization as design elements. However, device reproducibility was poor: the ON and OFF voltages varied by more than ± 0.2 V and the OFF current by nearly a factor of 2000. The reasons for this high variability are unclear, highlighting the need to understand RS mechanisms in general on a fundamental level.

In another example, the OFM was not used as the active material, but instead served as a dielectric coating over the switching material. Huang et al. coated 2D nanomaterials such as graphene oxide or $MoS_2$ with the 3D MOF ZIF-8.[532] Although interesting as hybrid materials, the

Final edited form was published in "Chemical Reviews 2020, 120(1), S. 8581-8640. ISSN 1520-6890.
https://doi.org/10.1021/acs.chemrev.0c00033

exact relevance to RS is not clear. A device comprised of $MoS_2$ coated with ZIF-8 (ZIF-8@$MoS_2$) was fabricated by spin-coating a suspension of the hybrid material onto a reduced graphene oxide (rGO) electrode, with rGO also used as the top electrode. The MOF apparently serves only as an insulating layer. This device exhibited WRITE-once, READ-many (WORM) characteristics, with high write voltage of 3.3 V. The resulting high-conductivity state was maintained for 1500 s at a READ voltage of 0.5 V. The write mechanism was thought to be thermionic emission and charge injection into the ZIF-8@$MoS_2$ layer, with the MOF layer (20 – 30 nm thick) serving as an insulating layer to prevent charge leakage and consequent decay of the write state. Although the MOF is certainly a good insulator, it is unclear whether any real advantage of using this material exists compared with a conventional low-κ dielectric.

### 5.3 COF-based Memristors

The high strength of covalent bonds enables COFs to exhibit high stability in many solvents and high-temperature environments. Additionally, 2D COFs are stable in the form of monolayers with sub-nanometer thickness. At present, large-area monolayer 2D COF films have been successfully prepared. Their ultrathinness is expected to reduce the filament length to the atomic scale, which not only facilitates miniaturization of the memristor but also helps minimize the need for energy to form and rupture the conductive filaments. More strikingly, 2D COFs are intrinsically porous and the structure and the pore environment can be intentionally engineered through monomer design and post synthetic modification. This has yielded promising applications requiring ion conduction,[390-392,533,534] which is also a key consideration when selecting memristive materials. Therefore, these unique characteristics of 2D COFs are highly desirable in the field of memristors. However, to date there are rather limited reports of the use of 2D COFs for the preparation of memristive devices.

Very recently, Hu, Lei and co-workers synthesized a wafer-scale 2D COF film ($2DP_{BTA+PDA}$, shown in Figure 25a) with tunable thickness at the air-liquid interface via the condensation between benzene-1,3,5-tricarbaldehyde (BTA) and p-phenylenediamine (PDA).[535] Figure 25b presents the as-grown ultrathin 2D COF film with a thickness of 1.8 ± 0.2 nm and good freestanding ability. The intrinsic porosity, the coordination ability of the imine groups, and the high uniformity of this $2DP_{BTA+PDA}$ film make it a desired resistive switching medium layer in electrochemical metallization (ECM) memories. Memristors based on these ultrathin 2D COF films (Ag/$2DP_{BTA+PDA}$/ITO) exhibited nonvolatile bipolar resistive switching behavior with high reliability and reproducibility, with on/off ratios in the range of $10^2$ to $10^5$ depending on the thickness of the film (Figures 25c and d). Furthermore, the typical two-terminal device behaved high thermal stability with an operating temperature of up to 400 °C, together with good resistance to many organic solvents. Finally, the intrinsic flexibility of this film enabled its application in flexible devices (Figures 25e), in which it displayed as reliable performance as that on a rigid substrate. Inspired by these results, a new research field for the production of flexible 2D COF-based memory devices is emerging and could allow high-temperature resistance and high robustness to satisfy future demands in wearable devices.

The bipolar switching behavior of this imine-based COF clearly occurs by an electroforming mechanism. Typically, devices operating on this principle require an electrolyte or ion-conducting oxide through which metal ions diffuse upon application of a positive voltage to the anode (the Ag electrode in this case). In this case, however, no electrolyte was employed, although water was almost certainly present in the pores following initial fabrication. Contradicting the hypothesis of water-assisted $Ag^+$ transport is that the device continues to display bipolar switching even after

Final edited form was published in "Chemical Reviews 2020, 120(1), S. 8581-8640. ISSN 1520-6890.
https://doi.org/10.1021/acs.chemrev.0c00033

annealing for 2 hours at 300 °C, at which point any water remaining from fabrication should be gone. The results suggest that the nanopores of the film serve as channels for ion transport.

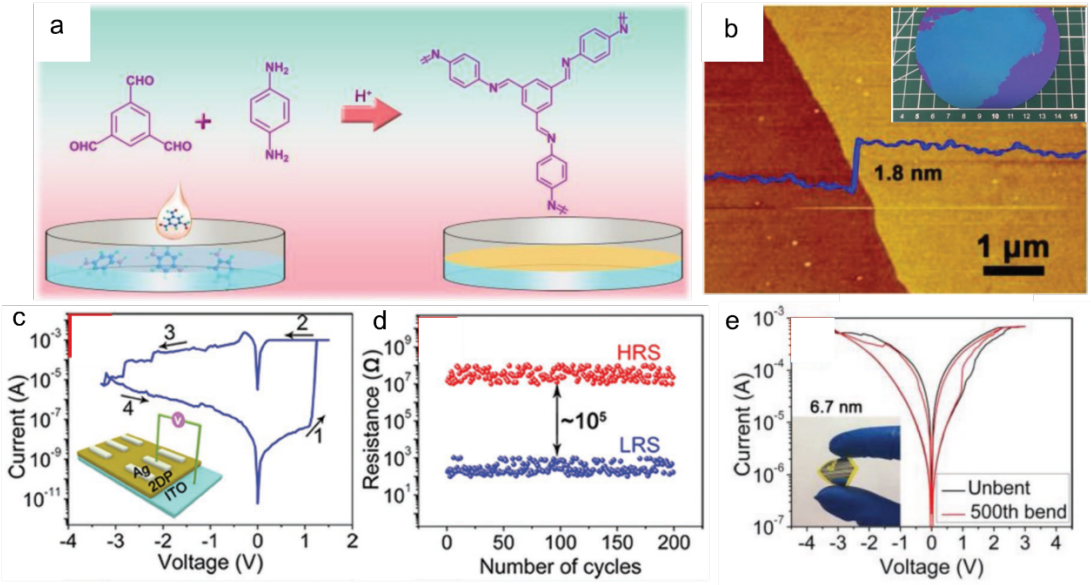


**Figure 25.** (a) A schematic illustration of the synthesis of $2DP_{BTA+PDA}$ films through the Schiff-base reaction of the monomers. (b) AFM image of a 1.8 ± 0.2 nm thick $2DP_{BTA+PDA}$ film on a silicon wafer. (c) *I*-V plots for the initial formation process (Inset: the schematic diagram of the resistive switching device with a Ag/$2DP_{BTA+PDA}$/ITO configuration). d) Endurance performance of the on/off resistances plotted as a function of the number of cycles. Reproduced with permission from Ref. 535. Copyright 2019 Wiley & Sons.

## 6. Perspective and outlook

The literature discussed here leaves no doubt that the extension of OFM (both MOFs and COFs) to electronic device applications is a highly active area of research. It is particularly noteworthy that several of the major challenges identified in the two roadmap documents, although not yet solved, are the focus of vigorous research efforts. In the roughly three years since the updated MOF roadmap was published,[9] several hundred articles have appeared describing the development of new OFM film growth methods and serving as semiconductors, dielectrics, and ionic conductors. Proof-of-concept demonstrations of several device types have appeared as well, including FETs of various architectures for logic and memory, memristors operating by a variety of mechanisms, and electrically transduced strain sensors and photodetectors. New OFM subclasses are also appearing, increasing the possibilities for both improved charge transport properties relative to 3D MOFs and COFs and device-compatible fabrication methods.

These developments are highly encouraging and validate the hypothesis that OFM are a legitimate class of electronic materials with unique properties. Although it is still the case that commercialized OFM-based devices are yet to be realized, thus far the field has not encountered any show-stopping problems. It is worth remembering that, historically, approximately two decades are required to move a new material from the laboratory to production.[536,537] A useful

Final edited form was published in "Chemical Reviews 2020, 120(1), S. 8581-8640. ISSN 1520-6890.
https://doi.org/10.1021/acs.chemrev.0c00033

comparison in this regard can be made with organic semiconductors. Molecular organic semiconductors became known in the 1960s and the first conducting organic polymers were reported by Heeger and others in 1977,[538,539] but these materials did not begin to be commercialized until about a decade ago.[540]

Creating OFM with ionic or electronic charge transport properties sufficient for applications remains a great challenge. The need for OFM with tailorable charge transport, including mobility, carrier concentration, band gap, and band dispersion was already highlighted in the first roadmap[8] as well as in the second.[9] Particularly encouraging is the recent expansion of the category of 2D frameworks (Section 4), some of which have very high electrical conductivity and mobility.[49,126,541] Only recently was an example of a 3D OFM with comparable properties reported.[371] This suggests that the close stacking of the layers in 2D materials is the most efficient for enhancing charge transport in OFM and highlights the need to develop strategies for more effective through-bond or guest-induced transport.[542]

An important aspect relevant to OFM charge transport as well as other properties is the poor understanding of defects in these materials. The heterogeneous features originating from small crystalline domains, crystal boundaries, and lattice defects as well as the random orientation of nanocrystals can limit the long-range charge transport. The recently developed MOF glasses with permanent porosity[543] present an additional twist on the structure-property relationship. Although as yet none have been reported that are electrically conducting, the absence grain boundaries could lead to enhanced charge transport. Although defects and their effects on gas sorption and catalytic behavior have been studied,[544] their influence on properties such as bandgap and conductivity are only beginning to be probed. The oft-repeated axiom that "defects are the material" is illustrated by DFT modeling of $Ni_3(HITP)_2$, the prototype MOF graphene analogue,[125]which predicts a startling sensitivity of the bandgap to very slight changes in the stacking arrangement.[368] It is clear that defects in OFM must be understood at a much deeper level before the true structure-property relationships governing OFM optoelectronic properties can be determined.

The need for reliable methods to integrate OFM with other materials is unchanged and has been highlighted here as well as in both roadmaps. There is no doubt that major efforts are still needed to develop controlled, reproducible, and scaleable fabrication routes. Although as Section 2 illustrates, the number of fabrication routes and materials deposited continues to increase, it is still the case that very few methods are applicable to a wide range of OFM. Films of these materials are typically polycrystalline, unoriented, and have a range of crystallite sizes that can affect their properties. Single-crystal films have not been achieved on the scale of electronic devices and wide-area growth of oriented films has only been achieved in a few cases. Solvothermal methods have the greatest generality, but these do not produce oriented films and control of thickness and morphology can be difficult. To enable facile insertion into a CMOS process, a gas-phase method is highly desirable, but the number of OFM for which such processes (PVD, CVD, and ALD) have been developed remains very small. Moreover, a significant complicating factor is the high-temperature "burn-in" step at the CMOS back end of the line. The temperatures used typically exceed the stability limits of even the most robust frameworks. A similar problem exists for organics but can be circumvented by using evaporation techniques that do not affect the integrity of the CMOS substrate. Unfortunately, most OFM growth methods require solvents and potentially corrosive conditions that can be incompatible with prefabricated semiconductor devices. In spite of these limitations, the research discussed in Sections 3, 4, and 5 demonstrate that OFM-enabled devices useful for specific applications can be fabricated.

Final edited form was published in "Chemical Reviews 2020, 120(1), S. 8581-8640. ISSN 1520-6890.
https://doi.org/10.1021/acs.chemrev.0c00033

Perhaps the most important overarching conclusion from the research summarized in this review is that OFM should not be considered as a replacement (or even an alternative) for either inorganic semiconductors or organic conductors (molecular or polymeric). Instead, as mentioned in the introduction, OFM possess a unique combination of properties that make them ideal for applications for which conventional conductors are unsuitable. Nanoporosity is of course the most obvious of these properties, but mechanical flexibility, high-temperature stability compared with organics, and long-range crystalline order are also important benefits. Although electrical conductivity does not match the best organic conductors, in many reported examples the charge transport is intrinsic to the framework, i.e., it can be achieved without doping. This simplifies device fabrication and contributes to higher long-term stability, as dopant migration and reactivity are not issues. Finally, examples in Section 5 demonstrate that the potential for fast ion transport makes OFM promising candidates for advanced memory and logic concepts that could address limitations of CMOS such as power consumption.

We conclude that, not discounting the major challenges still facing their use for electronic devices, OFM remain an exciting possibility for next-generation electronics and sensing. Unlike all other categories of nanoporous materials, as well as inorganic and organic conductors, OFM are remarkable in the scope of potential uses for both well-explored venues such as gas storage, separations, and catalysis, as well as high-tech applications as diverse as memory, energy conversion, and biocompatible sensing. The acceleration of research in an application space that was first considered only in the late 2000s is remarkable. With the pace of development continuing to increase, it seems plausible that OFM-enabled electronic devices could be commercialized within the next decade.

Final edited form was published in "Chemical Reviews 2020, 120(1), S. 8581-8640. ISSN 1520-6890.
https://doi.org/10.1021/acs.chemrev.0c00033

## AUTHOR INFORMATION

### Corresponding Author

* mdallen@sandia.gov

### ORCID

Mark D. Allendorf: 0000-0001-5645-8246

Renhao Dong 0000-0002-4125-9284

Xinliang Feng 0000-0003-3885-2703

Stefan Kaskel 0000-0003-4572-0303

Dariusz Matoga 0000-0002-0064-5541

Vitalie Stavila: 0000-0003-0981-0432

### Notes

The authors declare no competing financial interest.

### Biographies

**Mark D. Allendorf** is Co-Director of the Hydrogen Advanced Materials Research Consortium (HyMARC) and a Senior Scientist at Sandia National Laboratories in Livermore, California. He holds degrees in chemistry from Washington University in St. Louis (A.B.) and a Ph.D. in inorganic chemistry at Stanford University. At Sandia, his research focuses on the fundamental science and applications of metal-organic frameworks (MOFs) and on hydrogen storage. His interests include nanoscale metal hydrides and MOFs for hydrogen storage, chemical and radiation sensing, gas separations, MOFs for electronic devices, and catalysts for biofuels production. He is President Emeritus and Fellow of The Electrochemical Society and has received awards for research, leadership, and teamwork, including a 2014 R&D100 Award for a novel approach to radiation detection.

**Renhao Dong** is an independent research group leader in the Faculty of Chemistry and Food Chemistry at Technical University of Dresden. He obtained his B.S. degree in chemistry from Shandong University in 2008 and completed his Ph.D. study with a focus on colloid and interface chemistry under the supervision of Prof. Jingcheng Hao at Shandong University (China) in 2013. Then he joined Prof. Klaus Müllen's group as a Postdoctoral Fellow at Max Planck Institute for Polymer Research (Mainz, Germany) in August 2013. In 2015, he joined Prof. Xinliang Feng's group as an Alexander von Humboldt Foundation Fellow at Technical University of Dresden (Dresden, Germany). Since 2017, he has been a research group leader. His current research interest focuses on chemistry of organic 2D materials such as 2D polymers, 2D supramolecular polymers, 2D covalent organic frameworks, and 2D conjugated metal-organic frameworks as well as their functions in electronics and energy storage/conversion.

Final edited form was published in "Chemical Reviews 2020, 120(1), S. 8581-8640. ISSN 1520-6890.
https://doi.org/10.1021/acs.chemrev.0c00033

**Xinliang Feng** is a full professor and has been the head of the Chair for Molecular Functional Materials at Technische Universität Dresden since 2014. His current scientific interests include organic synthetic methodology, organic synthesis and supramolecular chemistry of π-conjugated system, bottom-up synthesis of graphene and graphene nanoribbons, electrochemical exfoliation of 2D crystals, 2D polymers and supramolecular polymers as well as 2D carbon-rich conjugated polymers for opto-electronic applications, energy storage and conversion, new energy devices and technologies. He has published more than 480 research articles which have attracted more than 52000 citations with H-index of 109.

**Stefan Kaskel** studied chemistry and received his Ph.D. in Tübingen (1997). After a postdoctoral stay in the group of J. D. Corbett (Ames, USA), he obtained his habilitation degree at Bochum University on the design and functionality of new porous materials (2003). At the same time, he was a group leader at the Max Planck Institute for Coal Research from 2002 to 2004. Since June 2004, he has been a Professor of Inorganic Chemistry at Dresden University of Technology, and from 2008 onward, also the head of the business unit Chemical Surface Technology at the Fraunhofer Institute for Material and Beam Technology (IWS). His research interests are focused on porous and nanostructured materials (high surface area carbons and MOFs) for applications in energy storage, catalysis, batteries and separation technologies. Stefan Kaskel has authored more than 440 publications with > 27000 citations (google scholar h-index 90) and has contributed as inventor to more than 50 patent applications. Since 2016 he was recognized annually as a Highly Cited Researcher by Thomson Reuters and Clarivate Analytics. He is a Fellow of the Royal Chemical Society and a Fellow of the European Academy of Sciences (EurASc).

**Dariusz Matoga** is a University Professor at Faculty of Chemistry, Jagiellonian University in Kraków, Poland. After graduation from interdisciplinary Studies in Mathematics and Natural Sciences, he received an MSc degree in chemistry followed by PhD and habilitation degrees in chemical sciences from Jagiellonian University. In the meantime, he worked as a post-doctoral fellow at Kwansei Gakuin University in Sanda, Japan and as a visiting consultant and lecturer at Sultan Qaboos University in Muscat, Oman. His current research interests comprise synthesis of new metal-organic frameworks with a particular focus on flexible networks, structure-property correlations and applications of these materials including proton conduction and sensing.

**Vitalie Stavila** is a Principal Member of Technical Staff at Sandia National Laboratories in Livermore, CA. He earned his Ph.D. in inorganic chemistry in 2002 from State University of Moldova. His projects in the area of open framework materials are focused on studying the fundamental processes (thermodynamic, kinetic, and mechanical) that lead to different structures and morphologies, and utilizing this knowledge to create novel materials for (opto)electronic applications. A central theme in Dr. Stavila's research is the rational design of new materials by changing the chemical composition, the arrangement of the atoms or molecules in crystalline or amorphous configurations, and the size, shape, and orientation of nano- or macroscopic objects.

## Acknowledgements

M.A. and V.S. gratefully acknowledge the support of the Sandia Laboratory Directed Research and Development (LDRD) Program. R.D. gratefully acknowledges ERC Starting Grant (FC2DMOF, No. 852909) and DFG funding (SPP1928, COORNET). X.F. thanks the financial support from EU Graphene Flagship (No.785219) and ERC Consolidator Grant (T2DCP). S.K. acknowledges DFG funding (FOR2433, SPP1928). D.M. gratefully acknowledges the National Science Centre (NCN, Poland) for the financial support (Grant no. 2015/17/B/ST5/01190). Sandia

Final edited form was published in "Chemical Reviews 2020, 120(1), S. 8581-8640. ISSN 1520-6890.
https://doi.org/10.1021/acs.chemrev.0c00033

National Laboratories is a multimission laboratory managed and operated by National Technology and Engineering Solutions of Sandia, LLC., a wholly owned subsidiary of Honeywell International, Inc., for the U.S. Department of Energy's National Nuclear Security Administration under contract DE-NA-0003525. Sandia National Laboratories is a multimission laboratory managed and operated by National Technology and Engineering Solutions of Sandia, LLC., a wholly owned subsidiary of Honeywell International, Inc., for the U.S. Department of Energy's National Nuclear Security Administration under contract DE-NA-0003525.

## Abbreviations

| | |
|---|---|
| AC | alternating current |
| ALD | atomic layer deposition |
| AFM | atomic force miscroscopy |
| ANN | artificial neural network |
| BC | bottom-contact |
| BDC | 1,4-benzenedicarboxylate |
| BDP | 1,4-benzenedipyrazolate |
| BDT | benzodithiophene |
| BDTBA | benzo[1,2-b:4,5-b′]dithiophene-2,6-diyldiboronic acid |
| BG | bottom-gate |
| BHS | benzenehexaselenol |
| BHT | benzenehexathiolate |
| bpy | 4,4'-bipyridine |
| BTA | benzene-1,3,5-tricarbaldehyde |
| BTC | 1,3,5-benzenetricarboxylate |
| CE | counter electrode |
| COF | covalent-organic framework |
| CMOS | complementary metal oxide semiconductor |
| CNP | carbon nanoparticles |
| CPD | contact potential difference |
| CVD | chemical vapor deposition |
| DABCO | 1,4-diazabicyclo(2,2,2)octane |
| DBA | 1,4-phenylenediboronic acid |
| DBC | dibenzo[g,p]chrysene |
| DC | direct current |
| DFT | density functional theory |
| DMF | *N,N′*-dimethylformamide |
| DMMP | dimethylmethylphosphonate |
| DPNI | *N,N′*-di(4-pyridyl)- 1,4,5,8-naphthalenetetracarboxydiimide |
| DPP | 1,3-di(4-pyridyl)propane |
| EDOT | 3,4-ethylenedioxythiophene |
| EDS | energy-dispersive X-ray spectroscopy |
| en | ethylenediamine |

Final edited form was published in "Chemical Reviews 2020, 120(1), S. 8581-8640. ISSN 1520-6890.
https://doi.org/10.1021/acs.chemrev.0c00033

| | |
|---|---|
| EPR | electron paramagnetic resonance |
| FET | field-effect transistor |
| FP-TMRC | flash photolysis time-resolved microwave conductivity |
| F-RAM | ferroelectric random access memory |
| FTO | fluorine-doped tin oxide |
| fum | fumarate |
| GCE | glassy carbon electrode |
| GIXRD | grazing incidence X-Ray diffraction |
| GO | graphene oxide |
| GR | graphite |
| HAB | hexaaminobenzene |
| HAADF | high-angle annular dark-field imaging |
| HATP | 2,3,6,7,10,11-hexaaminotriphenylene |
| HHB | hexahydroxybenzene |
| HHTP | 2,3,6,7,10,11-hexahydroxytriphenylene |
| HIB | hexaiminobenzene |
| HITP | 2,3,6,7,10,11-hexaiminotriphenylene |
| HOPG | highly oriented pyrolytic graphite |
| HOMO | highest occupied molecular orbital |
| HRTEM | high-resolution transmission electron microscopy |
| HTB | benzenehexathiolate |
| HTTP | 2,3,6,7,10,11-hexathiolatedtriphenylene |
| IDE | interdigitated electrode |
| im | imidazolate |
| INA | isonicotinate |
| ISE | ion-selective electrode |
| ISM | ion-selective membrane |
| ITO | indium tin oxide |
| IVCT | intervalence charge transfer |
| KP | Kelvin probe |
| LbL | layer-by-layer |
| LOD | limit of detection |
| LUMO | lowest unoccupied molecular orbital |
| mim | 2-methylimidazolate |
| 6-mn | 6-mercaptonicotinate |
| mpca | 2-pyrazine-5-methyl-carboxylate |
| MOF | metal-organic framework |
| MOG | metal-organic graphene |
| MOL | metal-organic layer |
| NDC | 2,7-naphthalene dicarboxylate |
| *o*-CbPhH$_2$IDC | 2-(2-carboxylphenyl)-1*H*-imidazole-4,5-dicarboxylate |
| OFM | open framework materials |
| OER | oxygen evolution reaction |
| PC | polycarbonate |
| Pc | phthalocyanine |

Final edited form was published in "Chemical Reviews 2020, 120(1), S. 8581-8640. ISSN 1520-6890.
https://doi.org/10.1021/acs.chemrev.0c00033

| | |
|---|---|
| pdt | 2,3-pyrazinedithiolate |
| PANI | polyaniline |
| PBBA | 1,4-phenylenebis(boronic acid) |
| PDA | *p*-phenylenediamine |
| PE | polyethylene |
| PEDOT | poly(3,4-ethylenedioxythiophene) |
| PEM | proton-exchange membrane; polymer electrolyte membrane |
| *p*-IPhHIDC | 2-(*p*-N-imidazol-1-yl)-phenyl-1*H*-imidazole-4,5-dicarboxylate |
| PLD | pulsed layer deposition |
| polyTB | poly(toluidine blue) |
| POM | polyoxometalate |
| PPDA | *p*-phenylenediamine |
| PTC | perthiolatedcoronene |
| PTFE | polytetrafluoroethylene |
| PS | polystyrene |
| PVD | physical vapor deposition |
| pyz, pz | pyrazine |
| pzdc | pyrazine-2,3-dicarboxylate |
| QCM | quartz crystal microbalance |
| RAM | random access memory |
| RE | reference electrode |
| rGO | reduced graphene oxide |
| RH | relative humidity |
| RRAM | resistive random access memory |
| RS | resistive switching |
| RT | room temperature |
| SAED | selected area electron diffraction |
| SAM | self-assembled monolayer |
| SEM | scanning electron microscopy |
| SOC | spin-orbital coupling |
| SLG | single-layer graphene |
| SMO | semiconductor metal oxide |
| SOFT | self-assembled framework on textiles |
| STEM | scanning transmission electron microscopy |
| SURMOF | surface-mounted MOF |
| TATTB | triaminotrithiolatedbenzene |
| TBAPy | 1,3,6,8-tetrakis(p-benzoic acid)pyrene |
| TBTC | 1,3,5-tris[4-(carboxyphenyl)-oxamethyl]-2,4,6-trimethylbenzene |
| TC | top-contact |
| TCA | tricarboxytriphenylamine |
| TCNQ | 7,7,8,8-tetracyanoquinododimethane |
| TCPP | tetrakis(4-carboxyphenyl)porphyrin |
| TDA | 2,5-thiophene-dicarboxylate |
| TEA | triethylamine |
| TEM | transmission electron microscopy |

| | |
|---|---|
| TFPy | 1,3,6,8-tetrakis(*p*- formylphenyl)pyrene |
| TFT | thin-film transistor |
| TG | top-gate |
| thf | tetrahydrofuran |
| THT | 2,3,6,7,10,11-triphenylenehexathiol |
| TI | topological insulator |
| TMA | 3-thiophenemalonate |
| TRTS | time-resolved terahertz spectroscopy |
| TX | truxene, 10,15-dihydro-5*H*-diindeno[1,2-*a*:1′,2′-*c*]fluorene |
| UMOFN | ultrathin metal-organic framework nanosheet |
| VFET | vertical field-effect transistor |
| VOC | volatile organic compound |
| WE | working electrode |
| XPS | X-ray photoelectron spectroscopy |
| XRD | X-ray diffraction |
| ZIF | zeolitic imidazolate framework |

Final edited form was published in "Chemical Reviews 2020, 120(1), S. 8581-8640. ISSN 1520-6890.
https://doi.org/10.1021/acs.chemrev.0c00033

## REFERENCES

(1) Furukawa, H.; Cordova, K. E.; O'Keeffe, M.; Yaghi, O. M. The Chemistry and Applications of Metal-Organic Frameworks. *Science* **2013,** *341*, 1230444.
(2) *The Chemistry of Metal–Organic Frameworks: Synthesis, Characterization, and Applications, Vol. 1*; Kaskel, S., Ed.; Wiley: Weinheim, 2016; Vol. 1.
(3) Diercks, C. S.; Yaghi, O. M. The Atom, the Molecule, and the Covalent Organic Framework. *Science* **2017,** *355*, 923-930.
(4) Canivet, J.; Fateeva, A.; Guo, Y. M.; Coasne, B.; Farrusseng, D. Water Adsorption in Mofs: Fundamentals and Applications. *Chem. Soc. Rev.* **2014,** *43*, 5594-5617.
(5) Wang, C. H.; Liu, X. L.; Demir, N. K.; Chen, J. P.; Li, K. Applications of Water Stable Metal-Organic Frameworks. *Chem. Soc. Rev.* **2016,** *45*, 5107-5134.
(6) DeSantis, D.; Mason, J. A.; James, B. D.; Houchins, C.; Long, J. R.; Veenstra, M. Techno-Economic Analysis of Metal-Organic Frameworks for Hydrogen and Natural Gas Storage. *Energy Fuels* **2017,** *31*, 2024-2032.
(7) "2015 International Technology Roadmap for Semiconductors (Itrs)," Semiconductor Industry Association, 2015.
(8) Allendorf, M. D.; Schwartzberg, A.; Stavila, V.; Talin, A. A. A Roadmap to Implementing Metal-Organic Frameworks in Electronic Devices: Challenges and Critical Directions. *Chem. Eur. J.* **2011,** *17*, 11372-11388.
(9) Stassen, I.; Burtch, N.; Talin, A.; Falcaro, P.; Allendorf, M.; Ameloot, R. An Updated Roadmap for the Integration of Metal-Organic Frameworks with Electronic Devices and Chemical Sensors. *Chem. Soc. Rev.* **2017,** *46*, 3185-3241.
(10) Anik, U.; Timur, S.; Dursun, Z. Metal Organic Frameworks in Electrochemical and Optical Sensing Platforms: A Review. *Microchim. Acta* **2019,** *186*, 196.
(11) Campbell, M. G.; Dinca, M. Metal-Organic Frameworks as Active Materials in Electronic Sensor Devices. *Sensors* **2017,** *17*.
(12) Chen, K.; Wu, C. D. Development of Photoluminescence Metal-Organic Framework Sensors Consisting of Dual-Emission Centers. *Chinese Chem. Lett.* **2018,** *29*, 823-826.
(13) Chidambaram, A.; Stylianou, K. C. Electronic Metal-Organic Framework Sensors. *Inorg. Chem. Front.* **2018,** *5*, 979-998.
(14) Dolgopolova, E. A.; Rice, A. M.; Martin, C. R.; Shustova, N. B. Photochemistry and Photophysics of Mofs: Steps Towards Mof-Based Sensing Enhancements. *Chem. Soc. Rev.* **2018,** *47*, 4710-4728.
(15) Fang, X.; Zong, B. Y.; Mao, S. Metal-Organic Framework-Based Sensors for Environmental Contaminant Sensing. *Nano-Micro Lett.* **2018,** *10*.
(16) Hao, Y. Q.; Chen, S.; Zhou, Y. L.; Zhang, Y. T.; Xu, M. T. Recent Progress in Metal-Organic Framework (Mof) Based Luminescent Chemodosimeters. *Nanomater.* **2019,** *9*.
(17) Jiang, X. X.; Zhao, C. J.; Zhong, C. J.; Li, J. P. The Electrochemical Sensors Based on Mof and Their Applications. *Prog. Chem.* **2017,** *29*, 1206-1214.
(18) Kempahanumakkagari, S.; Vellingiri, K.; Deep, A.; Kwon, E. E.; Bolan, N.; Kim, K. H. Metal-Organic Framework Composites as Electrocatalysts for Electrochemical Sensing Applications. *Coord. Chem. Rev.* **2018,** *357*, 105-129.
(19) Koo, W. T.; Jang, J. S.; Kim, I. D. Metal-Organic Frameworks for Chemiresistive Sensors. *Chem* **2019,** *5*, 1938-1963.

(20) Liao, Z. L.; Xia, T. F.; Yu, E. Y.; Cui, Y. J. Luminescent Metal-Organic Framework Thin Films: From Preparation to Biomedical Sensing Applications. *Crystals* **2018,** *8*.
(21) Liu, L. T.; Zhou, Y. L.; Liu, S.; Xu, M. T. The Applications of Metal-Organic Frameworks in Electrochemical Sensors. *ChemElectroChem* **2018,** *5*, 6-19.
(22) Liu, X. G.; Huang, D. L.; Lai, C.; Zeng, G. M.; Qin, L.; Wang, H.; Yi, H.; Li, B. S.; Liu, S. Y.; Zhang, M. M.et al. Recent Advances in Covalent Organic Frameworks (Cofs) as a Smart Sensing Material. *Chem. Soc. Rev.* **2019,** *48*, 5266-5302.
(23) Liu, Y.; Xie, X. Y.; Cheng, C.; Shao, Z. S.; Wang, H. S. Strategies to Fabricate Metal-Organic Framework (Mof)-Based Luminescent Sensing Platforms. *J. Mater. Chem. A* **2019,** *7*, 10743-10763.
(24) Lustig, W. P.; Mukherjee, S.; Rudd, N. D.; Desai, A. V.; Li, J.; Ghosh, S. K. Metal-Organic Frameworks: Functional Luminescent and Photonic Materials for Sensing Applications. *Chem. Soc. Rev.* **2017,** *46*, 3242-3285.
(25) Mahata, P.; Mondal, S. K.; Singha, D. K.; Majee, P. Luminescent Rare-Earth-Based Mofs as Optical Sensors. *Dalton Trans.* **2017,** *46*, 301-328.
(26) Mako, T. L.; Racicot, J. M.; Levine, M. Supramolecular Luminescent Sensors. *Chem. Rev.* **2019,** *119*, 322-477.
(27) Mandal, T. N.; Karmakar, A.; Sharma, S.; Ghosh, S. K. Metal-Organic Frameworks (Mofs) as Functional Supramolecular Architectures for Anion Recognition and Sensing. *Chem. Record* **2018,** *18*, 154-164.
(28) Tong, P. H.; Liang, J. Y.; Jiang, X. X.; Li, J. P. Research Progress on Metal-Organic Framework Composites in Chemical Sensors. *Crit. Rev. Anal. Chem.*, DOI:10.1080/10408347.2019.1642732 10.1080/10408347.2019.1642732.
(29) Zhang, Q.; Wang, C. F.; Lv, Y. K. Luminescent Switch Sensors for the Detection of Biomolecules Based on Metal-Organic Frameworks. *Analyst* **2018,** *143*, 4221-4229.
(30) Zhang, Y. M.; Yuan, S.; Day, G.; Wang, X.; Yang, X. Y.; Zhou, H. C. Luminescent Sensors Based on Metal-Organic Frameworks. *Coord. Chem. Rev.* **2018,** *354*, 28-45.
(31) Zhao, F.; Sun, T.; Geng, F. Y.; Chen, P. Y.; Gao, Y. P. Metal-Organic Frameworks-Based Electrochemical Sensors and Biosensors. *Int. J. Electrochem. Sci.* **2019,** *14*, 5287-5304.
(32) Zhao, S. N.; Wang, G. B.; Poelman, D.; Van der Voort, P. Luminescent Lanthanide Mofs: A Unique Platform for Chemical Sensing. *Materials* **2018,** *11*.
(33) Nguyen, T. N.; Ebrahim, F. M.; Stylianou, K. C. Photoluminescent, Upconversion Luminescent and Nonlinear Optical Metal-Organic Frameworks: From Fundamental Photophysics to Potential Applications. *Coord. Chem. Rev.* **2018,** *377*, 259-306.
(34) Xie, L. S.; Skorupskii, G.; Dincă, M. Electrically Conductive Metal–Organic Frameworks. *Chem. Rev.* **2020**, DOI:10.1021/acs.chemrev.9b00766 10.1021/acs.chemrev.9b00766.
(35) Xue, R.; Guo, H.; Wang, T.; Gong, L.; Wang, Y. N.; Ai, J. B.; Huang, D. D.; Chen, H. Q.; Yang, W. Fluorescence Properties and Analytical Applications of Covalent Organic Frameworks. *Anal. Meth.* **2017,** *9*, 3737-3750.
(36) Gu, Z. G.; Zhang, J. Epitaxial Growth and Applications of Oriented Metal-Organic Framework Thin Films. *Coord. Chem. Rev.* **2019,** *378*, 513-532.
(37) Liu, J. X.; Woll, C. Surface-Supported Metal-Organic Framework Thin Films: Fabrication Methods, Applications, and Challenges. *Chem. Soc. Rev.* **2017,** *46*, 5730-5770.

(38) Wang, H.; Zeng, Z. T.; Xu, P.; Li, L. S.; Zeng, G. M.; Xiao, R.; Tang, Z. Y.; Huang, D. L.; Tang, L.; Lai, C.et al. Recent Progress in Covalent Organic Framework Thin Films: Fabrications, Applications and Perspectives. *Chem. Soc. Rev.* **2019,** *48*, 488-516.
(39) Zhao, M. T.; Huang, Y.; Peng, Y. W.; Huang, Z. Q.; Ma, Q. L.; Zhang, H. Two-Dimensional Metal-Organic Framework Nanosheets: Synthesis and Applications. *Chem. Soc. Rev.* **2018,** *47*, 6267-6295.
(40) Zhao, W. W.; Peng, J. L.; Wang, W. K.; Liu, S. J.; Zhao, Q.; Huang, W. Ultrathin Two-Dimensional Metal-Organic Framework Nanosheets for Functional Electronic Devices. *Coord. Chem. Rev.* **2018,** *377*, 44-63.
(41) Moore, G. E. Cramming More Components onto Integrated Circuits. *Electronics* **1965,** *86*, 114.
(42) Moore, G. E. 1975 International Electron Devices, Washington, D.C., 1975; p 11.
(43) Moore, S. K. Another Step toward the End of Moore's Law. *IEEE Spectrum* **2019,** *56*, 9-10.
(44) Theis, T. N.; Wong, H. S. P. The End of Moore's Law: A New Beginning for Information Technology. *Computing Sci. Eng.* **2017,** *19*, 41-50.
(45) Hilbert, M.; Lopez, P. The World's Technological Capacity to Store, Communicate, and Compute Information. *Science* **2011,** *332*, 60-65.
(46) Allendorf, M. D.; Foster, M. E.; Leonard, F.; Stavila, V.; Feng, P. L.; Doty, F. P.; Leong, K.; Ma, E. Y.; Johnston, S. R.; Talin, A. A. Guest-Induced Emergent Properties in Metal-Organic Frameworks. *J. Phys. Chem. Lett.* **2015,** *6*, 1182-1195.
(47) Auslender, M.; Hava, S. In *Springer Handbook of Electronic and Photonic Materials*; Kasap, S.;Capper, P., Eds.; Springer International Publishing: Cham, 2017, DOI:10.1007/978-3-319-48933-9_21 10.1007/978-3-319-48933-9_21.
(48) Huang, X.; Sheng, P.; Tu, Z.; Zhang, F.; Wang, J.; Geng, H.; Zou, Y.; Di, C.-a.; Yi, Y.; Sun, Y.et al. A Two-Dimensional Π–D Conjugated Coordination Polymer with Extremely High Electrical Conductivity and Ambipolar Transport Behaviour. *Nat. Commun.* **2015,** *6*, 7408.
(49) Dong, R.; Han, P.; Arora, H.; Ballabio, M.; Karakus, M.; Zhang, Z.; Shekhar, C.; Adler, P.; Petkov, P. S.; Erbe, A.et al. High-Mobility Band-Like Charge Transport in a Semiconducting Two-Dimensional Metal–Organic Framework. *Nat. Mater.* **2018,** *17*, 1027-1032.
(50) Fratini, S.; Nikolka, M.; Salleo, A.; Schweicher, G.; Sirringhaus, H. Charge Transport in High-Mobility Conjugated Polymers and Molecular Semiconductors. *Nat. Mater.* **2020,** *19*, 491-502.
(51) Windischmann, H. Intrinsic Stress in Sputter-Deposited Thin-Films. *Crit. Rev. Anal. Chem.* **1992,** *17*, 547-596.
(52) Kang, D.; Kim, T. W.; Kubota, S. R.; Cardiel, A. C.; Cha, H. G.; Choi, K. S. Electrochemical Synthesis of Photoelectrodes and Catalysts for Use in Solar Water Splitting. *Chem. Rev.* **2015,** *115*, 12839-12887.
(53) Hu, J. Q.; Bando, Y.; Golberg, D. Novel Semiconducting Nanowire Heterostructures: Synthesis, Properties and Applications. *J. Mater. Chem.* **2009,** *19*, 330-343.
(54) He, L.; Kou, X. F.; Wang, K. L. Review of 3d Topological Insulator Thin-Film Growth by Molecular Beam Epitaxy and Potential Applications. *Phys. Status Solidi-R* **2013,** *7*, 50-63.

(55) Liu, B. L.; Abbas, A.; Zhou, C. W. Two-Dimensional Semiconductors: From Materials Preparation to Electronic Applications. *Adv. Electron. Mater.* **2017,** *3*, 1700045.
(56) Biyikli, N.; Haider, A. Atomic Layer Deposition: An Enabling Technology for the Growth of Functional Nanoscale Semiconductors. *Semicon. Sci. Tech.* **2017,** *32*.
(57) Kumah, D. P.; Ngai, J. H.; Kornblum, L. Epitaxial Oxides on Semiconductors: From Fundamentals to New Devices. *Adv. Funct. Mater.*, DOI:10.1002/adfm.201901597 10.1002/adfm.201901597.
(58) Christenson, H. K. Confinement Effects on Freezing and Melting. *J. Phys. Condensed Matter* **2001,** *13*, R95-R133.
(59) Stiff-Roberts, A. D.; Ge, W. Y. Organic/Hybrid Thin Films Deposited by Matrix-Assisted Pulsed Laser Evaporation (Maple). *Appl. Phys. Rev.* **2017,** *4*.
(60) Haick, H.; Cahen, D. Contacting Organic Molecules by Soft Methods: Towards Molecule-Based Electronic Devices. *Acc. Chem. Res.* **2008,** *41*, 359-366.
(61) Rullyani, C.; Ramesh, M.; Sung, C. F.; Lin, H. C.; Chu, C. W. Natural Polymers for Disposable Organic Thin Film Transistors. *Org. Electron.* **2018,** *54*, 154-160.
(62) Mähringer, A.; Jakowetz, A. C.; Rotter, J. M.; Bohn, B. J.; Stolarczyk, J. K.; Feldmann, J.; Bein, T.; Medina, D. D. Oriented Thin Films of Electroactive Triphenylene Catecholate-Based Two-Dimensional Metal–Organic Frameworks. *ACS Nano* **2019,** *13*, 6711-6719.
(63) Medina, D. D.; Rotter, J. M.; Hu, Y.; Dogru, M.; Werner, V.; Auras, F.; Markiewicz, J. T.; Knochel, P.; Bein, T. Room Temperature Synthesis of Covalent–Organic Framework Films through Vapor-Assisted Conversion. *J. Am. Chem. Soc.* **2015,** *137*, 1016-1019.
(64) Mushtaq, F.; Chen, X.; Torlakcik, H.; Steuer, C.; Hoop, M.; Siringil, E. C.; Marti, X.; Limburg, G.; Stipp, P.; Nelson, B. J.et al. Magnetoelectrically Driven Catalytic Degradation of Organics. *Adv. Mater.* **2019,** *31*, 1901378.
(65) Virmani, E.; Rotter, J. M.; Mähringer, A.; von Zons, T.; Godt, A.; Bein, T.; Wuttke, S.; Medina, D. D. On-Surface Synthesis of Highly Oriented Thin Metal–Organic Framework Films through Vapor-Assisted Conversion. *J. Am. Chem. Soc.* **2018,** *140*, 4812-4819.
(66) Haraguchi, T.; Otsubo, K.; Sokota, O.; Fujiwara, A.; Kitagawa, H. Guest-Induced Two-Way Structural Transformation in a Layered Metal-Organic Framework Thin Film. *J. Am. Chem. Soc.* **2016,** *138*, 16787-16793.
(67) Haraguchi, T.; Otsubo, K.; Kitagawa, H. Emergence of Surface- and Interface-Induced Structures and Properties in Metal-Organic Framework Thin Films. *Eur. J. Inorg. Chem.* **2018**, 1697-1706.
(68) Scherb, C.; Schödel, A.; Bein, T. Directing the Structure of Metal–Organic Frameworks by Oriented Surface Growth on an Organic Monolayer. *Angew. Chem. Int. Ed.* **2008,** *47*, 5777-5779.
(69) Hermes, S.; Zacher, D.; Baunemann, A.; Woll, C.; Fischer, R. A. Selective Growth and Mocvd Loading of Small Single Crystals of Mof-5 at Alumina and Silica Surfaces Modified with Organic Self-Assembled Monolayers. *Chem. Mater.* **2007,** *19*, 2168-2173.
(70) Kubo, M.; Chaikittisilp, W.; Okubo, T. Oriented Films of Porous Coordination Polymer Prepared by Repeated in Situ Crystallization. *Chem. Mater.* **2008,** *20*, 2887-2889.
(71) Ameloot, R.; Stappers, L.; Fransaer, J.; Alaerts, L.; Sels, B. F.; De Vos, D. E. Patterned Growth of Metal-Organic Framework Coatings by Electrochemical Synthesis. *Chem. Mater.* **2009,** *21*, 2580-2582.

(72) Ameloot, R.; Pandey, L.; Van der Auweraer, M.; Alaerts, L.; Sels, B. F.; De Vos, D. E. Patterned Film Growth of Metal-Organic Frameworks Based on Galvanic Displacement. *Chem. Commun.* **2010,** *46*, 3735-3737.

(73) Demessence, A.; Horcajada, P.; Serre, C.; Boissiere, C.; Grosso, D.; Sanchez, C.; Ferey, G. Elaboration and Properties of Hierarchically Structured Optical Thin Films of Mil-101(Cr). *Chem. Commun.* **2009**, 7149-7151.

(74) Gascon, J.; Aguado, S.; Kapteijn, F. Manufacture of Dense Coatings of Cu-3(Btc)(2) (Hkust-1) on Alpha-Alumina. *Microporous Mesoporous Mater.* **2008,** *113*, 132-138.

(75) Horcajada, P.; Serre, C.; Grosso, D.; Boissiere, C.; Perruchas, S.; Sanchez, C.; Ferey, G. Colloidal Route for Preparing Optical Thin Films of Nanoporous Metal-Organic Frameworks. *Adv. Mater.* **2009,** *21*, 1931-1935.

(76) Li, Y. S.; Bux, H.; Feldhoff, A.; Li, G. L.; Yang, W. S.; Caro, J. Controllable Synthesis of Metal-Organic Frameworks: From Mof Nanorods to Oriented Mof Membranes. *Adv. Mater.* **2010,** *22*, 3322-3326.

(77) Li, Y. S.; Liang, F. Y.; Bux, H.; Feldhoff, A.; Yang, W. S.; Caro, J. Molecular Sieve Membrane: Supported Metal-Organic Framework with High Hydrogen Selectivity. *Angew. Chem. Int. Ed.* **2010,** *49*, 548-551.

(78) Bradshaw, D.; Garai, A.; Huo, J. Metal-Organic Framework Growth at Functional Interfaces: Thin Films and Composites for Diverse Applications. *Chem. Soc. Rev.* **2012,** *41*, 2344-2381.

(79) Denny, M. S.; Moreton, J. C.; Benz, L.; Cohen, S. M. Metal-Organic Frameworks for Membrane-Based Separations. *Nat. Rev. Mater.* **2016,** *1*.

(80) Furukawa, S.; Reboul, J.; Diring, S.; Sumida, K.; Kitagawa, S. Structuring of Metal-Organic Frameworks at the Mesoscopic/Macroscopic Scale. *Chem. Soc. Rev.* **2014,** *43*, 5700-5734.

(81) Gimenez-Marques, M.; Hidalgo, T.; Serre, C.; Horcajada, P. Nanostructured Metal-Organic Frameworks and Their Bio-Related Applications. *Coord. Chem. Rev.* **2016,** *307*, 342-360.

(82) Gu, Z. Y.; Yang, C. X.; Chang, N.; Yan, X. P. Metal-Organic Frameworks for Analytical Chemistry: From Sample Collection to Chromatographic Separation. *Acc. Chem. Res.* **2012,** *45*, 734-745.

(83) Huang, N.; Wang, P.; Jiang, D. L. Covalent Organic Frameworks: A Materials Platform for Structural and Functional Designs. *Nat. Rev. Mater.* **2016,** *1*.

(84) Kang, Z. X.; Fan, L. L.; Sun, D. F. Recent Advances and Challenges of Metal-Organic Framework Membranes for Gas Separation. *J. Mater. Chem. A* **2017,** *5*, 10073-10091.

(85) Kuyuldar, S.; Genna, D. T.; Burda, C. On the Potential for Nanoscale Metal-Organic Frameworks for Energy Applications. *J. Mater. Chem. A* **2019,** *7*, 21545-21576.

(86) Li, W.-J.; Tu, M.; Cao, R.; Fischer, R. A. Metal–Organic Framework Thin Films: Electrochemical Fabrication Techniques and Corresponding Applications & Perspectives. *J. Mater. Chem. A* **2016,** *4*, 12356-12369.

(87) Liao, P. Q.; Shen, J. Q.; Zhang, J. P. Metal-Organic Frameworks for Electrocatalysis. *Coord. Chem. Rev.* **2018,** *373*, 22-48.

(88) Liu, B.; Fischer, R. A. Liquid-Phase Epitaxy of Metal Organic Framework Thin Films. *Science China-Chem.* **2011,** *54*, 1851-1866.

(89) Ma, X. J.; Chai, Y. T.; Li, P.; Wang, B. Metal-Organic Framework Films and Their Potential Applications in Environmental Pollution Control. *Acc. Chem. Res.* **2019,** *52*, 1461-1470.
(90) Rodriguez-San-Miguel, D.; Zamora, F. Processing of Covalent Organic Frameworks: An Ingredient for a Material to Succeed. *Chem. Soc. Rev.* **2019,** *48*, 4375-4386.
(91) Sumida, K.; Liang, K.; Reboul, J.; Ibarra, I. A.; Furukawa, S.; Falcaro, P. Sol-Gel Processing of Metal-Organic Frameworks. *Chem. Mater.* **2017,** *29*, 2626-2645.
(92) Tu, M.; Wannapaiboon, S.; Fischer, R. A. Liquid Phase Stepwise Growth of Surface Mounted Metal-Organic Frameworks for Exploratory Research and Development of Applications. *Inorg. Chem. Front.* **2014,** *1*, 442-463.
(93) Van Vleet, M. J.; Weng, T. T.; Li, X. Y.; Schmidt, J. R. In Situ, Time-Resolved, and Mechanistic Studies of Metal-Organic Framework Nucleation and Growth. *Chem. Rev.* **2018,** *118*, 3681-3721.
(94) Waller, P. J.; Gandara, F.; Yaghi, O. M. Chemistry of Covalent Organic Frameworks. *Acc. Chem. Res.* **2015,** *48*, 3053-3063.
(95) Yuan, S. S.; Li, X.; Zhu, J. Y.; Zhang, G.; Van Puyvelde, P.; Van der Bruggen, B. Covalent Organic Frameworks for Membrane Separation. *Chem. Soc. Rev.* **2019,** *48*, 2665-2681.
(96) Zacher, D.; Shekhah, O.; Woll, C.; Fischer, R. A. Thin Films of Metal-Organic Frameworks. *Chem. Soc. Rev.* **2009,** *38*, 1418-1429.
(97) Lu, C. J.; Ben, T.; Xu, S. X.; Qiu, S. L. Electrochemical Synthesis of a Microporous Conductive Polymer Based on a Metal-Organic Framework Thin Film. *Angew. Chem. Int. Ed.* **2014,** *53*, 6454-6458.
(98) Falcaro, P.; Ricco, R.; Doherty, C. M.; Liang, K.; Hill, A. J.; Styles, M. J. Mof Positioning Technology and Device Fabrication. *Chem. Soc. Rev.* **2014,** *43*, 5513-5560.
(99) Stavila, V.; Talin, A. A.; Allendorf, M. D. Mof-Based Electronic and Opto-Electronic Devices. *Chem. Soc. Rev.* **2014,** *43*, 5994-6010.
(100) Park, M. J.; Lee, J. S. Zeolitic-Imidazole Framework Thin Film-Based Flexible Resistive Switching Memory. *RSC Adv.* **2017,** *7*, 21045-21049.
(101) Sun, B.; Zhu, C. H.; Liu, Y.; Wang, C.; Wan, L. J.; Wang, D. Oriented Covalent Organic Framework Film on Graphene for Robust Ambipolar Vertical Organic Field-Effect Transistor. *Chem. Mater.* **2017,** *29*, 4367-4374.
(102) Zhao, Y.; Guo, L.; Gándara, F.; Ma, Y.; Liu, Z.; Zhu, C.; Lyu, H.; Trickett, C. A.; Kapustin, E. A.; Terasaki, O.et al. A Synthetic Route for Crystals of Woven Structures, Uniform Nanocrystals, and Thin Films of Imine Covalent Organic Frameworks. *J. Am. Chem. Soc.* **2017,** *139*, 13166-13172.
(103) Li, F.-L.; Shao, Q.; Huang, X.; Lang, J.-P. Nanoscale Trimetallic Metal–Organic Frameworks Enable Efficient Oxygen Evolution Electrocatalysis. *Angew. Chem. Int. Ed.* **2018,** *57*, 1888-1892.
(104) Howarth, A. J.; Liu, Y.; Li, P.; Li, Z.; Wang, T. C.; Hupp, J. T.; Farha, O. K. Chemical, Thermal and Mechanical Stabilities of Metal–Organic Frameworks. *Nat. Rev. Mater.* **2016,** *1*, 15018.
(105) Shi, W.; Cao, L.; Zhang, H.; Zhou, X.; An, B.; Lin, Z.; Dai, R.; Li, J.; Wang, C.; Lin, W. Surface Modification of Two-Dimensional Metal–Organic Layers Creates Biomimetic Catalytic Microenvironments for Selective Oxidation. *Angew. Chem. Int. Ed.* **2017,** *56*, 9704-9709.

(106) Cao, L.; Lin, Z.; Shi, W.; Wang, Z.; Zhang, C.; Hu, X.; Wang, C.; Lin, W. Exciton Migration and Amplified Quenching on Two-Dimensional Metal–Organic Layers. *J. Am. Chem. Soc.* **2017,** *139*, 7020-7029.
(107) Ahrenholtz, S. R.; Epley, C. C.; Morris, A. J. Solvothermal Preparation of an Electrocatalytic Metalloporphyrin Mof Thin Film and Its Redox Hopping Charge-Transfer Mechanism. *J. Am. Chem. Soc.* **2014,** *136*, 2464-2472.
(108) Zhang, H.; Gao, X. W.; Wang, L.; Zhao, X. S.; Li, Q. Y.; Wang, X. J. Microwave-Assisted Synthesis of Urea-Containing Zirconium Metal-Organic Frameworks for Heterogeneous Catalysis of Henry Reactions. *CrystEngComm* **2019,** *21*, 1358-1362.
(109) Thomas-Hillman, I.; Stevens, L. A.; Lange, M.; Mollmer, J.; Lewis, W.; Dodds, C.; Kingman, S. W.; Laybourn, A. Developing a Sustainable Route to Environmentally Relevant Metal-Organic Frameworks: Ultra-Rapid Synthesis of Mfm-300(Al) Using Microwave Heating. *Green Chem.* **2019,** *21*, 5039-5045.
(110) Chen, C. W.; Feng, X. B.; Zhu, Q.; Dong, R.; Yang, R.; Cheng, Y.; He, C. Microwave-Assisted Rapid Synthesis of Well-Shaped Mof-74 (Ni) for Co2 Efficient Capture. *Inorg. Chem.* **2019,** *58*, 2717-2728.
(111) Thomas-Hillman, I.; Laybourn, A.; Dodds, C.; Kingman, S. W. Realising the Environmental Benefits of Metal-Organic Frameworks: Recent Advances in Microwave Synthesis. *J. Mater. Chem. A* **2018,** *6*, 11564-11581.
(112) Tannert, N.; Gokpinar, S.; Hasturk, E.; Niessing, S.; Janiak, C. Microwave-Assisted Dry-Gel Conversion-a New Sustainable Route for the Rapid Synthesis of Metal-Organic Frameworks with Solvent Re-Use. *Dalton Trans.* **2018,** *47*, 9850-9860.
(113) Hillman, F.; Brito, J.; Jeong, H. K. Rapid One-Pot Microwave Synthesis of Mixed-Linker Hybrid Zeolitic-Imidazolate Framework Membranes for Tunable Gas Separations. *ACS Appl. Mater. Interfaces* **2018,** *10*, 5586-5593.
(114) Laybourn, A.; Katrib, J.; Ferrari-John, R. S.; Morris, C. G.; Yang, S. H.; Udoudo, O.; Easun, T. L.; Dodds, C.; Champness, N. R.; Kingman, S. W.et al. Metal-Organic Frameworks in Seconds Via Selective Microwave Heating. *J. Mater. Chem. A* **2017,** *5*, 7333-7338.
(115) Laybourn, A.; Katrib, J.; Palade, P. A.; Easun, T. L.; Champness, N. R.; Schroder, M.; Kingman, S. W. Understanding the Electromagnetic Interaction of Metal Organic Framework Reactants in Aqueous Solution at Microwave Frequencies. *Phys. Chem. Chem. Phys.* **2016,** *18*, 5419-5431.
(116) Liang, W. B.; D'Alessandro, D. M. Microwave-Assisted Solvothermal Synthesis of Zirconium Oxide Based Metal-Organic Frameworks. *Chem. Commun.* **2013,** *49*, 3706-3708.
(117) Wang, S. Z.; McGuirk, C. M.; d'Aquino, A.; Mason, J. A.; Mirkin, C. A. Metal-Organic Framework Nanoparticles. *Adv. Mater.* **2018,** *30*.
(118) Ni, Z.; Masel, R. I. Rapid Production of Metal-Organic Frameworks Via Microwave-Assisted Solvothermal Synthesis. *J. Am. Chem. Soc.* **2006,** *128*, 12394-12395.
(119) Campbell, N. L.; Clowes, R.; Ritchie, L. K.; Cooper, A. I. Rapid Microwave Synthesis and Purification of Porous Covalent Organic Frameworks. *Chem. Mater.* **2009,** *21*, 204-206.
(120) Ding, S. Y.; Wang, W. Covalent Organic Frameworks (Cofs): From Design to Applications. *Chem. Soc. Rev.* **2013,** *42*, 548-568.

(121) Chalati, T.; Horcajada, P.; Gref, R.; Couvreur, P.; Serre, C. Optimisation of the Synthesis of Mof Nanoparticles Made of Flexible Porous Iron Fumarate Mil-88a. *J. Mater. Chem.* **2011,** *21*, 2220-2227.
(122) Chen, Y.; Ni, D.; Yang, X.; Liu, C.; Yin, J.; Cai, K. Microwave-Assisted Synthesis of Honeycomblike Hierarchical Spherical Zn-Doped Ni-Mof as a High-Performance Battery-Type Supercapacitor Electrode Material. *Electrochim. Acta* **2018,** *278*, 114-123.
(123) Yoo, Y.; Jeong, H. K. Rapid Fabrication of Metal Organic Framework Thin Films Using Microwave-Induced Thermal Deposition. *Chem. Commun.* **2008**, 2441-2443.
(124) Ren, J.; Dyosiba, X.; Musyoka, N. M.; Langmi, H. W.; Mathe, M.; Liao, S. Review on the Current Practices and Efforts Towards Pilot-Scale Production of Metal-Organic Frameworks (Mofs). *Coord. Chem. Rev.* **2017,** *352*, 187-219.
(125) Sheberla, D.; Sun, L.; Blood-Forsythe, M. A.; Er, S.; Wade, C. R.; Brozek, C. K.; Aspuru-Guzik, A.; Dinca, M. High Electrical Conductivity in Ni-3(2,3,6,7,10,11-Hexaiminotriphenylene)(2), a Semiconducting Metal-Organic Graphene Analogue. *J. Am. Chem. Soc.* **2014,** *136*, 8859-8862.
(126) Clough, A. J.; Orchanian, N. M.; Skelton, J. M.; Neer, A. J.; Howard, S. A.; Downes, C. A.; Piper, L. F. J.; Walsh, A.; Melot, B. C.; Marinescu, S. C. Room Temperature Metallic Conductivity in a Metal–Organic Framework Induced by Oxidation. *J. Am. Chem. Soc.* **2019,** *141*, 16323-16330.
(127) Clough, A. J.; Skelton, J. M.; Downes, C. A.; de la Rosa, A. A.; Yoo, J. W.; Walsh, A.; Melot, B. C.; Marinescu, S. C. Metallic Conductivity in a Two-Dimensional Cobalt Dithiolene Metal–Organic Framework. *J. Am. Chem. Soc.* **2017,** *139*, 10863-10867.
(128) Chen, I.-F.; Lu, C.-F.; Su, W.-F. Highly Conductive 2d Metal–Organic Framework Thin Film Fabricated by Liquid–Liquid Interfacial Reaction Using One-Pot-Synthesized Benzenehexathiol. *Langmuir* **2018,** *34*, 15754-15762.
(129) Biemmi, E.; Scherb, C.; Bein, T. Oriented Growth of the Metal Organic Framework Cu3(Btc)2(H2o)3·Xh2o Tunable with Functionalized Self-Assembled Monolayers. *J. Am. Chem. Soc.* **2007,** *129*, 8054-8055.
(130) Hermes, S.; Schröder, F.; Chelmowski, R.; Wöll, C.; Fischer, R. A. Selective Nucleation and Growth of Metalâˆ’organic Open Framework Thin Films on Patterned Cooh/Cf3-Terminated Self-Assembled Monolayers on Au(111). *J. Am. Chem. Soc.* **2005,** *127*, 13744-13745.
(131) McCarthy, M. C.; Varela-Guerrero, V.; Barnett, G. V.; Jeong, H. K. Synthesis of Zeolitic Imidazolate Framework Films and Membranes with Controlled Microstructures. *Langmuir* **2010,** *26*, 14636-14641.
(132) Huang, A.; Dou, W.; Caro, J. r. Steam-Stable Zeolitic Imidazolate Framework Zif-90 Membrane with Hydrogen Selectivity through Covalent Functionalization. *J. Am. Chem. Soc.* **2010,** *132*, 15562-15564.
(133) Lu, G.; Hupp, J. T. Metal-Organic Frameworks as Sensors: A Zif-8 Based Fabry-Perot Device as a Selective Sensor for Chemical Vapors and Gases. *J. Am. Chem. Soc.* **2010,** *132*, 7832-7833.
(134) Yoo, J.; Lee, S.; Hirata, S.; Kim, C.; Lee, C. K.; Shiraki, T.; Nakashima, N.; Shim, J. K. In Situ Synthesis of Covalent Organic Frameworks (Cofs) on Carbon Nanotubes and Graphenes by Sonochemical Reaction for Co2 Adsorbents. *Chem. Lett.* **2015,** *44*, 560-562.

(135) Yang, S. T.; Kim, J.; Cho, H. Y.; Kim, S.; Ahn, W. S. Facile Synthesis of Covalent Organic Frameworks Cof-1 and Cof-5 by Sonochemical Method. *RSC Adv.* **2012,** *2*, 10179-10181.
(136) Abuzalat, O.; Wong, D.; Elsayed, M.; Park, S.; Kim, S. Sonochemical Fabrication of Cu(Ii) and Zn(Ii) Metal-Organic Framework Films on Metal Substrates. *Ultrasonics Sonochem.* **2018,** *45*, 180-188.
(137) Marandi, F.; Hashemi, L.; Morsali, A.; Krautscheid, H. Sonochemical Synthesis and Characterization of Three Nano Zinc(Ii) Coordination Polymers; Precursors for Preparation of Zinc(Ii) Oxide Nanoparticles. *Ultrasonics Sonochem.* **2016,** *32*, 86-94.
(138) Lee, Y. R.; Cho, S. M.; Baeck, S. H.; Ahn, W. S.; Cho, W. S. Ti-Mil-125-Nh2 Membrane Grown on a Tio2 Disc by Combined Microwave/Ultrasonic Heating: Facile Synthesis for Catalytic Application. *RSC Adv.* **2016,** *6*, 63286-63290.
(139) Lee, Y. R.; Cho, S. M.; Ahn, W. S.; Lee, C. H.; Lee, K. H.; Cho, W. S. Facile Synthesis of an Irmof-3 Membrane on Porous Al2o3 Substrate Via a Sonochemical Route. *Microporous Mesoporous Mater.* **2015,** *213*, 161-168.
(140) Tahmasian, A.; Morsali, A. Ultrasonic Synthesis of a 3d Ni(Ii) Metal-Organic Framework at Ambient Temperature and Pressure: New Precursor for Synthesis of Nickel(Ii) Oxide Nano-Particles. *Inorg. Chim. Acta* **2012,** *387*, 327-331.
(141) Carson, C. G.; Brown, A. J.; Sholl, D. S.; Nair, S. Sonochemical Synthesis and Characterization of Submicrometer Crystals of the Metal-Organic Framework Cu (Hfipbb)(H(2)Hfipbb)(0.5). *Cryst. Growth Des.* **2011,** *11*, 4505-4510.
(142) Vaitsis, C.; Sourkouni, G.; Argirusis, C. Metal Organic Frameworks (Mofs) and Ultrasound: A Review. *Ultrasonics Sonochem.* **2019,** *52*, 106-119.
(143) Haque, E.; Khan, N. A.; Park, J. H.; Jhung, S. H. Synthesis of a Metal-Organic Framework Material, Iron Terephthalate, by Ultrasound, Microwave, and Conventional Electric Heating: A Kinetic Study. *Chem. Eur. J.* **2010,** *16*, 1046-1052.
(144) Cao, F.; Zhao, M.; Yu, Y.; Chen, B.; Huang, Y.; Yang, J.; Cao, X.; Lu, Q.; Zhang, X.; Zhang, Z.et al. Synthesis of Two-Dimensional Cos1.097/Nitrogen-Doped Carbon Nanocomposites Using Metal–Organic Framework Nanosheets as Precursors for Supercapacitor Application. *J. Am. Chem. Soc.* **2016,** *138*, 6924-6927.
(145) Ning, Y.; Lou, X.; Li, C.; Hu, X.; Hu, B. Ultrathin Cobalt-Based Metal–Organic Framework Nanosheets with Both Metal and Ligand Redox Activities for Superior Lithium Storage. *Chem. Eur. J.* **2017,** *23*, 15984-15990.
(146) Li, Z.-Q.; Qiu, L.-G.; Wang, W.; Xu, T.; Wu, Y.; Jiang, X. Fabrication of Nanosheets of a Fluorescent Metal–Organic Framework [Zn(Bdc)(H2o)]N (Bdc=1,4-Benzenedicarboxylate): Ultrasonic Synthesis and Sensing of Ethylamine. *Inorg. Chem. Commun.* **2008,** *11*, 1375-1377.
(147) Li, C.; Hu, X.; Tong, W.; Yan, W.; Lou, X.; Shen, M.; Hu, B. Ultrathin Manganese-Based Metal–Organic Framework Nanosheets: Low-Cost and Energy-Dense Lithium Storage Anodes with the Coexistence of Metal and Ligand Redox Activities. *ACS Appl. Mater. Interfaces* **2017,** *9*, 29829-29838.
(148) Rui, K.; Zhao, G.; Chen, Y.; Lin, Y.; Zhou, Q.; Chen, J.; Zhu, J.; Sun, W.; Huang, W.; Dou, S. X. Hybrid 2d Dual-Metal–Organic Frameworks for Enhanced Water Oxidation Catalysis. *Adv. Funct. Mater.* **2018,** *28*, 1801554.

(149) Hosseini, M. S.; Zeinali, S. Capacitive Humidity Sensing Using a Metal-Organic Framework Nanoporous Thin Film Fabricated through Electrochemical in Situ Growth. *J. Mater. Sci.* **2019,** *30*, 3701-3710.
(150) Hauser, J. L.; Tso, M.; Fitchmun, K.; Oliver, S. R. J. Anodic Electrodeposition of Several Metal Organic Framework Thin Films on Indium Tin Oxide Glass. *Cryst. Growth Des.* **2019,** *19*, 2358-2365.
(151) Wei, J. Z.; Wang, X. L.; Sun, X. J.; Hou, Y.; Zhang, X.; Yang, D. D.; Dong, H.; Zhang, F. M. Rapid and Large-Scale Synthesis of Irmof-3 by Electrochemistry Method with Enhanced Fluorescence Detection Performance for Tnp. *Inorg. Chem.* **2018,** *57*, 3818-3824.
(152) Zhang, F.; Zhang, T. T.; Zou, X. Q.; Liang, X. Q.; Zhu, G. S.; Qu, F. Y. Electrochemical Synthesis of Metal Organic Framework Films with Proton Conductive Property. *Solid State Ionics* **2017,** *301*, 125-132.
(153) Van Assche, T. R. C.; Campagnol, N.; Muselle, T.; Terryn, H.; Fransaer, J.; Denayer, J. F. M. On Controlling the Anodic Electrochemical Film Deposition of Hkust-1 Metal-Organic Frameworks. *Microporous Mesoporous Mater.* **2016,** *224*, 302-310.
(154) Schafer, P.; van der Veen, A.; Domke, K. F. Unraveling a Two-Step Oxidation Mechanism in Electrochemical Cu-Mof Synthesis. *Chem. Commun.* **2016,** *52*, 4722-4725.
(155) Lan, H. Z.; Pan, D. D.; Sun, Y. Y.; Guo, Y. X.; Wu, Z. Thin Metal Organic Frameworks Coatings by Cathodic Electrodeposition for Solid-Phase Microextraction and Analysis of Trace Exogenous Estrogens in Milk. *Anal. Chim. Acta* **2016,** *937*, 53-60.
(156) Stassen, I.; Styles, M.; Van Assche, T.; Campagnol, N.; Fransaer, J.; Denayer, J.; Tan, J. C.; Falcaro, P.; De Vos, D.; Ameloot, R. Electrochemical Film Deposition of the Zirconium Metal-Organic Framework Uio-66 and Application in a Miniaturized Sorbent Trap. *Chem. Mater.* **2015,** *27*, 1801-1807.
(157) Li, M.; Dincă, M. On the Mechanism of Mof-5 Formation under Cathodic Bias. *Chem. Mater.* **2015,** *27*, 3203-3206.
(158) Al-Kutubi, H.; Gascon, J.; Sudholter, E. J. R.; Rassaei, L. Electrosynthesis of Metal-Organic Frameworks: Challenges and Opportunities. *ChemElectroChem* **2015,** *2*, 462-474.
(159) Alizadeh, S.; Nematollahi, D. Convergent and Divergent Paired Electrodeposition of Metal-Organic Framework Thin Films. *Sci. Reports* **2019,** *9*.
(160) Jian, M.; Liu, H.; Williams, T.; Ma, J.; Wang, H.; Zhang, X. Temperature-Induced Oriented Growth of Large Area, Few-Layer 2d Metal–Organic Framework Nanosheets. *Chem. Commun.* **2017,** *53*, 13161-13164.
(161) Hod, I.; Bury, W.; Karlin, D. M.; Deria, P.; Kung, C. W.; Katz, M. J.; So, M.; Klahr, B.; Jin, D. N.; Chung, Y. W.et al. Directed Growth of Electroactive Metal-Organic Framework Thin Films Using Electrophoretic Deposition. *Adv. Mater.* **2014,** *26*, 6295-6300.
(162) Campagnol, N.; Van Assche, T.; Boudewijns, T.; Denayer, J.; Binnemans, K.; De Vos, D.; Fransaer, J. High Pressure, High Temperature Electrochemical Synthesis of Metal-Organic Frameworks: Films of Mil-100 (Fe) and Hkust-1 in Different Morphologies. *J. Mater. Chem. A* **2013,** *1*, 5827-5830.
(163) Van Assche, T. R. C.; Desmet, G.; Ameloot, R.; De Vos, D. E.; Terryn, H.; Denayer, J. F. M. Electrochemical Synthesis of Thin Hkust-1 Layers on Copper Mesh. *Microporous Mesoporous Mater.* **2012,** *158*, 209-213.

(164) Li, H.; Eddaoudi, M.; O'Keeffe, M.; Yaghi, O. M. Design and Synthesis of an Exceptionally Stable and Highly Porous Metal-Organic Framework. *Nature* **1999,** *402*, 276-279.
(165) Stassen, I.; De Vos, D.; Ameloot, R. Vapor-Phase Deposition and Modification of Metal-Organic Frameworks: State-of-the-Art and Future Directions. *Chem. Eur. J.* **2016,** *22*, 14452-14460.
(166) Fischer, D.; Meyer, L. V.; Jansen, M.; Muller-Buschbaum, K. Highly Luminescent Thin Films of the Dense Framework (3)(Infinity) Euim(2) with Switchable Transparency Formed by Scanning Femtosecond-Pulse Laser Deposition. *Angew. Chem. Int. Ed.* **2014,** *53*, 706-710.
(167) Meyer, L. V.; Vogt, J.; Schafer, H.; Steinhart, M.; Bottcher, R.; Poppl, A.; Mai, M.; Feldmann, C.; Muller-Buschbaum, K. Organic Melt, Electride, and Cvd Induced in Situ Deposition of Luminescent Lanthanide Imidazolate Mofs on Nanostructured Alumina. *Inorg. Chem. Front.* **2015,** *2*, 237-245.
(168) Fischer, D.; von Mankowski, A.; Ranft, A.; Vasa, S. K.; Linser, R.; Mannhart, J.; Lotsch, B. V. Zif-8 Films Prepared by Femtosecond Pulsed-Laser Deposition. *Chem. Mater.* **2017,** *29*, 5148-5155.
(169) Stassen, I.; Styles, M.; Grenci, G.; Van Gorp, H.; Vanderlinden, W.; De Feyter, S.; Falcaro, P.; De Vos, D.; Vereecken, P.; Ameloot, R. Chemical Vapour Deposition of Zeolitic Imidazolate Framework Thin Films. *Nat. Mater.* **2016,** *15*, 304-310.
(170) Lausund, K. B.; Nilsen, O. All-Gas-Phase Synthesis of Uio-66 through Modulated Atomic Layer Deposition. *Nat. Commun.* **2016,** *7*.
(171) Majewski, M. B.; Noh, H.; Islamoglu, T.; Farha, O. K. Nanomofs: Little Crystallites for Substantial Applications. *J. Mater. Chem. A* **2018,** *6*, 7338-7350.
(172) Lollar, C. T.; Qin, J. S.; Pang, J. D.; Yuan, S.; Becker, B.; Zhou, H. C. Interior Decoration of Stable Metal-Organic Frameworks. *Langmuir* **2018,** *34*, 13795-13807.
(173) Lan, H. Z.; Salmi, L. D.; Ronkko, T.; Parshintsev, J.; Jussila, M.; Hartonen, K.; Kemell, M.; Riekkola, M. L. Integrated Atomic Layer Deposition and Chemical Vapor Reaction for the Preparation of Metal Organic Framework Coatings for Solid-Phase Microextraction Arrow. *Anal. Chim. Acta* **2018,** *1024*, 93-100.
(174) Rimoldi, M.; Bernales, V.; Borycz, J.; Vjunov, A.; Gallington, L. C.; Platero-Prats, A. E.; Kim, I. S.; Fulton, J. L.; Martinson, A. B. F.; Lercher, J. A.et al. Atomic Layer Deposition in a Metal-Organic Framework: Synthesis, Characterization, and Performance of a Solid Acid. *Chem. Mater.* **2017,** *29*, 1058-1068.
(175) Lee, D. T.; Zhao, J. J.; Peterson, G. W.; Parsons, G. N. Catalytic "Mof-Cloth" Formed Via Directed Supramolecular Assembly of Uio-66-Nh2 Crystals on Atomic Layer Deposition-Coated Textiles for Rapid Degradation of Chemical Warfare Agent Simulants. *Chem. Mater.* **2017,** *29*, 4894-4903.
(176) Lausund, K. B.; Petrovic, V.; Nilsen, O. All-Gas-Phase Synthesis of Amino-Functionalized Uio-66 Thin Films. *Dalton Trans.* **2017,** *46*, 16983-16992.
(177) Peters, A. W.; Li, Z. Y.; Farha, O. K.; Hupp, J. T. Atomically Precise Growth of Catalytically Active Cobalt Sulfide on Flat Surfaces and within a Metal-Organic Framework Via Atomic Layer Deposition. *ACS Nano* **2015,** *9*, 8484-8490.
(178) Zhao, J. J.; Losego, M. D.; Lemaire, P. C.; Williams, P. S.; Gong, B.; Atanasov, S. E.; Blevins, T. M.; Oldham, C. J.; Walls, H. J.; Shepherd, S. D.et al. Highly Adsorptive, Mof-

Functionalized Nonwoven Fiber Mats for Hazardous Gas Capture Enabled by Atomic Layer Deposition. *Adv. Mater. Interfaces* **2014,** *1*.

(179) Salmi, L. D.; Heikkila, M. J.; Puukilainen, E.; Sajavaara, T.; Grosso, D.; Ritala, M. Studies on Atomic Layer Deposition of Mof-5 Thin Films. *Microporous Mesoporous Mater.* **2013,** *182*, 147-154.

(180) Ahvenniemi, E.; Karppinen, M. Atomic/Molecular Layer Deposition: A Direct Gas-Phase Route to Crystalline Metal-Organic Framework Thin Films. *Chem. Commun.* **2016,** *52*, 1139-1142.

(181) Zhang, M. D.; Wang, G.; Zheng, B. H.; Li, L. Y.; Lv, B. N.; Cao, H.; Chen, M. D. 3-Layer Conductive Metal-Organic Nanosheets as Electrocatalysts to Enable an Ultralow Detection Limit of H2o2. *Nanoscale* **2019,** *11*, 5058-5063.

(182) Ishihara, K. M.; Tian, F. Y. Semiconducting Langmuir-Blodgett Films of Porphyrin Paddle-Wheel Frameworks for Photoelectric Conversion. *Langmuir* **2018,** *34*, 15689-15699.

(183) Aulakh, D.; Xie, H. M.; Shen, Z.; Harley, A.; Zhang, X.; Yakovenko, A. A.; Dunbar, K. R.; Wriedt, M. Systematic Investigation of Controlled Nanostructuring of Mn-12 Single-Molecule Magnets Templated by Metal-Organic Frameworks. *Inorg. Chem.* **2017,** *56*, 6965-6972.

(184) Benito, J.; Sorribas, S.; Lucas, I.; Coronas, J.; Gascon, I. Langmuir-Blodgett Films of the Metal-Organic Framework Mil-101(Cr): Preparation, Characterization, and Co2 Adsorption Study Using a Qcm-Based Setup. *ACS Appl. Mater. Interfaces* **2016,** *8*, 16486-16492.

(185) Makiura, R.; Motoyama, S.; Umemura, Y.; Yamanaka, H.; Sakata, O.; Kitagawa, H. Surface Nano-Architecture of a Metal–Organic Framework. *Nat. Mater.* **2010,** *9*, 565-571.

(186) Shekhah, O.; Wang, H.; Paradinas, M.; Ocal, C.; Schupbach, B.; Terfort, A.; Zacher, D.; Fischer, R. A.; Woll, C. Controlling Interpenetration in Metal-Organic Frameworks by Liquid-Phase Epitaxy. *Nat. Mater.* **2009,** *8*, 481-484.

(187) Fischer, R. A.; Woll, C. Layer-by-Layer Liquid-Phase Epitaxy of Crystalline Coordination Polymers at Surfaces. *Angew. Chem. Int. Ed.* **2009,** *48*, 6205-6208.

(188) Shekhah, O.; Wang, H.; Kowarik, S.; Schreiber, F.; Paulus, M.; Tolan, M.; Sternemann, C.; Evers, F.; Zacher, D.; Fischer, R. A.et al. Step-by-Step Route for the Synthesis of Metal-Organic Frameworks. *J. Am. Chem. Soc.* **2007,** *129*, 15118-15119.

(189) Shekhah, O.; Wang, H.; Strunskus, T.; Cyganik, P.; Zacher, D.; Fischer, R.; Wöll, C. Layer-by-Layer Growth of Oriented Metal Organic Polymers on a Functionalized Organic Surface. *Langmuir* **2007,** *23*, 7440-7442.

(190) Shekhah, O.; Wang, H.; Zacher, D.; Fischer, R. A.; Woll, C. Growth Mechanism of Metal-Organic Frameworks: Insights into the Nucleation by Employing a Step-by-Step Route. *Angew. Chem. Int. Ed.* **2009,** *48*, 5038-5041.

(191) Darbandi, M.; Arslan, H. K.; Shekhah, O.; Bashir, A.; Birkner, A.; Woll, C. Fabrication of Free-Standing Ultrathin Films of Porous Metal-Organic Frameworks by Liquid-Phase Epitaxy and Subsequent Delamination. *Phys. Status Solidi-R* **2010,** *4*, 197-199.

(192) Shekhah, O. Layer-by-Layer Method for the Synthesis and Growth of Surface Mounted Metal-Organic Frameworks (Surmofs). *Materials* **2010,** *3*, 1302-1315.

(193) Yusenko, K.; Meilikhov, M.; Zacher, D.; Wieland, F.; Sternemann, C.; Stammer, X.; Ladnorg, T.; Woll, C.; Fischer, R. A. Step-by-Step Growth of Highly Oriented and

Continuous Seeding Layers of Cu-2(Ndc)(2)(Dabco) on Bare Oxide and Nitride Substrates. *CrystEngComm* **2010,** *12*, 2086-2090.

(194) Liu, Y.; Yang, Y.; Sun, Q.; Wang, Z.; Huang, B.; Dai, Y.; Qin, X.; Zhang, X. Chemical Adsorption Enhanced Co2 Capture and Photoreduction over a Copper Porphyrin Based Metal Organic Framework. *ACS Appl. Mater. Interfaces* **2013,** *5*, 7654-7658.

(195) Hinman, J. G.; Turner, J. G.; Hofmann, D. M.; Murphy, C. J. Layer-by-Layer Synthesis of Conformal Metal–Organic Framework Shells on Gold Nanorods. *Chem. Mater.* **2018,** *30*, 7255-7261.

(196) Yu, D.; Ge, L.; Wei, X.; Wu, B.; Ran, J.; Wang, H.; Xu, T. A General Route to the Synthesis of Layer-by-Layer Structured Metal Organic Framework/Graphene Oxide Hybrid Films for High-Performance Supercapacitor Electrodes. *J. Mater. Chem. A* **2017,** *5*, 16865-16872.

(197) Müller, K.; Helfferich, J.; Zhao, F.; Verma, R.; Kanj, A. B.; Meded, V.; Bléger, D.; Wenzel, W.; Heinke, L. Switching the Proton Conduction in Nanoporous, Crystalline Materials by Light. *Adv. Mater.* **2018,** *30*, 1706551.

(198) Haldar, R.; Jakoby, M.; Mazel, A.; Zhang, Q.; Welle, A.; Mohamed, T.; Krolla, P.; Wenzel, W.; Diring, S.; Odobel, F.et al. Anisotropic Energy Transfer in Crystalline Chromophore Assemblies. *Nat. Commun.* **2018,** *9*, 4332.

(199) Heinke, L.; Wöll, C. Surface-Mounted Metal–Organic Frameworks: Crystalline and Porous Molecular Assemblies for Fundamental Insights and Advanced Applications. *Adv. Mater.* **2019,** *31*, 1806324.

(200) Armon, N.; Greenberg, E.; Edri, E.; Kenigsberg, A.; Piperno, S.; Kapon, O.; Fleker, O.; Perelshtein, I.; Cohen-Taguri, G.; Hod, I.et al. Simultaneous Laser-Induced Synthesis and Micro-Patterning of a Metal Organic Framework. *Chem. Commun.* **2019,** *55*, 12773-12776.

(201) Li, R.; Yuan, S.; Zhang, W.; Zheng, H.; Zhu, W.; Li, B.; Zhou, M.; Wing-Keung Law, A.; Zhou, K. 3d Printing of Mixed Matrix Films Based on Metal–Organic Frameworks and Thermoplastic Polyamide 12 by Selective Laser Sintering for Water Applications. *ACS Appl. Mater. Interfaces* **2019,** *11*, 40564-40574.

(202) Zhang, M.; Li, L.; Lin, Q.; Tang, M.; Wu, Y.; Ke, C. Hierarchical-Coassembly-Enabled 3d-Printing of Homogeneous and Heterogeneous Covalent Organic Frameworks. *J. Am. Chem. Soc.* **2019,** *141*, 5154-5158.

(203) Ruigomez, A. D.; Rodriguez-San-Miguel, D.; Stylianou, K. C.; Cavallini, M.; Gentili, D.; Liscio, F.; Milita, S.; Roscioni, O. M.; Ruiz-Gonzalez, M. L.; Carbonell, C.et al. Direct on-Surface Patterning of a Crystalline Laminar Covalent Organic Framework Synthesized at Room Temperature. *Chem. Eur. J.* **2015,** *21*, 10666-10670.

(204) Kung, C. W.; Wang, T. C.; Mondloch, J. E.; Fairen-Jimenez, D.; Gardner, D. M.; Bury, W.; Klingsporn, J. M.; Barnes, J. C.; Van Duyne, R.; Stoddart, J. F.et al. Metal-Organic Framework Thin Films Composed of Free-Standing Acicular Nanorods Exhibiting Reversible Electrochromism. *Chem. Mater.* **2013,** *25*, 5012-5017.

(205) Usov, P. M.; Fabian, C.; D'Alessandro, D. M. Rapid Determination of the Optical and Redox Properties of a Metal-Organic Framework Via in Situ Solid State Spectroelectrochemistry. *Chem. Commun.* **2012,** *48*, 3945-3947.

(206) Halls, J. E.; Hernán-Gómez, A.; Burrows, A. D.; Marken, F. Metal–Organic Frameworks Post-Synthetically Modified with Ferrocenyl Groups: Framework Effects on Redox Processes and Surface Conduction. *Dalton Trans.* **2012,** *41*, 1475-1480.
(207) Meilikhov, M.; Yusenko, K.; Fischer, R. A. Turning Mil-53(Al) Redox-Active by Functionalization of the Bridging Oh-Group with 1,1'-Ferrocenediyl-Dimethylsilane. *J. Am. Chem. Soc.* **2009,** *131*, 9644-9645.
(208) Hod, I.; Bury, W.; Gardner, D. M.; Deria, P.; Roznyatovskiy, V.; Wasielewski, M. R.; Farha, O. K.; Hupp, J. T. Bias-Switchable Permselectivity and Redox Catalytic Activity of a Ferrocene-Functionalized, Thin-Film Metal-Organic Framework Compound. *J. Phys. Chem. Lett.* **2015,** *6*, 586-591.
(209) Dragasser, A.; Shekhah, O.; Zybaylo, O.; Shen, C.; Buck, M.; Woll, C.; Schlettwein, D. Redox Mediation Enabled by Immobilised Centres in the Pores of a Metal-Organic Framework Grown by Liquid Phase Epitaxy. *Chem. Commun.* **2012,** *48*, 663-665.
(210) Chang, Z.; Gao, N.; Li, Y.; He, X. Preparation of Ferrocene Immobilized Metal–Organic-Framework Modified Electrode for the Determination of Acetaminophen. *Anal. Meth.* **2012,** *4*, 4037-4041.
(211) Talin, A. A.; Centrone, A.; Ford, A. C.; Foster, M. E.; Stavila, V.; Haney, P.; Kinney, R. A.; Szalai, V.; El Gabaly, F.; Yoon, H. P.et al. Tunable Electrical Conductivity in Metal-Organic Framework Thin-Film Devices. *Science* **2014,** *343*, 66-69.
(212) Erickson, K. J.; Leonard, F.; Stavila, V.; Foster, M. E.; Spataru, C. D.; Jones, R. E.; Foley, B. M.; Hopkins, P. E.; Allendorf, M. D.; Talin, A. A. Thin Film Thermoelectric Metal-Organic Framework with High Seebeck Coefficient and Low Thermal Conductivity. *Adv. Mater.* **2015,** *27*, 3453-3459.
(213) Zhou, S.; Wei, Y. Y.; Zhuang, L. B.; Ding, L. X.; Wang, H. H. Introduction of Metal Precursors by Electrodeposition for the in Situ Growth of Metalorganic Framework Membranes on Porous Metal Substrates. *J. Mater. Chem. A* **2017,** *5*, 1948-1951.
(214) Wang, S. J.; Kitao, T.; Guillou, N.; Wahiduzzaman, M.; Martineau-Corcos, C.; Nouar, F.; Tissot, A.; Binet, L.; Ramsahye, N.; Devautour-Vinot, S.et al. A Phase Transformable Ultrastable Titanium-Carboxylate Framework for Photoconduction. *Nat. Commun.* **2018,** *9*.
(215) Marshall, N.; James, W.; Fulmer, J.; Crittenden, S.; Thompson, A. B.; Ward, P. A.; Rowe, G. T. Polythiophene Doping of the Cu-Based Metal-Organic Framework (Mof) Hkust-1 Using Innate Mof-Initiated Oxidative Polymerization. *Inorg. Chem.* **2019,** *58*, 5561-5575.
(216) Kreno, L. E.; Leong, K.; Farha, O. K.; Allendorf, M.; Van Duyne, R. P.; Hupp, J. T. Metal–Organic Framework Materials as Chemical Sensors. *Chem. Rev.* **2012,** *112*, 1105-1125.
(217) Wongkaew, N.; Simsek, M.; Griesche, C.; Baeumner, A. J. Functional Nanomaterials and Nanostructures Enhancing Electrochemical Biosensors and Lab-on-a-Chip Performances: Recent Progress, Applications, and Future Perspective. *Chem. Rev.* **2018,** *119*, 120-194.
(218) Yin, M.-J.; Gu, B.; An, Q.-F.; Yang, C.; Guan, Y. L.; Yong, K.-T. Recent Development of Fiber-Optic Chemical Sensors and Biosensors: Mechanisms, Materials, Micro/Nano-Fabrications and Applications. *Coord. Chem. Rev.* **2018,** *376*, 348-392.
(219) Hromadka, J.; Tokay, B.; Correia, R.; Morgan, S. P.; Korposh, S. Highly Sensitive Volatile Organic Compounds Vapour Measurements Using a Long Period Grating Optical Fibre

Sensor Coated with Metal Organic Framework Zif-8. *Sens. Actuators B Chem.* **2018,** *260*, 685-692.

(220) Kim, K.-J.; Lu, P.; Culp, J. T.; Ohodnicki, P. R. Metal-Organic Framework Thin Film Coated Optical Fiber Sensors: A Novel Waveguide-Based Chemical Sensing Platform. *ACS Sensors* **2018,** *3*, 386-394.

(221) Kim, K.-J.; Culp, J. T.; Ohodnicki, P. R.; Cvetic, P. C.; Sanguinito, S.; Goodman, A. L.; Kwon, H. T. Alkylamine-Integrated Metal-Organic Framework-Based Waveguide Sensors for Efficient Detection of Carbon Dioxide from Humid Gas Streams. *ACS Appl. Mater. Interfaces* **2019,** *11*, 33489-33496.

(222) Hromadka, J.; Tokay, B.; Correia, R.; Morgan, S. P.; Korposh, S. Carbon Dioxide Measurements Using Long Period Grating Optical Fibre Sensor Coated with Metal Organic Framework Hkust-1. *Sens. Actuators B Chem.* **2018,** *255*, 2483-2494.

(223) Zhu, C.; Perman, J. A.; Gerald, R. E., II; Ma, S.; Huang, J. Chemical Detection Using a Metal-Organic Framework Single Crystal Coupled to an Optical Fiber. *ACS Appl. Mater. Interfaces* **2019,** *11*, 4393-4398.

(224) Zhang, R.; Zhang, D.; Yao, Y.; Zhang, Q.; Xu, Y.; Wu, Y.; Yu, H.; Lu, G. Metal-Organic Framework Crystal-Assembled Optical Sensors for Chemical Vapors: Effects of Crystal Sizes and Missing-Linker Defects on Sensing Performances. *ACS Appl. Mater. Interfaces* **2019,** *11*, 21010-21017.

(225) Sun, L.; Campbell, M. G.; Dincă, M. Electrically Conductive Porous Metal-Organic Frameworks. *Angew. Chem. Int. Ed.* **2016,** *55*, 3566-3579.

(226) Ko, M.; Mendecki, L.; Mirica, K. A. Conductive Two-Dimensional Metal–Organic Frameworks as Multifunctional Materials. *Chem. Commun.* **2018,** *54*, 7873-7891.

(227) Kitao, T.; Zhang, Y.; Kitagawa, S.; Wang, B.; Uemura, T. Hybridization of Mofs and Polymers. *Chem. Soc. Rev.* **2017,** *46*, 3108-3133.

(228) Zheng, Y.; Zheng, S.; Xue, H.; Pang, H. Metal-Organic Frameworks/Graphene-Based Materials: Preparations and Applications. *Adv. Funct. Mater.* **2018,** *28*, 1804950.

(229) Zhu, Q.-L.; Xu, Q. Metal–Organic Framework Composites. *Chem. Soc. Rev.* **2014,** *43*, 5468-5512.

(230) Chen, E.-X.; Yang, H.; Zhang, J. Zeolitic Imidazolate Framework as Formaldehyde Gas Sensor. *Inorg. Chem.* **2014,** *53*, 5411-5413.

(231) Chen, E.-X.; Fu, H.-R.; Lin, R.; Tan, Y.-X.; Zhang, J. Highly Selective and Sensitive Trimethylamine Gas Sensor Based on Cobalt Imidazolate Framework Material. *ACS Appl. Mater. Interfaces* **2014,** *6*, 22871-22875.

(232) Campbell, M. G.; Sheberla, D.; Liu, S. F.; Swager, T. M.; Dincă, M. Cu3(Hexaiminotriphenylene)2: An Electrically Conductive 2d Metal-Organic Framework for Chemiresistive Sensing. *Angew. Chem. Int. Ed.* **2015,** *54*, 4349-4352.

(233) Campbell, M. G.; Liu, S. F.; Swager, T. M.; Dincă, M. Chemiresistive Sensor Arrays from Conductive 2d Metal–Organic Frameworks. *J. Am. Chem. Soc.* **2015,** *137*, 13780-13783.

(234) Smith, M. K.; Jensen, K. E.; Pivak, P. A.; Mirica, K. A. Direct Self-Assembly of Conductive Nanorods of Metal–Organic Frameworks into Chemiresistive Devices on Shrinkable Polymer Films. *Chem. Mater.* **2016,** *28*, 5264-5268.

(235) Hmadeh, M.; Lu, Z.; Liu, Z.; Gándara, F.; Furukawa, H.; Wan, S.; Augustyn, V.; Chang, R.; Liao, L.; Zhou, F.et al. New Porous Crystals of Extended Metal-Catecholates. *Chem. Mater.* **2012,** *24*, 3511-3513.
(236) Smith, M. K.; Mirica, K. A. Self-Organized Frameworks on Textiles (Soft): Conductive Fabrics for Simultaneous Sensing, Capture, and Filtration of Gases. *J. Am. Chem. Soc.* **2017,** *139*, 16759-16767.
(237) Yao, M.-S.; Lv, X.-J.; Fu, Z.-H.; Li, W.-H.; Deng, W.-H.; Wu, G.-D.; Xu, G. Layer-by-Layer Assembled Conductive Metal-Organic Framework Nanofilms for Room-Temperature Chemiresistive Sensing. *Angew. Chem. Int. Ed.* **2017,** *56*, 1651-1654.
(238) Hoppe, B.; Hindricks, K. D. J.; Warwas, D. P.; Schulze, H. A.; Mohmeyer, A.; Pinkvos, T. J.; Zailskas, S.; Krey, M. R.; Belke, C.; König, S.et al. Graphene-Like Metal–Organic Frameworks: Morphology Control, Optimization of Thin Film Electrical Conductivity and Fast Sensing Applications. *CrystEngComm* **2018,** *20*, 6458-6471.
(239) Rubio-Giménez, V.; Almora-Barrios, N.; Escorcia-Ariza, G.; Galbiati, M.; Sessolo, M.; Tatay, S.; Martí-Gastaldo, C. Origin of the Chemiresistive Response of Ultrathin Films of Conductive Metal–Organic Frameworks. *Angew. Chem. Int. Ed.* **2018,** *130*, 15086-15090.
(240) Day, R. W.; Bediako, D. K.; Rezaee, M.; Parent, L. R.; Skorupskii, G.; Arguilla, M. Q.; Hendon, C. H.; Stassen, I.; Gianneschi, N. C.; Kim, P.et al. Single Crystals of Electrically Conductive Two-Dimensional Metal–Organic Frameworks: Structural and Electrical Transport Properties. *ACS Central Sci.* **2019,** *5*, 1959-1964.
(241) Meng, Z.; Stolz, R. M.; Mirica, K. A. Two-Dimensional Chemiresistive Covalent Organic Framework with High Intrinsic Conductivity. *J. Am. Chem. Soc.* **2019,** *141*, 11929-11937.
(242) Aubrey, M. L.; Kapelewski, M. T.; Melville, J. F.; Oktawiec, J.; Presti, D.; Gagliardi, L.; Long, J. R. Chemiresistive Detection of Gaseous Hydrocarbons and Interrogation of Charge Transport in Cu[Ni(2,3-Pyrazinedithiolate)2] by Gas Adsorption. *J. Am. Chem. Soc.* **2019,** *141*, 5005-5013.
(243) Dmello, M. E.; Sundaram, N. G.; Singh, A.; Singh, A. K.; Kalidindi, S. B. An Amine Functionalized Zirconium Metal–Organic Framework as an Effective Chemiresistive Sensor for Acidic Gases. *Chem. Commun.* **2019,** *55*, 349-352.
(244) Musho, T.; Wu, N. Ab Initio Calculation of Electronic Charge Mobility in Metal–Organic Frameworks. *Phys. Chem. Chem. Phys.* **2015,** *17*, 26160-26165.
(245) Lohse, M. S.; Bein, T. Covalent Organic Frameworks: Structures, Synthesis, and Applications. *Adv. Func. Mater.* **2018,** *28*.
(246) Medina, D. D.; Sick, T.; Bein, T. Photoactive and Conducting Covalent Organic Frameworks. *Adv. Energy Mater.* **2017,** *7*, 1700387-n/a.
(247) Sharma, N.; Sharma, N.; Srinivasan, P.; Kumar, S.; Rayappan, J. B. B.; Kailasam, K. Heptazine Based Organic Framework as a Chemiresistive Sensor for Ammonia Detection at Room Temperature. *J. Mater. Chem. A* **2018,** *6*, 18389-18395.
(248) Tian, H.; Fan, H.; Li, M.; Ma, L. Zeolitic Imidazolate Framework Coated Zno Nanorods as Molecular Sieving to Improve Selectivity of Formaldehyde Gas Sensor. *ACS Sensors* **2015,** *1*, 243-250.
(249) Drobek, M.; Kim, J.-H.; Bechelany, M.; Vallicari, C.; Julbe, A.; Kim, S. S. Mof-Based Membrane Encapsulated Zno Nanowires for Enhanced Gas Sensor Selectivity. *ACS Appl. Mater. Interfaces* **2016,** *8*, 8323-8328.

(250) Yao, M.-S.; Tang, W.-X.; Wang, G.-E.; Nath, B.; Xu, G. Mof Thin Film-Coated Metal Oxide Nanowire Array: Significantly Improved Chemiresistor Sensor Performance. *Adv. Mater.* **2016,** *28*, 5229-5234.
(251) Wu, X. N.; Xiong, S. S.; Mao, Z. H.; Hu, S.; Long, X. G. A Designed Zno@Zif-8 Core-Shell Nanorod Film as a Gas Sensor with Excellent Selectivity for H-2 over Co. *Chem. Eur. J.* **2017,** *23*, 7969-7975.
(252) Zhou, T. T.; Sang, Y. T.; Wang, X. X.; Wu, C. Y.; Zeng, D. W.; Xie, C. S. Pore Size Dependent Gas-Sensing Selectivity Based on Zno@Zif Nanorod Arrays. *Sens. Actuators B Chem.* **2018,** *258*, 1099-1106.
(253) Liu, Y.; Wang, R.; Zhang, T.; Liu, S.; Fei, T. Zeolitic Imidazolate Framework-8 (Zif-8)-Coated In2o3 Nanofibers as an Efficient Sensing Material for Ppb-Level No2 Detection. *J. Colloid Interface Sci.* **2019,** *541*, 249-257.
(254) Dmello, M. E.; Sundaram, N. G.; Kalidindi, S. B. Assembly of Zif-67 Metal-Organic Framework over Tin Oxide Nanoparticles for Synergistic Chemiresistive Co2 Gas Sensing. *Chem. Eur. J.* **2018,** *24*, 9220-9223.
(255) Ren, G. J.; Li, Z. M.; Yang, W. T.; Faheem, M.; Xing, J. B.; Zou, X. Q.; Pan, Q. H.; Zhu, G. S.; Du, Y. Zno@Zif-8 Core-Shell Microspheres for Improved Ethanol Gas Sensing. *Sens. Actuators B Chem.* **2019,** *284*, 421-427.
(256) Weber, M.; Kim, J.-H.; Lee, J.-H.; Kim, J.-Y.; Iatsunskyi, I.; Coy, E.; Drobek, M.; Julbe, A.; Bechelany, M.; Kim, S. S. High-Performance Nanowire Hydrogen Sensors by Exploiting the Synergistic Effect of Pd Nanoparticles and Metal–Organic Framework Membranes. *ACS Appl. Mater. Interfaces* **2018,** *10*, 34765-34773.
(257) Wang, D.; Li, Z.; Zhou, J.; Fang, H.; He, X.; Jena, P.; Zeng, J.-B.; Wang, W.-N. Simultaneous Detection and Removal of Formaldehyde at Room Temperature: Janus Au@Zno@Zif-8 Nanoparticles. *Nano-Micro Lett.* **2018,** *10: 4*.
(258) Wang, P. Y.; Zou, X. Q.; Tan, H. Q.; Wu, S.; Jiang, L. C.; Zhu, G. S. Ultrathin Zif-8 Film Containing Polyoxometalate as an Enhancer for Selective Formaldehyde Sensing. *J. Mater. Chem. C* **2018,** *6*, 5412-5419.
(259) Travlou, N. A.; Singh, K.; Rodriguez-Castellon, E.; Bandosz, T. J. Cu-Btc Mof-Graphene-Based Hybrid Materials as Low Concentration Ammonia Sensors. *J. Mater. Chem. A* **2015,** *3*, 11417-11429.
(260) Ko, M.; Aykanat, A.; Smith, M. K.; Mirica, K. A. Drawing Sensors with Ball-Milled Blends of Metal-Organic Frameworks and Graphite. *Sensors* **2017,** *17*, 2192.
(261) Freund, P.; Senkovska, I.; Kaskel, S. Switchable Conductive Mof–Nanocarbon Composite Coatings as Threshold Sensing Architectures. *ACS Appl. Mater. Interfaces* **2017,** *9*, 43782-43789.
(262) Freund, P.; Mielewczyk, L.; Rauche, M.; Senkovska, I.; Ehrling, S.; Brunner, E.; Kaskel, S. Mil-53(Al)/Carbon Films for Co2-Sensing at High Pressure. *ACS Sustain. Chem. Eng.* **2019,** *7*, 4012-4018.
(263) Roztocki, K.; Formalik, F.; Krawczuk, A.; Senkovska, I.; Kuchta, B.; Kaskel, S.; Matoga, D. Collective Breathing in an Eightfold Interpenetrated Metal–Organic Framework: From Mechanistic Understanding Towards Threshold Sensing Architectures. *Angew. Chem. Int. Ed* **2020,** *59*, 4491-4497.

(264) Le Ouay, B.; Boudot, M.; Kitao, T.; Yanagida, T.; Kitagawa, S.; Uemura, T. Nanostructuration of Pedot in Porous Coordination Polymers for Tunable Porosity and Conductivity. *J. Am. Chem. Soc.* **2016,** *138*, 10088-10091.
(265) Kung, C.-W.; Platero-Prats, A. E.; Drout, R. J.; Kang, J.; Wang, T. C.; Audu, C. O.; Hersam, M. C.; Chapman, K. W.; Farha, O. K.; Hupp, J. T. Inorganic "Conductive Glass" Approach to Rendering Mesoporous Metal–Organic Frameworks Electronically Conductive and Chemically Responsive. *ACS Appl. Mater. Interfaces* **2018,** *10*, 30532-30540.
(266) Achmann, S.; Hagen, G.; Kita, J.; Malkowsky, I.; Kiener, C.; Moos, R. Metal-Organic Frameworks for Sensing Applications in the Gas Phase. *Sensors* **2009,** *9*, 1574-1589.
(267) Zhang, Y.; Chen, Y.; Zhang, Y.; Cong, H.; Fu, B.; Wen, S.; Ruan, S. A Novel Humidity Sensor Based on Nh2-Mil-125(Ti) Metal Organic Framework with High Responsiveness. *J. Nanoparticle Res.* **2013,** *15*, 2014.
(268) Zhang, Y.; Fu, B.; Liu, K.; Zhang, Y.; Li, X.; Wen, S.; Chen, Y.; Ruan, S. Humidity Sensing Properties of Fecl3-Nh2-Mil-125(Ti) Composites. *Sens. Actuators B Chem.* **2014,** *201*, 281-285.
(269) Zhang, J.; Sun, L.; Chen, C.; Liu, M.; Dong, W.; Guo, W.; Ruan, S. High Performance Humidity Sensor Based on Metal Organic Framework Mil-101(Cr) Nanoparticles. *J. Alloys Compounds* **2017,** *695*, 520-525.
(270) Bao, S.-S.; Li, N.-Z.; Taylor, J. M.; Shen, Y.; Kitagawa, H.; Zheng, L.-M. Co–Ca Phosphonate Showing Humidity-Sensitive Single Crystal to Single Crystal Structural Transformation and Tunable Proton Conduction Properties. *Chem. Mater.* **2015,** *27*, 8116-8125.
(271) Gao, Y.; Jing, P.; Yan, N.; Hilbers, M.; Zhang, H.; Rothenberg, G.; Tanase, S. Dual-Mode Humidity Detection Using a Lanthanide-Based Metal–Organic Framework: Towards Multifunctional Humidity Sensors. *Chem. Commun.* **2017,** *53*, 4465-4468.
(272) Yin, Y.-Y.; Xing, Y.; Li, M.-W.; Li, Y.-N.; Wang, J.-N.; Li, T.; Zhang, L.-X. A 3d Pillared-Layer Cadmium (Ii) Metal-Organic Framework for Chemiresistive Humidity Sensing with High Performance. *Inorg. Chem. Commun.* **2018,** *97*, 49-55.
(273) Singh, H.; Tomer, V. K.; Jena, N.; Bala, I.; Sharma, N.; Nepak, D.; De Sarkar, A.; Kailasam, K.; Pal, S. K. A Porous, Crystalline Truxene-Based Covalent Organic Framework and Its Application in Humidity Sensing. *J. Mater. Chem. A* **2017,** *5*, 21820-21827.
(274) Guo, K.; Zhao, L.; Yu, S.; Zhou, W.; Li, Z.; Li, G. A Water-Stable Proton-Conductive Barium(Ii)-Organic Framework for Ammonia Sensing at High Humidity. *Inorg. Chem.* **2018,** *57*, 7104-7112.
(275) Sun, Z.; Yu, S.; Zhao, L.; Wang, J.; Li, Z.; Li, G. A Highly Stable Two-Dimensional Copper(Ii) Organic Framework for Proton Conduction and Ammonia Impedance Sensing. *Chem. Eur. J.* **2018,** *24*, 10829-10839.
(276) Liu, J.; Sun, F.; Zhang, F.; Wang, Z.; Zhang, R.; Wang, C.; Qiu, S. In Situ Growth of Continuous Thin Metal–Organic Framework Film for Capacitive Humidity Sensing. *J. Mater. Chem.* **2011,** *21*, 3775.
(277) Hosseini, M. S.; Zeinali, S.; Sheikhi, M. H. Fabrication of Capacitive Sensor Based on Cu-Btc (Mof-199) Nanoporous Film for Detection of Ethanol and Methanol Vapors. *Sens. Actuators B Chem.* **2016,** *230*, 9-16.

(278) Homayoonnia, S.; Zeinali, S. Design and Fabrication of Capacitive Nanosensor Based on Mof Nanoparticles as Sensing Layer for Vocs Detection. *Sens. Actuators B Chem.* **2016,** *237*, 776-786.
(279) Sachdeva, S.; Venkatesh, M. R.; El Mansouri, B.; Wei, J.; Bossche, A.; Kapteijn, F.; Zhang, G. Q.; Gascon, J.; de Smet, L.; Sudholter, E. J. R. Sensitive and Reversible Detection of Methanol and Water Vapor by in Situ Electrochemically Grown Cubtc Mofs on Interdigitated Electrodes
. *Small* **2017,** *13*, 1604150.
(280) Weiss, A.; Reimer, N.; Stock, N.; Tiemann, M.; Wagner, T. Surface-Modified Cau-10 Mof Materials as Humidity Sensors: Impedance Spectroscopic Study on Water Uptake. *Phys. Chem. Chem. Phys.* **2015,** *17*, 21634-21642.
(281) Weiss, A.; Reimer, N.; Stock, N.; Tiemann, M.; Wagner, T. Screening of Mixed-Linker Cau-10 Mof Materials for Humidity Sensing by Impedance Spectroscopy. *Microporous Mesoporous Mater.* **2016,** *220*, 39-43.
(282) Sapsanis, C.; Omran, H.; Chernikova, V.; Shekhah, O.; Belmabkhout, Y.; Buttner, U.; Eddaoudi, M.; Salama, K. Insights on Capacitive Interdigitated Electrodes Coated with Mof Thin Films: Humidity and Vocs Sensing as a Case Study. *Sensors* **2015,** *15*, 18153-18166.
(283) Sachdeva, S.; Soccol, D.; Gravesteijn, D. J.; Kapteijn, F.; Sudhölter, E. J. R.; Gascon, J.; de Smet, L. C. P. M. Polymer–Metal Organic Framework Composite Films as Affinity Layer for Capacitive Sensor Devices. *ACS Sensors* **2016,** *1*, 1188-1192.
(284) Sachdeva, S.; Koper, S. J. H.; Sabetghadam, A.; Soccol, D.; Gravesteijn, D. J.; Kapteijn, F.; Sudhölter, E. J. R.; Gascon, J.; de Smet, L. C. P. M. Gas Phase Sensing of Alcohols by Metal Organic Framework–Polymer Composite Materials. *ACS Appl. Mater. Interfaces* **2017,** *9*, 24926-24935.
(285) Yassine, O.; Shekhah, O.; Assen, A. H.; Belmabkhout, Y.; Salama, K. N.; Eddaoudi, M. H2s Sensors: Fumarate-Based Fcu-Mof Thin Film Grown on a Capacitive Interdigitated Electrode. *Angew. Chem. Int. Ed.* **2016,** *55*, 15879-15883.
(286) Chernikova, V.; Yassine, O.; Shekhah, O.; Eddaoudi, M.; Salama, Khaled N. Highly Sensitive and Selective So2 Mof Sensor: The Integration of Mfm-300 Mof as a Sensitive Layer on a Capacitive Interdigitated Electrode. *J. Mater. Chem. A* **2018,** *6*, 5550-5554.
(287) Chappanda, K. N.; Tchalala, M. R.; Shekhah, O.; Surya, S. G.; Eddaoudi, M.; Salama, K. N. A Comparative Study of Interdigitated Electrode and Quartz Crystal Microbalance Transduction Techniques for Metal–Organic Framework-Based Acetone Sensors. *Sensors* **2018,** *18*, 3898.
(288) Li, H.; Shi, W.; Song, J.; Jang, H.-J.; Dailey, J.; Yu, J.; Katz, H. E. Chemical and Biomolecule Sensing with Organic Field-Effect Transistors. *Chem. Rev.* **2019,** *119*, 3-35.
(289) Meng, Z.; Stolz, R. M.; Mendecki, L.; Mirica, K. A. Electrically-Transduced Chemical Sensors Based on Two-Dimensional Nanomaterials. *Chem. Rev.* **2019,** *119*, 478-598.
(290) Bodkhe, G. A.; Deshmukh, M. A.; Patil, H. K.; Shirsat, S. M.; Srihari, V.; Pandey, K. K.; Panchal, G.; Phase, D. M.; Mulchandani, A.; Shirsat, M. D. Field Effect Transistor Based on Proton Conductive Metal Organic Framework (Cubtc). *J. Phys. D* **2019,** *52*.

(291) Lahiri, N.; Lotfizadeh, N.; Tsuchikawa, R.; Deshpande, V. V.; Louie, J. Hexaaminobenzene as a Building Block for a Family of 2d Coordination Polymers. *J. Am. Chem. Soc.* **2017,** *139*, 19-22.
(292) Panda, T.; Banerjee, R. High Charge Carrier Mobility in Two Dimensional Indium (Iii) Isophthalic Acid Based Frameworks. *Proc. Nat. Acad. Sci. India A* **2014,** *84*, 331-336.
(293) Wu, G. D.; Huang, J. H.; Zang, Y.; He, J.; Xu, G. Porous Field-Effect Transistors Based on a Semiconductive Metal-Organic Framework. *J. Am. Chem. Soc.* **2017,** *139*, 1360-1363.
(294) Aubrey, M. L.; Wiers, B. M.; Andrews, S. C.; Sakurai, T.; Reyes-Lillo, S. E.; Hamed, S. M.; Yu, C. J.; Darago, L. E.; Mason, J. A.; Baeg, J. O.et al. Electron Delocalization and Charge Mobility as a Function of Reduction in a Metal-Organic Framework. *Nat. Mater.* **2018,** *17*, 625-+.
(295) Surya, S. G.; Nagarkar, S. S.; Ghosh, S. K.; Sonar, P.; Ramgopal Rao, V. Ofet Based Explosive Sensors Using Diketopyrrolopyrrole and Metal Organic Framework Composite Active Channel Material. *Sens. Actuators B Chem.* **2016,** *223*, 114-122.
(296) Gu, Z.-G.; Chen, S.-C.; Fu, W.-Q.; Zheng, Q.; Zhang, J. Epitaxial Growth of Mof Thin Film for Modifying the Dielectric Layer in Organic Field-Effect Transistors. *ACS Appl. Mater. Interfaces* **2017,** *9*, 7259-7264.
(297) Jang, Y. J.; Jung, Y. E.; Kwon, E. H.; Lee, C. Y.; Park, Y. D. Built-in Water Capture in a Polythiophene Film Blended with Metal-Organic Frameworks. *Macrolmolec. Res.* **2019,** *27*, 421-426.
(298) Davydovskaya, P.; Pohle, R.; Tawil, A.; Fleischer, M. Work Function Based Gas Sensing with Cu-Btc Metal-Organic Framework for Selective Aldehyde Detection. *Sens. Actuators B Chem.* **2013,** *187*, 142-146.
(299) Davydovskaya, P.; Ranft, A.; Lotsch, B. V.; Pohle, R. Selective and Sensitive Detection of C3 Molecules with Cu-Btc Metal-Organic Framework by Means of Mass Sensitive and Work Function Based Read-Out. *Procedia Eng.* **2014,** *87*, 1433-1436.
(300) Pentyala, V.; Davydovskaya, P.; Ade, M.; Pohle, R.; Urban, G. Metal–Organic Frameworks for Alcohol Gas Sensor. *Sens. Actuators B Chem.* **2016,** *222*, 904-909.
(301) Pentyala, V.; Davydovskaya, P.; Ade, M.; Pohle, R.; Urban, G. Carbon Dioxide Gas Detection by Open Metal Site Metal Organic Frameworks and Surface Functionalized Metal Organic Frameworks. *Sens. Actuators B Chem.* **2016,** *225*, 363-368.
(302) Pentyala, V.; Davydovskaya, P.; Pohle, R.; Urban, G.; Yurchenko, O. Mg-Mof74 and Co-Mof74 as Sensing Layers for Co2 Detection. *Procedia Eng.* **2014,** *87*, 1071-1074.
(303) Pohle, R.; Tawil, A.; Davydovskaya, P.; Fleischer, M. Metal Organic Frameworks as Promising High Surface Area Material for Work Function Gas Sensors. *Procedia Eng.* **2011,** *25*, 108-111.
(304) Stassen, I.; Bueken, B.; Reinsch, H.; Oudenhoven, J. F. M.; Wouters, D.; Hajek, J.; Van Speybroeck, V.; Stock, N.; Vereecken, P. M.; Van Schaijk, R.et al. Towards Metal–Organic Framework Based Field Effect Chemical Sensors: Uio-66-Nh2 for Nerve Agent Detection. *Chem. Sci.* **2016,** *7*, 5827-5832.
(305) Xu, Y. X.; Li, Q.; Xue, H. G.; Pang, H. Metal-Organic Frameworks for Direct Electrochemical Applications. *Coord. Chem. Rev.* **2018,** *376*, 292-318.

(306) Wang, L.; Liang, H. H.; Xu, M. L.; Wang, L. Y.; Xie, Y.; Song, Y. H. Ratiometric Electrochemical Biosensing Based on Double-Enzymes Loaded on Two-Dimensional Dual-Pore Cofetta-Tpal. *Sens. Actuators B Chem.* **2019,** *298*, 126859.
(307) Liang, C.; Lin, H.; Wang, Q.; Shi, E.; Zhou, S.; Zhang, F.; Qu, F.; Zhu, G. A Redox-Active Covalent Organic Framework for the Efficient Detection and Removal of Hydrazine. *J. Hazardous Mater.* **2020,** *381*, 120983.
(308) Su, D.; Feng, B.; Xu, P.; Zeng, Q.; Shan, B.; Song, Y. Covalent Organic Frameworks and Electron Mediator-Based Open Circuit Potential Biosensor for in Vivo Electrochemical Measurements. *Anal. Meth.* **2018,** *10*, 4320-4328.
(309) Sun, Y. F.; Xu, L. H.; Waterhouse, G. I. N.; Wang, M. L.; Qiao, X. G.; Xu, Z. X. Novel Three-Dimensional Electrochemical Sensor with Dual Signal Amplification Based on Mos2 Nanosheets and High-Conductive Nh2-Mwcnt@Cof for Sulfamerazine Determination. *Sens. Actuators B Chem.* **2019,** *281*, 107-114.
(310) Xu, M.; Wang, L.; Xie, Y.; Song, Y.; Wang, L. Ratiometric Electrochemical Sensing and Biosensing Based on Multiple Redox-Active State Cofdhta-Tta. *Sens. Actuators B Chem.* **2019,** *281*, 1009-1015.
(311) Zhang, T.; Chen, Y.; Huang, W.; Wang, Y.; Hu, X. A Novel Aunps-Doped Cofs Composite as Electrochemical Probe for Chlorogenic Acid Detection with Enhanced Sensitivity and Stability. *Sens. Actuators B Chem.* **2018,** *276*, 362-369.
(312) Zhang, T.; Gao, C.; Huang, W.; Chen, Y.; Wang, Y.; Wang, J. Covalent Organic Framework as a Novel Electrochemical Platform for Highly Sensitive and Stable Detection of Lead. *Talanta* **2018,** *188*, 578-583.
(313) Zhou, N.; Ma, Y.; Hu, B.; He, L.; Wang, S.; Zhang, Z.; Lu, S. Construction of Ce-Mof@Cof Hybrid Nanostructure: Label-Free Aptasensor for the Ultrasensitive Detection of Oxytetracycline Residues in Aqueous Solution Environments. *Biosensors Bioelectron.* **2019,** *127*, 92-100.
(314) Wang, Y.; Wang, L.; Huang, W.; Zhang, T.; Hu, X.; Perman, J. A.; Ma, S. A Metal–Organic Framework and Conducting Polymer Based Electrochemical Sensor for High Performance Cadmium Ion Detection. *J. Mater. Chem. A* **2017,** *5*, 8385-8393.
(315) Wei, Z.; Zhu, W.; Li, Y.; Ma, Y.; Wang, J.; Hu, N.; Suo, Y.; Wang, J. Conductive Leaflike Cobalt Metal–Organic Framework Nanoarray on Carbon Cloth as a Flexible and Versatile Anode toward Both Electrocatalytic Glucose and Water Oxidation. *Inorg. Chem.* **2018,** *57*, 8422-8428.
(316) Wang, Z.; Liu, T.; Asif, M.; Yu, Y.; Wang, W.; Wang, H.; Xiao, F.; Liu, H. Rimelike Structure-Inspired Approach toward in Situ-Oriented Self-Assembly of Hierarchical Porous Mof Films as a Sweat Biosensor. *ACS Applied Materials & Interfaces* **2018,** *10*, 27936-27946.
(317) Ling, W.; Liew, G.; Li, Y.; Hao, Y.; Pan, H.; Wang, H.; Ning, B.; Xu, H.; Huang, X. Materials and Techniques for Implantable Nutrient Sensing Using Flexible Sensors Integrated with Metal–Organic Frameworks. *Adv. Mater.* **2018,** *30*, 1800917.
(318) Mendecki, L.; Mirica, K. A. Conductive Metal–Organic Frameworks as Ion-to-Electron Transducers in Potentiometric Sensors. *ACS Appl. Mater. Interfaces* **2018,** *10*, 19248-19257.

(319) Pan, L.; Liu, G.; Shi, W.; Shang, J.; Leow, W. R.; Liu, Y.; Jiang, Y.; Li, S.; Chen, X.; Li, R.-W. Mechano-Regulated Metal–Organic Framework Nanofilm for Ultrasensitive and Anti-Jamming Strain Sensing. *Nat. Commun.* **2018,** *9*, 3813.
(320) Allendorf, M. D.; Houk, R. J. T.; Andruszkiewicz, L.; Talin, A. A.; Pikarsky, J.; Choudhury, A.; Gall, K. A.; Hesketh, P. J. Stress-Induced Chemical Detection Using Flexible Metal-Organic Frameworks. *J. Am. Chem. Soc.* **2008,** *130*, 14404-14405.
(321) Arora, H.; Dong, R.; Venanzi, T.; Zscharschuch, J.; Schneider, H.; Helm, M.; Feng, X.; Cánovas, E.; Erbe, A. Demonstration of a Broadband Photodetector Based on a Two-Dimensional Metal–Organic Framework. *Adv. Mater.* **2020,** *32*, 1907063.
(322) Meng, Z.; Aykanat, A.; Mirica, K. A. Welding Metallophthalocyanines into Bimetallic Molecular Meshes for Ultrasensitive, Low-Power Chemiresistive Detection of Gases. *J. Am. Chem. Soc.* **2019,** *141*, 2046-2053.
(323) Davydovskaya, P.; Pentyala, V.; Yurchenko, O.; Hussein, L.; Pohle, R.; Urban, G. A. Work Function Based Sensing of Alkanes and Alcohols with Benzene Tricarboxylate Linked Metal Organic Frameworks. *Sens. Actuators B Chem.* **2014,** *193*, 911-917.
(324) Davydovskaya, P.; Ranft, A.; Lotsch, B. V.; Pohle, R. Analyte Detection with Cu-Btc Metal–Organic Framework Thin Films by Means of Mass-Sensitive and Work-Function-Based Readout. *Anal. Chem.* **2014,** *86*, 6948-6958.
(325) Dong, R.; Zhang, T.; Feng, X. Interface-Assisted Synthesis of 2d Materials: Trend and Challenges. *Chem. Rev.* **2018,** *118*, 6189-6235.
(326) Klauk, H. Organic Thin-Film Transistors. *Chem. Soc. Rev.* **2010,** *39*, 2643-2666.
(327) Braga, D.; Horowitz, G. High-Performance Organic Field-Effect Transistors. *Adv. Mater.* **2009,** *21*, 1473-1486.
(328) Wentz, H. C.; Skorupskii, G.; Bonfim, A. B.; Mancuso, J. L.; Hendon, C. H.; Oriel, E. H.; Sazama, G. T.; Campbell, M. G. Switchable Electrical Conductivity in a Three-Dimensional Metal–Organic Framework Via Reversible Ligand N-Doping. *Chem. Sci.* **2020,** *11*, 1342-1346.
(329) Kobayashi, Y.; Jacobs, B.; Allendorf, M. D.; Long, J. R. Conductivity, Doping, and Redox Chemistry of a Microporous Dithiolene-Based Metal−Organic Framework. *Chem. Mater.* **2010,** *22*, 4120-4122.
(330) Takaishi, S.; Hosoda, M.; Kajiwara, T.; Miyasaka, H.; Yamashita, M.; Nakanishi, Y.; Kitagawa, Y.; Yamaguchi, K.; Kobayashi, A.; Kitagawa, H. Electroconductive Porous Coordination Polymer Cu[Cu(Pdt)2] Composed of Donor and Acceptor Building Units. *Inorg. Chem.* **2009,** *48*, 9048-9050.
(331) Butler, S. Z.; Hollen, S. M.; Cao, L.; Cui, Y.; Gupta, J. A.; Gutiérrez, H. R.; Heinz, T. F.; Hong, S. S.; Huang, J.; Ismach, A. F.et al. Progress, Challenges, and Opportunities in Two-Dimensional Materials Beyond Graphene. *ACS Nano* **2013,** *7*, 2898-2926.
(332) Wang, L.; Sahabudeen, H.; Zhang, T.; Dong, R. Liquid-Interface-Assisted Synthesis of Covalent-Organic and Metal-Organic Two-Dimensional Crystalline Polymers. *npj 2D Mater. Appl.* **2018,** *2*, 26.
(333) Dong, R.; Pfeffermann, M.; Liang, H.; Zheng, Z.; Zhu, X.; Zhang, J.; Feng, X. Large-Area, Free-Standing, Two-Dimensional Supramolecular Polymer Single-Layer Sheets for Highly Efficient Electrocatalytic Hydrogen Evolution. *Angew. Chem. Int. Ed.* **2015,** *54*, 12058-12063.

(334) Cui, Y.; Yan, J.; Chen, Z.; Xing, W.; Ye, C.; Li, X.; Zou, Y.; Sun, Y.; Liu, C.; Xu, W.et al. Synthetic Route to a Triphenylenehexaselenol-Based Metal Organic Framework with Semi-Conductive and Glassy Magnetic Properties. *iScience* **2020,** *23*, 100812.
(335) Kambe, T.; Sakamoto, R.; Hoshiko, K.; Takada, K.; Miyachi, M.; Ryu, J.-H.; Sasaki, S.; Kim, J.; Nakazato, K.; Takata, M.et al. Π-Conjugated Nickel Bis(Dithiolene) Complex Nanosheet. *J. Am. Chem. Soc.* **2013,** *135*, 2462-2465.
(336) Dou, J.-H.; Sun, L.; Ge, Y.; Li, W.; Hendon, C. H.; Li, J.; Gul, S.; Yano, J.; Stach, E. A.; Dincă, M. Signature of Metallic Behavior in the Metal–Organic Frameworks M3(Hexaiminobenzene)2 (M = Ni, Cu). *J. Am. Chem. Soc.* **2017,** *139*, 13608-13611.
(337) Sun, X.; Wu, K.-H.; Sakamoto, R.; Kusamoto, T.; Maeda, H.; Ni, X.; Jiang, W.; Liu, F.; Sasaki, S.; Masunaga, H.et al. Bis(Aminothiolato)Nickel Nanosheet as a Redox Switch for Conductivity and an Electrocatalyst for the Hydrogen Evolution Reaction. *Chem. Sci.* **2017,** *8*, 8078-8085.
(338) Park, J.; Hinckley, A. C.; Huang, Z.; Feng, D.; Yakovenko, A. A.; Lee, M.; Chen, S.; Zou, X.; Bao, Z. Synthetic Routes for a 2d Semiconductive Copper Hexahydroxybenzene Metal–Organic Framework. *J. Am. Chem. Soc.* **2018,** *140*, 14533-14537.
(339) Cui, Y.; Yan, J.; Chen, Z.; Zhang, J.; Zou, Y.; Sun, Y.; Xu, W.; Zhu, D. [Cu3(C6se6)]N: The First Highly Conductive 2d Π–D Conjugated Coordination Polymer Based on Benzenehexaselenolate. *Adv. Sci.* **2019,** *6*, 1802235.
(340) Nagatomi, H.; Yanai, N.; Yamada, T.; Shiraishi, K.; Kimizuka, N. Synthesis and Electric Properties of a Two-Dimensional Metal-Organic Framework Based on Phthalocyanine. *Chem. Eur. J.* **2018,** *24*, 1806-1810.
(341) Jia, H.; Yao, Y.; Zhao, J.; Gao, Y.; Luo, Z.; Du, P. A Novel Two-Dimensional Nickel Phthalocyanine-Based Metal–Organic Framework for Highly Efficient Water Oxidation Catalysis. *J. Mater. Chem. A* **2018,** *6*, 1188-1195.
(342) Zhong, H.; Ly, K. H.; Wang, M.; Krupskaya, Y.; Han, X.; Zhang, J.; Zhang, J.; Kataev, V.; Büchner, B.; Weidinger, I. M.et al. A Phthalocyanine-Based Layered Two-Dimensional Conjugated Metal–Organic Framework as a Highly Efficient Electrocatalyst for the Oxygen Reduction Reaction. *Angew. Chem. Int. Ed.* **2019,** *58*, 10677-10682.
(343) Yang, C.; Dong, R.; Wang, M.; Petkov, P. S.; Zhang, Z.; Wang, M.; Han, P.; Ballabio, M.; Bräuninger, S. A.; Liao, Z.et al. A Semiconducting Layered Metal-Organic Framework Magnet. *Nat. Commun.* **2019,** *10*, 3260.
(344) Dong, R.; Pfeffermann, M.; Skidin, D.; Wang, F.; Fu, Y.; Narita, A.; Tommasini, M.; Moresco, F.; Cuniberti, G.; Berger, R.et al. Persulfurated Coronene: A New Generation of "Sulflower". *J. Am. Chem. Soc.* **2017,** *139*, 2168-2171.
(345) Liu, J.; Zhou, Y.; Xie, Z.; Li, Y.; Liu, Y.; Sun, J.; Ma, Y.; Terasaki, O.; Chen, L. Conjugated Copper-Catecholate Framework Electrodes for Efficient Energy Storage. *Angew. Chem. Int. Ed.* **2019,** *n/a*.
(346) Kambe, T.; Sakamoto, R.; Kusamoto, T.; Pal, T.; Fukui, N.; Hoshiko, K.; Shimojima, T.; Wang, Z.; Hirahara, T.; Ishizaka, K.et al. Redox Control and High Conductivity of Nickel Bis(Dithiolene) Complex Π-Nanosheet: A Potential Organic Two-Dimensional Topological Insulator. *J. Am. Chem. Soc.* **2014,** *136*, 14357-14360.
(347) Dong, R.; Zheng, Z.; Tranca, D. C.; Zhang, J.; Chandrasekhar, N.; Liu, S.; Zhuang, X.; Seifert, G.; Feng, X. Immobilizing Molecular Metal Dithiolene–Diamine Complexes on 2d

Metal–Organic Frameworks for Electrocatalytic H2 Production. *Chem. Eur. J.* **2017,** *23*, 2255-2260.

(348) Clough, A. J.; Yoo, J. W.; Mecklenburg, M. H.; Marinescu, S. C. Two-Dimensional Metal–Organic Surfaces for Efficient Hydrogen Evolution from Water. *J. Am. Chem. Soc.* **2015,** *137*, 118-121.

(349) Miner, E. M.; Fukushima, T.; Sheberla, D.; Sun, L.; Surendranath, Y.; Dincă, M. Electrochemical Oxygen Reduction Catalysed by Ni3(Hexaiminotriphenylene)2. *Nat. Commun.* **2016,** *7*, 10942.

(350) Miner, E. M.; Gul, S.; Ricke, N. D.; Pastor, E.; Yano, J.; Yachandra, V. K.; Van Voorhis, T.; Dincă, M. Mechanistic Evidence for Ligand-Centered Electrocatalytic Oxygen Reduction with the Conductive Mof Ni3(Hexaiminotriphenylene)2. *ACS Catal.* **2017,** *7*, 7726-7731.

(351) Zhang, M.; Zheng, B.-H.; Xu, J.; Pan, N.; Yu, J.; Chen, M.; Cao, H. Fewer-Layer Conductive Metal–Organic Nanosheets Enable Ultrahigh Mass Activity for the Oxygen Evolution Reaction. *Chem. Commun.* **2018,** *54*, 13579-13582.

(352) Miner, E. M.; Wang, L.; Dincă, M. Modular O2 Electroreduction Activity in Triphenylene-Based Metal–Organic Frameworks. *Chem. Sci.* **2018,** *9*, 6286-6291.

(353) Zhong, H.; Ghorbani-Asl, M.; Ly, K. H.; Zhang, J.; Ge, J.; Wang, M.; Liao, Z.; Makarov, D.; Zschech, E.; Brunner, E.et al. Synergistic Electroreduction of Carbon Dioxide to Carbon Monoxide on Bimetallic Layered Conjugated Metal-Organic Frameworks. *Nat. Commun.* **2020,** *11*, 1409.

(354) Sheberla, D.; Bachman, J. C.; Elias, J. S.; Sun, C.-J.; Shao-Horn, Y.; Dincă, M. Conductive Mof Electrodes for Stable Supercapacitors with High Areal Capacitance. *Nat. Mater.* **2016,** *16*, 220.

(355) Li, W.-H.; Ding, K.; Tian, H.-R.; Yao, M.-S.; Nath, B.; Deng, W.-H.; Wang, Y.; Xu, G. Conductive Metal–Organic Framework Nanowire Array Electrodes for High-Performance Solid-State Supercapacitors. *Adv. Funct. Mater.* **2017,** *27*, 1702067-n/a.

(356) Feng, D.; Lei, T.; Lukatskaya, M. R.; Park, J.; Huang, Z.; Lee, M.; Shaw, L.; Chen, S.; Yakovenko, A. A.; Kulkarni, A.et al. Robust and Conductive Two-Dimensional Metal−Organic Frameworks with Exceptionally High Volumetric and Areal Capacitance. *Nat. Energy* **2018,** *3*, 30-36.

(357) Wu, H.; Zhang, W.; Kandambeth, S.; Shekhah, O.; Eddaoudi, M.; Alshareef, H. N. Conductive Metal–Organic Frameworks Selectively Grown on Laser-Scribed Graphene for Electrochemical Microsupercapacitors. *Adv. Ener. Mater.* **2019,** *9*, 1900482.

(358) Park, J.; Lee, M.; Feng, D.; Huang, Z.; Hinckley, A. C.; Yakovenko, A.; Zou, X.; Cui, Y.; Bao, Z. Stabilization of Hexaaminobenzene in a 2d Conductive Metal–Organic Framework for High Power Sodium Storage. *J. Am. Chem. Soc.* **2018,** *140*, 10315-10323.

(359) Wada, K.; Sakaushi, K.; Sasaki, S.; Nishihara, H. Multielectron-Transfer-Based Rechargeable Energy Storage of Two-Dimensional Coordination Frameworks with Non-Innocent Ligands. *Angew. Chem. Int. Ed.* **2018,** *57*, 8886-8890.

(360) Li, Y.-L.; Zhou, J.-J.; Wu, M.-K.; Chen, C.; Tao, K.; Yi, F.-Y.; Han, L. Hierarchical Two-Dimensional Conductive Metal–Organic Framework/Layered Double Hydroxide Nanoarray for a High-Performance Supercapacitor. *Inorg. Chem.* **2018,** *57*, 6202-6205.

(361) Wang, Z.; Wang, G.; Qi, H.; Wang, M.; Wang, M.; Park, S.; Wang, H.; Yu, M.; Kaiser, U.; Fery, A.et al. Ultrathin Two-Dimensional Conjugated Metal–Organic Framework Single-

Crystalline Nanosheets Enabled by Surfactant-Assisted Synthesis. *Chem. Sci.* **2020**, DOI:10.1039/D0SC01408G 10.1039/D0SC01408G.

(362) M. Wang, H. S., P. Zhang, Z. Liao, M. Wang, H. Zhong, F. Schwotzer, A. Shaygan Nia, E. Zschech, S. Zhou, S. Kaskel, R. Dong, and X. Feng. Phthalocyanine-Based Two-Dimensional Conjugated Metal-Organic Framework Nanosheets for High-Performance Micro-Supercapacitors. *Adv. Func. Mater.* **2020**, DOI:0.1002/adfm.202002664 0.1002/adfm.202002664.

(363) Huang, X.; Zhang, S.; Liu, L.; Yu, L.; Chen, G.; Xu, W.; Zhu, D. Superconductivity in a Copper(Ii)-Based Coordination Polymer with Perfect Kagome Structure. *Angew. Chem. Int. Ed.* **2018,** *57*, 146-150.

(364) Ulbricht, R.; Hendry, E.; Shan, J.; Heinz, T. F.; Bonn, M. Carrier Dynamics in Semiconductors Studied with Time-Resolved Terahertz Spectroscopy. *Rev. Modern Phys.* **2011,** *83*, 543-586.

(365) Wang, Z. F.; Su, N.; Liu, F. Prediction of a Two-Dimensional Organic Topological Insulator. *Nano Lett.* **2013,** *13*, 2842-2845.

(366) Shojaei, F.; Kang, H. S. Continuous Tuning of Band Gap for Π-Conjugated Ni Bis(Dithiolene) Complex Bilayer. *J. Phys. Chem. C* **2014,** *118*, 25626-25632.

(367) Dong, L.; Kim, Y.; Er, D.; Rappe, A. M.; Shenoy, V. B. Two-Dimensional Pi-Conjugated Covalent-Organic Frameworks as Quantum Anomalous Hall Topological Insulators. *Phys. Rev. Lett.* **2016,** *116*, 096601.

(368) Foster, M. E.; Sohlberg, K.; Allendorf, M. D.; Talin, A. A. Unraveling the Semiconducting/Metallic Discrepancy in Ni3(Hitp)2. *J. Phys. Chem. Lett.* **2018,** *9*, 481-486.

(369) Foster, M. E.; Sohlberg, K.; Spataru, C. D.; Allendorf, M. D. Proposed Modification of the Graphene Analogue Ni3(Hitp)2 to Yield a Semiconducting Material. *J. Phys. Chem. C* **2016,** *120*, 15001-15008.

(370) Sun, L.; Liao, B.; Sheberla, D.; Kraemer, D.; Zhou, J.; Stach, E. A.; Zakharov, D.; Stavila, V.; Talin, A. A.; Ge, Y.et al. A Microporous and Naturally Nanostructured Thermoelectric Metal-Organic Framework with Ultralow Thermal Conductivity. *Joule* **2017,** *1*, 168-177.

(371) Skorupskii, G.; Trump, B. A.; Kasel, T. W.; Brown, C. M.; Hendon, C. H.; Dincă, M. Efficient and Tunable One-Dimensional Charge Transport in Layered Lanthanide Metal–Organic Frameworks. *Nat. Chem.* **2020,** *12*, 131-136.

(372) Dong, R.; Zhang, Z.; Tranca, D. C.; Zhou, S.; Wang, M.; Adler, P.; Liao, Z.; Liu, F.; Sun, Y.; Shi, W.et al. A Coronene-Based Semiconducting Two-Dimensional Metal-Organic Framework with Ferromagnetic Behavior. *Nat. Commun.* **2018,** *9*, 2637.

(373) Narayan, T. C.; Miyakai, T.; Seki, S.; Dincă, M. High Charge Mobility in a Tetrathiafulvalene-Based Microporous Metal–Organic Framework. *J. Am. Chem. Soc.* **2012,** *134*, 12932-12935.

(374) He, Y. P.; Spataru, C. D.; Leonard, F.; Jones, R. E.; Foster, M. E.; Allendorf, M. D.; Talin, A. A. Two-Dimensional Metal-Organic Frameworks with High Thermoelectric Efficiency through Metal Ion Selection. *Phys. Chem. Chem. Phys.* **2017,** *19*, 19461-19467.

(375) Xie, L. S.; Sun, L.; Wan, R.; Park, S. S.; DeGayner, J. A.; Hendon, C. H.; Dincă, M. Tunable Mixed-Valence Doping toward Record Electrical Conductivity in a Three-Dimensional Metal–Organic Framework. *J. Am. Chem. Soc.* **2018,** *140*, 7411-7414.

(376) Sun, L.; Hendon, C. H.; Park, S. S.; Tulchinsky, Y.; Wan, R.; Wang, F.; Walsh, A.; Dincă, M. Is Iron Unique in Promoting Electrical Conductivity in Mofs? *Chem. Sci.* **2017,** *8*, 4450-4457.

(377) Pathak, A.; Shen, J.-W.; Usman, M.; Wei, L.-F.; Mendiratta, S.; Chang, Y.-S.; Sainbileg, B.; Ngue, C.-M.; Chen, R.-S.; Hayashi, M.et al. Integration of a (–Cu–S–)N Plane in a Metal–Organic Framework Affords High Electrical Conductivity. *Nat. Commun.* **2019,** *10*, 1721.

(378) Feng, X.; Chen, L.; Honsho, Y.; Saengsawang, O.; Liu, L.; Wang, L.; Saeki, A.; Irle, S.; Seki, S.; Dong, Y.et al. An Ambipolar Conducting Covalent Organic Framework with Self-Sorted and Periodic Electron Donor-Acceptor Ordering. *Adv. Mater.* **2012,** *24*, 3026-3031.

(379) Côté, A. P.; Benin, A. I.; Ockwig, N. W.; O'Keeffe, M.; Matzger, A. J.; Yaghi, O. M. Porous, Crystalline, Covalent Organic Frameworks. *Science* **2005,** *310*, 1166-1170.

(380) Furukawa, H.; Yaghi, O. M. Storage of Hydrogen, Methane, and Carbon Dioxide in Highly Porous Covalent Organic Frameworks for Clean Energy Applications. *J. Am. Chem. Soc.* **2009,** *131*, 8875-8883.

(381) Zeng, Y.; Zou, R.; Zhao, Y. Covalent Organic Frameworks for Co2 Capture. *Adv. Mater.* **2016,** *28*, 2855-2873.

(382) Zhang, C.; Wu, B.-H.; Ma, M.-Q.; Wang, Z.; Xu, Z.-K. Ultrathin Metal/Covalent–Organic Framework Membranes Towards Ultimate Separation. *Chem. Soc. Rev.* **2019,** *48*, 3811-3841.

(383) Kuehl, V. A.; Yin, J.; Duong, P. H. H.; Mastorovich, B.; Newell, B.; Li-Oakey, K. D.; Parkinson, B. A.; Hoberg, J. O. A Highly Ordered Nanoporous, Two-Dimensional Covalent Organic Framework with Modifiable Pores, and Its Application in Water Purification and Ion Sieving. *J. Am. Chem. Soc.* **2018,** *140*, 18200-18207.

(384) Matsumoto, M.; Valentino, L.; Stiehl, G. M.; Balch, H. B.; Corcos, A. R.; Wang, F.; Ralph, D. C.; Mariñas, B. J.; Dichtel, W. R. Lewis-Acid-Catalyzed Interfacial Polymerization of Covalent Organic Framework Films. *Chem* **2018,** *4*, 308-317.

(385) Dey, K.; Pal, M.; Rout, K. C.; Kunjattu H, S.; Das, A.; Mukherjee, R.; Kharul, U. K.; Banerjee, R. Selective Molecular Separation by Interfacially Crystallized Covalent Organic Framework Thin Films. *J. Am. Chem. Soc.* **2017,** *139*, 13083-13091.

(386) Ding, S.-Y.; Gao, J.; Wang, Q.; Zhang, Y.; Song, W.-G.; Su, C.-Y.; Wang, W. Construction of Covalent Organic Framework for Catalysis: Pd/Cof-Lzu1 in Suzuki–Miyaura Coupling Reaction. *J. Am. Chem. Soc.* **2011,** *133*, 19816-19822.

(387) Xu, H.; Gao, J.; Jiang, D. Stable, Crystalline, Porous, Covalent Organic Frameworks as a Platform for Chiral Organocatalysts. *Nat. Chem.* **2015,** *7*, 905.

(388) Han, X.; Xia, Q.; Huang, J.; Liu, Y.; Tan, C.; Cui, Y. Chiral Covalent Organic Frameworks with High Chemical Stability for Heterogeneous Asymmetric Catalysis. *J. Am. Chem. Soc.* **2017,** *139*, 8693-8697.

(389) Li, Z.; Huang, N.; Lee, K. H.; Feng, Y.; Tao, S.; Jiang, Q.; Nagao, Y.; Irle, S.; Jiang, D. Light-Emitting Covalent Organic Frameworks: Fluorescence Improving Via Pinpoint Surgery and Selective Switch-on Sensing of Anions. *J. Am. Chem. Soc.* **2018,** *140*, 12374-12377.

(390) Xie, Z.; Wang, B.; Yang, Z.; Yang, X.; Yu, X.; Xing, G.; Zhang, Y.; Chen, L. Stable 2d Heteroporous Covalent Organic Frameworks for Efficient Ionic Conduction. *Angew. Chem. Int. Ed.* **2019,** *58*, 15742-15746.

(391) Sasmal, H. S.; Aiyappa, H. B.; Bhange, S. N.; Karak, S.; Halder, A.; Kurungot, S.; Banerjee, R. Superprotonic Conductivity in Flexible Porous Covalent Organic Framework Membranes. *Angew. Chem. Int. Ed.* **2018,** *57*, 10894-10898.
(392) Xu, H.; Tao, S.; Jiang, D. Proton Conduction in Crystalline and Porous Covalent Organic Frameworks. *Nat. Mater.* **2016,** *15*, 722.
(393) Biswal, B. P.; Valligatla, S.; Wang, M.; Banerjee, T.; Saad, N. A.; Mariserla, B. M. K.; Chandrasekhar, N.; Becker, D.; Addicoat, M.; Senkovska, I.et al. Nonlinear Optical Switching in Regioregular Porphyrin Covalent Organic Frameworks. *Angew. Chem. Int. Ed.* **2019,** *58*, 6896-6900.
(394) Phan, H.; Herng, T. S.; Wang, D.; Li, X.; Zeng, W.; Ding, J.; Loh, K. P.; Shen Wee, A. T.; Wu, J. Room-Temperature Magnets Based on 1,3,5-Triazine-Linked Porous Organic Radical Frameworks. *Chem* **2019,** *5*, 1223-1234.
(395) Jiang, Y.; Oh, I.; Joo, S. H.; Buyukcakir, O.; Chen, X.; Lee, S. H.; Huang, M.; Seong, W. K.; Kim, J. H.; Rohde, J.-U.et al. Organic Radical-Linked Covalent Triazine Framework with Paramagnetic Behavior. *ACS Nano* **2019,** *13*, 5251-5258.
(396) Wu, S.; Li, M.; Phan, H.; Wang, D.; Herng, T. S.; Ding, J.; Lu, Z.; Wu, J. Toward Two-Dimensional Π-Conjugated Covalent Organic Radical Frameworks. *Angew. Chem. Int. Ed.* **2018,** *57*, 8007-8011.
(397) Jin, E.; Asada, M.; Xu, Q.; Dalapati, S.; Addicoat, M. A.; Brady, M. A.; Xu, H.; Nakamura, T.; Heine, T.; Chen, Q.et al. Two-Dimensional Sp2 Carbon–Conjugated Covalent Organic Frameworks. *Science* **2017,** *357*, 673-676.
(398) Sick, T.; Hufnagel, A. G.; Kampmann, J.; Kondofersky, I.; Calik, M.; Rotter, J. M.; Evans, A.; Döblinger, M.; Herbert, S.; Peters, K.et al. Oriented Films of Conjugated 2d Covalent Organic Frameworks as Photocathodes for Water Splitting. *J. Am. Chem. Soc.* **2018,** *140*, 2085-2092.
(399) Wang, G.; Chandrasekhar, N.; Biswal, B. P.; Becker, D.; Paasch, S.; Brunner, E.; Addicoat, M.; Yu, M.; Berger, R.; Feng, X. A Crystalline, 2d Polyarylimide Cathode for Ultrastable and Ultrafast Li Storage. *Adv. Mater.* **2019,** *31*, 1901478.
(400) Xu, S.; Wang, G.; Biswal, B. P.; Addicoat, M.; Paasch, S.; Sheng, W.; Zhuang, X.; Brunner, E.; Heine, T.; Berger, R.et al. A Nitrogen-Rich 2d Sp2-Carbon-Linked Conjugated Polymer Framework as a High-Performance Cathode for Lithium-Ion Batteries. *Angew. Chem. Int. Ed.* **2019,** *58*, 849-853.
(401) Liu, W.; Ulaganathan, M.; Abdelwahab, I.; Luo, X.; Chen, Z.; Rong Tan, S. J.; Wang, X.; Liu, Y.; Geng, D.; Bao, Y.et al. Two-Dimensional Polymer Synthesized Via Solid-State Polymerization for High-Performance Supercapacitors. *ACS Nano* **2018,** *12*, 852-860.
(402) Duan, H.; Lyu, P.; Liu, J.; Zhao, Y.; Xu, Y. Semiconducting Crystalline Two-Dimensional Polyimide Nanosheets with Superior Sodium Storage Properties. *ACS Nano* **2019,** *13*, 2473-2480.
(403) Chen, X.; Li, Y.; Wang, L.; Xu, Y.; Nie, A.; Li, Q.; Wu, F.; Sun, W.; Zhang, X.; Vajtai, R.et al. High-Lithium-Affinity Chemically Exfoliated 2d Covalent Organic Frameworks. *Adv. Mater.* **2019,** *31*, 1901640.
(404) Wang, L.; Tranca, D. C.; Zhang, J.; Qi, Y.; Sfaelou, S.; Zhang, T.; Dong, R.; Zhuang, X.; Zheng, Z.; Seifert, G. Toward Activity Origin of Electrocatalytic Hydrogen Evolution

Reaction on Carbon-Rich Crystalline Coordination Polymers. *Small* **2017,** *13*, 1700783-n/a.

(405) Wan, S.; Guo, J.; Kim, J.; Ihee, H.; Jiang, D. A Belt-Shaped, Blue Luminescent, and Semiconducting Covalent Organic Framework. *Angew. Chem. Int. Ed.* **2008,** *47*, 8826-8830.

(406) Martínez-Abadía, M.; Stoppiello, C. T.; Strutynski, K.; Lerma-Berlanga, B.; Martí-Gastaldo, C.; Saeki, A.; Melle-Franco, M.; Khlobystov, A. N.; Mateo-Alonso, A. A Wavy Two-Dimensional Covalent Organic Framework from Core-Twisted Polycyclic Aromatic Hydrocarbons. *J. Am. Chem. Soc.* **2019,** *141*, 14403-14410.

(407) Spitler, E. L.; Dichtel, W. R. Lewis Acid-Catalysed Formation of Two-Dimensional Phthalocyanine Covalent Organic Frameworks. *Nat. Chem.* **2010,** *2*, 672-677.

(408) Wan, S.; Gándara, F.; Asano, A.; Furukawa, H.; Saeki, A.; Dey, S. K.; Liao, L.; Ambrogio, M. W.; Botros, Y. Y.; Duan, X.et al. Covalent Organic Frameworks with High Charge Carrier Mobility. *Chem. Mater.* **2011,** *23*, 4094-4097.

(409) Calik, M.; Auras, F.; Salonen, L. M.; Bader, K.; Grill, I.; Handloser, M.; Medina, D. D.; Dogru, M.; Löbermann, F.; Trauner, D.et al. Extraction of Photogenerated Electrons and Holes from a Covalent Organic Framework Integrated Heterojunction. *J. Am. Chem. Soc.* **2014,** *136*, 17802-17807.

(410) Dalapati, S.; Addicoat, M.; Jin, S.; Sakurai, T.; Gao, J.; Xu, H.; Irle, S.; Seki, S.; Jiang, D. Rational Design of Crystalline Supermicroporous Covalent Organic Frameworks with Triangular Topologies. *Nat. Commun.* **2015,** *6*, 7786.

(411) Feldblyum, J. I.; McCreery, C. H.; Andrews, S. C.; Kurosawa, T.; Santos, E. J. G.; Duong, V.; Fang, L.; Ayzner, A. L.; Bao, Z. Few-Layer, Large-Area, 2d Covalent Organic Framework Semiconductor Thin Films. *Chem. Commun.* **2015,** *51*, 13894-13897.

(412) Zhuang, X.; Zhao, W.; Zhang, F.; Cao, Y.; Liu, F.; Bi, S.; Feng, X. A Two-Dimensional Conjugated Polymer Framework with Fully Sp2-Bonded Carbon Skeleton. *Polymer Chem.* **2016,** *7*, 4176-4181.

(413) Liu, W.; Luo, X.; Bao, Y.; Liu, Y. P.; Ning, G.-H.; Abdelwahab, I.; Li, L.; Nai, C. T.; Hu, Z. G.; Zhao, D.et al. A Two-Dimensional Conjugated Aromatic Polymer Via C–C Coupling Reaction. *Nat. Chem.* **2017,** *9*, 563-570.

(414) Guo, J.; Xu, Y.; Jin, S.; Chen, L.; Kaji, T.; Honsho, Y.; Addicoat, M. A.; Kim, J.; Saeki, A.; Ihee, H.et al. Conjugated Organic Framework with Three-Dimensionally Ordered Stable Structure and Delocalized Π Clouds. *Nat. Commun.* **2013,** *4*, 2736.

(415) Mahmood, J.; Lee, E. K.; Jung, M.; Shin, D.; Jeon, I.-Y.; Jung, S.-M.; Choi, H.-J.; Seo, J.-M.; Bae, S.-Y.; Sohn, S.-D.et al. Nitrogenated Holey Two-Dimensional Structures. *Nat. Commun.* **2015,** *6*, 6486.

(416) Thomas, S.; Li, H.; Zhong, C.; Matsumoto, M.; Dichtel, W. R.; Bredas, J.-L. Electronic Structure of Two-Dimensional Π-Conjugated Covalent Organic Frameworks. *Chem. Mater.* **2019,** *31*, 3051-3065.

(417) Kim, T. W.; Jun, S.; Ha, Y.; Yadav, R. K.; Kumar, A.; Yoo, C.-Y.; Oh, I.; Lim, H.-K.; Shin, J. W.; Ryoo, R.et al. Ultrafast Charge Transfer Coupled with Lattice Phonons in Two-Dimensional Covalent Organic Frameworks. *Nat. Commun.* **2019,** *10*, 1873.

(418) Bessinger, D.; Ascherl, L.; Auras, F.; Bein, T. Spectrally Switchable Photodetection with near-Infrared-Absorbing Covalent Organic Frameworks. *J. Am. Chem. Soc.* **2017,** *139*, 12035-12042.
(419) Sahabudeen, H.; Qi, H.; Glatz, B. A.; Tranca, D.; Dong, R.; Hou, Y.; Zhang, T.; Kuttner, C.; Lehnert, T.; Seifert, G.et al. Wafer-Sized Multifunctional Polyimine-Based Two-Dimensional Conjugated Polymers with High Mechanical Stiffness. *Nat. Commun.* **2016,** *7*, 13461.
(420) Cai, S.-L.; Zhang, Y.-B.; Pun, A. B.; He, B.; Yang, J.; Toma, F. M.; Sharp, I. D.; Yaghi, O. M.; Fan, J.; Zheng, S.-R.et al. Tunable Electrical Conductivity in Oriented Thin Films of Tetrathiafulvalene-Based Covalent Organic Framework. *Chem. Sci.* **2014,** *5*, 4693-4700.
(421) Chen, L.; Furukawa, K.; Gao, J.; Nagai, A.; Nakamura, T.; Dong, Y.; Jiang, D. Photoelectric Covalent Organic Frameworks: Converting Open Lattices into Ordered Donor–Acceptor Heterojunctions. *J. Am. Chem. Soc.* **2014,** *136*, 9806-9809.
(422) Ding, H.; Li, Y.; Hu, H.; Sun, Y.; Wang, J.; Wang, C.; Wang, C.; Zhang, G.; Wang, B.; Xu, W.et al. A Tetrathiafulvalene-Based Electroactive Covalent Organic Framework. *Chem. Eur. J.* **2014,** *20*, 14614-14618.
(423) Ding, X.; Chen, L.; Honsho, Y.; Feng, X.; Saengsawang, O.; Guo, J.; Saeki, A.; Seki, S.; Irle, S.; Nagase, S.et al. An N-Channel Two-Dimensional Covalent Organic Framework. *J. Am. Chem. Soc.* **2011,** *133*, 14510-14513.
(424) Dogru, M.; Bein, T. On the Road Towards Electroactive Covalent Organic Frameworks. *Chem. Commun.* **2014,** *50*, 5531-5546.
(425) Dogru, M.; Handloser, M.; Auras, F.; Kunz, T.; Medina, D.; Hartschuh, A.; Knochel, P.; Bein, T. A Photoconductive Thienothiophene-Based Covalent Organic Framework Showing Charge Transfer Towards Included Fullerene. *Angewandte Chemie* **2013,** *125*, 2992-2996.
(426) Feng, X.; Liu, L.; Honsho, Y.; Saeki, A.; Seki, S.; Irle, S.; Dong, Y.; Nagai, A.; Jiang, D. High-Rate Charge-Carrier Transport in Porphyrin Covalent Organic Frameworks: Switching from Hole to Electron to Ambipolar Conduction. *Angewandte Chemie* **2012,** *124*, 2672-2676.
(427) Jin, S.; Sakurai, T.; Kowalczyk, T.; Dalapati, S.; Xu, F.; Wei, H.; Chen, X.; Gao, J.; Seki, S.; Irle, S.et al. Two-Dimensional Tetrathiafulvalene Covalent Organic Frameworks: Towards Latticed Conductive Organic Salts. *Chem. Eur. J.* **2014,** *20*, 14608-14613.
(428) Medina, D. D.; Petrus, M. L.; Jumabekov, A. N.; Margraf, J. T.; Weinberger, S.; Rotter, J. M.; Clark, T.; Bein, T. Directional Charge-Carrier Transport in Oriented Benzodithiophene Covalent Organic Framework Thin Films. *ACS Nano* **2017,** *11*, 2706-2713.
(429) Noda, Y.; Merschjann, C.; Tarábek, J.; Amsalem, P.; Koch, N.; Bojdys, M. J. Directional Charge Transport in Layered Two-Dimensional Triazine-Based Graphitic Carbon Nitride. *Angew. Chem. Int. Ed.* **2019,** *58*, 9394-9398.
(430) Rager, S.; Jakowetz, A. C.; Gole, B.; Beuerle, F.; Medina, D. D.; Bein, T. Scaffold-Induced Diketopyrrolopyrrole Molecular Stacks in a Covalent Organic Framework. *Chem. Mater.* **2019,** *31*, 2707-2712.
(431) Stegbauer, L.; Schwinghammer, K.; Lotsch, B. V. A Hydrazone-Based Covalent Organic Framework for Photocatalytic Hydrogen Production. *Chem. Sci.* **2014,** *5*, 2789-2793.

(432) Vyas, V. S.; Haase, F.; Stegbauer, L.; Savasci, G.; Podjaski, F.; Ochsenfeld, C.; Lotsch, B. V. A Tunable Azine Covalent Organic Framework Platform for Visible Light-Induced Hydrogen Generation. *Nat. Commun.* **2015,** *6*, 8508.
(433) Wan, S.; Guo, J.; Kim, J.; Ihee, H.; Jiang, D. A Photoconductive Covalent Organic Framework: Self-Condensed Arene Cubes Composed of Eclipsed 2d Polypyrene Sheets for Photocurrent Generation. *Angew. Chem. Int. Ed.* **2009,** *48*, 5439-5442.
(434) Wang, M.; Ballabio, M.; Wang, M.; Lin, H.-H.; Biswal, B. P.; Han, X.; Paasch, S.; Brunner, E.; Liu, P.; Chen, M.et al. Unveiling Electronic Properties in Metal–Phthalocyanine-Based Pyrazine-Linked Conjugated Two-Dimensional Covalent Organic Frameworks. *J. Am. Chem. Soc.* **2019,** *141*, 16810-16816.
(435) Wang, L.; Zeng, C.; Xu, H.; Yin, P.; Chen, D.; Deng, J.; Li, M.; Zheng, N.; Gu, C.; Ma, Y. A Highly Soluble, Crystalline Covalent Organic Framework Compatible with Device Implementation. *Chem. Sc.* **2019,** *10*, 1023-1028.
(436) Solomos, M. A.; Claire, F. J.; Kempa, T. J. 2d Molecular Crystal Lattices: Advances in Their Synthesis, Characterization, and Application. *J. Mater. Chem. A* **2019,** *7*, 23537-23562.
(437) Zhong, Y.; Cheng, B.; Park, C.; Ray, A.; Brown, S.; Mujid, F.; Lee, J.-U.; Zhou, H.; Suh, J.; Lee, K.-H.et al. Wafer-Scale Synthesis of Monolayer Two-Dimensional Porphyrin Polymers for Hybrid Superlattices. *Science* **2019**, *366*, 1379-1384.
(438) Gao, X.; Liu, H.; Wang, D.; Zhang, J. Graphdiyne: Synthesis, Properties, and Applications. *Chem. Soc. Rev.* **2019,** *48*, 908-936.
(439) Dai, W.; Shao, F.; Szczerbiński, J.; McCaffrey, R.; Zenobi, R.; Jin, Y.; Schlüter, A. D.; Zhang, W. Synthesis of a Two-Dimensional Covalent Organic Monolayer through Dynamic Imine Chemistry at the Air/Water Interface. *Angew. Chem. Int. Ed.* **2016,** *55*, 213-217.
(440) Bhola, R.; Payamyar, P.; Murray, D. J.; Kumar, B.; Teator, A. J.; Schmidt, M. U.; Hammer, S. M.; Saha, A.; Sakamoto, J.; Schlüter, A. D.et al. A Two-Dimensional Polymer from the Anthracene Dimer and Triptycene Motifs. *J. Am. Chem. Soc.* **2013,** *135*, 14134-14141.
(441) Gourdon, A. On-Surface Covalent Coupling in Ultrahigh Vacuum. *Angew. Chem. Int. Ed.* **2008,** *47*, 6950-6953.
(442) Dienstmaier, J. F.; Gigler, A. M.; Goetz, A. J.; Knochel, P.; Bein, T.; Lyapin, A.; Reichlmaier, S.; Heckl, W. M.; Lackinger, M. Synthesis of Well-Ordered Cof Monolayers: Surface Growth of Nanocrystalline Precursors Versus Direct on-Surface Polycondensation. *ACS Nano* **2011,** *5*, 9737-9745.
(443) Dienstmaier, J. F.; Medina, D. D.; Dogru, M.; Knochel, P.; Bein, T.; Heckl, W. M.; Lackinger, M. Isoreticular Two-Dimensional Covalent Organic Frameworks Synthesized by on-Surface Condensation of Diboronic Acids. *ACS Nano* **2012,** *6*, 7234-7242.
(444) Liu, X.-H.; Guan, C.-Z.; Ding, S.-Y.; Wang, W.; Yan, H.-J.; Wang, D.; Wan, L.-J. On-Surface Synthesis of Single-Layered Two-Dimensional Covalent Organic Frameworks Via Solid–Vapor Interface Reactions. *J. Am. Chem. Soc.* **2013,** *135*, 10470-10474.
(445) Colson, J. W.; Woll, A. R.; Mukherjee, A.; Levendorf, M. P.; Spitler, E. L.; Shields, V. B.; Spencer, M. G.; Park, J.; Dichtel, W. R. Oriented 2d Covalent Organic Framework Thin Films on Single-Layer Graphene. *Science* **2011,** *332*, 228-231.
(446) Medina, D. D.; Werner, V.; Auras, F.; Tautz, R.; Dogru, M.; Schuster, J.; Linke, S.; Döblinger, M.; Feldmann, J.; Knochel, P.et al. Oriented Thin Films of a Benzodithiophene Covalent Organic Framework. *ACS Nano* **2014,** *8*, 4042-4052.

(447) McDonald, T. M.; Mason, J. A.; Kong, X.; Bloch, E. D.; Gygi, D.; Dani, A.; Crocellà, V.; Giordanino, F.; Odoh, S. O.; Drisdell, W. S.et al. Cooperative Insertion of Co2 in Diamine-Appended Metal-Organic Frameworks. *Nature* **2015,** *519*, 303.

(448) Park, S.; Liao, Z. Q.; Ibarlucea, B.; Qi, H. Y.; Lin, H. H.; Becker, D.; Melidonie, J.; Zhang, T.; Sahabudeen, H.; Baraban, L.et al. Two-Dimensional Boronate Ester Covalent Organic Framework Thin Films with Large Single Crystalline Domains for a Neuromorphic Memory Device. *Angew. Chem. Int. Ed.*, **2020,** DOI:10.1002/anie.201916595 10.1002/anie.201916595.

(449) Biswal, B. P.; Chandra, S.; Kandambeth, S.; Lukose, B.; Heine, T.; Banerjee, R. Mechanochemical Synthesis of Chemically Stable Isoreticular Covalent Organic Frameworks. *J. Am. Chem. Soc.* **2013,** *135*, 5328-5331.

(450) Bunck, D. N.; Dichtel, W. R. Bulk Synthesis of Exfoliated Two-Dimensional Polymers Using Hydrazone-Linked Covalent Organic Frameworks. *J. Am. Chem. Soc.* **2013,** *135*, 14952-14955.

(451) Chandra, S.; Kandambeth, S.; Biswal, B. P.; Lukose, B.; Kunjir, S. M.; Chaudhary, M.; Babarao, R.; Heine, T.; Banerjee, R. Chemically Stable Multilayered Covalent Organic Nanosheets from Covalent Organic Frameworks Via Mechanical Delamination. *J. Am. Chem. Soc.* **2013,** *135*, 17853-17861.

(452) Khayum, M. A.; Kandambeth, S.; Mitra, S.; Nair, S. B.; Das, A.; Nagane, S. S.; Mukherjee, R.; Banerjee, R. Chemically Delaminated Free-Standing Ultrathin Covalent Organic Nanosheets. *Angew. Chem. Int. Ed.* **2016,** *55*, 15604-15608.

(453) Kissel, P.; Erni, R.; Schweizer, W. B.; Rossell, M. D.; King, B. T.; Bauer, T.; Götzinger, S.; Schlüter, A. D.; Sakamoto, J. A Two-Dimensional Polymer Prepared by Organic Synthesis. *Nat. Chem.* **2012,** *4*, 287.

(454) Lei, Z.; Chen, X.; Sun, W.; Zhang, Y.; Wang, Y. Exfoliated Triazine-Based Covalent Organic Nanosheets with Multielectron Redox for High-Performance Lithium Organic Batteries. *Adv. Ener. Mater.* **2019,** *9*, 1801010.

(455) Peng, Y.; Huang, Y.; Zhu, Y.; Chen, B.; Wang, L.; Lai, Z.; Zhang, Z.; Zhao, M.; Tan, C.; Yang, N.et al. Ultrathin Two-Dimensional Covalent Organic Framework Nanosheets: Preparation and Application in Highly Sensitive and Selective DNA Detection. *J. Am. Chem. Soc.* **2017,** *139*, 8698-8704.

(456) Wang, S.; Wang, Q.; Shao, P.; Han, Y.; Gao, X.; Ma, L.; Yuan, S.; Ma, X.; Zhou, J.; Feng, X.et al. Exfoliation of Covalent Organic Frameworks into Few-Layer Redox-Active Nanosheets as Cathode Materials for Lithium-Ion Batteries. *J. Am. Chem. Soc.* **2017,** *139*, 4258-4261.

(457) Sirringhaus, H.; Brown, P. J.; Friend, R. H.; Nielsen, M. M.; Bechgaard, K.; Langeveld-Voss, B. M. W.; Spiering, A. J. H.; Janssen, R. A. J.; Meijer, E. W.; Herwig, P.et al. Two-Dimensional Charge Transport in Self-Organized, High-Mobility Conjugated Polymers. *Nature* **1999,** *401*, 685-688.

(458) Kim, J.; Swager, T. M. Control of Conformational and Interpolymer Effects in Conjugated Polymers. *Nature* **2001,** *411*, 1030-1034.

(459) Joseph Kline, R.; McGehee, M. D.; Toney, M. F. Highly Oriented Crystals at the Buried Interface in Polythiophene Thin-Film Transistors. *Nat. Mater.* **2006,** *5*, 222-228.

(460) Zhang, W.; Xiong, R.-G. Ferroelectric Metal–Organic Frameworks. *Chem. Rev.* **2012,** *112*, 1163-1195.
(461) Mendiratta, S.; Usman, M.; Lu, K. L. Expanding the Dimensions of Metal-Organic Framework Research Towards Dielectrics. *Coord. Chem. Rev.* **2018,** *360*, 77-91.
(462) Li, W.-J.; Liu, J.; Sun, Z.-H.; Liu, T.-F.; Lü, J.; Gao, S.-Y.; He, C.; Cao, R.; Luo, J.-H. Integration of Metal-Organic Frameworks into an Electrochemical Dielectric Thin Film for Electronic Applications. *Nat. Commun.* **2016,** *7*, 11830.
(463) Zhao, J.-P.; Xu, J.; Han, S.-D.; Wang, Q.-L.; Bu, X.-H. A Niccolite Structural Multiferroic Metal–Organic Framework Possessing Four Different Types of Bistability in Response to Dielectric and Magnetic Modulation. *Adv. Mater.* **2017,** *29*, 1606966.
(464) Lu, S.-Q.; Chen, X.-G.; Gao, J.-X.; Lu, Y.; Hua, X.-N.; Liao, W.-Q. High-Temperature Sequential Structural Transitions with Distinct Switchable Dielectric Behaviors in Two Organic Ionic Plastic Crystals: [C4h11nbr] [Clo4] and [C4h11nbr] [Bf4]. *CrystEngComm* **2018,** *20*, 454-459.
(465) Mączka, M.; Kucharska, E.; Gągor, A.; Pikul, A.; Hanuza, J. Synthesis, Magnetic and Vibrational Properties of Two Novel Mixed-Valence Iron(Ii)-Iron(Iii) Formate Frameworks. *J. Sol. State Chem.* **2018,** *258*, 163-169.
(466) Wang, K.; Xiong, J.-B.; Xia, B.; Wang, Q.-L.; Tong, Y.-Z.; Ma, Y.; Bu, X.-H. Ferroelastic Phase Transition and Switchable Dielectric Constant in Heterometallic Niccolite Formate Frameworks. *Inorg. Chem.* **2018,** *57*, 537-540.
(467) Wang, K.; Xiong, J.-B.; Xia, B.; Wang, Q.-L.; Tong, Y.-Z.; Ma, Y.; Wang, Z.-M.; Gao, S. Alkylamine-Templated Niccolite Frameworks of [Gaiiimii(Hcoo)6]− (M = Fe, Ni): Structure, Magnetism, and Dielectricity. *Inorg. Chem.* **2018,** *57*, 3941-3947.
(468) Eslava, S.; Zhang, L.; Esconjauregui, S.; Yang, J.; Vanstreels, K.; Baklanov, M. R.; Saiz, E. Metal-Organic Framework Zif-8 Films as Low-K Dielectrics in Microelectronics. *Chem. Mater.* **2013,** *25*, 27-33.
(469) Redel, E.; Wang, Z.; Walheim, S.; Liu, J.; Gliemann, H.; Wöll, C. On the Dielectric and Optical Properties of Surface-Anchored Metal-Organic Frameworks: A Study on Epitaxially Grown Thin Films. *Appl. Phys. Lett.* **2013,** *103*, 091903.
(470) Usman, M.; Lee, C.-H.; Hung, D.-S.; Lee, S.-F.; Wang, C.-C.; Luo, T.-T.; Zhao, L.; Wu, M.-K.; Lu, K.-L. Intrinsic Low Dielectric Behaviour of a Highly Thermally Stable Sr-Based Metal–Organic Framework for Interlayer Dielectric Materials. *J. Mater. Chem. C* **2014,** *2*, 3762-3768.
(471) Krishtab, M.; Stassen, I.; Stassin, T.; Cruz, A. J.; Okudur, O. O.; Armini, S.; Wilson, C.; De Gendt, S.; Ameloot, R. Vapor-Deposited Zeolitic Imidazolate Frameworks as Gap-Filling Ultra-Low-K Dielectrics. *Nat. Commun.* **2019,** *10*, 3729.
(472) Shao, P. P.; Li, J.; Chen, F.; Ma, L.; Li, Q. B.; Zhang, M. X.; Zhou, J. W.; Yin, A. X.; Feng, X.; Wang, B. Flexible Films of Covalent Organic Frameworks with Ultralow Dielectric Constants under High Humidity. *Angew. Chem. Int. Ed.* **2018,** *57*, 16501-16505.
(473) Galli, S.; Cimino, A.; Ivy, J. F.; Giacobbe, C.; Arvapally, R. K.; Vismara, R.; Checchia, S.; Rawshdeh, M. A.; Cardenas, C. T.; Yaseen, W. K.et al. Fluorous Metal-Organic Frameworks and Nonporous Coordination Polymers as Low-Kappa Dielectrics. *Adv. Func. Mater.* **2019,** *29*.

(474) Kao, Y. C.; Mendiratta, S.; Usman, M.; Wen, Y. S.; Wang, C. M.; Zhao, L.; Wu, M. K.; Lu, K. L. Exceptional Low Dielectric Behavior of Chemically Robust, Guest-Free Co- and Mn-Based Coordination Polymers. *Chemelectrochem* **2019,** *6*, 623-626.
(475) Xu, W.; Yu, S. S.; Zhang, H.; Duan, H. B. A Three-Dimensional Metal-Organic Framework for a Guest-Free Ultra-Low Dielectric Material. *RSC Adv.* **2019,** *9*, 16183-16186.
(476) Guo, H. L.; Wang, M.; Liu, J. J.; Zhu, S. J.; Liu, C. G. Facile Synthesis of Nanoscale High Porosity Ir-Mofs for Low-K Dielectrics Thin Films. *Microporous Mesoporous Mater.* **2016,** *221*, 40-47.
(477) Mezenov, Y. A.; Krasilin, A. A.; Dzyuba, V. P.; Nominé, A.; Milichko, V. A. Metal–Organic Frameworks in Modern Physics: Highlights and Perspectives. *Adv. Mater.* **2019,** *6*, 1900506.
(478) Wang, B.; Huang, W.; Chi, L.; Al-Hashimi, M.; Marks, T. J.; Facchetti, A. High-K Gate Dielectrics for Emerging Flexible and Stretchable Electronics. *Chem. Rev.* **2018,** *118*, 5690-5754.
(479) Robertson, J. High Dielectric Constant Oxides. *Eur. Phys. J. Appl. Phys.* **2004,** *28*, 265-291.
(480) Ryder, M. R.; Zeng, Z. X.; Titov, K.; Sun, Y. T.; Mandi, E. M.; Flyagina, I.; Bennett, T. D.; Civalleri, B.; Kelley, C. S.; Frogley, M. D.et al. Dielectric Properties of Zeolitic Imidazolate Frameworks in the Broad-Band Infrared Regime. *Journal of Physical Chemistry Letters* **2018,** *9*, 2678-2684.
(481) Scatena, R.; Guntern, Y. T.; Macchi, P. Electron Density and Dielectric Properties of Highly Porous Mofs: Binding and Mobility of Guest Molecules in Cu-3(Btc)(2) and Zn-3(Btc)(2). *J. Am. Chem. Soc.* **2019,** *141*, 9382-9390.
(482) Babal, A. S.; Dona, L.; Ryder, M. R.; Titov, K.; Chaudhari, A. K.; Zeng, Z. X.; Kelley, C. S.; Frogley, M. D.; Cinque, G.; Civalleri, B.et al. Impact of Pressure and Temperature on the Broadband Dielectric Response of the Hkust-1 Metal-Organic Framework. *Journal of Physical Chemistry C* **2019,** *123*, 29427-29435.
(483) Bermudez-Garcia, J. M.; Vicent-Luna, J. M.; Yanez-Vilar, S.; Hamad, S.; Sanchez-Andujar, M.; Castro-Garcia, S.; Calero, S.; Senaris-Rodriguez, M. A. Liquid Self-Diffusion of H2o and Dmf Molecules in Co-Mof-74: Molecular Dynamics Simulations and Dielectric Spectroscopy Studies. *Phys. Chem. Chem. Phys.* **2016,** *18*, 19605-19612.
(484) Wang, H. L.; Li, N.; Hu, Z. B.; Bennett, T. D.; Zhao, X. J.; Ching, W. Y. Structural, Electronic, and Dielectric Properties of a Large Random Network Model of Amorphous Zeolitic Imidazolate Frameworks and Its Analogues. *J. Am. Ceram. Soc.* **2019,** *102*, 4602-4611.
(485) Jain, A. K.; Mao, J. C.; Mohiuddin, K. M. Artificial Neural Networks: A Tutorial. *Computer* **1996,** *29*, 31.
(486) Strukov, D. B.; Snider, G. S.; Stewart, D. R.; Williams, R. S. The Missing Memristor Found. *Nature* **2008,** *453*, 80-83.
(487) Kwon, D.-H.; Kim, K. M.; Jang, J. H.; Jeon, J. M.; Lee, M. H.; Kim, G. H.; Li, X.-S.; Park, G.-S.; Lee, B.; Han, S.et al. Atomic Structure of Conducting Nanofilaments in Tio2 Resistive Switching Memory. *Nat. Nanotech.* **2010,** *5*, 148-153.
(488) Yang, J. J.; Strukov, D. B.; Stewart, D. R. Memristive Devices for Computing. *Nat. Nanotech.* **2013,** *8*, 13-24.
(489) Zhou, Y.; Ramanathan, S. Mott Memory and Neuromorphic Devices. *Proc. IEEE* **2015,** *103*, 1289-1310.

(490) Yang, J. J.; Pickett, M. D.; Li, X. M.; Ohlberg, D. A. A.; Stewart, D. R.; Williams, R. S. Memristive Switching Mechanism for Metal/Oxide/Metal Nanodevices. *Nat. Nanotech.* **2008,** *3*, 429-433.

(491) Wang, Z. Y.; Wang, L. Y.; Nagai, M.; Xie, L. H.; Yi, M. D.; Huang, W. Nanoionics-Enabled Memristive Devices: Strategies and Materials for Neuromorphic Applications. *Adv. Electron. Mater.* **2017,** *3*.

(492) Xia, Q. F.; Yang, J. J. Memristive Crossbar Arrays for Brain-Inspired Computing. *Nat. Mater.* **2019,** *18*, 309-323.

(493) Friedlein, J. T.; Rivnay, J.; Dunlap, D. H.; McCulloch, I.; Shaheen, S. E.; McLeod, R. R.; Malliaras, G. G. Influence of Disorder on Transfer Characteristics of Organic Electrochemical Transistors. *Appl. Phys. Lett.* **2017,** *111*.

(494) Rivnay, J.; Inal, S.; Salleo, A.; Owens, R. M.; Berggren, M.; Malliaras, G. G. Organic Electrochemical Transistors. *Nat. Rev. Mater.* **2018,** *3*.

(495) Bureekaew, S.; Horike, S.; Higuchi, M.; Mizuno, M.; Kawamura, T.; Tanaka, D.; Yanai, N.; Kitagawa, S. One-Dimensional Imidazole Aggregate in Aluminium Porous Coordination Polymers with High Proton Conductivity. *Nat. Mater.* **2009,** *8*, 831-836.

(496) Hurd, J. A.; Vaidhyanathan, R.; Thangadurai, V.; Ratcliffe, C. I.; Moudrakovski, I. L.; Shimizu, G. K. H. Anhydrous Proton Conduction at 150 Degrees C in a Crystalline Metal-Organic Framework. *Nat. Chem.* **2009,** *1*, 705-710.

(497) Kim, S.; Joarder, B.; Hurd, J. A.; Zhang, J.; Dawson, K. W.; Gelfand, B. S.; Wong, N. E.; Shimizu, G. K. H. Achieving Superprotonic Conduction in Metal-Organic Frameworks through Iterative Design Advances. *J. Am. Chem. Soc.* **2018,** *140*, 1077-1082.

(498) Umeyama, D.; Horike, S.; Inukai, M.; Hijikata, Y.; Kitagawa, S. Confinement of Mobile Histamine in Coordination Nanochannels for Fast Proton Transfer. *Angew. Chem. Int. Ed.* **2011,** *50*, 11706-11709.

(499) Horike, S.; Umeyama, D.; Kitagawa, S. Ion Conductivity and Transport by Porous Coordination Polymers and Metal-Organic Frameworks. *Acc. Chem. Res.* **2013,** *46*, 2376-2384.

(500) Munjal, S.; Khare, N. Advances in Resistive Switching Based Memory Devices. *J. Phys. D* **2019,** *52*.

(501) Goswami, S.; Matula, A. J.; Rath, S. P.; Hedström, S.; Saha, S.; Annamalai, M.; Sengupta, D.; Patra, A.; Ghosh, S.; Jani, H.et al. Robust Resistive Memory Devices Using Solution-Processable Metal-Coordinated Azo aromatics. *Nat. Mater.* **2017,** *16*, 1216.

(502) Noriega, R.; Rivnay, J.; Vandewal, K.; Koch, F. P. V.; Stingelin, N.; Smith, P.; Toney, M. F.; Salleo, A. A General Relationship between Disorder, Aggregation and Charge Transport in Conjugated Polymers. *Nat. Mater.* **2013,** *12*, 1038-1044.

(503) Tessler, N.; Preezant, Y.; Rappaport, N.; Roichman, Y. Charge Transport in Disordered Organic Materials and Its Relevance to Thin-Film Devices: A Tutorial Review. *Adv. Mater.* **2009,** *21*, 2741-2761.

(504) Meng, X.; Wang, H.-N.; Song, S.-Y.; Zhang, H.-J. Proton-Conducting Crystalline Porous Materials. *Chem. Soc. Rev.* **2017,** *46*, 464-480.

(505) Yamada, T.; Otsubo, K.; Makiura, R.; Kitagawa, H. Designer Coordination Polymers: Dimensional Crossover Architectures and Proton Conduction. *Chem. Soc. Rev.* **2013,** *42*, 6655-6669.

(506) Gorodokin, V.; Zemlyanov, D. Metallic Contamination in Silicon Processing. in *23rd IEEE Convention of Electrical and Electronics Engineers in Israel, Proceedings*, **2004,** DOI:10.1109/eeei.2004.1361113 10.1109/EEEI.2004.1361113.

(507) Yao, Z. Z.; Pan, L.; Liu, L. Z.; Zhang, J. D.; Lin, Q. J.; Ye, Y. X.; Zhang, Z. J.; Xiang, S. C.; Chen, B. L. Simultaneous Implementation of Resistive Switching and Rectifying Effects in a Metal-Organic Framework with Switched Hydrogen Bond Pathway. *Sci. Advances* **2019,** *5,* DOI: 10.1126/sciadv.aaw4515.

(508) Colomban, P. *Protonconductors:Solids,Membranesandgels—Materials and Devices*; Cambridge University Press: Cambridge, U.K., 1992.

(509) Nagarkar, S. S.; Unni, S. M.; Sharma, A.; Kurungot, S.; Ghosh, S. K. Two-in-One: Inherent Anhydrous and Water-Assisted High Proton Conduction in a 3d Metal-Organic Framework. *Angew. Chem. Int. Ed.* **2014,** *53*, 2638-2642.

(510) Ponomareva, V. G.; Kovalenko, K. A.; Chupakhin, A. P.; Dybtsev, D. N.; Shutova, E. S.; Fedin, V. P. Imparting High Proton Conductivity to a Metal-Organic Framework Material by Controlled Acid Impregnation. *J. Am. Chem. Soc.* **2012,** *134*, 15640-15643.

(511) Domenech, A.; Garcia, H.; Domenech-Carbo, M. T.; Xamena, F. Electrochemistry of Metal-Organic Frameworks: A Description from the Voltammetry of Microparticles Approach. *J. Phys. Chem. C* **2007,** *111*, 13701-13711.

(512) Ji, L. D.; Wang, J.; Wu, K. B.; Yang, N. J. Tunable Electrochemistry of Electrosynthesized Copper Metal-Organic Frameworks. *Adv. Funct. Mater.* **2018,** *28*.

(513) Li, M. Y.; Dinca, M. Reductive Electrosynthesis of Crystalline Metal-Organic Frameworks (N). *J. Am. Chem. Soc.* **2011,** *133*, 12926-12929.

(514) Li, M. Y.; Dinca, M. Selective Formation of Biphasic Thin Films of Metal-Organic Frameworks by Potential-Controlled Cathodic Electrodeposition. *Chem. Sci.* **2014,** *5*, 107-111.

(515) Mueller, U.; Schubert, M.; Teich, F.; Puetter, H.; Schierle-Arndt, K.; Pastre, J. Metal-Organic Frameworks - Prospective Industrial Applications. *J. Mater. Chem.* **2006,** *16*, 626-636.

(516) Worrall, S. D.; Bissett, M. A.; Hirunpinyopas, W.; Attfield, M. P.; Dryfe, R. A. W. Facile Fabrication of Metal-Organic Framework Hkust-1-Based Rewritable Data Storage Devices. *J. Mater. Chem. C* **2016,** *4*, 8687-8695.

(517) Thurmer, K.; Schneider, C.; Stavila, V.; Friddle, R. W.; Leonard, F.; Fischer, R. A.; Allendorf, M. D.; Talin, A. A. Surface Morphology and Electrical Properties of Cu3btc2 Thin Films before and after Reaction with Tcnq. *ACS Appl. Mater. Interfaces* **2018,** *10*, 39400-39410.

(518) Yoon, S. M.; Warren, S. C.; Grzybowski, B. A. Storage of Electrical Information in Metal-Organic-Framework Memristors. *Angew. Chem. Int. Ed.* **2014,** *53*, 4437-4441.

(519) Wang, Z.; Nminibapiel, D.; Shrestha, P.; Liu, J.; Guo, W.; Weidler, P. G.; Baumgart, H.; Woell, C.; Redel, E. Resistive Switching Nanodevices Based on Metal-Organic Frameworks. *ChemNanoMat* **2016,** *2*, 67-73.

(520) Liu, Y.; Wang, H.; Shi, W.; Zhang, W.; Yu, J.; Chandran, B. K.; Cui, C.; Zhu, B.; Liu, Z.; Li, B.et al. Alcohol-Mediated Resistance-Switching Behavior in Metal-Organic Framework-Based Electronic Devices. *Angew. Chem. Int. Ed.* **2016,** *55*, 8884-8888.

(521) Meena, J. S.; Sze, S. M.; Chand, U.; Tseng, T. Y. Overview of Emerging Nonvolatile Memory Technologies. *Nanoscale Res. Lett.* **2014,** *9*.
(522) Ye, H.-Y.; Tang, Y.-Y.; Li, P.-F.; Liao, W.-Q.; Gao, J.-X.; Hua, X.-N.; Cai, H.; Shi, P.-P.; You, Y.-M.; Xiong, R.-G. Metal-Free Three-Dimensional Perovskite Ferroelectrics. *Science* **2018,** *361*, 151-155.
(523) Chen, X.; Han, X.; Shen, Q. D. Pvdf-Based Ferroelectric Polymers in Modern Flexible Electronics. *Adv. Electron. Mater.* **2017,** *3*, 1600460.
(524) Asadi, K.; van der Veen, M. A. Ferroelectricity in Metal–Organic Frameworks: Characterization and Mechanisms. *Chem. Eur. J.* **2016,** *2016*, 4332-4344.
(525) Pan, L.; Liu, G.; Li, H.; Meng, S.; Han, L.; Shang, J.; Chen, B.; Platero-Prats, A. E.; Lu, W.; Zou, X. D.et al. A a Resistance-Switchable and Ferroelectric Metal Organic Framework. *J. Am. Chem. Soc.* **2014,** *136*, 17477-17483.
(526) Allendorf, M. D.; Medishetty, R.; Fischer, R. A. Guest Molecules as a Design Element for Metal–Organic Frameworks. *MRS Bull.* **2016,** *41*, 865-869.
(527) Halder, A.; Ghoshal, D. Structure and Properties of Dynamic Metal-Organic Frameworks: A Brief Accounts of Crystalline-to-Crystalline and Crystalline-to-Amorphous Transformations. *CrystEngComm* **2018,** *20*, 1322-1345.
(528) Taniguchi, K.; Narushima, K.; Sagayama, H.; Kosaka, W.; Shito, N.; Miyasaka, H. In Situ Reversible Ionic Control for Nonvolatile Magnetic Phases in a Donor/Acceptor Metal-Organic Framework. *Adv. Funct. Mater.* **2017,** *27*.
(529) Cheng, Y.; Peng, B.; Hu, Z.; Zhou, Z.; Liu, M. Recent Development and Status of Magnetoelectric Materials and Devices. *Phys. Lett. A* **2018,** *382*, 3018-3025.
(530) Pan, L.; Ji, Z.; Yi, X.; Zhu, X.; Chen, X.; Shang, J.; Liu, G.; Li, R.-W. Metal-Organic Framework Nanofilm for Mechanically Flexible Information Storage Applications. *Adv. Funct. Mater.* **2015,** *25*, 2677-2685.
(531) Ding, G. L.; Wang, Y. X.; Zhang, G. X.; Zhou, K.; Zeng, K. L.; Li, Z. X.; Zhou, Y.; Zhang, C.; Chen, X. L.; Han, S. T. 2d Metal-Organic Framework Nanosheets with Time-Dependent and Multilevel Memristive Switching. *Adv. Funct. Mater.* **2019,** *29*.
(532) Huang, X.; Zheng, B.; Liu, Z. D.; Tan, C. L.; Liu, J. Q.; Chen, B.; Li, H.; Chen, J. Z.; Zhang, X.; Fan, Z. X.et al. Coating Two-Dimensional Nanomaterials with Metal-Organic Frameworks. *ACS Nano* **2014,** *8*, 8695-8701.
(533) Hu, Y.; Dunlap, N.; Wan, S.; Lu, S.; Huang, S.; Sellinger, I.; Ortiz, M.; Jin, Y.; Lee, S.-h.; Zhang, W. Crystalline Lithium Imidazolate Covalent Organic Frameworks with High Li-Ion Conductivity. *J. Am. Chem. Soc.* **2019,** *141*, 7518-7525.
(534) Xu, Q.; Tao, S.; Jiang, Q.; Jiang, D. Ion Conduction in Polyelectrolyte Covalent Organic Frameworks. *J. Am. Chem. Soc.* **2018,** *140*, 7429-7432.
(535) Liu, J.; Yang, F.; Cao, L.; Li, B.; Yuan, K.; Lei, S.; Hu, W. A Robust Nonvolatile Resistive Memory Device Based on a Freestanding Ultrathin 2d Imine Polymer Film. *Adv. Mater.* **2019,** *31*, 1902264.
(536) Eagar, T. W. Bringing New Materials to Market. *Technol. Rev.* **1995,** *98*, 43-49.
(537) Wadia, C., 2012.
(538) Chiang, C. K.; Fincher, C. R.; Park, Y. W.; Heeger, A. J.; Shirakawa, H.; Louis, E. J.; Gau, S. C.; Macdiarmid, A. G. Electrical-Conductivity in Doped Polyacetylene. *Phys. Rev. Lett.* **1977,** *39*, 1098-1101.

(539) Shirakawa, H.; Louis, E. J.; Macdiarmid, A. G.; Chiang, C. K.; Heeger, A. J. Synthesis of Electrically Conducting Organic Polymers - Halogen Derivatives of Polyacetylene, (Ch)X *J. Chem. Soc., Chem. Commun.* **1977**, 578-580.
(540) Loo, Y.-L.; McCulloch, I. Progress and Challenges in Commercialization of Organic Electronics. *MRS Bulletin* **2008,** *33*, 653-662.
(541) Huang, X.; Li, H. S.; Tu, Z. Y.; Liu, L. Y.; Wu, X. Y.; Chen, J.; Liang, Y. Y.; Zou, Y.; Yi, Y. P.; Sun, J. L.et al. Highly Conducting Neutral Coordination Polymer with Infinite Two-Dimensional Silver-Sulfur Networks. *J. Am. Chem. Soc.* **2018,** *140*, 15153-15156.
(542) Claire, F. J.; Tenney, S. M.; Li, M. M.; Siegler, M. A.; Wagner, J. S.; Hall, A. S.; Kempa, T. J. Hierarchically Ordered Two-Dimensional Coordination Polymers Assembled from Redox-Active Dimolybdenum Clusters. *J. Am. Chem. Soc.* **2018,** *140*, 10673-10676.
(543) Zhou, C.; Longley, L.; Krajnc, A.; Smales, G. J.; Qiao, A.; Erucar, I.; Doherty, C. M.; Thornton, A. W.; Hill, A. J.; Ashling, C. W.et al. Metal-Organic Framework Glasses with Permanent Accessible Porosity. *Nat. Commun.* **2018,** *9*, 5042.
(544) Dissegna, S.; Epp, K.; Heinz, W. R.; Kieslich, G.; Fischer, R. A. Defective Metal-Organic Frameworks. *Adv. Mater.* **2018,** *30*.